A study of high energy muons inextensive air showers

Wafiq Shakir Rada

A STUDY OF HIGH ENERGY MUONS

IN

EXTENSIVE AIR SHOWERS

BY

Wafiq Shakir Rada, B.Sc.

A thesis submitted to the University of Durham for the degree of Doctor of Philosophy.

Department of Physics,
Durham University, U.K.

MARCH , 1978.

ABSTRACT

An automated air shower array to investigate the properties of showers accompanied by high energy muons has been constructed to run in conjunction with the Durham magnetic automated muon spectrograph (M.A.R.S.). Measurements of the lateral distribution of muons have been obtained for muon energies $\geqslant$ 50, $\geqslant$ 100, $\geqslant$ 200, and $\geqslant$ 300 GeV in showers of size $5 \times 10^4 - 3 \times 10^6$ particles for core distance of up to 50 metres.

Details are given of the construction of the array, the computer handling of the collected data, its treatment and its analysis.

Based on the current high energy nuclear interaction models, theoretical predictions of the muon lateral distributions have been examined and it is shown that the assumptions on which these models are based may be valid for high energy muons in E.A.S. Broad agreement is found with the predictions of the C.K.P. and the Slow Multiple Fire Ball (S.M.F.B.) models as applied to extensive air showers by Olejnizhack (1975) and Greider (1977). A comparison of the data is made with the predictions of the Feynman scaling model (Goned, 1975, and Fishbane et al, 1974) and it is shown that the scaling model and an assumed pure proton primary predicts lower values of muon densities than those observed in the present experiment. In contrast, it would appear that a combination of a scaling model and an assumed iron primary spectrum gives a better agreement with experimental data.

In a preliminary experiment a small air shower array around the spectrograph was constructed and used to measure the sea level rate of muons having energies $\geq$ 5 GeV in small air showers. Experimental results are also presented on the sea level rate of these showers, their angular distribution, density and size spectra. In this experiment, comparison is made between the experimental data and theoretical predictions and the results of other workers wherever possible.

An account of the properties of the primary cosmic radiation and the showers they initiate is given in Chapters 1 and 2 with special reference to the muon component of E.A.S.

PREFACE

This thesis is an account of the work carried out by the author under the supervision of Dr. M.G.Thompson during the period 1973 - 1977 in the Department of Physics in the University of Durham. The author was responsible for the construction of the 1 m^2 and 2 m^2 detectors of the Durham Air Shower Array, the design and operation of the array coincidence recording system and the calibration and normal operation of the array detectors. With his colleagues the author has shared in the running and data collection of all experiments concerned with the air shower array. Following the analysis techniques of Wells (1972), Daniels (internal report) and Smith (1976), the author has been responsible for the analysis of both the spectrograph and array data as well as the treatment and interpretation of the experimental results with respect to the predictions of the high energy interaction models. The design and construction of the preliminary experiment, described in Chapter 3, has been the sole responsibility of the author together with the running of the apparatus, analysis of the experimental data, and the theoretical predictions, as described in Chapter 4.

Publications of the author relating to the Durham Air Shower Array include,

1. Rada et al (1975) Proceedings of the 14th International Conference on Cosmic Rays (Munich).
2. Rada et al (1977), Nucl.Inst. and Methods, 145, 283.
3. Rada et al (1977), to be published in the Proceedings of the 15th International Conference on Cosmic Rays (Plovdiv).
4. Ashton et al ; a,b,c,d and e to be published in the Proceedings of the 15th International Cosmic Ray Conference (Plovdiv).

ACKNOWLEDGMENT

I am indebted to Professor A. W. Wolfendale, F.R.S., for the privilege of working in his laboratories and for his encouragement through all stages of this work.

It is a pleasure to record a deep gratitude to my supervisor, Dr. M. G. Thompson, for his advice, guidance and many invaluable suggestions throughout this work. I wish to thank all the members of the M.A.R.S. group, both past and present, for their friendly co-operation and assistance ; it has been a pleasure to work with them. In particular, I would like to express my sincere thanks to Dr. A.C.Smith for many constructive discussions, valuable suggestions, and constant help.

I would like to take this opportunity of expressing my thanks to Dr. C.A.Ayre and Dr. M.R.Whalley for reading the manuscript and making valuable criticisms and suggestions. I also acknowledge the assistance of my colleagues, Dr. R.C.Hawkes, Mr. T.R.Stewart, Mr. R. Thornley, and Mr. J.M.Baxendale, for their help in data collection and useful discussions on countless occasions. I wish to extend my thanks to the group computer programmer, Mrs.S.E.Davidson, who has willingly helped in the data handling and transfer through the computer systems. Mr. K. Tindale is thanked for his skilled assistance in the laboratory and in the maintenance of the air shower experiments.

Thanks are due to Mrs. A. Gregory and Mrs. J. Johnson for preparing the figures and diagrams for this thesis. The staff of the department electronics workshop are thanked for their assistance in many electronic devices.

Dr. J. Wdowczyk, Dr. B.A. Khrenov, Dr. A. Goned and Dr. J. Olejniczak are thanked for many suggestions and beneficial discussions. The assistance of the Northumbrian Universities Multiple Access Computer staff both at Durham and Newcastle Universities is well appreciated. The British Science Research Council is acknowledged for funding this research project. Thanks are due to Mrs. Mellanby and Mrs. F.Stubbs for typing this thesis.

Finally, the Government of the Republic of Iraq is thanked for the provision of a research scholarship without which the author would not have been able to participate in the work of the Durham laboratory.

CONTENTS

CHAPTER 2 Continued:

CHAPTER 6 Continued:

Page Nos

CHAPTER 7 Continued:

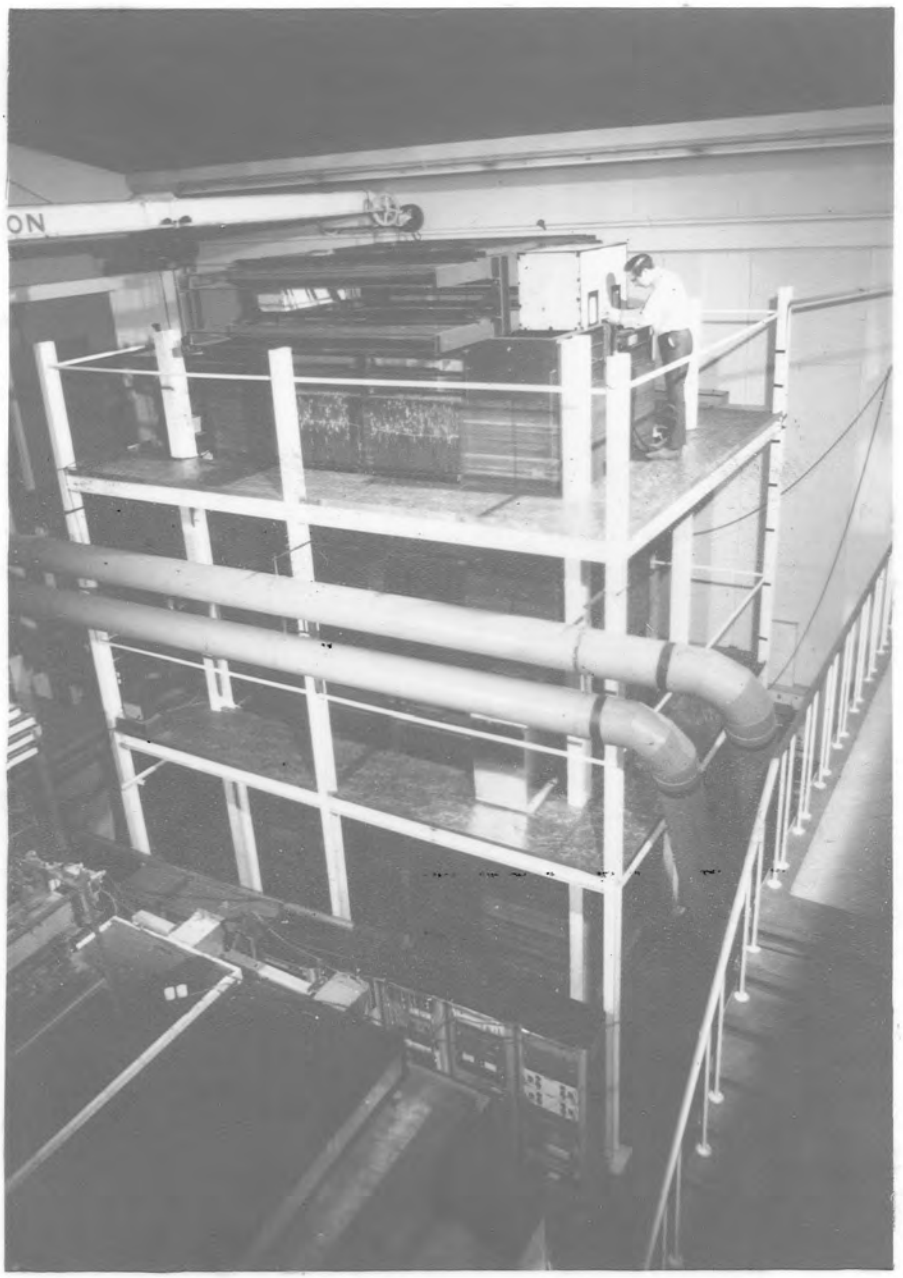

Plate 1. Magnetic Automated Research Spectrograph (M.A.R.S.)

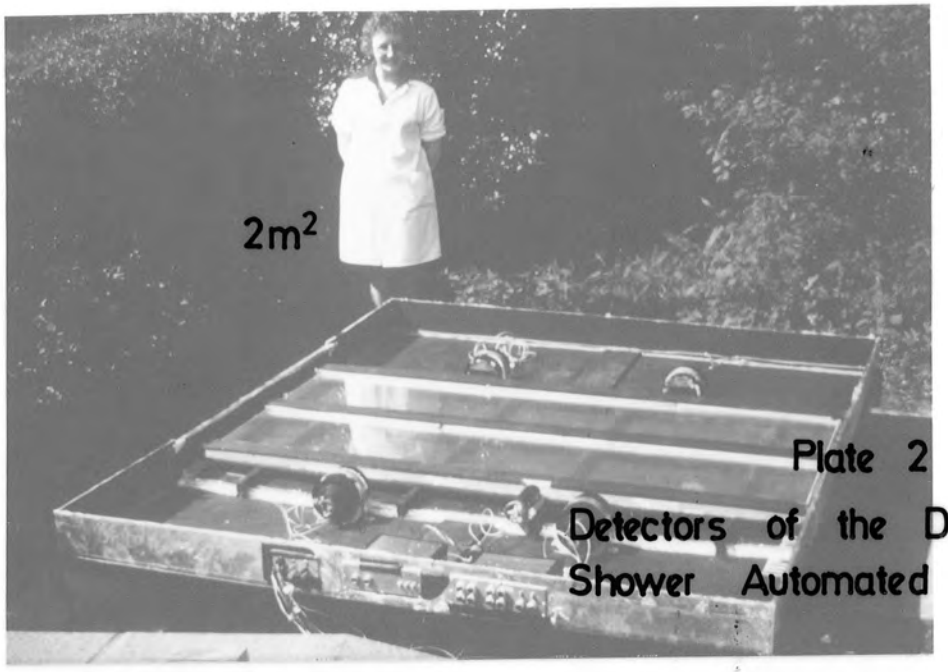

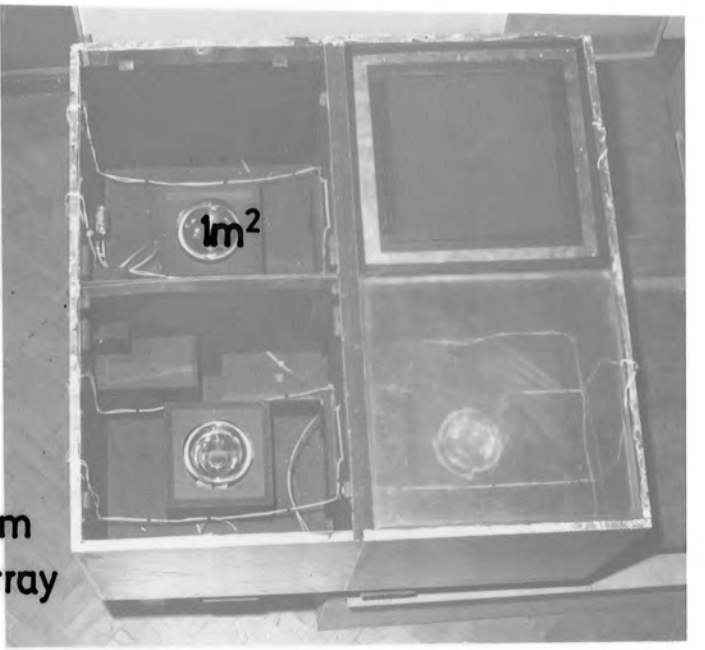

Plate 2

Detectors of the Durham Shower Automated Array

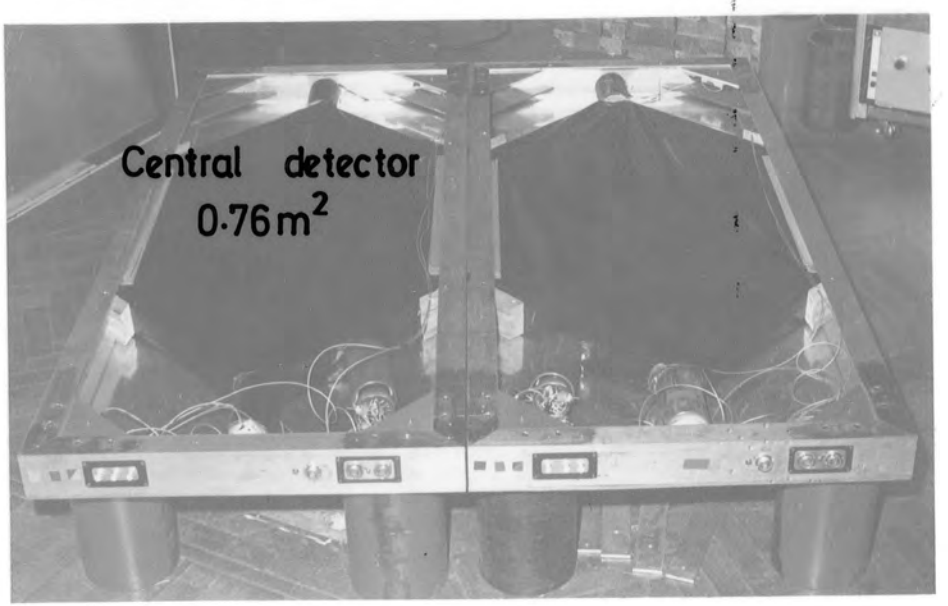

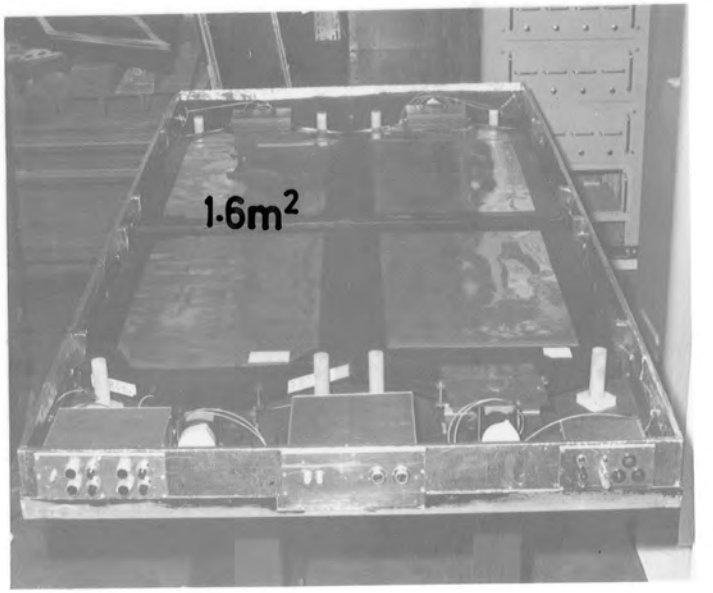

CHAPTER 1

THE COSMIC RADIATION

1.1. INTRODUCTION

Cosmic radiation is continuously incident on the earth's atmosphere. This radiation consists of subatomic nuclei (having energies from less than a GeV up to about 10^{10} GeV), X-rays, low energy electrons, neutrinos, γ-rays and possibly neutrons. Some of the particles incident on the earth originate at the place where they were accelerated and others are the result of interactions of the cosmic radiation and the interstellar medium.

Up-to-date the question of the origin of cosmic rays has not been answered satisfactorily. The sources of cosmic radiation have not been uniquely identified but one likely possibility is that cosmic rays are produced in Supernova explosions (Fowler, 1975).

The correlation between the bursts of cosmic ray activity and the occurrence of solar flares shows that the sun is a source of part of the low-energy cosmic ray flux that arrives at the top of the earth's atmosphere. During solar flares there are emitted particles with energy as large as 10 GeV, but difficulties associated with the acceleration of these particles to energies very much greater than this limit leads to the fact that there are other sources contributing significantly to the flux of high energy primary cosmic rays.

Theoretical studies have shown that it is possible that cosmic rays have been subjected to an acceleration process in the galactic magnetic field in which particles deviate many times from their original directions as a consequence of diffusion between regions of different magnetic field strengths (Wolfendale, 1973). Due to the high complexity and uncertainty of the diffusion process, particles lose the "information" of the direction

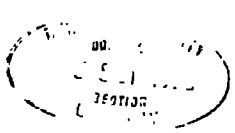

of origin and produce a nearly isotropic distribution on top of the earth's atmosphere. The degree of isotropy of the cosmic rays bombarding the earth's atmosphere is expected to depend upon many parameters. For example, the regularity of the galactic magnetic field, its strength, the distribution of matter in the galaxies and the energy of the cosmic ray. At the present time no significant anisotropies in the cosmic radiation to 10^{20} eV have been found. Significant advances in the last few years in high energy γ-ray astronomy have been made and a considerable amount of information concerning the energy spectrum and distribution of γ-rays is now available. This information is currently interpreted in the light of interactions between very high energy electrons and photons, matter and magnetic fields, and alternatively, in connection with p-interstellar matter interactions which via π^o production lead to γ-rays. Not only our galaxy but the Universe also is transparent to γ-rays, therefore, these photons retain the information concerning the direction from which they originated and the temporal features set at their origin.

1.2 THE PRIMARY SPECTRUM OF COSMIC RADIATION

The most important problem of Cosmic Ray Physics at the present time is the origin of the radiation, and to investigate the origin of prime importance,is a knowledge of the primary energy spectrum. Because of the wide range of energy and intensities of the cosmic ray primaries it is not possible to measure the whole range of the energy spectrum in a single experiment. Wolfendale (1973) summarizes the results of the primary cosmic ray spectrum over the entire range of energies obtained by various workers using various experimental techniques. The results of the summary are shown in Figure 1.1.

Studies of the primary energy spectrum can be classified into three broad energy intervals as follows : below 10^{10} eV, the region 10^{10}-10^{14} eV

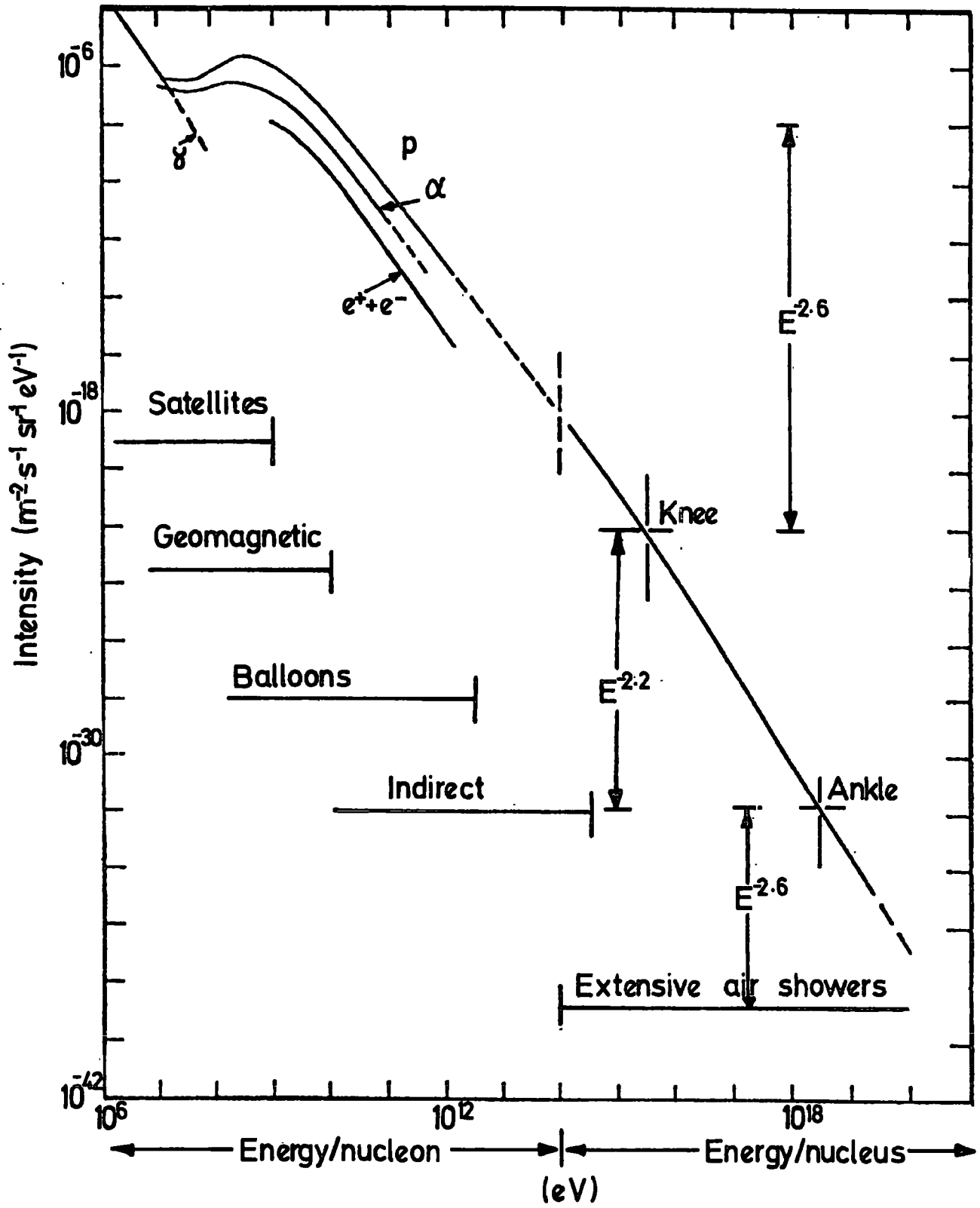

Figure 1.1. The energy spectrum of primary cosmic rays. (After Wolfendale, 1973).

and the E.A.S. region beyond about 10^{14} eV. Each range is discussed in the following sections.

1.2.1 The Spectral Region Below 10^{10} eV

Cosmic ray particles with energies less than 10^{10} eV arriving at the earth's atmosphere do not all come from the sun, rather the greater proportion comes from the distant parts of the galaxy. Figure 1.2 presents a survey of the measured differential primary spectrum in the low energy region from the summary of Bell (1974) for various primary components. Below 2 GeV/nucleon the primary cosmic ray intensity does not follow a power law. The deviation from a power law is due to the effect of solar modulation. The lack of knowledge of the nature of the solar modulation mechanism prevents accurate determination of the true primary spectrum. At these low energies the primary spectrum is continually changing with the time due to the random occurrence of magnetic storms and solar flares. These phenomenological effects have no appreciable importance in the intermediate and E.A.S. region of the primary energy.

1.2.2 The Spectrum in the Region 10^{10}-10^{14} eV

The spectral results in this energy range have been obtained using both indirect or direct methods. The indirect methods comprise those in which the primary spectrum is derived from the measurements of the secondary components carried out at high altitudes by balloons, aeroplanes and at mountain altitudes. Further, at sea level and underground, high energy muons have been used. The direct methods include measurements of the primary particles carried out using ionization calorimeters on board satellites or as the payloads of balloons flown at high altitudes. The "all particle" spectrum in the region 10^{10}-10^{14} eV obtained by both methods seem to be well represented by a power law having an exponent 2.6 - 2.7. This value of the exponent is in agreement with most of the measurements in this region. According to the Proton satellite experiments of Grigorov, et al (1971),

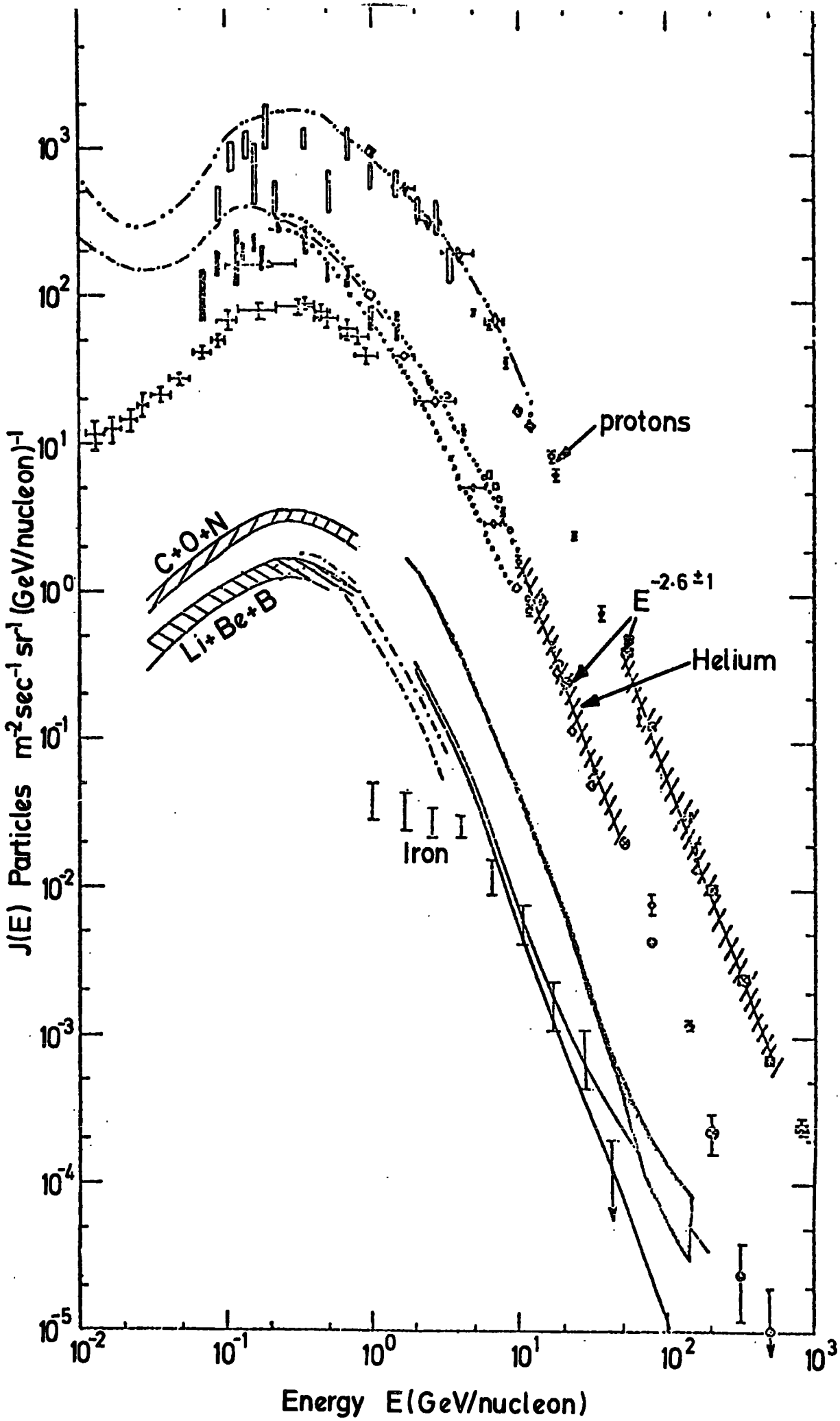

Figure 1.2. The differential energy spectrum of various primary nuclei (After Bell, 1974).

the spectrum of protons steepens around 10^{12} eV although the "all particle" spectrum does not show any significant change in slope. The results of experiments by Ryan, et al (1972), carried out with balloons do not support the steepening in the proton spectrum beyond 10^{12} eV, and therefore there is some doubt as to the form of the proton spectrum in this region. Results concerning the α-particle spectrum are available in the range 5×10^{10}-10^{12} eV, and the exponent of this spectrum appears to be essentially the same as that of "all particle" spectrum. Recently the independent observations of various groups have shown an increase in the relative abundance of heavy nuclei (especially iron) with increasing primary energy towards the E.A.S. region (e.g. Balasubrahmanian and Ormes, 1973 ; Juliussen, 1974 ; and Schmidt, et al, 1976). Although this work could give more understanding on the mass composition up to E.A.S. energies, some care has to be taken in interpreting these results. Figure 1.3 shows the differential energy spectrum above 10^{10} eV taken from a very recent summary presented by Wdowczyk, et al (1976). It is worthwhile pointing out that the very flat iron spectrum is not universally accepted. From Figure 1.3 it can be seen that the recent data of Schmidt, et al (1976) exhibit a steeper spectrum as indicated by the line VH.

1.2.3 The Energy Spectrum in the Region Above 10^{14} eV (E.A.S.Region)

In the energy range 10^{14} - 10^{17} eV, measurements on the primary energy spectrum,obtained from E.A.S. experiments, e.g. Bradt, et al (1965) ; Aseikin, et al (1971); Brownlee, et al (1970) & Greisen (1966), show a gradual change of the slope of the differential spectrum from 2.7 to 3.2. A comparison of the spectra composed by these authors shows that the spectrum steepens at approximately 3×10^{15} eV, and this position is known as the "knee" (Figure 1.1). It is difficult to establish the position of the "knee" in the observed energy spectrum exactly due to uncertainties in the energy calibration of the different experiments, the structure function fitted

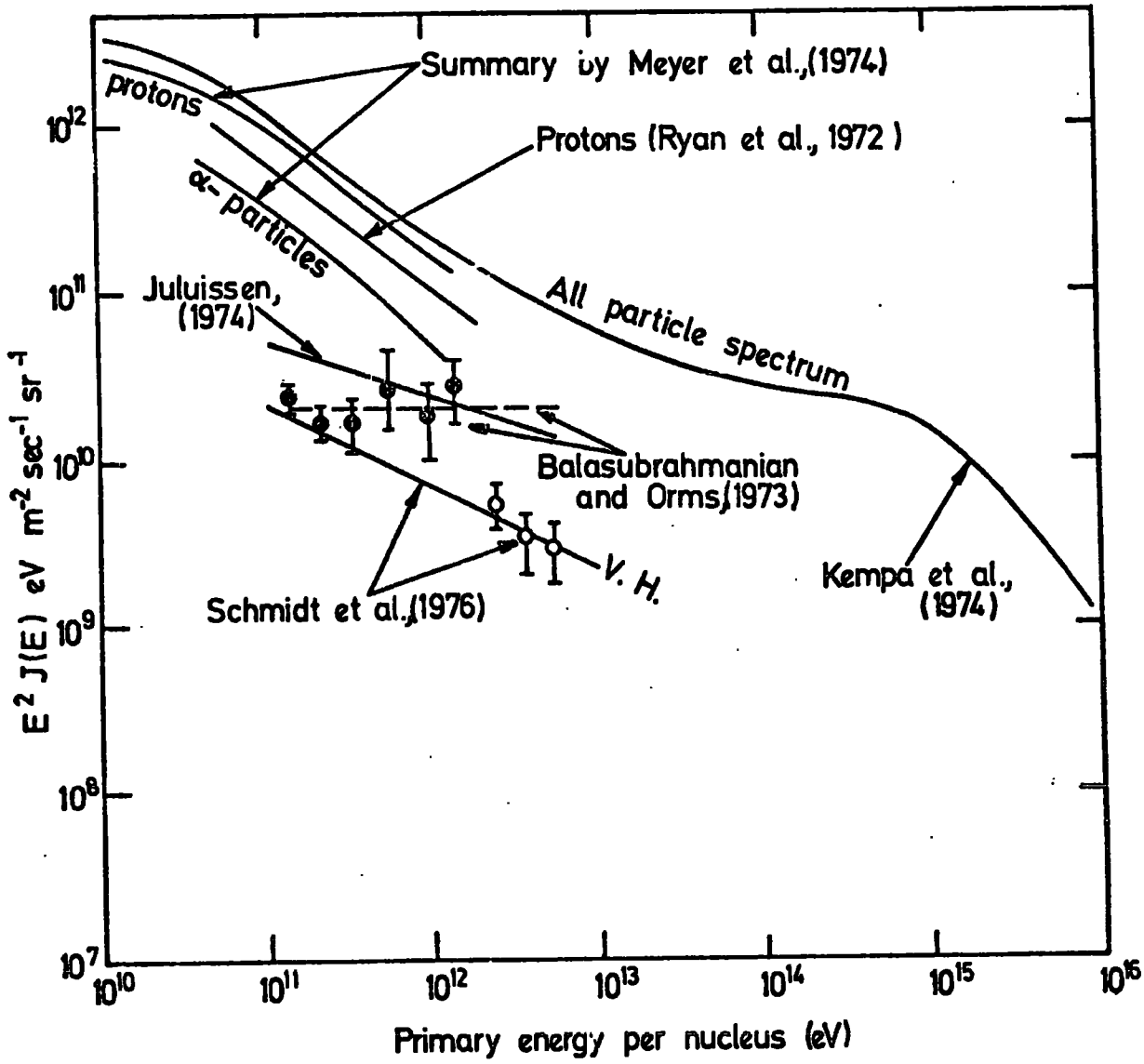

FIGURE 1.3 The differential primary energy spectrum of cosmic rays in the range 10^{10} - 10^{14} eV. (After Wdowszyk et al, 1976).

to the observed data, and in the modelling of the development of E.A.S. The change in slope is believed to be due to the failure of the galactic magnetic fields to contain the particles as their rigidity cut-off is exceeded. A recent explanation of the observed energy spectrum in this range is reported by Bell (1974), using a model of cosmic ray diffusion in the spiral arm of the galaxy. Bell (1974) has suggested the possibility of producing cosmic rays at energies below that of the "knee" by a supernova explosion, and those beyond the "knee" being produced in other parts of the galaxy. Hence, the change in the slope at the position of the "knee" could be explained either by differences in the production mechanism at the sources of the primary cosmic radiation below and above the "knee", or alternatively, cosmic rays however produced have the same production spectrum, and the change in the slope is due to the fact that cosmic rays below the "knee" have originated at local sources, while those above have had their energies modulated on their way through the interstellar matter. Knowledge of the shape and the magnitude of the primary spectrum contributes to the understanding of the origin of cosmic rays and their acceleration mechanism. Figure 1.4 shows the integral spectrum of cosmic ray primaries as summarised by Kempa, et al (1974) from the available data. The most important aspect of this spectrum is the evidence of a "bump" in the region 10^{14} - 10^{15} eV. The best fitted line to the spectrum has been plotted in the differential form as seen in Figure 1.5 and compared with the results of other workers, as indicated in the figure. It is seen that the spectrum of Kempa, et al, shows significantly higher intensities than other workers, e.g. Edge, et al, (1973) ; Bell, et al (1974). Several workers, e.g. Kempa,et al(1974);Karakula et al, (1974) have attempted to explain the "bump" in the spectrum as being the result of contributions from Pulsars. The agreement with experimental observations in this region is very interesting. Wdowczyk, et al (1976) have pointed out that there is no evidence against pulsar contributions. If this

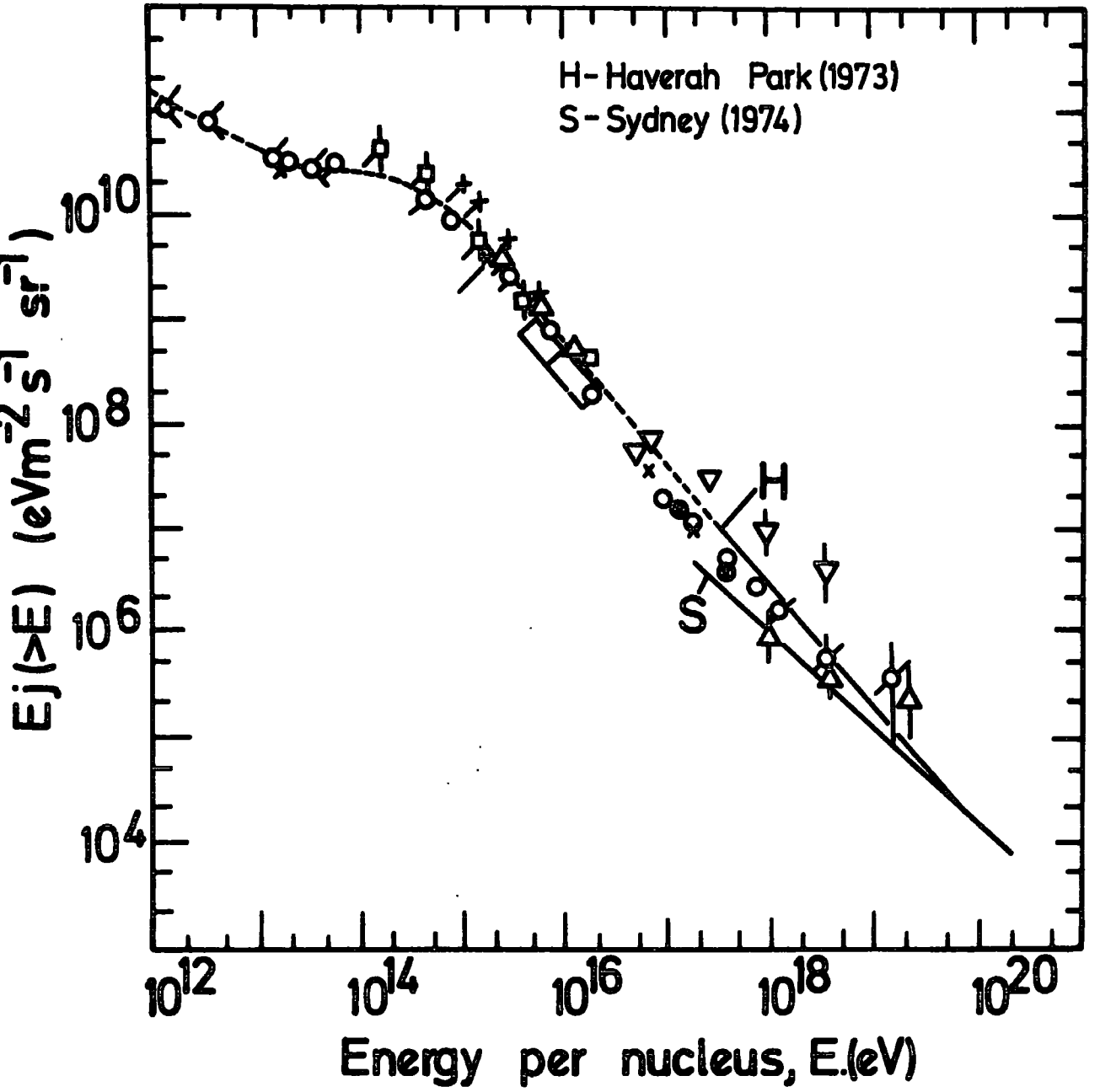

Figure 1.4. The integral primary cosmic ray spectrum. (After Kempa et al. (1974))

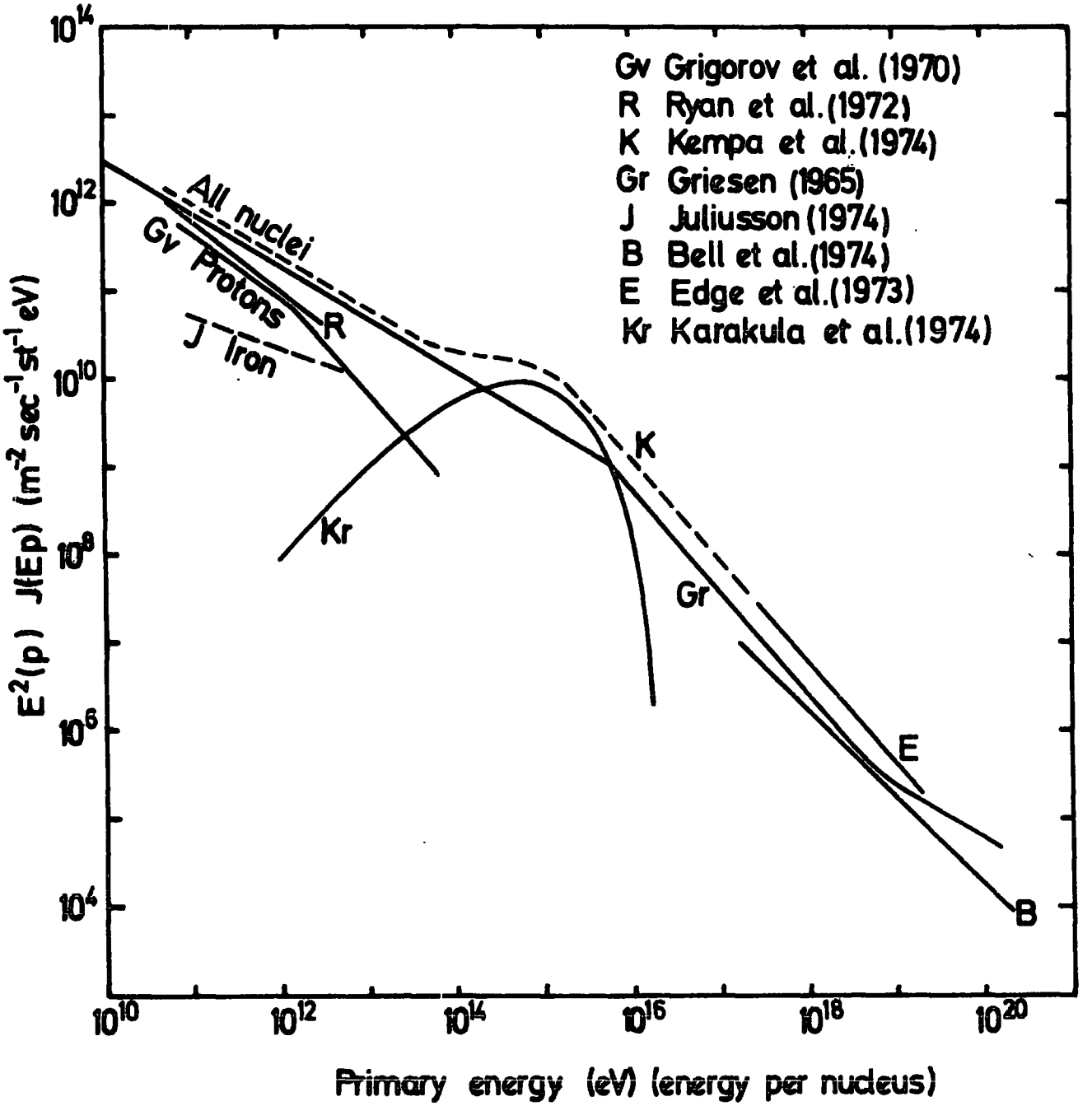

FIGURE 1.5 The differential energy spectrum of primary cosmic rays obtained from the results of various workers.

feature is confirmed, then this will imply a galactic contribution to the primary flux.

The shape of the energy spectrum at the ultra high energy region is rather uncertain and the interpretation of the primary spectrum is rather complicated. A number of workers have explained the existence of the possible "ankle" at $\sim 10^{18}$ eV (first reported by Linsley (1963)), as being due to the disappearance of galactic nuclei at ultra high energies and most of the radiation is expected to be of extra-galactic origin. Berenzinky and Zatsepin (1969 & 1971) have suggested that the cosmic ray energy spectrum $\gtrsim 10^{19}$ eV comes from neutrinos produced in the interactions of protons with the microwave photons that fill the metagalaxy.

From the discovery of the 2.7 K black body radiation in space (Penzias and Wilson (1965), Roll and Wilkinson (1967)) has arisen the problem of a conflict between the primary spectrum and the universal background (2.7 K black body radiation of universal origin). The interactions between cosmic rays and the 2.7 K radiation would produce a cut-off in the cosmic ray spectrum at about 6×10^{19} eV (Greisen,(1966) ; Zatsepin and Kuzmin (1966)). Recently, however, observations of large E.A.S. at the highest energies, notably by the Sydney array (Bell, et al, 1974) and by the Haverah Park array (Edge, et al, 1974) have shown that no cut-off exists.

Concerning the isotropy of cosmic rays, the primary radiation in total shows a high degree of isotropy right up to 10^{18} eV and indications of anisotropies are found only with showers attributed to primary gamma rays at relatively low energies.

1.3 THE COMPOSITION OF PRIMARY RADIATION

The radiation which comes across the earth from outside consists of two types, namely particles and waves. Both types have contributed enormously to the great advances made in Physics and Astronomy. Over the

past thirty years a large number of atomic nuclei and subatomic particles have been discovered and identified. The observed spectrum has been extended into the Ultraviolet, X- and γ-ray regions at the shorter wave lengths, and into the Infra-red and Radio-wave regions at the longer wave lengths. Concerning the mechanism of primary cosmic ray production and their mean lifetime, the primary mass composition offers valuable and important information in these aspects. Recently, significant knowledge of the mass composition has been obtained using nuclear emulsions, counter techniques and ionization calorimeters carried by balloons and satellites. The relative abundances of the principal elements in the primary radiations are approximately 89% protons, 10% α-particles and 1% other elements.

After helium, carbon and oxygen are the next most abundant elements, followed by N, Ne, Mg, Si, Fe, Li, and Be. A summary of the recent experimental results is given by Wolfendale (1972). Table 1.1 shows the cosmic ray composition of the more abundant elements relative to carbon as measured by different workers. Although detection of very heavy nuclei as large as Uranium has been reported (Fowler, (1975)), iron is still the most abundant of the heavier nuclei. The energy spectra are fairly well established in the energy region 50 MeV up to 10 GeV (Figure 1.2). The results for some light elements are shown in Figure 1.2. The intensity reaches a maximum at a few hundred MeV and at higher energies it falls off with a differential exponent of -2.6.

1.4 HIGH ENERGY NUCLEAR INTERACTIONS

Air shower development is mostly due to the collisions of particles with energies greater than a few hundred GeV. The nuclear cascade produced, plays an important role in understanding the characteristics of high energy interactions. The physics of nuclear interactions have been studied in accelerator experiments with equivalent laboratory energies up to

* This value applies to source spectra that follow a power law in energy per nucleon.

H	5×10^4 *	$29 \leq Z \leq 43$	$\approx 10^{-2}$
He	$(2.7 \pm 0.5) \times 10^3$		
C	100	$44 \leq Z \leq 59$	$\approx 3 \times 10^{-4}$
N	12 ± 3		
O	102 ± 6	$68 \leq Z \leq 83$	$\approx 3 \times 10^{-4}$
Ne	20 ± 3		
Mg	27 ± 4	$90 \leq Z \leq 96$	$\approx 2 \times 10^{-4}$
Si	23 ± 4		
Fe	23 ± 5		

TABLE 1.1 : Primordial composition of the more abundant cosmic rays at energies below 1 GeV per nucleon

(The data is normalized to carbon.(after Shapiro et al, 1971)

$\simeq 2 \times 10^{12}$ eV. These energies are still many orders of magnitude lower than those involved in the early interactions of particles in extensive air showers. Extrapolation of the particle accelerator data to air shower energies ($\geqslant 10^{14}$ eV) is the only possible way of establishing a model of propogation of an air shower. For a number of years, empirical models of nuclear interactions have been adopted, the most extensively used being the model proposed by Cocconi, et al (1961) ; the so called C.K.P. model. This was based upon accelerator measurements of proton-light nucleus interactions in the 10-30 GeV region. This model assumes an exponential distribution of energy for the secondary particles with some mean energy depending on the incident particle energy. One of the main features of this model is the dependence of pion multiplicity, n_s, on the primary energy, E_p, (Figure 1.6) having the form $n_s \propto E_p^{\frac{1}{4}}$. Extensive calculations have been made for a variety of E.A.S. characteristics (e.g. De Beer, et al, 1966 ; Hillas, 1970, and Dixon, 1973) showing that many E.A.S. phenomena are consistent with this model. Wdowczyk and Wolfendale (1973) have shown that the C.K.P. model is valid if the bulk of primary particles are protons up to at least 10^6 GeV. This conclusion was based upon the measurements of the Utah group (Cannon, et al, 1971) of the relative frequency of multiple muons. Also, Adcock, et al (1971) have concluded that there is evidence of a slow rise in transverse momentum with increasing primary energy which is consistent with the predictions of the C.K.P. model. New ideas have been generated by the "scaling" model of Feynman (1969) which assumes a limiting shape of the energy distribution of secondary particles which carry a particular fraction of the primary energy expressed as x, x being $\frac{E\pi}{Ep}$. A logarithmic dependence of the mean multiplicity (Figure 1.6) upon energy is predicted from this model as well as a rapid saturation of the mean transverse momentum $\langle P_t \rangle$ of these secondaries at a value of 0.4 GeV/c. The scaling model has been shown to be reasonably valid for several character-

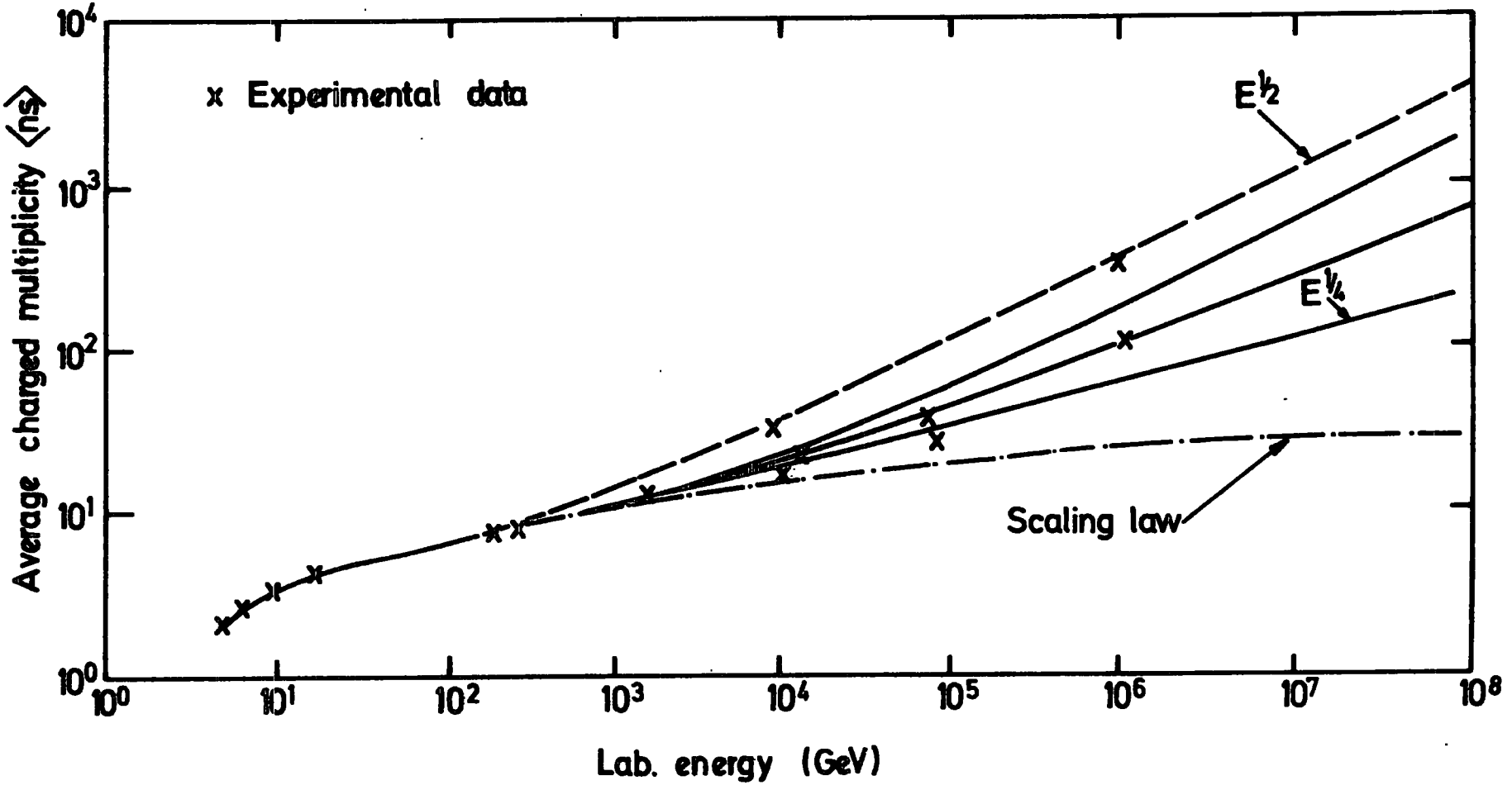

FIGURE 1.6 The average charged multiplicity for different models (After Grieder, (1977)).

istics of the proton-proton collisions at the I.S.R. energies by Jacob (1973). The question is whether or not scaling is valid at higher energies, also, if the scaling hypothesis is valid for nucleon-air nucleus collisions, as well as for nucleon-nucleon collisions. From calculations done on cosmic ray data (Wdowczyk and Wolfendale, 1972, 1973) it has been shown that the scaling model becomes less and less applicable as the energy exceeds 10^{12} eV, Also, it is suggested that scaling is valid at higher energies only if an increase in the primary mass is allowed. Very recently Wdowczyk, et al, (1976 in the press) have concluded that the scaling model should cease to be valid for proton-air nucleus interactions above about 10^{13} eV. This conclusion was obtained by examining the recent measurements of the Moscow State University group (Rozhdestvensky, et al, 1975) on the lateral distribution and energy spectrum of muons in E.A.S. in the energy range 10-100 GeV, as well as the measurements of the Utah group (Mason, et al, 1975) on the decoherence curve of muon pairs. Wdowczyk, et al, also point out that air showers require a higher multiplicity dependence than $E^{\frac{1}{4}}$ when the primaries are all assumed to be protons. Further, even if the primaries are all iron, the multiplicity should be greater than that predicted by the scaling hypothesis.

1.5 HIGH ENERGY MUONS

Experimental studies of high energy cosmic ray muons can be divided into two groups. The first is that concerned with examining the electromagnetic interactions of muons with matter. The second concerns the use of muons in order to obtain information about their parent pions and the mechanism of their production. Single unaccompanied muons that reach sea level are usually formed along with low energy "old" showers that are absorbed in the atmosphere. These muons are mainly initiated by primary particles in the energy range 10^{10} - 10^{13} eV. At higher energies muons observed at

sea level are expected to be accompanied by extensive air showers and form one of the major components of the E.A.S. Recent reviews on the electromagnetic interactions of muons, their energy spectra, charge ratio and other aspects, are given by Thompson (1973).

Studies of high energy muons in E.A.S. are of interest from the view point of the characteristics of nuclear interactions at ultra high energies, as well as the nature and mass composition of the primary cosmic radiation. High energy muons usually originate from pions produced in the early interactions of the high energy primaries. Those with energy $E_\mu \geqslant 20$ GeV lose a small fraction of their energy as they traverse the atmosphere. However, high energy muons observed in E.A.S. contain information about all the nuclear interactions which have taken place in the atmosphere in the development of the shower, and data pertaining to the muon energy spectra and lateral distribution should reveal some of the basic parameters of the nuclear interaction process. Detailed theoretical studies of muons in E.A.S. have shown that the muon lateral distribution can give information on the mean transverse momenta of the parent pions in the energy range 10^{14} - 10^{16} eV. The frequency of multiple muons and the decoherence curve of muon pairs as measured by the Utah group (Mason, 1975) could be related to the multiplicity of the pion productions and the nature of the primary spectrum. Theoretical studies on the measurements of the last two phenomena have been carried out by Goned, et al, (1975), and Mason, et al, (1975). In an attempt to derive some information on the primary spectrum from the measurements of the Utah group, it was found by Wdowczyk, et al (1976) that the resulting spectrum is sensitive to the absolute number of muons above a particular threshold energy. Information on the nature of the primary particles can be obtained from the studies of the fluctuations in measurements of muons in E.A.S. Evidence of normal mixed composition of the primary spectrum came from the work of

Khristiansen, et al (1966) and Alexander (1968). To date, the work of De Beer, et al (1966), Hillas (1966), Turver (1974),Goned (1975) and Greider (1977) has provided a satisfactory overall account of the measurements of the distributions of muons with energy and radial distance in the showers. The spatial and temporal characteristics of E.A.S. muons have been considered in detail by Dixon and Turver (1974) and Turver (1974). Such works form the basis on which experimental data are interpreted and which leads to a greater understanding of the high energy interactions, and increased knowledge of the nature of primary cosmic rays.

CHAPTER 2

EXTENSIVE AIR SHOWERS

2.1 INTRODUCTION

Extensive air showers (E.A.S.) can be considered as the result of a complicated chain of strong nuclear interactions initiated by primary cosmic ray particles which, on entering the earth's atmosphere interact with air nuclei. Many secondary particles are produced due to a series of collisions of a primary particle with an air nucleus, which move through the atmosphere in almost the same direction as the primary particles and give rise to a cascade of particles through the atmosphere. Consequently, the total number of particles in the shower can be very large and the particles are scattered over a very large area at sea level. The principal features in the development of an air shower are shown in Fig. 2.1. The particles in a shower are distributed symmetrically around the shower axis due to the following processes that take place during their traversal of the atmosphere :-

1. The finite transverse momentum of the secondary particles of the interactions.
2. The multiple scattering of charged particles in the atmosphere.
3. The angular divergence of muons and other particles produced in the decay process.
4. The deflection of charged particles due to their movement in the earth's magnetic field.

The nature of the E.A.S. depends upon the nuclear interaction characteristics such as the multiplicity of secondaries and the inelasticity of the collisions. Also the size of the E.A.S. produced (the total number of particles in the shower) depends on the level of the first interaction and the level of the observation. The lateral extension of showers ensures the

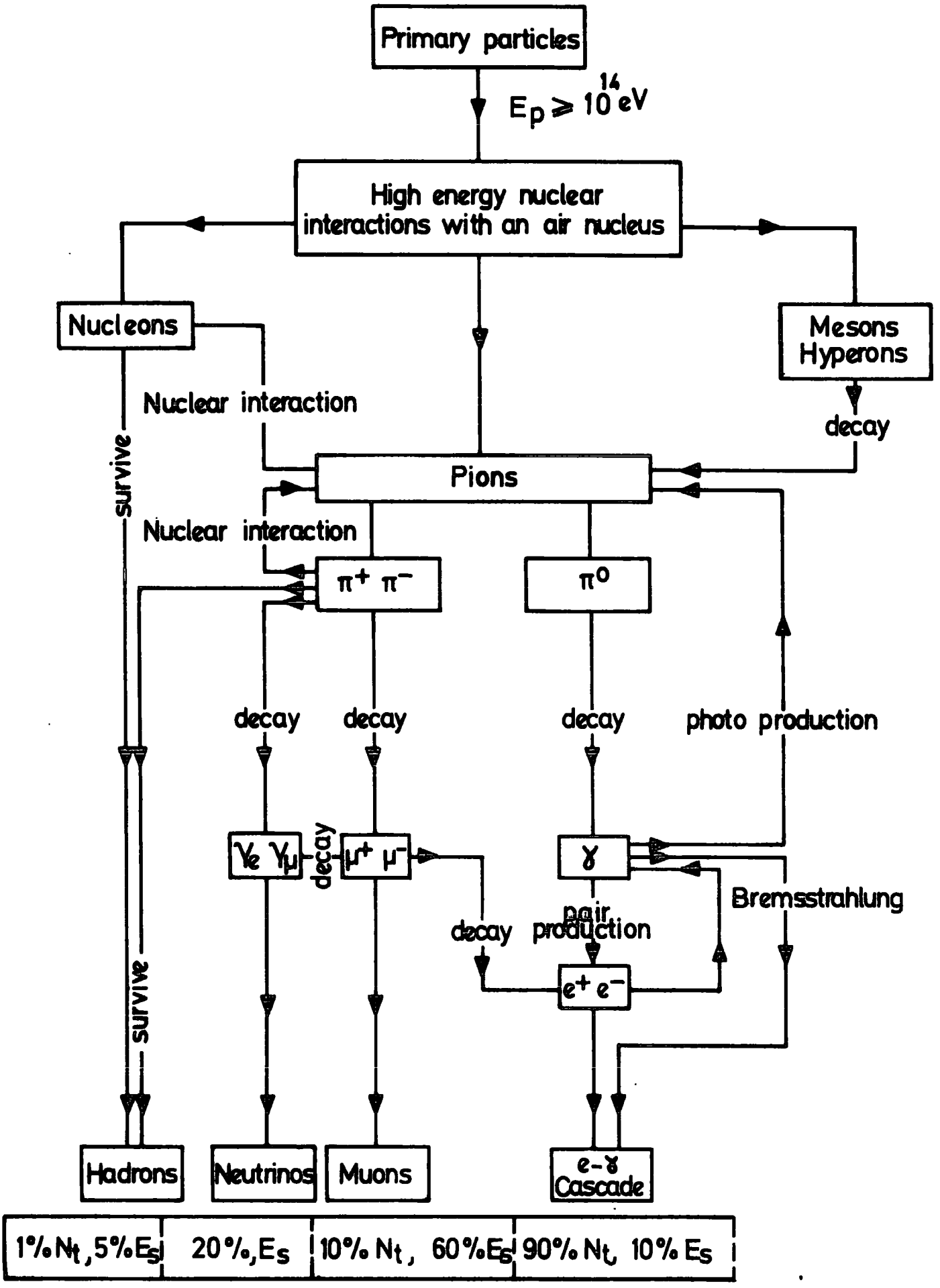

FIGURE 2.1 The development of an E.A.S. arriving at sea level, N_t is the number of particles in the shower at sea level and E_s is the total energy of the shower at the same level.

detection near sea level of showers initiated by primaries on the top of the atmosphere over quite a large area. The observations of E.A.S. provide a unique method of detecting ultra high energy particles ($\gtrsim 10^{14}$ eV). By studying various parameters of the different components of E.A.S. and the relationship between them, the primary spectrum, mass composition and the characteristics of high energy nuclear interactions can be deduced. The three major components of an E.A.S. are discussed in the following sections.

2.2 THE ELECTRON-PHOTON CASCADE

2.2.1 Introduction

The γ-rays that are produced by the decay of neutral pions produced in nucleon-nucleus interactions initiate the electron-photon cascade. This component has been investigated very well since it constitutes the largest fraction of charged particles in the shower. The ionization losses of the electrons in their passage through the atmosphere is the main process by which the shower particles lose energy and eventually the particles are absorbed. Coulomb scattering is the major process that influences the lateral spread of the electrons and photons in the shower. Although this component represents only $\sim$ 10% of the shower energy at sea level it is still an important measure of the stage of development of the shower. As the shower propagates through the atmosphere the number of shower particles reaches a maximum and subsequently decreases with increasing atmospheric depth.

The development of an air shower can be understood by studying the shower cascade curve which shows the dependence of shower size on the depth in the atmosphere for a fixed primary energy. The cascade curve is experimentally investigated by plotting the shower size as a function of depth for equal shower intensity. Figure 2.2 shows the experimental results obtained for many showers recorded by different experiments at various

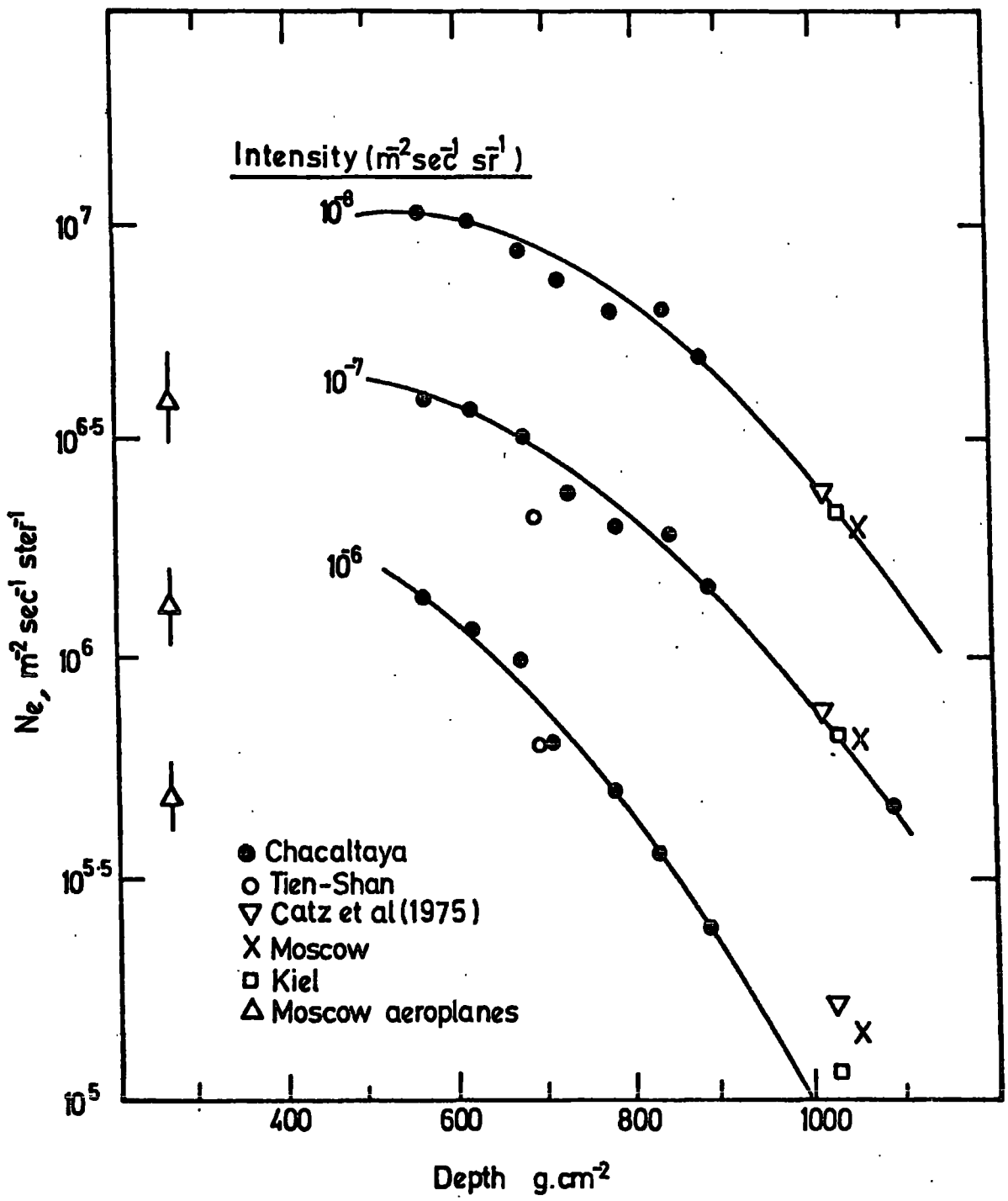

FIGURE 2.2 The longitudinal development of air showers, the experimental data shown are derived from equi-intensity cuts of size spectra (After Catz et al, 1975).

observational levels.

Information on the character of nuclear interactions at high energies ($\gtrsim 10^{14}$ eV) can be obtained from the measurements of the energy spectrum of the electron-photon component at mountain altitudes. Gaisser (1974) has studied the longitudinal development curves using the Chacaltaya results of Bradt, et al (1965) and La Pointe, et al (1968), and has found that they are consistent with iron primaries when the scaling hypothesis is modified to allow for an increase in the production cross section with energy and some allowance for the intranuclear cascading is introduced. Khristiansen (1975) has pointed out that the experimental data obtained in studying the energy spectrum of this component at mountain altitudes are inconsistent with the extrapolations of the scaling hypothesis to the high energy regions (10^{14} - 10^{17} eV).

2.2.2 The Lateral Electron Density Distribution Function

Studies of the lateral distribution of all charged particles in a shower at sea level and mountain altitudes have produced a great deal of information on the development of air showers as well as determining the total number of particles in a shower at the level of observation. The lateral distribution of all charged particles in a shower plays an important role in the theoretical analysis of the observed experimental data. Nishimura and Kamata (1952, 1958) have derived the lateral structure function of E.A.S. particles. Their derivation was based on a purely electromagnetic cascade shower theory taking into account the multiple scattering of electrons. Greisen (1956) produced a simplified formula representing the lateral distribution of all charged particles in E.A.S. at sea level (known as the N.K.G. formula, i.e. Nishimura, Kamata, Greisen) which is given as :-

$$f\left\{\frac{r}{r_1}\right\} = C(S)\left\{\frac{r}{r_1}\right\}^{s-2}\left\{1 + \frac{r}{r_1}\right\}^{s-4.5} \qquad (2.1)$$

where s is the shower age parameter and is a measure of the stage of development of the shower, r is the distance to the shower axis, r_1 is the Moliere Unit having a value of 79 meters at sea level and C(S) is a normalisation factor related to the cascade age parameter as follows :-

$$C(S) = 0.443\ s^2(1.9 - s) \tag{2.2}$$

The shower electron density $\rho_e(N_e,r)$, assuming that the lateral structure function is independent of shower size N_e, is given by :-

$$\rho_e\ (N_e,\ r) = f\left\{\frac{r}{r_1}\right\}\frac{Ne}{r_1^2} \tag{2.3}$$

An empirical formula representing the lateral electron shower density has been suggested by Greisen (1960) which is based on experimental measurements done over a wide range of shower sizes (10^3 - 10^9) at core distances ranging from 5 cm to 500 m and at various atmospheric depths of observation varying from 537 gm cm^{-2} to 1800 gm cm^{-2} (zenith angles as large as 55^o). This formula is given as :-

$$\rho(N_e,r) = \frac{0.4\ Ne}{r_1^2}\left\{\frac{r_1}{r}\right\}^{0.75}\left\{\frac{r}{r + r_1}\right\}^{3.25}\left\{1 + \frac{r}{11.4\ r_1}\right\} \tag{2.4}$$

at s = 1.25. Measurements of the lateral structure function have been carried out by many workers using different measuring techniques and it has been found that the shape of the structure function is dependent slightly upon the type of the detectors employed. The measurements done with Geiger tubes give a good representation of the actual density distribution of the shower particles, while measurements with scintillation counters give slightly steeper distributions. This is attributed to the sensitivity of the scintillator to the photon component of the shower. Figure 2.3 illustrates

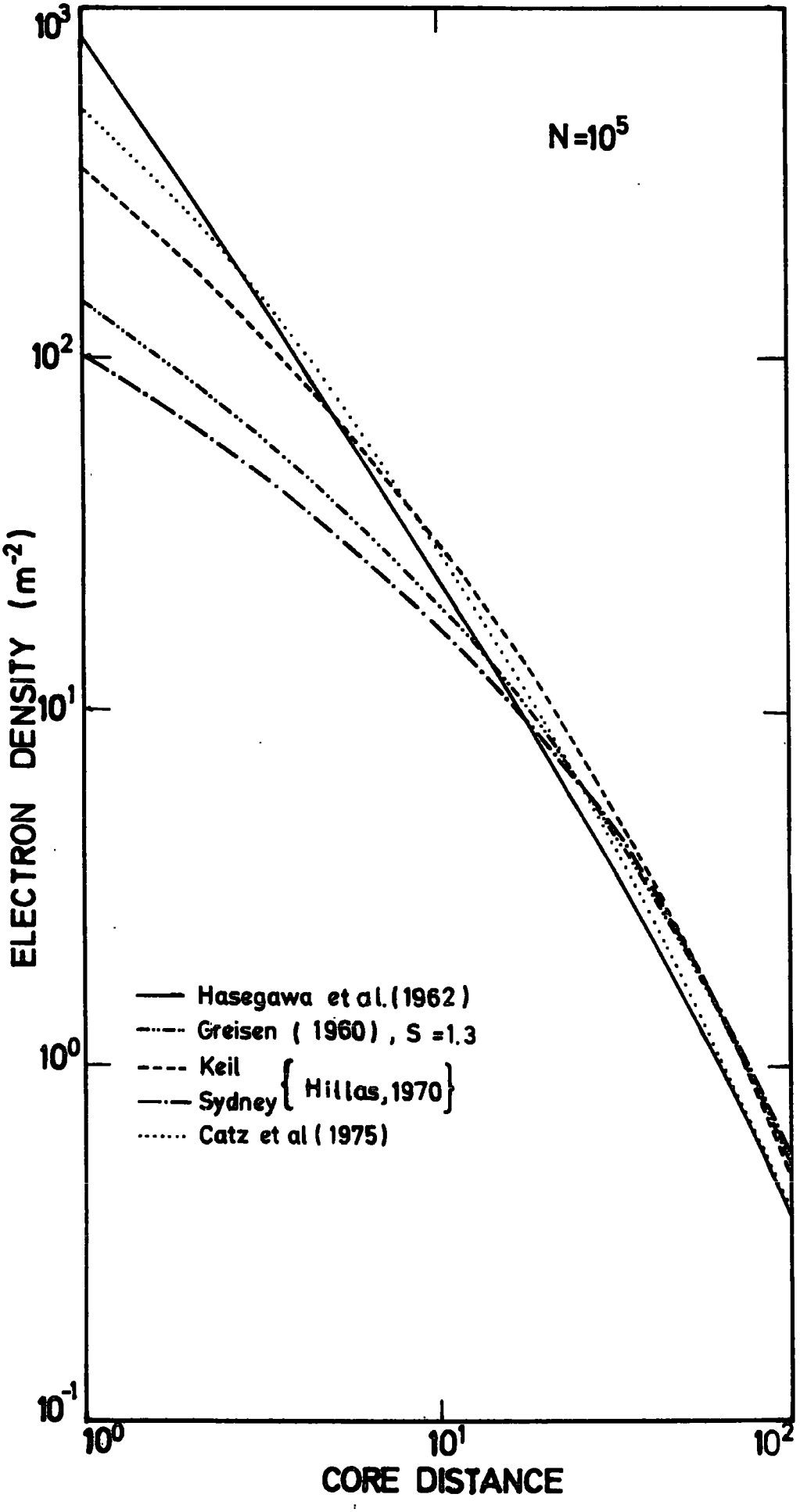

FIGURE 2.3 Measurements of the electrons lateral distribution obtained by different authors at sea level and normalised to a common shower size of 10^5 particles.

this fact, and shows a comparison of various electron lateral distributions (normalised to a common shower size of 10^5 particles) measured by different groups. The measurements of Hasegawa, et al (1962), who used an array of scintillation counters, show a steeper density distribution than that of Greisen (1960), for an age parameter of 1.25. Hasegawa et al found that their data could be represented by the following expression :-

$$\rho(N_e, r) = \frac{Ne}{2\pi\sqrt{120\ \pi}} \quad \frac{\exp(-r/120)}{r^{1.15}} \tag{2.5}$$

Detailed analysis of the experiment of Catz, et al (1975) has shown that the lateral distribution of particle densities recorded by scintillation counters can be described by the following relation :-

$$\rho(N, r) = \frac{1.57 \times 10^{-2} \times N_e}{(1 + r)^{1.62}} \exp(-r/120) \tag{2.6}$$

where r is the distance from the shower axis, and varies from about 2 meters to at least 70 meters. The lateral distribution of electrons in E.A.S. obtained by Catz, et al (see Figure 2.3) seems to agree well with the NKG relation for an age parameter of 1.25; it is also clear from the figure that this distribution is steeper than that suggested by Greisen (1960) in the region below 20 meters from the shower core. The distribution of particle densities observed by the Sydney group (Hillas, 1970) for large air showers gives a much flatter distribution. The flattening of the distribution can possibly be attributed to the detection of multi-cored showers induced by primaries of energies greater than 10^{15} eV. Nevertheless, it can be concluded from Figure 2.3 that there is a general agreement between the above mentioned distributions in the region 20 - 100 meters from the shower axis,

whilst there is some discrepancy between the measurements at distances near to the shower axis and at large distances ($\gtrsim$ 100 meters). This discrepancy could be due partly to inaccurate shower core determination and partly to the effect of the dependence of the measured lateral distributions on the type of particle detector in the apparatus.

2.2.3 The Shower Age Parameter

The behaviour of the electron-photon cascade is well described in terms of the cascade shower theory (Nishimura and Kamata, 1958). According to this theory, the stage of shower development is characterised by an age parameter (s) which is defined approximately as :-

$$s = 3t/(t + 2y_o + x) \qquad (2.7)$$

where $y_o = \ln(w_o/E_o)$, w_o being the energy of the photon that initiated the shower cascade and E_o is the electron critical energy in air, 84 MeV. Further, $x = \ln(r/r_1)$, r and r_1 are defined as in equation 2.1 and t is the atmospheric depth (gm cm^{-2}). If the age parameter is less than one, then the shower is in the early stages of development and is called a "young" shower, at maximum development the age parameter is assigned a value of unity while for age parameters larger than one, the shower has passed its maximum development and is decreasing in size, it is now defined as an old shower.

Equation 2.7 shows the dependence of the age parameter on radial distance. In practice, this dependence is rather weak for $-1<x<1$ because of the very large values of $t + 2y_o$. Only at very small distances ($\lesssim$20 meters) from the shower axis does the dependence become more important (see Figure 2.4). Moving far from the shower core ($r \gtrsim 100$ m) the energy of electrons becomes less than the critical energy E_o and hence they cannot travel far.

Figure 2.4 shows the effect of the age parameter on the lateral electron density distributions obtained using the N.K.G. distribution function. From

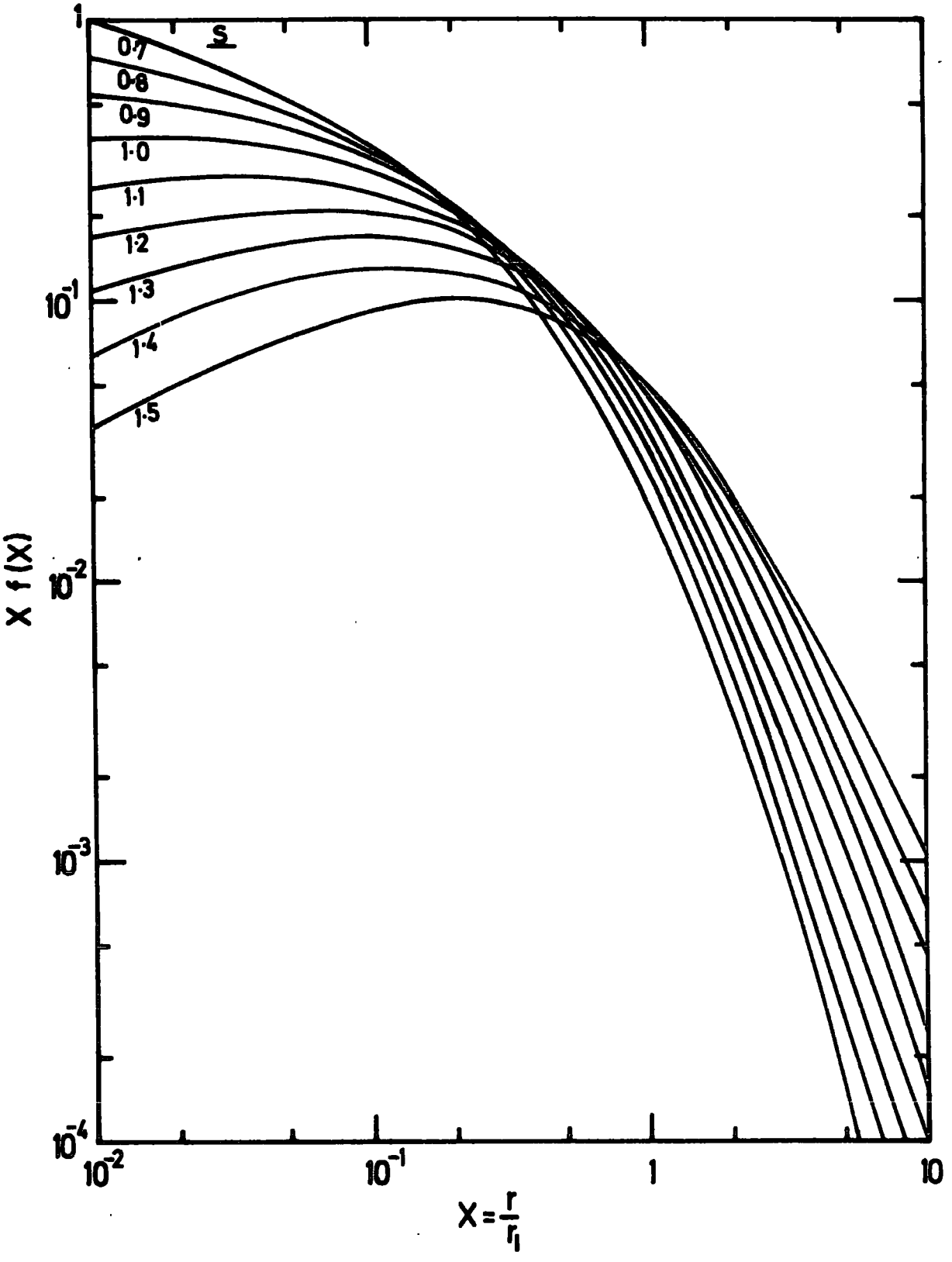

FIGURE 2.4 The dependence of the electron structure function on the age parameter for a fixed shower size, the curves are obtained by using the N.K.G. structure function.

the experimental observations on E.A.S. at sea level, Vernov et al (1970) have suggested a dependence between the average age parameter and shower size ; as the shower size increases the average age parameter increases. The mountain altitude observations of Miyake et al (1973) support this increase. These results are interesting since most of the measurements on the lateral electron density distribution indicate that this function is independent of shower size.

Figure 2.5 shows the shower age parameter for various shower sizes as predicted by Karakula, (1968) on the basis of the standard model of De Beer, et al (1966). It can be seen that although there is no significant variation in age parameters with shower size, the variation is still larger than that observed by Vernov et al. Monte Carlo simulations of air showers by Dixon and Turver (1974) show that the age parameter decreases with increasing shower size.

The increase in age parameters observed in the experiment of Vernov et al can be explained by the employment of a flatter lateral distribution than that given by the N.K.G . function, and also by the fact that the lateral distribution corresponding to the N.K.G. relation for a fixed age parameter tends to under-estimate the total number of particles at both large and small distances from the shower axis.

2.2.4 The Shower Size Spectrum :

Derivation and Spectral Measurements

The shower size spectrum is the frequency of occurrence of showers with a particular number of particles. To determine the spectrum, a knowledge of location of the shower axes of the individual showers is necessary and the lateral distribution function has to be fitted to the measured particle densities at the observation distances from the shower axis. The fit is usually made several meters away from the shower axis, and therefore extrapolation of the lateral structure function into the central core region is necessary. The

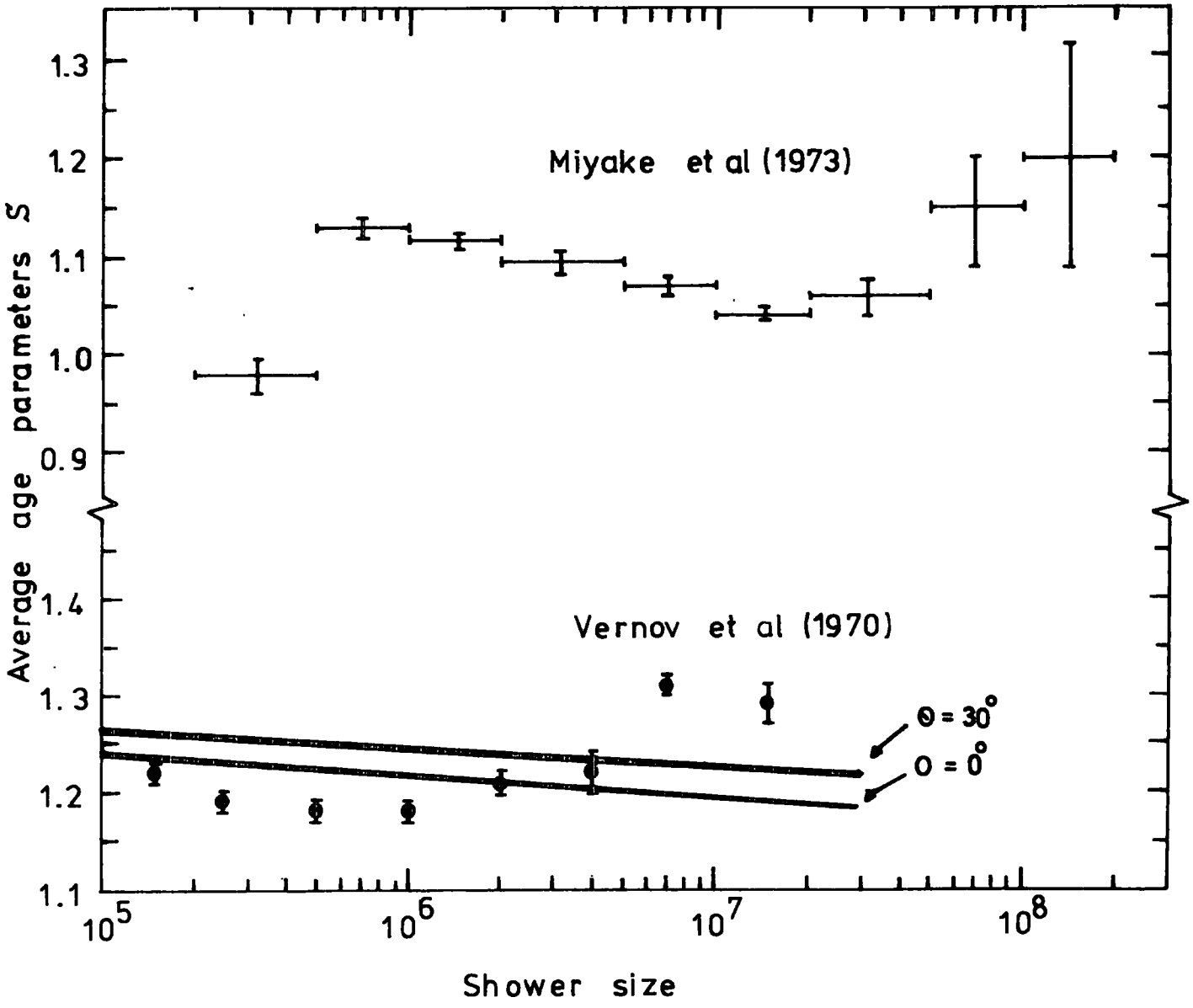

FIGURE 2.5 The dependence of age parameter on shower size. The experimental data are from Vernov et al (1970) and Miyake et al (1973).

shower size N is obtained by integrating the lateral distribution function over all values of r as follows :-

$$N = \int_0^\infty 2\pi r \; f(r) \; dr \qquad (2.8)$$

The determination of the shower size (N) is very dependent on the lateral structure function employed, and on shower core location. The shower size can be overestimated by assuming too steep lateral distribution function. There are many reasons why the spectral intensities determined by different experiments differ significantly from each other. These reasons are mainly technical due for example to the use of different types of detectors, a scintillation detectors, Geiger Müller counters or Cerenkov detectors, which all have different threshold energies, and to acceptance biases due to the various experimental arrays having different geometries. As a consequence it is not easy to compare the intensity at a particular shower size measured by one experiment with the intensity obtained at the same size in a second experiment. Therefore, in order to compare the results of different experiments it is often necessary to resort to a normalisation proceedure.

Figure 2.6 and Figure 2.7 show an accurate estimation of the integral size spectrum at sea level and mountain altitudes respectively (Summary of Bell, 1974), after being corrected for a variety of biases. The solid line represents the best fit to the summarised data in both figures. Examination of the sea level size spectrum and the spectrum at mountain altitudes indicates the following features :-

1. There is a transition from a region of practically constant exponent to another of greater exponent. The transition is rather short and exhibits a sharp change of slope at the position of the "knee".
2. The position of the "knee" appears to be at $N \approx 7 \times 10^5$ particles at sea level, and $N \simeq 1.5 \times 10^6$ at mountain altitudes.

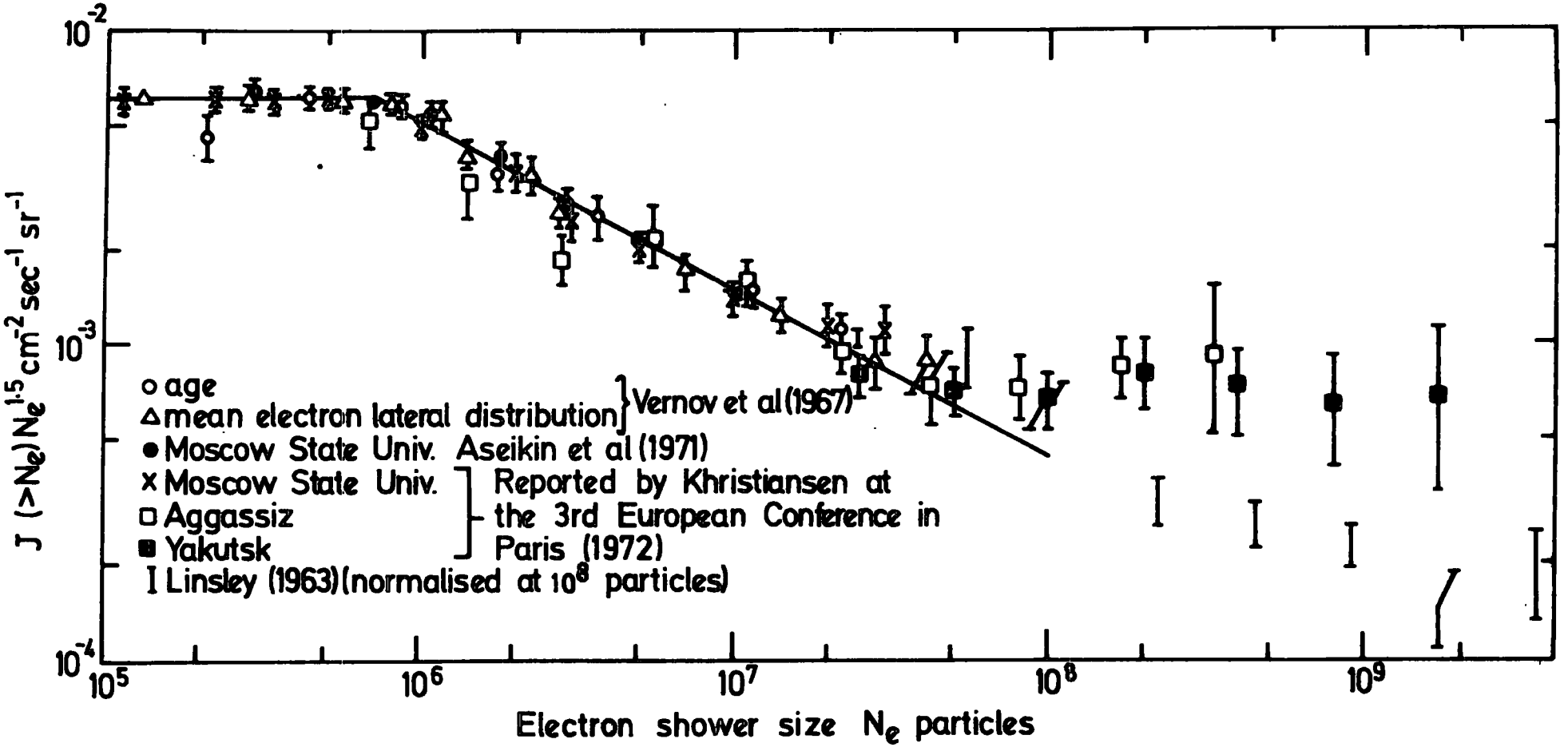

FIGURE 2.6 The integral shower size spectrum of E.A.S. at sea level, the solid line represents the least squares fit to the data beyond 10^6 particles (excluding Linsley and Paris data), after Bell M, 1974.)

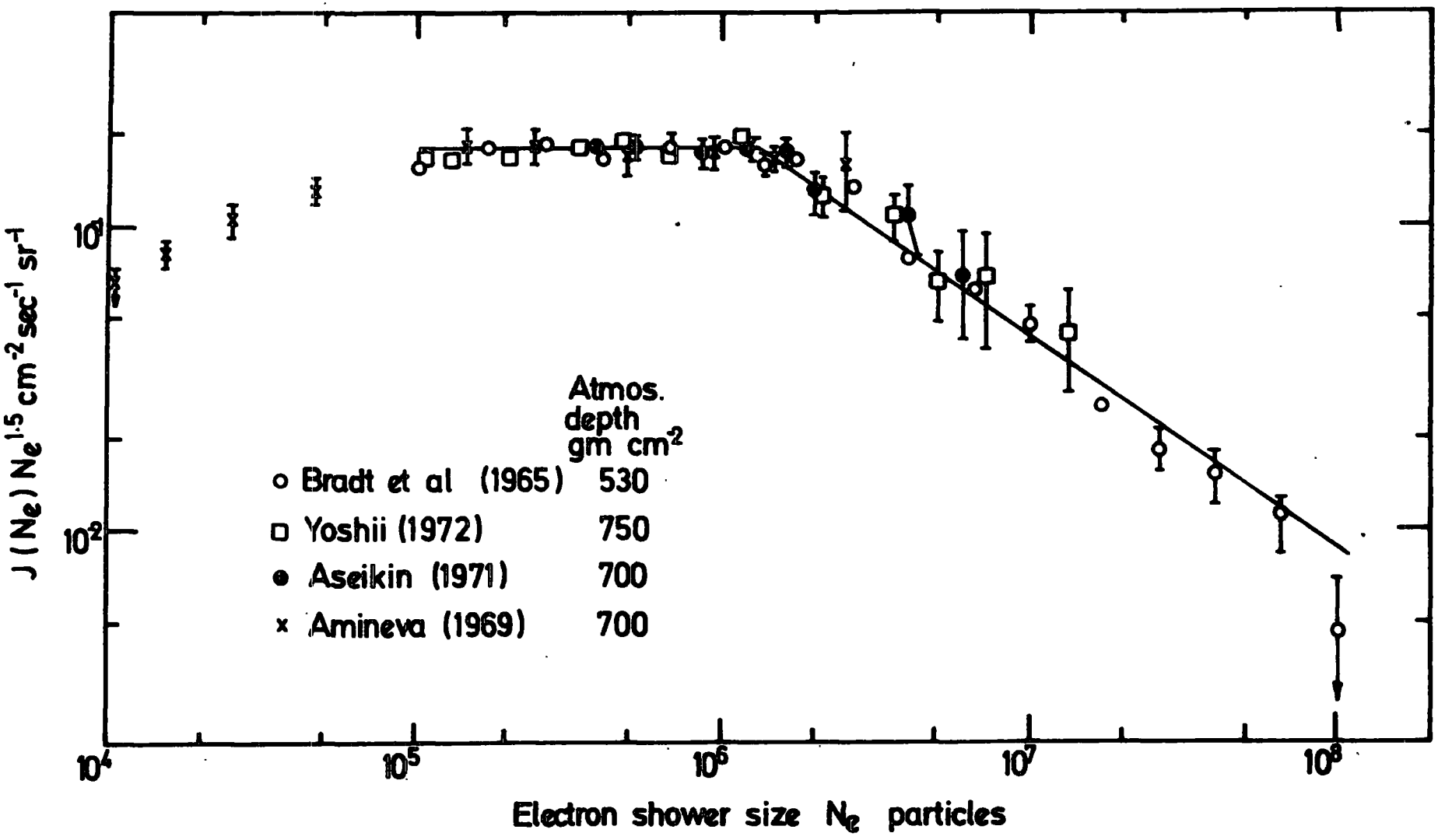

FIGURE 2.7 Integral size spectrum of E.A.S. measured at mountain altitudes, the solid line represents the least squares fit to the data (after Bell, 1974).

3. The absolute intensity of showers observed at mountain altitudes in the region below the "knee" is higher than that measured at sea level by a factor of 20.

It is not necessary for all showers plotted in the two figures to be at their maximum development since the determination of shower size depends upon the adopted experimental technique and on the method of analysis. This could be one reason for the change in the position of the "knee". An alternative reason is that showers due to primary particles of different energies reach their maximum of development at different depths in the atmosphere.

2.3 THE MUON COMPONENT

2.3.1 Introduction

The muon component of E.A.S. is formed mainly from the decay of charged pions and kaons. The decay of pions and kaons depends upon their energy and the atmospheric density in which they find themselves. The relative probability of their decay will be greatest in low atmospheric densities, thus, muons mainly originate very early in the nuclear cascade. The most energetic muons are produced near the first interaction of the incoming primary particle. By studying this muon component, information can be deduced about the primary particles, the production spectra of the parent pions and kaons, and the characteristics of nuclear interactions. Most of the muons survive to ground level due to their low probability of decay or interaction in the atmosphere.

Muons undergo some Coulomb scattering and geomagnetic deflection in traversing the atmosphere from their point of generation to the observation level, but the muons, particularly those of high energy, retain a considerable imprint of their level of production.

The number of muons in a shower is dependent mainly on the energy of

the primary particle. The ratio of the number of muons to electrons in a shower is dependent on the atomic number of the primary particles. As a consequence this ratio can give a measure of the chemical composition of the primary particles at high energies.

Muons form only a few percent of particles in the shower, though they carry much of the shower energy. At distances of a few hundred meters from the shower core they are relatively frequent. Showers containing only a very few percent of muons may be initiated by primary γ-rays, which in turn, may show anisotropies in their arrival directions since they will be unaffected by the galactic magnetic fields.

Theoretical and experimental studies of the muon component of E.A.S. have been made in recent years in order to obtain information on the shower characteristics, the nature of the primary particles and nuclear interactions. The theoretical predictions of De Beer, et al (1966), Hillas (1966) and Dixon and Turver (1974) and others have considered many aspects of the muon component of E.A.S.

The experimental measurements concerning muons are in broad agreement, but comparison of the measurements with theoretical predictions shows some discrepancies. At the present time more experimental observations of muons in showers are required. Most measurements of the lateral distribution and energy spectrum of E.A.S. muons have been made over restricted core distances and muon energy range. It is important to obtain information on E.A.S. muons over a wide energy range, particularly on muons of highest energy, for different shower parameters. The high momentum resolution magnetic spectrograph (M.A.R.S.) at Durham University is capable of making such measurements in conjunction with the Durham small air shower array. The apparatus is capable of making measurements of the muon energy spectrum in the energy range 7 - 2000 GeV at core distances ranging from 5 - 50 m measured with showers in the range $2 \times 10^4 - 2 \times 10^6$ particles.

2.3.2 The Lateral Distribution of Muons in the E.A.S.

The lateral distribution of muons at various distances from the shower core is mainly caused by the transverse momenta of the parent pions, thus, E.A.S. studies of the lateral distribution of the muon component will, in principle, give information about the transverse momenta of the parent particles.

The experimental results of the Cornell group (Clark, et al,(1958)) on the lateral distribution of muons of energy in excess of 1 GeV in showers whose size is in the range 2×10^5 - 2×10^8 particles form the basis for the empirical lateral distribution function proposed by Greisen (1960) :-

$$\rho_\mu\ (Ne,r) \;=\; 18 \left(\frac{Ne}{10^6} \right)^{0.75} r^{-0.75} \left(1 + \frac{r}{320} \right)^{-2.5} \qquad (2.9)$$

where $\rho_\mu(Ne,r)$ represents the muon density in m^{-2} measured at a distance r(m.) from the axis of a shower of size Ne.

Some measurements have been made of the muon lateral density distribution for various energy thresholds, and Bennett and Greisen (1961) propose the empirical formula :-

$$\rho_\mu\ (Ne,r,\geq E_\mu) = 14.4\ \frac{r^{-0.75}}{\left(1 + \frac{r}{320} \right)^{2.5}} \left(\frac{Ne}{10^6} \right)^{0.75} \left(\frac{51}{E_\mu + 51} \right) \left(\frac{3}{E_\mu + 2} \right)^{0.14r^{0.37}} \qquad (2.10)$$

where r is expressed in meters and E_μ in GeV. This formula is valid for muons with energies 1 - 10 GeV. Up to date most of the results on the muon lateral distribution in this energy range have shown no serious deviation from the above formula especially in the region greater than 20 meters from the shower axis. Predictions of the formula for muons with energies $E_\mu \geq 10$ GeV are shown in Figure 2.8 along with the results of various experiments. The

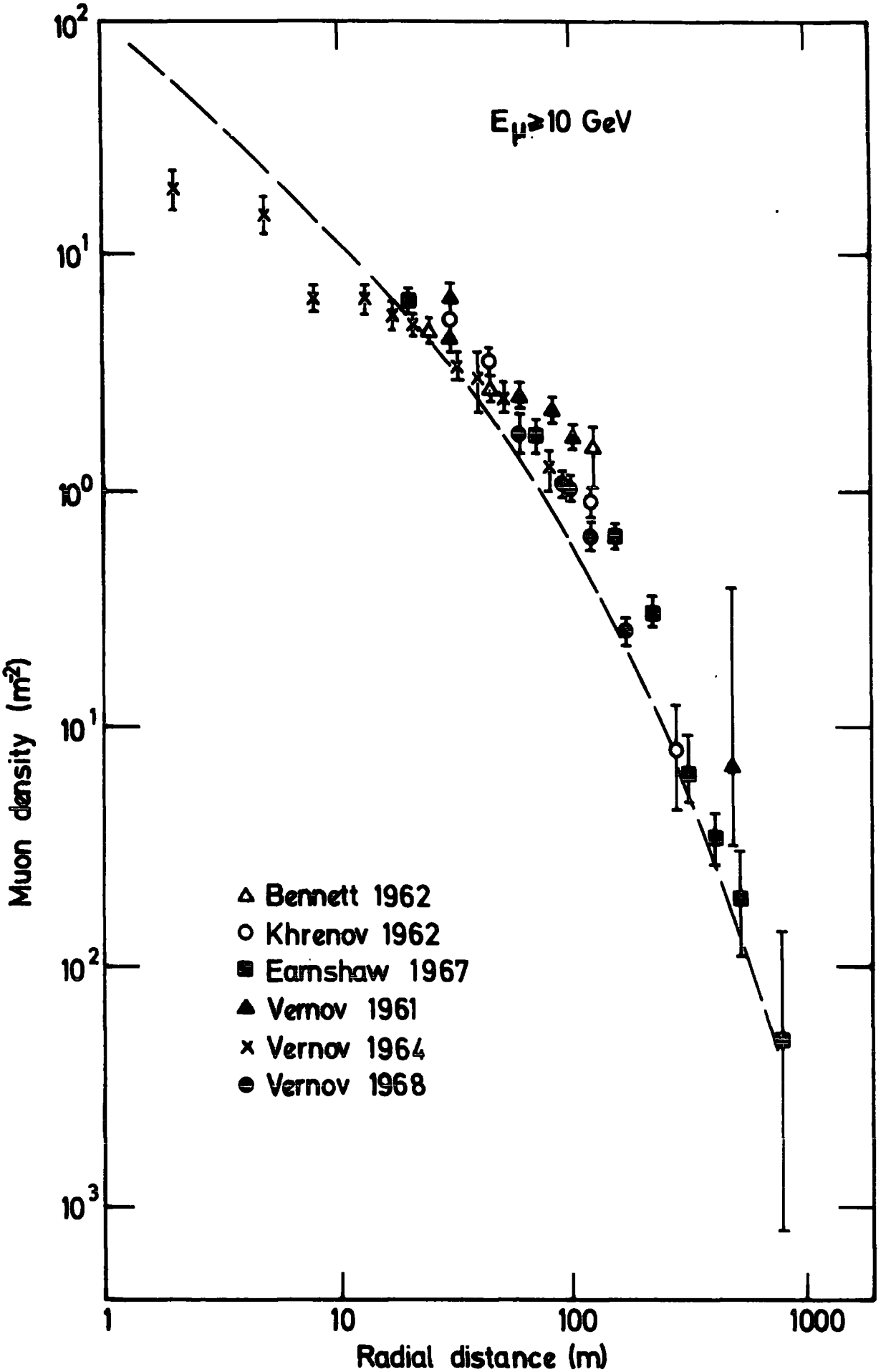

Figure 2·8· The muon lateral distribution for a 10 GeV energy threshold. Data are normalised to 2.10^7. (After Wdowczyk, 1973).

experimental data shows that the muon lateral distribution seems to be slightly flatter for the lesser radial distances ($\lesssim$ 20 meters). This may be attributable to uncertainties in the determination of the location of the shower core.

Measurements of the lateral distribution of muons at large and small distances from the shower core have been obtained by the Haverah Park group (Earnshaw,et al,1967) and recently by Moscow State University (Rozhdestvensky, et al, 1975) using a magnetic spectrograph at sea level for threshold energies 10 - 100 GeV. In the early work of Earnshaw, et al, (1967) the muon lateral distribution was obtained for threshold energy $E_\mu \gtrsim 1$ GeV by using the Haverah Park magnetic muon spectrograph as a range spectrograph. Their distribution fits well with the predictions of the model calculations of Hillas (1966) and De Beer, et al, (1966) except for core distances less than 100 meters and greater than about 700 meters. The discrepancy in the Haverah Park data at small distances is attributed by De Beer, et al, to the C.K.P. (Cocconi, Koester and Perkins (1961))relation, predicting too many secondaries with small transverse momenta. At higher energies (50 - 100 GeV), Machin,et al,, (1969) have reported too many high energy muons at large distances from the shower core. In this energy range the muon lateral distributions are not well fitted by models of either De Beer, et al, or Hillas. De Beer, et al, (1968) have explained the discrepancy as being due either to experimental bias or to the existence of secondaries possessing a very large mean transverse momentum. Orford and Turver (1969) have found that their results agreed well with a mean value of 0.4 - 0.6 GeV/c for the transverse momentum of the secondary pions of the nuclear interaction. The other important measurement of the muon lateral distribution is that of the Moscow State University group. Their distributions for threshold energies 10 - 90 GeV are shown in Figure 2.9 for radial distances less than 100 meters from the shower core. Comparison of the experimental distribution with the theoretically predicted distribution

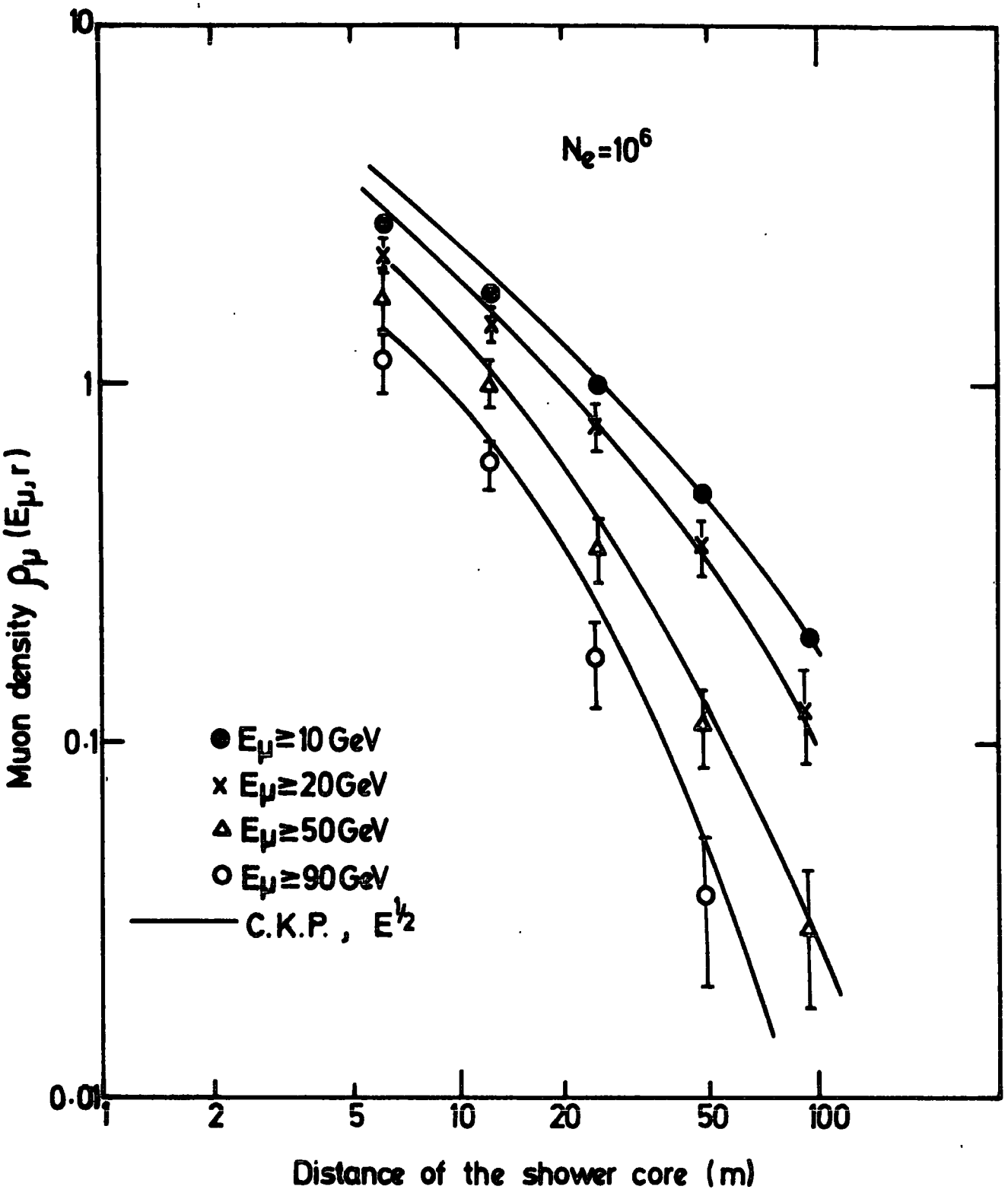

FIGURE 2.9 The muon lateral density distribution measured by the Moscow State University group. (After Rozhdesivensky et al, 1975).

based on the standard model (C.K.P. with n α $E^{-\frac{1}{4}}$) shows that the measured distribution is wider than the predicted distributions. This is illustrated in Figure 2.10 in which the muon lateral distribution for $E_\mu \geq 50$ GeV is plotted as $\rho_\mu \times r_\mu^2$ versus r_μ, and it is seen that in order to obtain an agreement the predicted curves must be widened by a factor of 1.6 (Wdowczyk, 1975). The widening of the distributions could be explained as either being due to a higher transverse momemtum or due to a higher level of muon origin. An alternative possibility is to assume an increase of the rate of degradation of the energy of the particles in the shower at the initial stage of the shower development (e.g. a transfer from an $E^{-\frac{1}{4}}$ multiplicity to an $E^{-\frac{1}{2}}$ law).

2.3.3 The Energy Spectrum of Muons in E.A.S.

The energy spectrum of muons in E.A.S. depends upon the distance from the shower core at which the muons are observed. The spectrum becomes steeper as the distance from the shower axis increases. The energy spectrum of high energy muons which originate in the early interactions of the shower may be expected to be sensitive to characteristics of the nuclear process such as inelasticity, transverse momentum and the mass composition of the primary particles.

The most comprehensive measurements of the muon energy spectra in E.A.S. is that of Bennett and Greisen (1961) which is based on the measurements of the 1 GeV muon lateral distribution obtained at Cornell University, as well as by Clark, et al (1958) and the measurements of the integral spectra of muons in the range 1 - 20 GeV using an air gap magnetic spectrograph. Bennett, et al, (1962) have found the integral energy spectrum of muons in E.A.S. can be well represented by the equation :-

$$N_\mu (\geq E_\mu) = 1.3 \times 10^5 \left(\frac{Ne}{10^6} \right)^{0.75} \left(\frac{2}{E_\mu + 2} \right)^{1.29} \qquad (2.11)$$

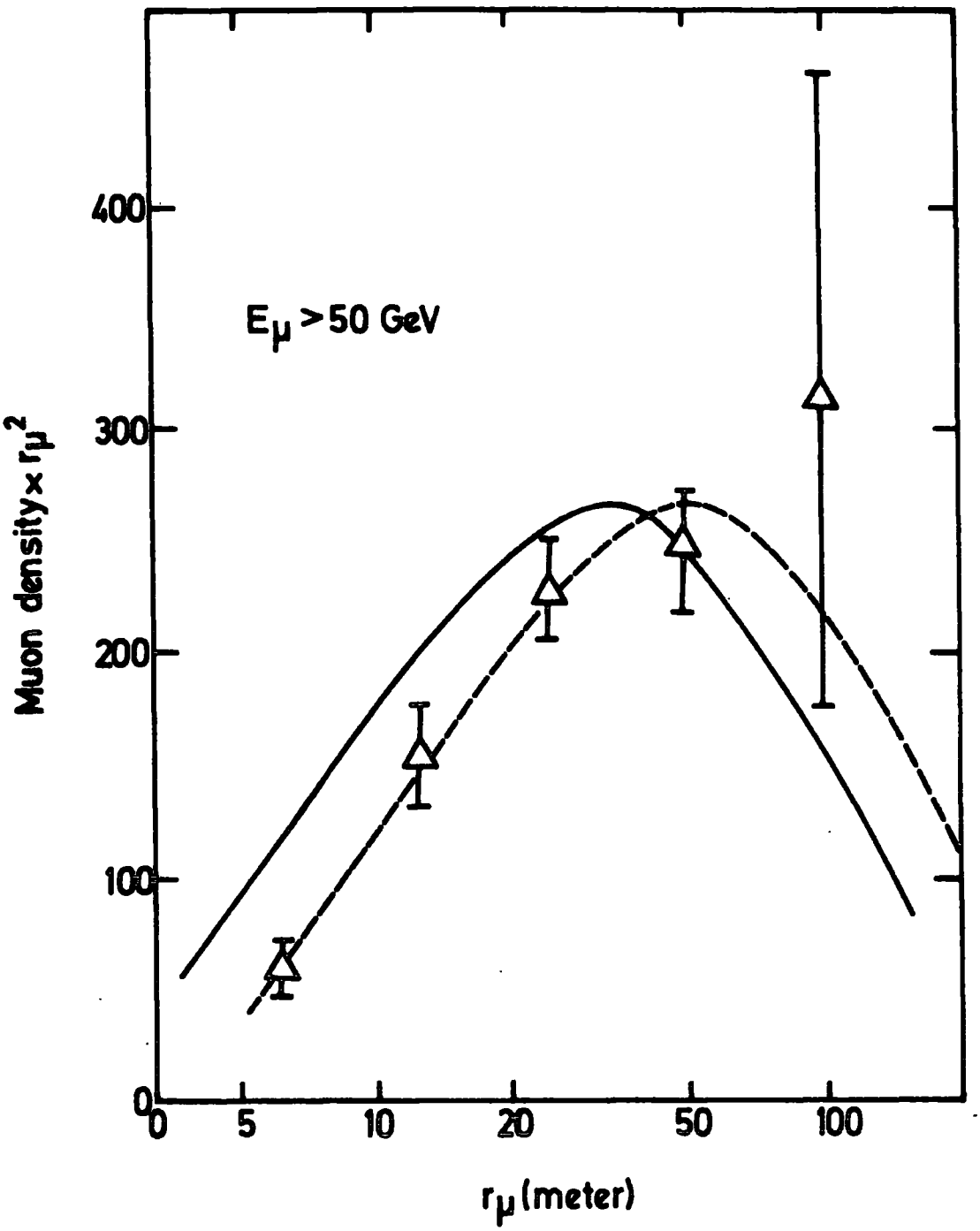

FIGURE 2.10 The lateral density distribution of high energy muons in E.A.S. (After Wdowczyk, 1975). The dotted line refers to the C.K.P. predicted distribution displaced to the right by 1.6.

where E_μ represents the threshold energy of the muon in GeV in a shower of N_e charged particles. Orford (1968) has made a comprehensive survey of the early work concerning the muon energy spectra and the muon lateral distribution carried out by various workers.

A magnetic spectrograph in association with the Haverah Park E.A.S. array has been used to measure the energy spectrum of muons with energies in the range 10 - 100 GeV falling at distances 50 - 800 meters from cores of showers covering the size range 10^5 - 10^8 particles. The results of the Haverah Park group (Earnshaw, et al, (1967))are in good agreement with those of Bennett and Greisen (1961). Generally, a fair agreement has been found with other experiments which use different techniques, with the exception of the work of De Beer, et al (1962) which shows a steeper spectrum at large distances from the shower core (100 - 500 meters).

Theoretical air shower simulations of the energy spectra of muons in E.A.S. have shown that the number of muons of energies greater than a certain energy threshold is sensitive to the primary energy. Figure 2.11 illustrates very clearly the dependence of the number of muons, $N_\mu(\geq E_\mu)$, on the primary energy in showers initiated by protons in the energy range 10^{14} - 10^{18} eV. The experimental data superimposed on the figure are those taken from the summary of Gaisser and Maurer (1972). Very recently the muon energy spectrum in E.A.S. has been measured using muon spectrographs in Moscow State University (Rozhdestvensky, et al, 1975), and in Kiel (Burger, et al, 1975). Comparison of the results of the Kiel group with the results of the Moscow State University group (see Figure 2.12) shows that the data obtained from the latter seem to give a flatter spectrum, but the difference still may not be significant.

2.3.4 The Heights of Origin of Muons

One of the important shower parameters that is the subject of investigation is the height of origin of the muons present in the air showers.

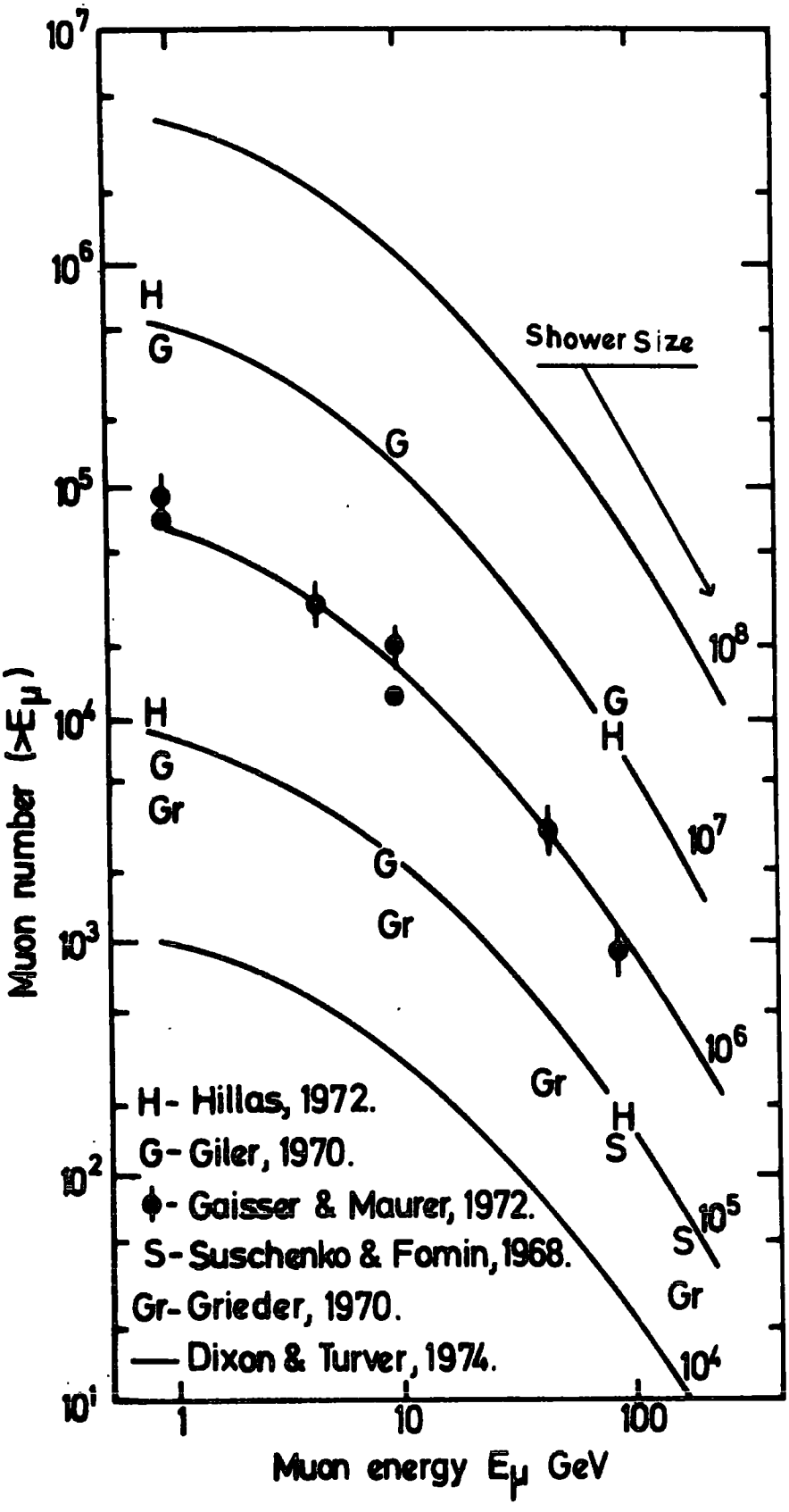

FIGURE 2.11 The energy spectra of muons in showers in the size range 10^4 - 10^8 particles obtained by various workers. (After Turver, 1974).

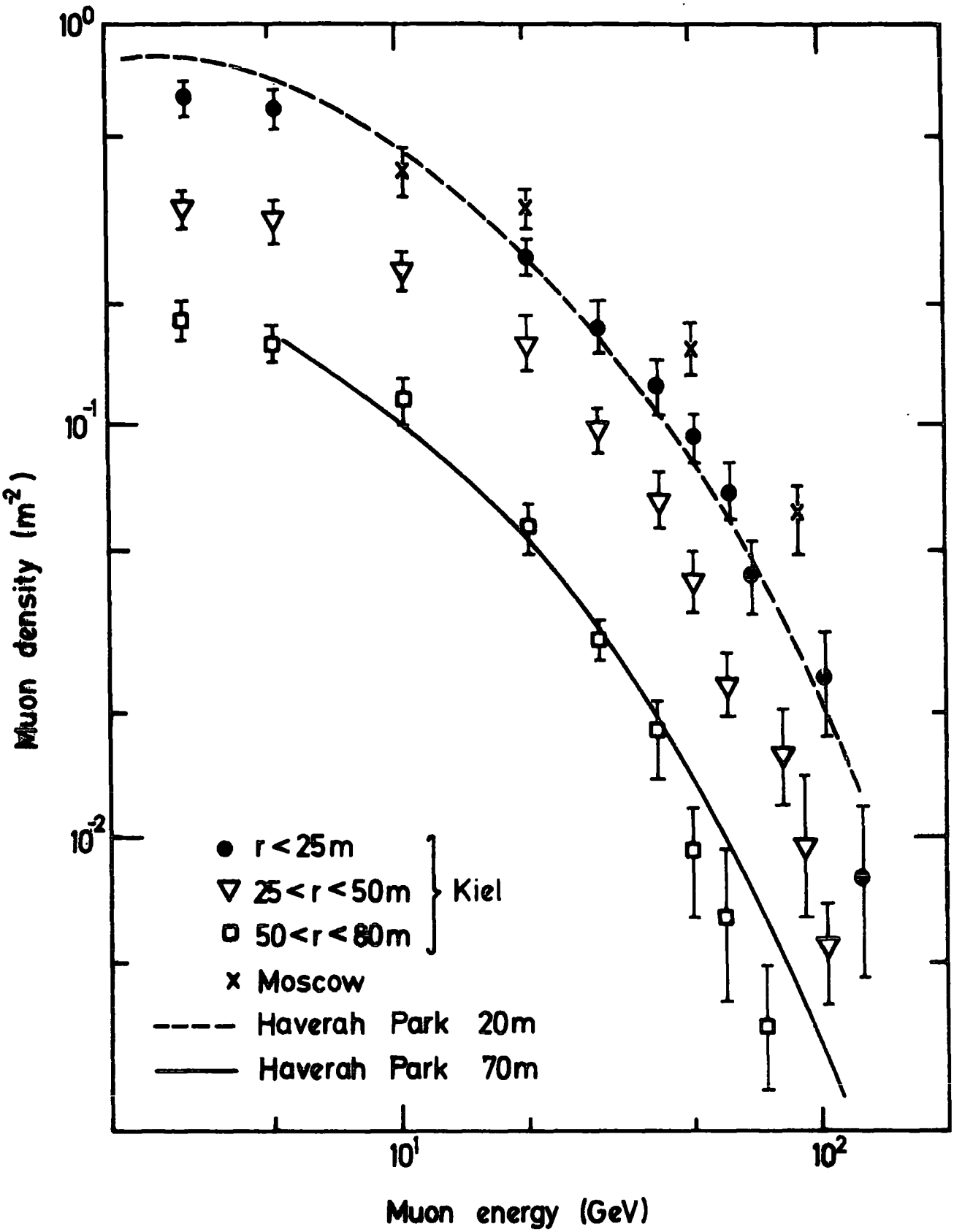

FIGURE 2.12 The energy spectrum of muons in E.A.S. obtained by various experiments using magnetic field technique in muon spectrographs. (After Burger et al, 1975).

Showers initiated by heavy primaries will have a higher level of production than proton initiated showers, due to the reduction in the nuclear interaction length. The mean height of origin of muons can be determined as follows :-

1. From a knowledge of the muon energy and core distance together with assumptions concerning the transverse momentum of secondaries of interactions.
2. From a knowledge of the time delay of muons of known energy and core distance.
3. From the separation of muons of opposite charges in the geomagnetic field.

It is hoped that with a knowledge of the production height, the distribution of muons of a given energy will enable an estimate of the characteristics of the nuclear cascade to be made from a different standpoint to that taken by studying the lateral distribution of muons.

A survey of the measurements of the mean height of muons at various energies derived from different experimental techniques is given by Turver, (1973). The summarised data (see Figure 2.13) shows a general agreement between the measurements when all are reduced to a common threshold energy of 0.3 GeV, in that they indicate the expected increase in the mean height of origin with increasing core distance. The measurements of Earnshaw, et al, (1973) have given further evidence of the increase. Recently, the mean height of origin has been measured directly by the Kiel group (Burger, et al, 1975) and the Lodz groups (Dzikowsky, et al, 1975). The results of Burger, et al, show an overall dependence of the mean production height on core distance, particularly for distances less than 50 meters from the shower axis. Their results also give a very low level of height of origin, compared with the general picture of E.A.S. obtained from most other data.

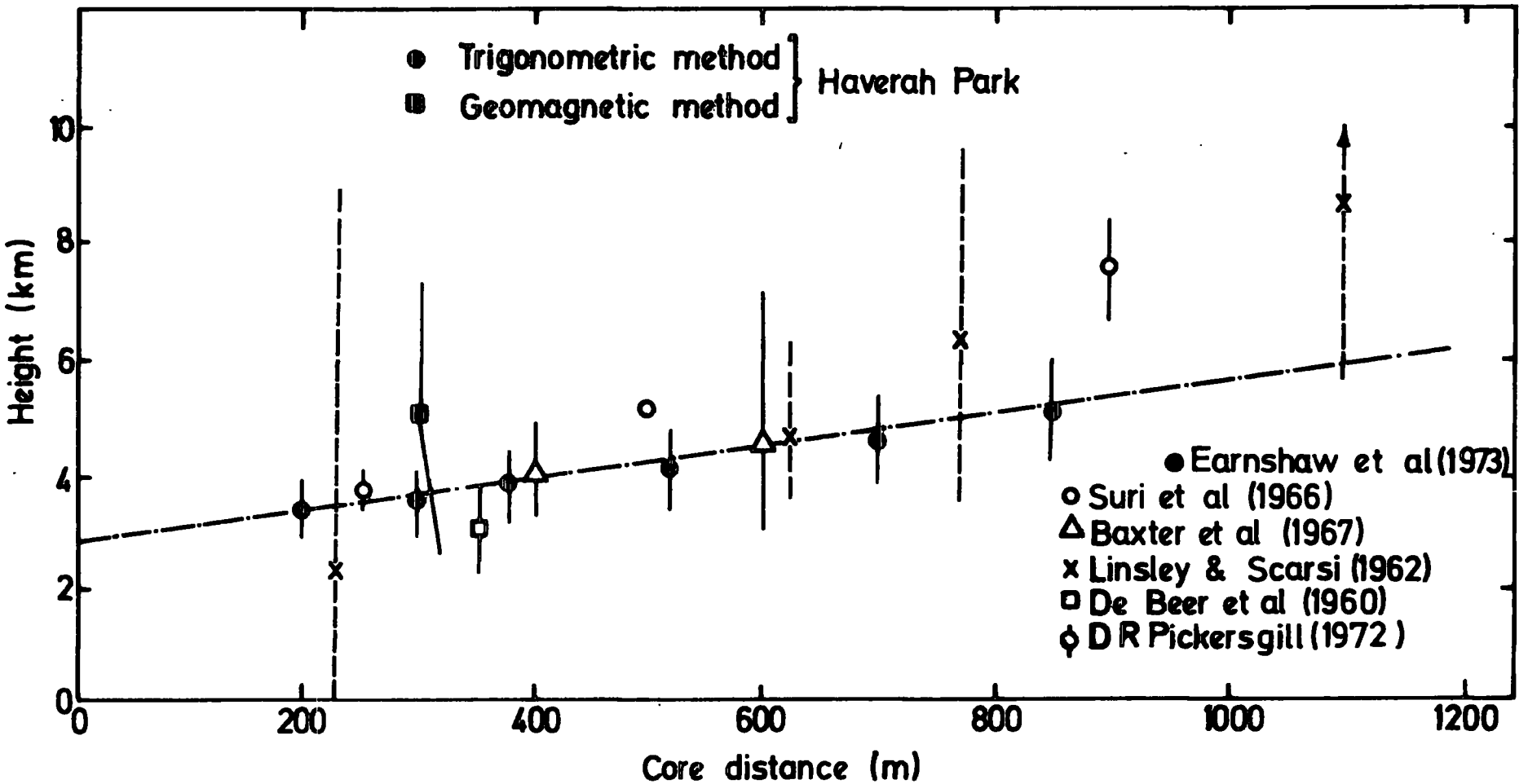

FIGURE 2.13 The height of origin of muons with energy greater than 0.3 GeV. in a shower of about 10^{17} eV. as a function of shower core distance. The line shown is the best fit to the data of Haverah Park. (After Earnshaw et al, 1973).

Dzikowsky, et al, estimate the height of origin of muons with energies > 5 GeV as 12.7 $\pm$ 1.8 Km, which , although exceeding the height predicted by the same authors on the basis of the standard model, is consistent with results obtained from muon lateral distribution investigations.

2.3.5 The Relationship Between the Total Number of Muons and Electrons and the Primary Cosmic Ray Energy

Converting the shower size spectrum into a primary spectrum is not a straight forward procedure,due to the lack of precise knowledge of the average parameters of the high energy nuclear interactions that control the development of the air shower, as well as the effect of the fluctuations in the air shower development. Detailed Monte Carlo calculations on this important aspect have shown that the effect of these uncertainties can be reduced if showers are measured near the depth of maximum development. Although most of the theoretical observations are still subject to some uncertainties, they predict an almost linear relationship between the primary energy and the shower size ; this relationship is model dependent. The size-energy relationship has been shown by De Beer, et al, (1966), for near vertical E.A.S. at sea level and initiated by primary protons of fixed energy, to be of the form :-

$$E_p = 9.5 \times 10^{13} \ (N_e \ 10^{-4})^{0.91} \ eV \qquad (2.12)$$

where N_e is the mean shower size. Also, De Beer, et al, define the mean primary energy for a fixed shower size as having the following form :-

$$E_p = 5.6 \times 10^{13} \ (N_e 10^{-4})^{0.93} \ eV \qquad (2.13)$$

Figure 2.14 shows the N_e - E_p relationship for vertical showers initiated by primary protons as defined by the shower simulations of Dixon,

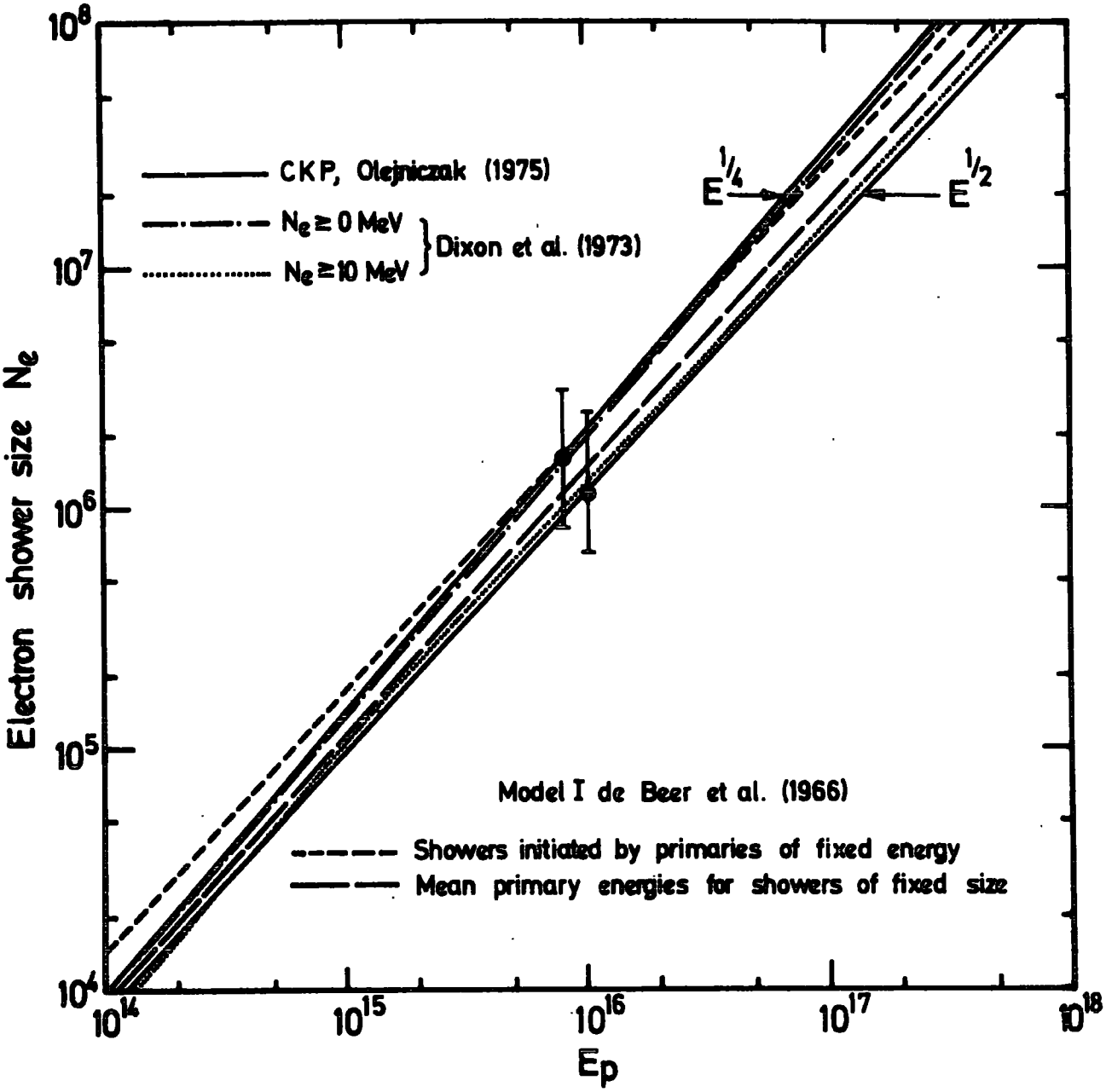

FIGURE 2.14 The dependence of the electron shower size on primary energy obtained by various models. The error bars represent the error in shower size as given in the work of Olejniczak (1975).

et al, (1973). The effect of the detector threshold energy (1 - 10 MeV) has been included when the $N_e - E_p$ relationship was established. Also in the same figure the results of De Beer, et al (1966) and the recent work of Olejniczak (1975) is plotted for primary proton energies.

For muons in air showers, investigations have been carried out to define the $N_\mu - E_p$ relationship. As has been mentioned earlier (Section 2.3.1) the total number of muons exceeding a certain energy threshold is a better representation of the energy primary spectrum than is the number of electrons. De Beer, et al, (1969) give for the $N_\mu - E_p$ relationship for muons with energies $\geq$ 1 GeV the following expression :-

$$E_p = 1.8 \times 10^5 \ (N_\mu \geq 1 \text{ GeV}) \ 10^{-4})^{1.13} \text{ eV} \qquad (2.14)$$

where N_μ is the number of muons in the shower.

The work on the $N_\mu - E_p$ conversion is shown in Figure 2.15 for $E_\mu \geq 1$ GeV and $E_\mu \geq 10$ GeV, calculated by various groups.

Concerning the relationship between N_μ and N_e, their dependence may be approximated by a power law of the form :-

$$N_\mu \ \alpha \ N_e^{\alpha} \qquad (2.15)$$

The exponent α in this relationship is not constant ; its value is sensitive to the primary composition. Figure 2.16 shows the variation of α with shower size as predicted by Mason et al, (1975) on this basis. The

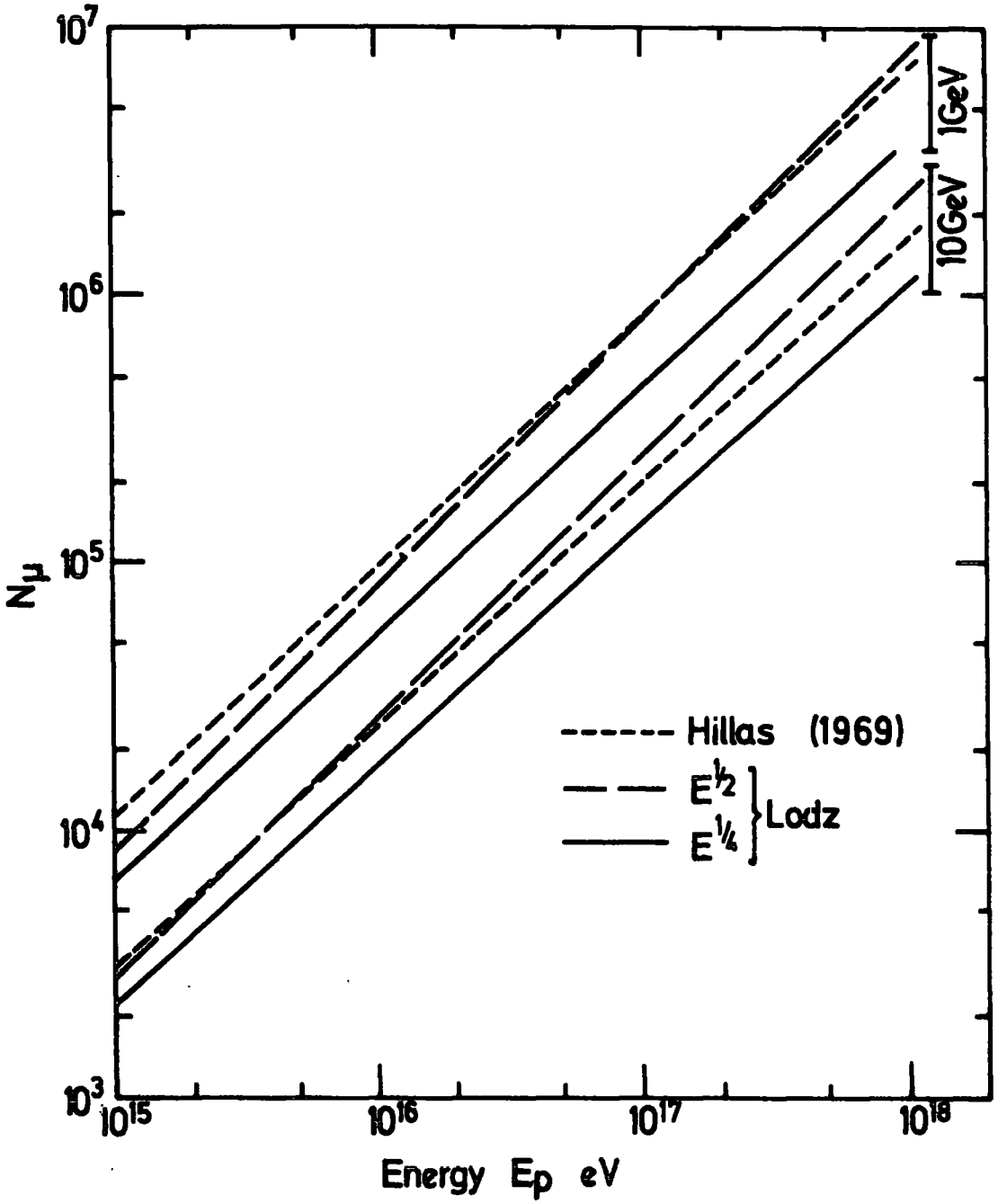

FIGURE 2.15 The dependence of the number of muons N above 1 and 10 GeV. on primary energy, for proton showers at 14° for model of Hillas (1971) compared with vertical showers of Giler (1969) marked Lodz. (After Bell, 1974).

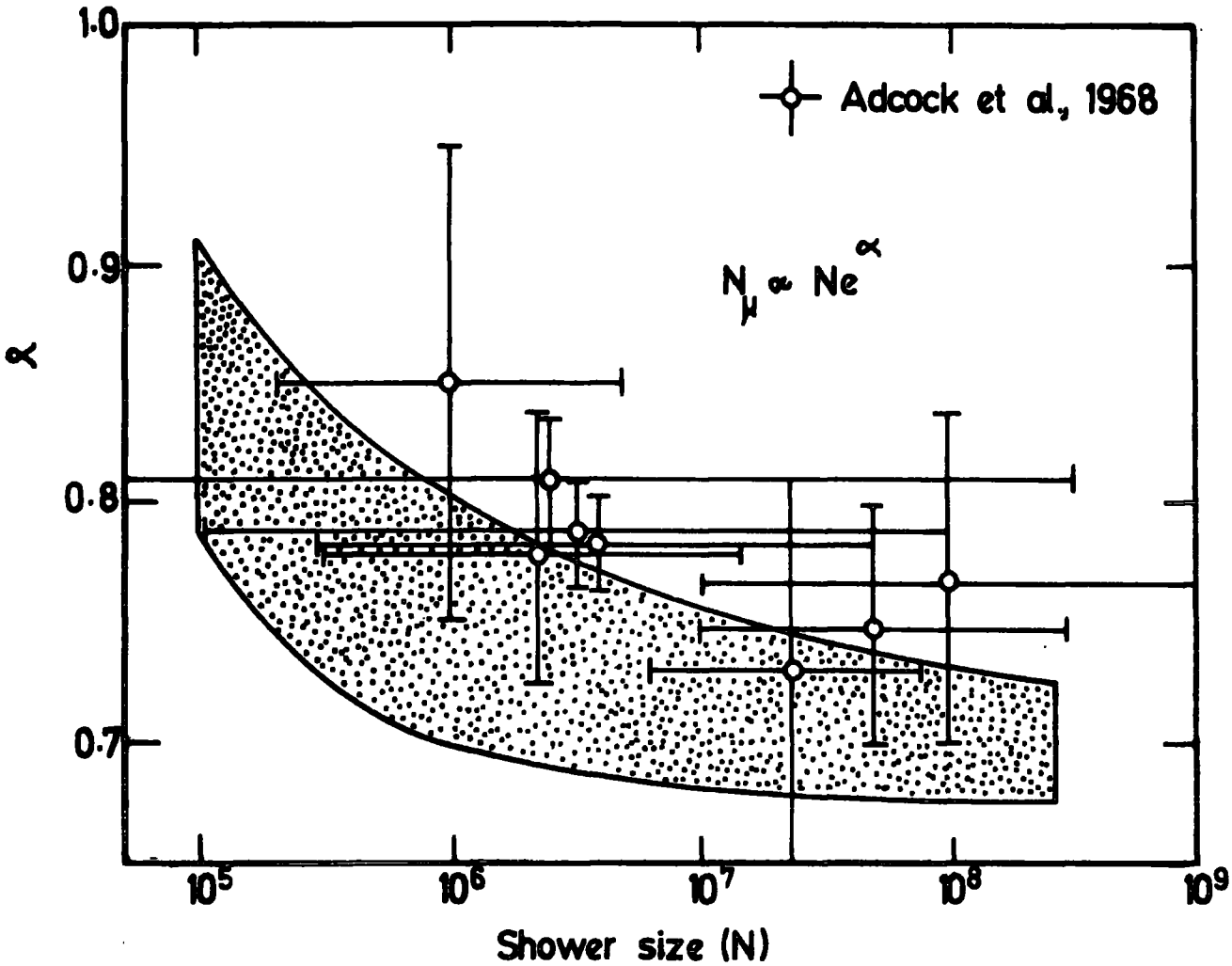

FIGURE 2.16 The size dependence of the number of low energy muons, N_μ is shown by the exponent, α, given by the $N_\mu \alpha N_e^{\alpha}$. The experimental data were taken from Adcock et al (1968). The shaded area represents the predictions of the trial composition of Mason et al (1975).

experimental data are those collected by Adcock, et al (1968). The dotted area is the theoretical prediction of Mason, et al. The agreement between theory and experimental results is fair and the decreasing trend of α with shower size is exhibited by the predictions of Mason, et al.

Besides the evidence from the longitudinal development of the electron component (Wdowczyk and Wolfendale, 1972, 1973, and Gaisser,1974) there exists evidence which shows that the muon to electron ratio in showers is greater than expected. De Beer, et al, (1966) carried out detailed calculations based on the C.K.P. model. For primary protons and showers at sea level the calculated muon to electron ratio was found to be less than the summarised experimental data which referred to muons in the energy range 1 - 100 GeV and near vertical E.A.S. of mean size $N_e = 10^6$ particles. This means that the muon to electron ratio for protons and scaling will be even smaller. Gaisser and Murer (1972) have demonstrated this case and found that the N_μ/N_e ratio for scaling is lower by a factor of 5 when compared with the C.K.P. predictions as shown in Figure 2.17.

New measurements by Kalmykov and Khristiansen (1975) on the character of N_μ (N_e) dependence for muons above 10 GeV have indicated the existence of a sharp contradiction when compared with the predictions calculated by the same authors for scaling and primary protons. Very recently Wdowczyk, et al, (1976) have summarised the case concerning the N_μ (N_e) dependence with the theoretical treatment of different authors as shown in Figure 2.18. Wdowczyk, et al, show that the scaling model predictions do not give a fit to the experimental data, even assuming that the primaries are all iron nuclei as is seen from the line "scaling and Fe". Also, it is of importance to mention that the slope of the experimentally determined relationship between N_μ and N_e is quite different from that for scaling. Wdowczyk, et al, point out that agreement with the observed slope could be achieved by having an increasing fraction of the primaries as iron, reaching 100% only at $N_e = 10^7$ particles

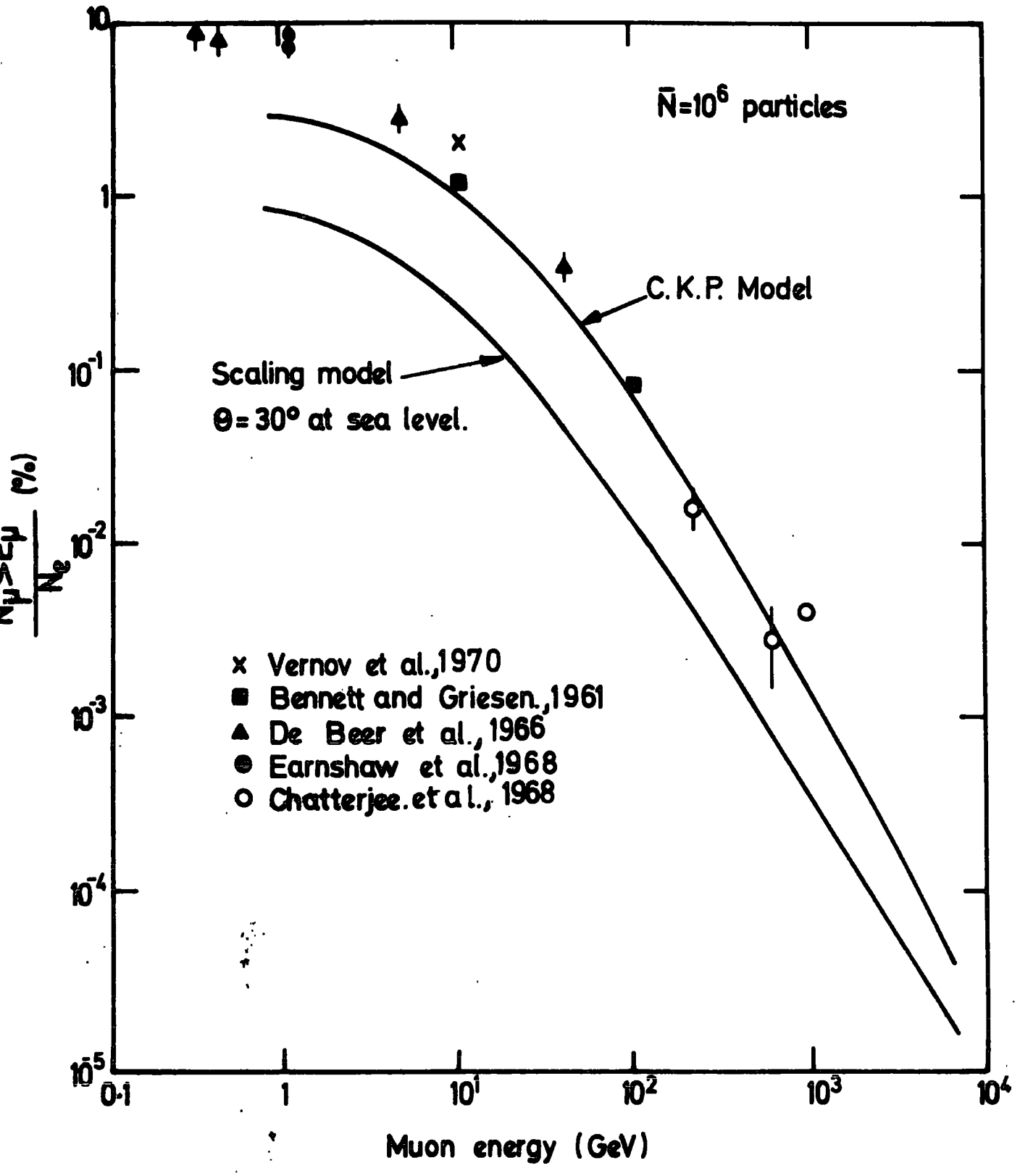

FIGURE 2.17 The integral number of muons as a per cent of shower size versus muon energy for showers of mean size 10^6 particles. (After Gaisser and Maurer, 1972).

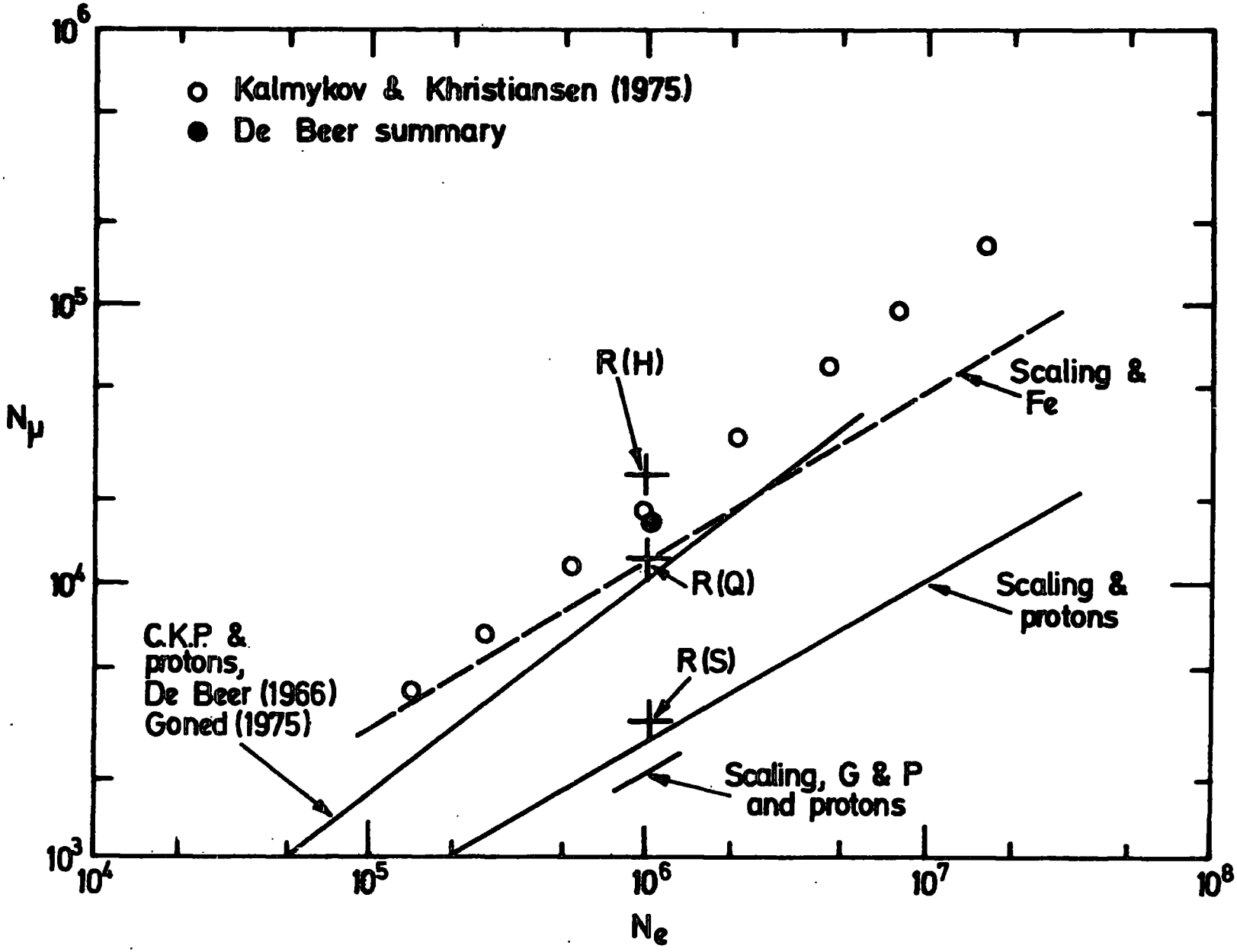

FIGURE 2.18 Muon number versus electron size for near vertical showers, for muon threshold energy of 10 GeV. Points denoted R refer to the predictions of Rozhdestvensky et al (1975) for normal composition, (After Wdowczyk et al, 1976).

R(s) ---- scaling, R(a) ---- $E_p^{\frac{1}{4}}$ multiplicity law, R(Q) ---- $E_p^{\frac{1}{2}}$ multiplicity law.

and comprising 30% iron at $N_e = 10^5$. This is consequently in contradiction with the results of the Utah data (Bergeson, et al, 1975) which indicate the need for 80% iron at 3×10^{14} eV. A further difficulty is that such a high percentage of iron would not explain the large fluctuations of the muon number in E.A.S. when N_e is fixed.

2.4 THE NUCLEAR CASCADE

2.4.1 Introduction

The nuclear cascade plays a principal role in the development of an air shower. The development of the whole shower depends on the properties of the individual nuclear interactions and on the development of the nuclear cascade. As a matter of illustration, if a primary particle of energy $\geq 10^{14}$ eV is considered to be incident vertically upon the atmosphere it will undergo a nuclear collision with a mean path in the range 75 - 90 gm cm^{-2}. This indicates that the first interaction could take place generally at 15 Km above sea level, but because of possible large fluctuations on this height, the production height distribution can be nearly flat between 10 - 30 Km above sea level.

As the cascade progresses through the atmosphere there will be on average about 12 nuclear interactions of the primary particle before it reaches sea level. The incident particle, after each collision, emerges with a flat energy spread with around 50% of its original energy ; the inelasticity of individual collisions may vary 0.3 - 0.9.

The nuclear cascade continues to develop due to the injection of pions, nucleons, kaons and hyperons as interaction products of the primary particle ; these secondaries either interact with the air nuclei, thus continuing the cascade, or they decay. The interacting pions will have an interaction mean free path of $\approx$ 120 gm cm^{-2}. Approximately one third of the pions produced in the nuclear cascade are neutral pions that have an extremely short life

time ($T_o \sim 10^{-16}$ sec.) and these probably decay. As long as nuclear active particles have sufficient energy to initiate other interactions, neutral pions produced will inject energy into the electromagnetic cascade of the shower. Since nuclear active particles that are produced in nuclear interactions are emitted with small transverse momenta ($\simeq 0.4$ GeV/c), those of high energy will form a bundle close to the core of the shower.

Studies of the multicore structure of the E.A.S. show some indication of a large increase in the transverse momenta of the nuclear active particles of such showers to about 6 GeV/c (Miyake, et al, 1970) and to about 10 GeV/c (Dake, et al, 1975). Such increases have not been accepted yet, and are doubtful.

2.4.2 The Transverse Momentum

It has been confirmed many times that the mean transverse momentum of secondary particles in high energy collisions is almost independent of the collision energy, having possibly a very slight increase with energy. Figure 2.19 shows the mean transverse momentum versus primary energy taken from Muraki (1975).

In the work on E.A.S. the following observable quantities are influenced by the transverse momentum :-

1. The muon lateral distribution.
2. The lateral spread of hadrons in shower cores.
3. The core structure of the electromagnetic component.

Some experiments have indicated the existence of large transverse momenta of the produced particles. Two arguments support this phenomenon, the first being the fact that the experimentally measured densities for muons with energies $\gtrsim 100$ GeV have flatter lateral distributions than those obtained by the Monte Carlo simulations. The second is the occurrence of multiple core showers where the energy of the individual cores, E, and their mutual distances, r, were so large that after having assumed reasonable heights of

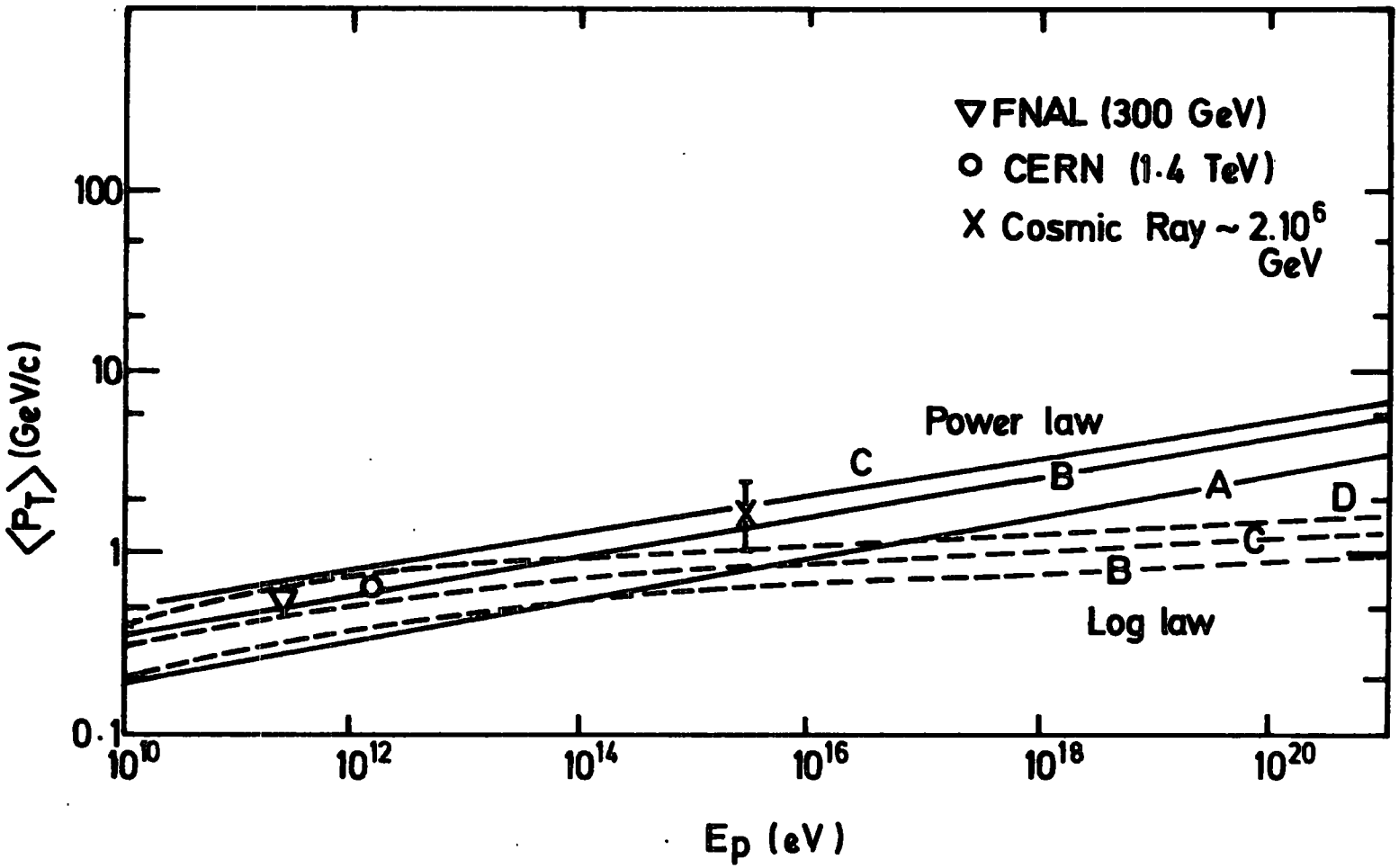

FIGURE 2.19 The mean Transverse momentum versus primary energy, (After Muraki, 1975), cases A B C and D represent the best ψ^2 fit to experimental data, obtained at the CERN ISR and FNAL, for three parameters that characterize the Pt-Ep dependence laws : for details see the same reference.

origin, h, the quantity (r/h)E turned out to be many times larger than 1 - 10 GeV. This quantity can be interpreted as the transverse momentum of the particle produced at the given height.

Evidence for high transverse momenta has been shown in the work of Hazen, et al, (1973) from studies of sub-cores in the electromagnetic component of E.A.S. using a cloud chamber, also, the earlier work of Shibata, et al, (1965) and Hasegawa, et al, (1966). The results of Guseva, et al, (1962) obtained from experiments using the emulsion technique show evidence for more secondaries with large transverse momenta than can be expected on the basis of the C.K.P. model. Halzen and Gaisser (1975) have pointed out that the E.A.S. observations of the secondary π^o produced in cosmic ray interactions in the energy primary range 10^4 - 10^7 GeV confirm the discovery of the FNAL and CERN ISR experiments of a component of the proton-proton interaction growing with energy yielding an unexpected number of high transverse momenta secondaries. These proton-proton interactions are very different from the hadron component interactions that yield the bulk of pions with small transverse momentum.

2.5 PREVIOUS STUDIES OF THE MUON COMPONENT USING THE MAGNETIC SPECTROGRAPH TECHNIQUE

2.5.1 The Cornell Group

In the pioneer work of Bennett and Greisen (1961) a vertical magnetic spectrograph was run in coincidence with an E.A.S. array. Figure 2.20 shows the relative position of the spectrometer in the array. The magnetic spectrometer consisted of an air-gap magnet with magnetic field strength of 12K Gauss and nominal aperture of 25 $cm^2 sr$. Muons were traced through the magnet by trays of Geiger-Müller counters. The array detecting elements were plastic scintillation counters arranged as in Figure 2.20, and showers in the size range 10^3 - 10^7 particles were recorded by the array.

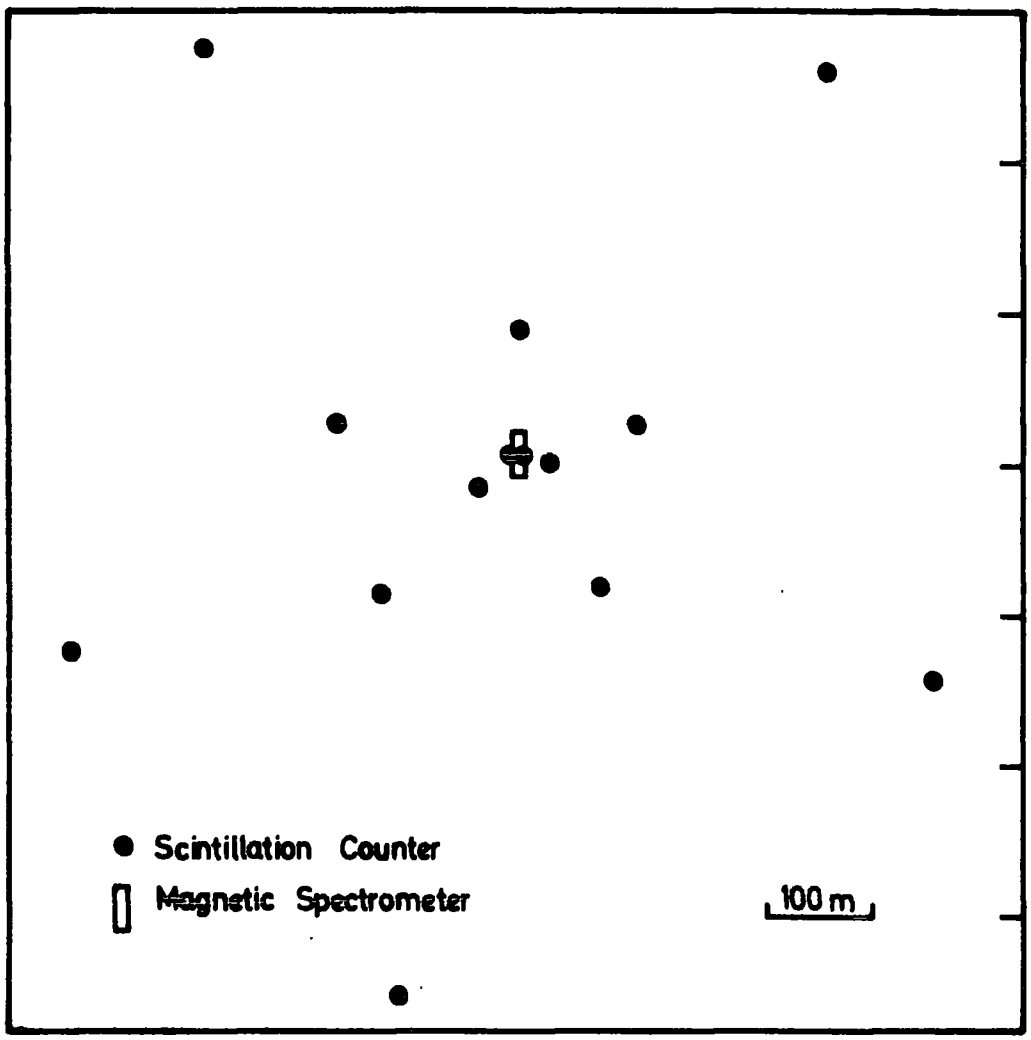

The experiment of Bennett & Griesen, 1961.

FIGURE 2.20 The experiment of Bennett and Griesen, (1961).

In this experiment the muon lateral distribution for momentum > 1 GeV/c and the integral muon energy spectrum in the range 10 - 20 GeV were measured. Bennett and Greisen (1961) express their results in the terms of the empirical relationships (equations 2.9, 2.10) which give the density of muons with a minimum energy in a shower of size N_e, at a certain distance from the shower core.

As it has been noted in Section 2.3.2, there is no serious discrepancy in the shape of the lateral distribution obtained in this experiment and those obtained by other workers.

2.5.2 The Haverah Park Experiment

A variety of air shower properties have been studied in this large scale experiment. The principal aim is to determine the primary energy spectrum at high energies, to examine the isotropy of arrival direction and to give as much information as possible about the primary mass composition. Studies of the muon component of E.A.S. have been achieved by operating a vertical magnetic spectrograph (Figure 2.21 a) of total sensitive area 1.8 m^2 for particles incident in the vertical direction, having a momentum resolution of $\sim$ 100 GeV/c.

For muons traversing the spectrograph, trays of neon flash tubes were used as visual detectors that provide four estimates of track location for the momentum determinations. The Haverah Park E.A.S. array consists of diffused light Cerenkov detectors arranged as shown in Figure 2.21 b. Also shown in the same figure is the location of the spectrograph relative to the array. The spectrograph was triggered and photographed whenever a shower was recorded on one of the small arrays of the whole installation.

The following aspects of E.A.S. muons have been measured by operating the array in conjunction with the spectrograph :-

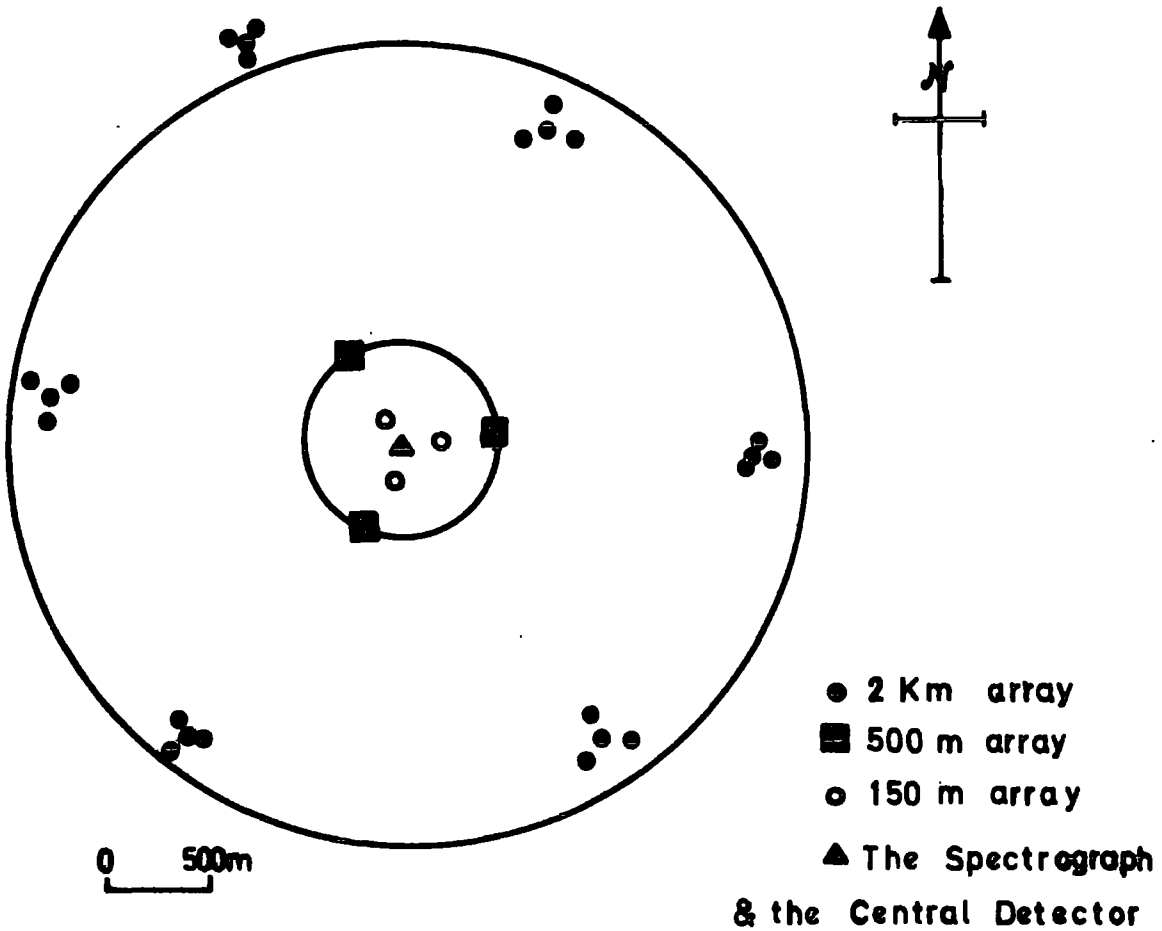

FIGURE 2.21b The Haverah Park E.A.S. Array (After Pickersgill, 1973).

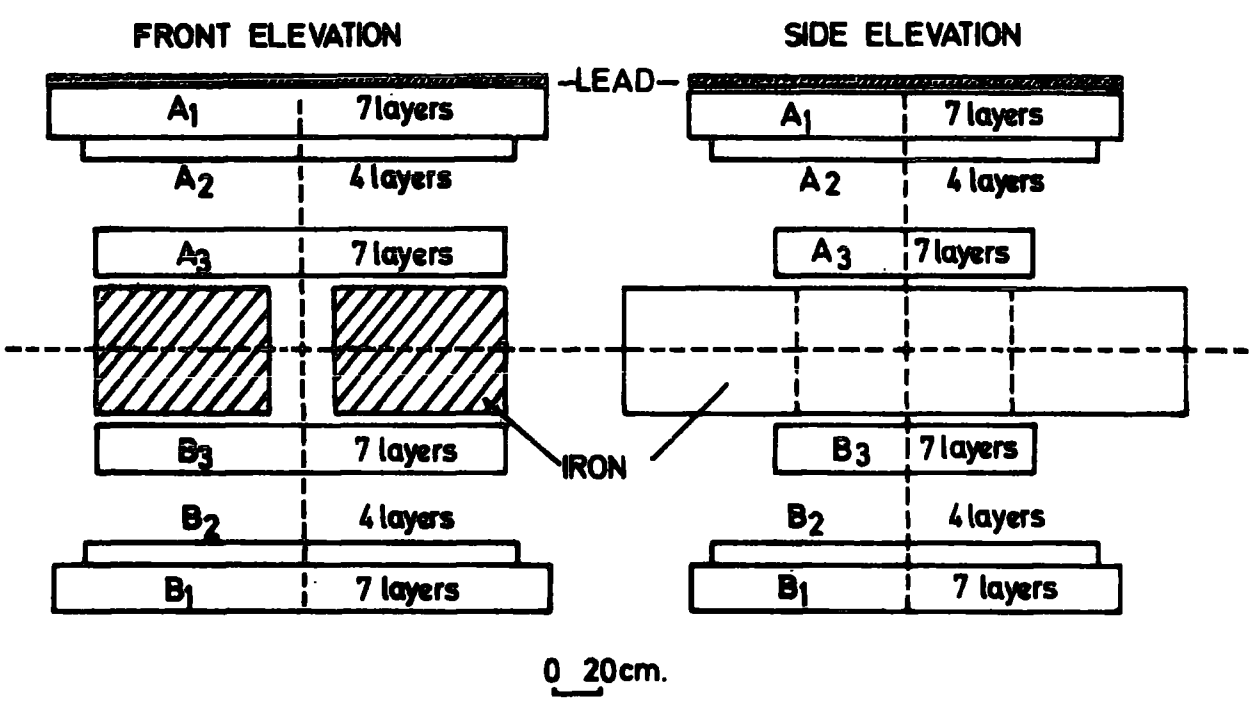

FIGURE 2.21a The muon magnetic spectrograph at Haverah Park. A, B are neon flash tubes trays (After Pickersgill, 1973).

1. The lateral distribution of muons in near vertical showers as a function of muon energy, to lateral distances of $\sim$ 1 Km and to energies of about 100 GeV.

2. The energy spectrum of muons as a function of core distance.

3. The production heights of the muons.

4. The charge ratio of E.A.S. muons.

5. The distribution of transverse momentum of the secondary particles of an interaction.

A comparison of the experimental results with model calculations has been made by Orford and Turver (1969). It has been shown that it is necessary to assume a high pion multiplicity law ($n_s \propto E^{\frac{1}{4}}$), or heavy primary mass in order to explain the observed high number of muons (particularly those with energies $\gtrsim$ 50 GeV) far from the shower core.

2.5.3 The Kiel Spectrograph

A solid iron magnetic spectrograph has been used in co-operation with the Kiel E.A.S. Array, (Figure 2.22 a) to study the energy spectra and production height of muons in E.A.S. in the energy range 3 - 200 GeV. The spectrograph (Figure 2.22 b) consists of a solid iron magnet of area 2.25 m^2. The muon momentum measurements are done using four sections of the magnet, each of area 0.25 m^2, where there is a homogeneous magnetic field. The visual detecting elements of the spectrograph are double gap spark chambers. The M.D.M. of the spectrograph is 210 GeV/c and the threshold momentum is 3 GeV/c (due to absorption in concrete and iron). The method used for data analysis was to select showers with exactly one muon passing through the spectrograph. The experimental results of Burger, et al, (1975) show an overall dependence of the production height on core distance for $\lesssim$ 50 meters from the shower core.

This result is in agreement with a mean transverse momentum of 0.4 GeV/c. Burger, et al, have found no significant change in the production height at distances 50 - 100 meters from the core. The

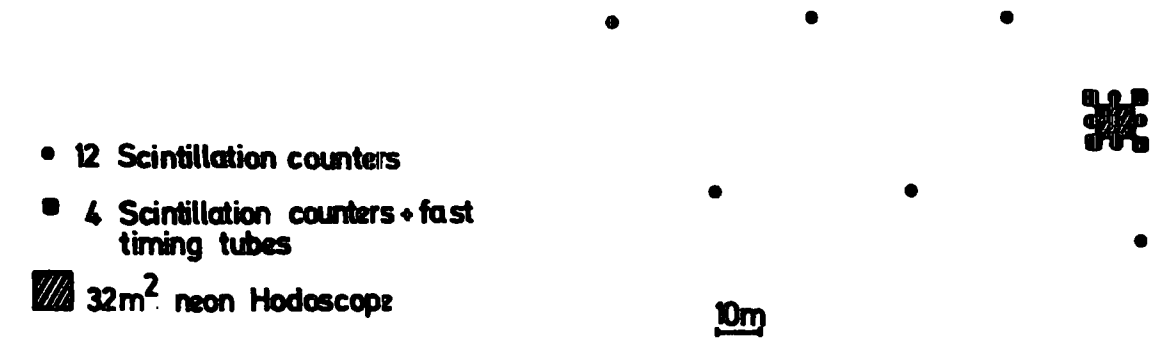

FIGURE 2.22a The Kiel E.A.S. Array (After Stauburt et al, 1970).

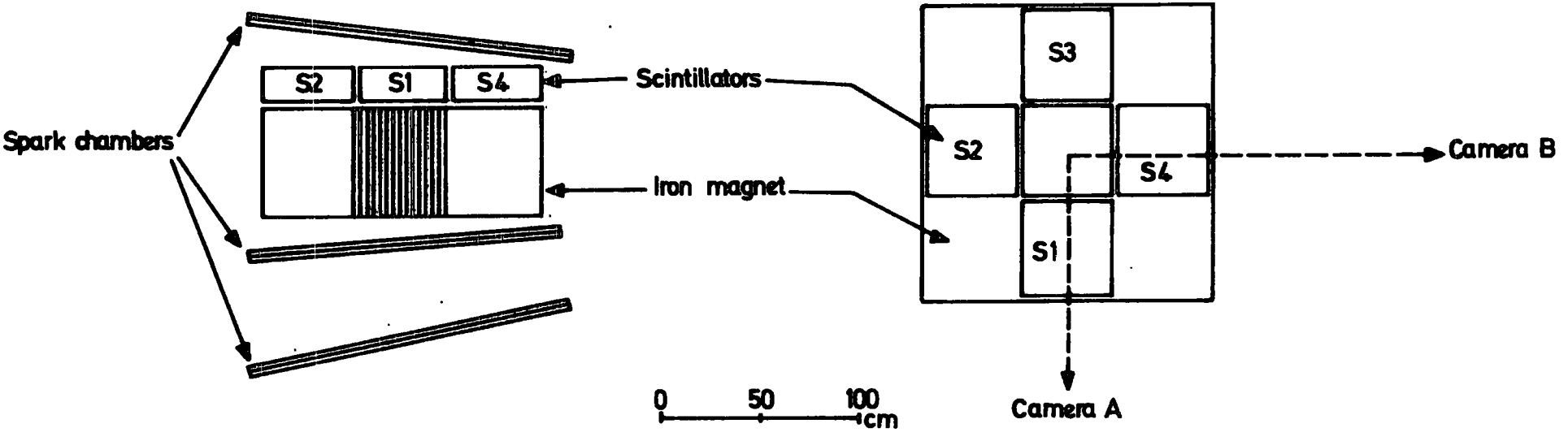

FIGURE 2.22b The muon spectrograph at Kiel (After Burger et al, 1975).

experimental results on the energy spectrum obtained by the same group agrees with the results from Haverah Park (Earnshaw et al, 1967).

2.5.4 The Moscow State University Experiment

Recently the Moscow State University has installed a magnetic muon spectrometer (Abrosimov et al, 1974) in the middle of the Moscow State University air shower array, (Figure 2.23a), at a depth of 40 m.w.e. underground. The spectrometer, (Figure 2.23b) consists of a magnetic iron body placed between arrays of wide gap spark chambers. Muon tracks were obtained by photographing the spark chamber after the muon has passed through the iron. Preliminary results of the Moscow State University spectrograph have been given by Rozhdestvensky, et al (1975). Figure 2.24 shows the muon energy spectrum in E.A.S. of size $N = 10^6$ as obtained by integrating the lateral distribution in the Figure (2.9) for muons with $E \geq 10$ GeV. The data are presented together with that obtained by Earnshaw et al (1967) for showers of size 2×10^7 particles. It is clear from the figure that the measured muon energy spectra are in contradiction with the predictions of the "scaling" hypothesis, and a good agreement is obtained with the C.K.P. model with multiplicity $n_s \alpha E^{\frac{1}{4}}$.

It is also found that the shape of energy spectra in the range 20-90 GeV is the same as that predicted by both models with $n \alpha E^{\frac{1}{4}}$ and $n \alpha E^{\frac{1}{2}}$. It is important to mention that in spite of the agreement between the experimental muon energy spectra and the standard model there exists some disagreement in the lateral distribution function. Furthermore, although the experimental shape of the muon spectra agrees with both multiplicity dependences, the energy spectrum at a given distance from the shower axis is more sensitive to the model, but the statistical accuracy

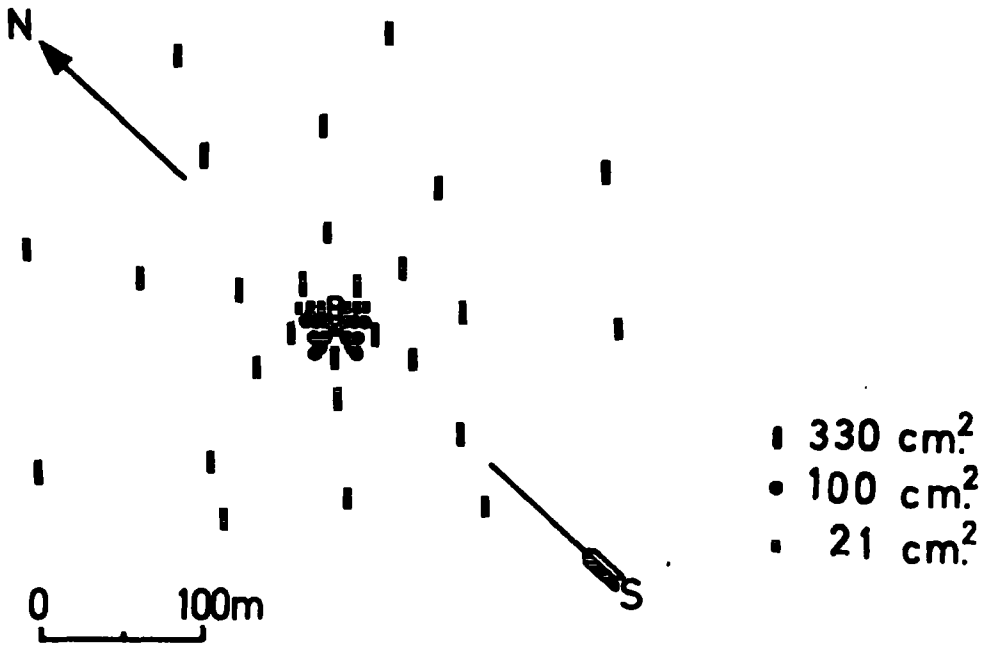

FIGURE 2.23a The Moscow State University E.A.S. Complex Array (After Vernov et al, 1970).

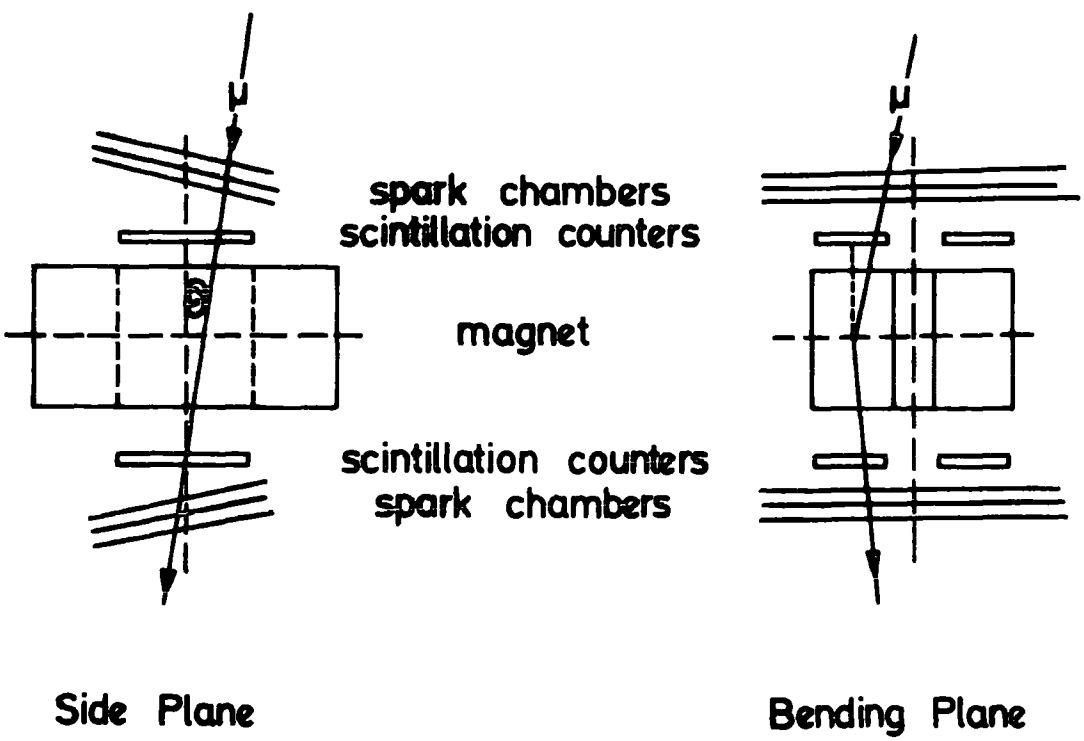

FIGURE 2.23b The magnetic spectrograph of the M.S.U. air shower array (After Abrozimov, et al, 1974).

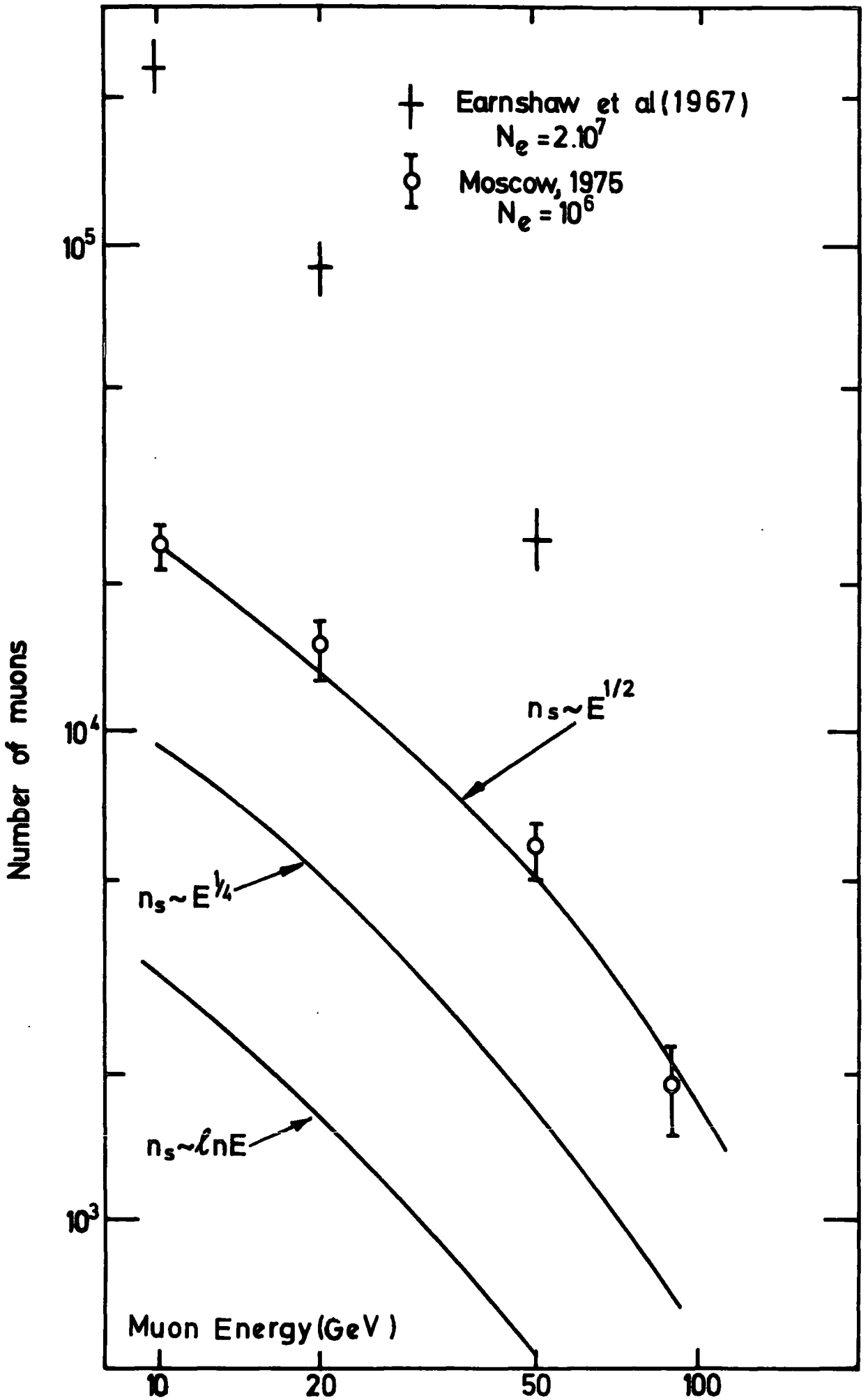

FIGURE 2.24 The integral muon energy spectrum in E.A.S. The theoretical predictions are those carried out at Moscow and Lodz University, The Haverah Park data are also presented, (After Rozhdestvensky, et al, (1975).

is not sufficient to rule out one of them.

2.6 THE PRESENT WORK

The work described in this thesis is based on employing two experiments in which some aspects of the electron and muon components of the air shower have been studied. In the first experiment an array of four plastic scintillation counters has been used to measure the density spectrum of small air showers and to determine the absolute rate of occurrence of the showers. Also this array has been used in conjunction with the muon magnetic spectrograph (M.A.R.S.) in which the absolute integral rate of muons associated with E.A.S. has been measured for muons with energy $\geq$ 5 GeV.

The second experiment employs an air shower array of plastic scintillation counters operated in conjunction with the M.A.R.S. spectrograph. This array measures the characteristics of air showers falling within a distance of 50 meters from the centre of the array and typically selects showers in the size range $8 \times 10^4 - 2 \times 10^6$ particles. The magnetic spectrograph provides an accurate measurement of the muon energy spectrum in the range 7 - 2000 GeV. Measurement of the muon lateral distribution has been made over radial distances 5 - 50 meters for various muon energy thresholds.

CHAPTER 3

THE EXPERIMENT - PART I

3.1 INTRODUCTION

An array of four E.A.S. detectors was designed to study the absolute integral intensity and the density spectrum of small air showers. The apparatus was designed to run in conjunction with the Durham Magnetic Automated Research Spectrograph (M.A.R.S), in which, by using a coincidence technique, the absolute integral intensity of E.A.S. muons with energies $\geq$ 5 GeV/c has been measured. The apparatus was constructed in the Sir James Knott laboratory in the Physics Department (50m above sea level and at a latitude 55^{o} N). It was placed directly beneath a roof of thickness $\approx$ 4 gm/cm^{2}. The array was operational for the period Oct. 1972 to April 1973, and a total of 293,361 showers were recorded including a total of 11,171 muon showers. There were two modes of operation of the apparatus. In the first, air shower detectors function alone, and in the second mode a coincidence is required between the array and the left-hand side of the magnetic spectrograph (the blue-side).

The coincidence rates,due to showers falling on the array, were measured for different combinations of the operational detectors. The "decoherence" curve of the measured showers was determined at six separations between the detectors. The exponent of the measured particle density spectrum was determined from the comparison of the 4-fold and 3-fold coincidence rates. The integral rates of muons associated with small air showers were measured with a variety of coincidences of the shower particle detectors and the main 3-fold coincidence pulse generated due to the passage of muons with $E\mu \geq 5$ GeV through the blue-side of the spectrograph.

The latter measurements were done using the spectrograph as a magnetised iron absorber (the magnetic field in the absorber was 16.3 kGauss and was positive or negative or comprised various sections of the absorber having crossed fields). Later, a run was done with the magnetic field reduced to 10 kGauss (reduced field).

3.2 GENERAL DESCRIPTION AND DESIGN OF THE APPARATUS

The geometrical arrangement of the array is shown in Figure 3.1a. The E.A.S. array consists of four identical scintillation detectors, S_1, S_2, S_3, S_4, all having a sensitive area of 0.5 m^2 arranged in a horizontal plane around the top of M.A.R.S. The geometry and location of the array around M.A.R.S. can be seen in Figure 3.1b. A shower is defined by a $\geq$ 2-fold coincidence between the four detectors of the array, and a third coincidence with the blue-side of M.A.R.S. is required to define a muon associated with a shower. Table 3.1 shows all coincidence categories used to select the data with and without the spectrograph.

3.3 THE E.A.S. DETECTOR

The type of detector used was a modified version of that described by Barnaby and Barton, (1960). Each detector in the array consists of a pair of similar individual scintillators attached together and separated by a partition as shown in Figure 3.2. Each individual scintillation counter is designed in such a manner that a square slab of phosphor material with mean dimensions of 50 x 50 x 5 cms fits the top of a box which is itself constructed of chipboard with dimensions 51 x 51 x 60 cms. The scintillator is viewed by a 5" diameter photomultiplier tube, (E.M.I. 9579B) with a useful cathode area of 121 cm^2. The photomultiplier in each part of the detector was at the centre of the base of the box. The top and side surfaces of the scintillator were covered with a highly reflecting

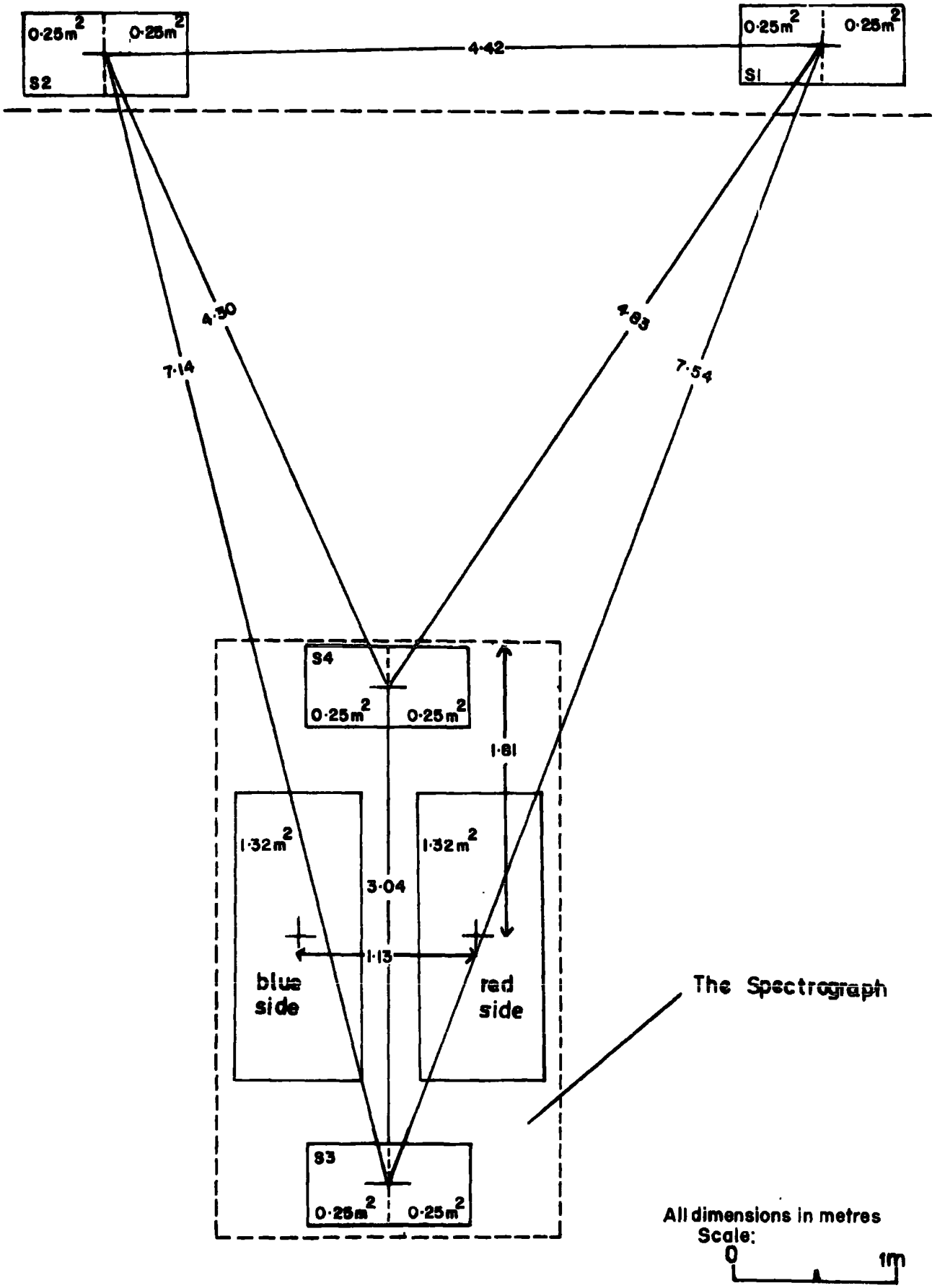

FIGURE 3.1a The small air shower array viewed at the top of the spectrograph.

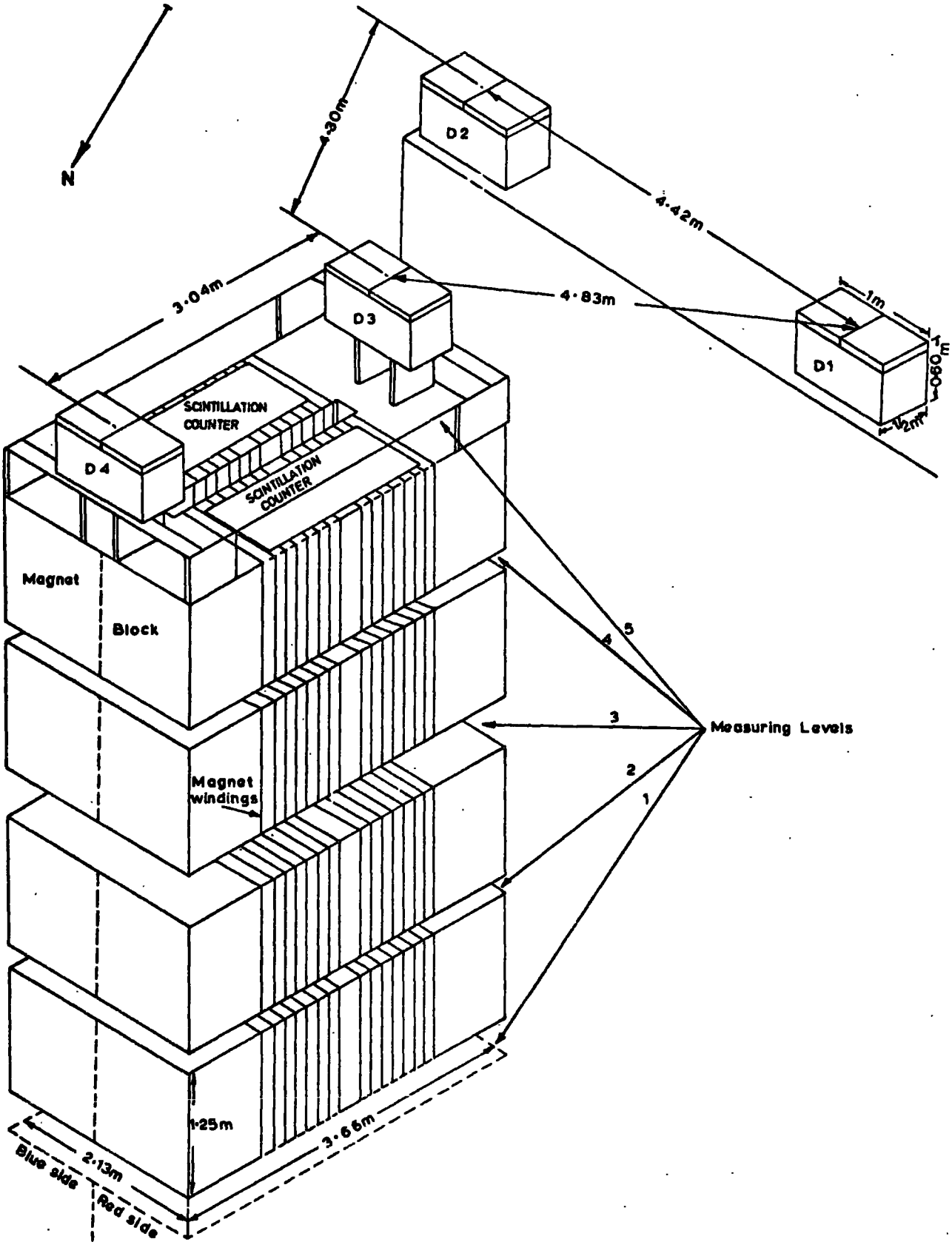

FIG. 31b: RELATIVE POSITION OF THE SHOWER ARRAY AROUND M.A.R.S.

TABLE 3.1

DETECTOR COINCIDENCE COMBINATION CATEGORY

SELECTED WITH AND WITHOUT THE SPECTROGRAPH.

Two fold	Three fold	Four fold
$S_3 + S_4$	$S_1 + S_2 + S_3$	All four detectors
$S_2 + S_4$	$S_1 + S_2 + S_4$	$S_1 + S_2 + S_3 + S_4$
$S_1 + S_4$	$S_1 + S_3 + S_4$	
$S_1 + S_2$	$S_2 + S_3 + S_4$	
$S_1 + S_3$		
$S_2 + S_3$		

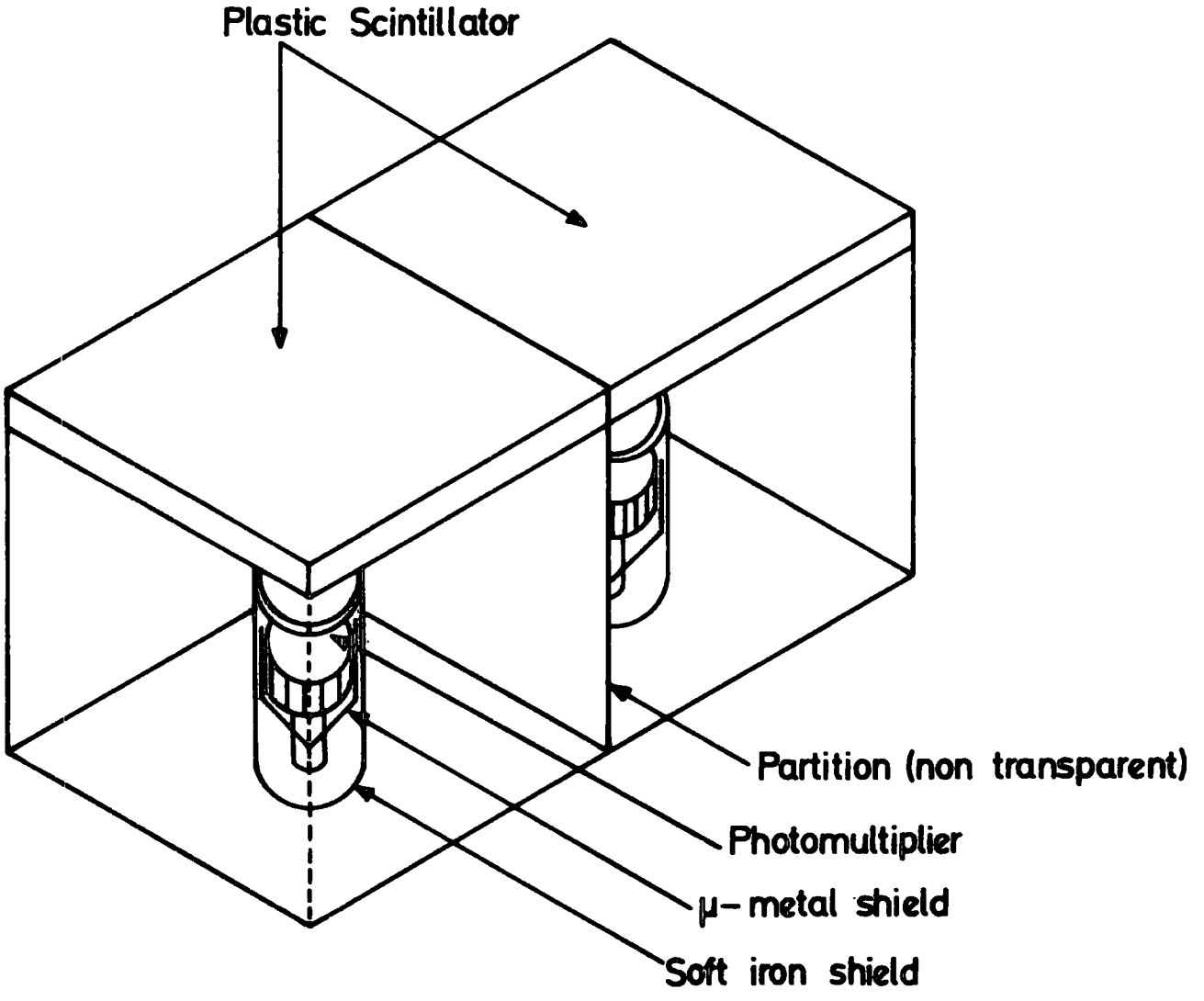

Figure 3.2: A typical detector.

aluminium foil to ensure the reflection of most of the light down to the photomultiplier tube. The top of the box was covered by hardboard of thickness 0.4 cm.

As a consequence of the passage of air shower particles through the plastic scintillator photons are generated in the scintillator. The total amount of light produced is proportional to the energy deposited by the shower particles in the scintillator. The photomultiplier can receive only a small proportion of the light emitted over the whole area of the scintillator.

Each photomultiplier has been run with the anode connected to a positive high voltage with respect to the cathode and the positive output pulse was taken from the last photomultiplier dynode, the pulse length (1.8 μsec) being determined by the R.C. network as shown in Figure 3.3. This figure shows the dynode resistor chain of the base of the photomultiplier tube used in each scintillation counter. The photomultipliers were tested individually by being used to view directly a 5" x 5" plastic scintillator. It was found that an unscreened photomultiplier placed in the vicinity of the spectrograph was affected by the stray magnetic field of the spectrograph. This effect can be explained as being due to the deflection of the secondary electrons as they pass between the photomultiplier dynodes, and this occurs mainly in the first dynode region. Clearly the effect of the magnetic field of the spectrograph on the photomultiplier must be avoided or minimised, and this was achieved by completely surrounding the tube by a μ-metal shield and an outer concentric soft iron cylinder, as shown in Figure 3.4.

Tests with the proper scintillation counters in their experimental location for positive and negative magnetic fields show no change in the shape of the pulse height distribution for single particles traversing the detectors, as is shown in Figure 3.5.

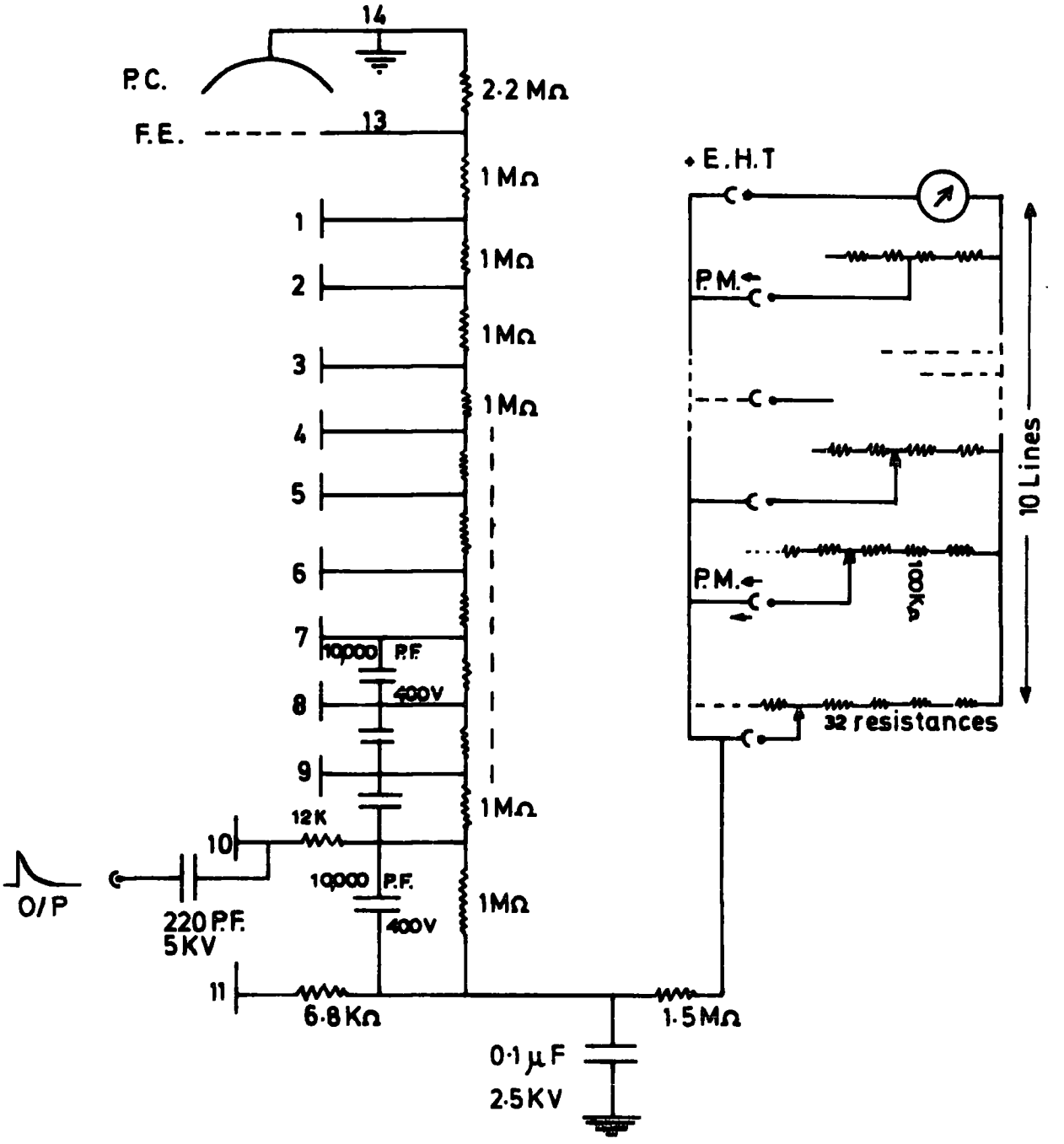

FIGURE 3.3 The dynode resistor chain for the photomultiplier tubes.

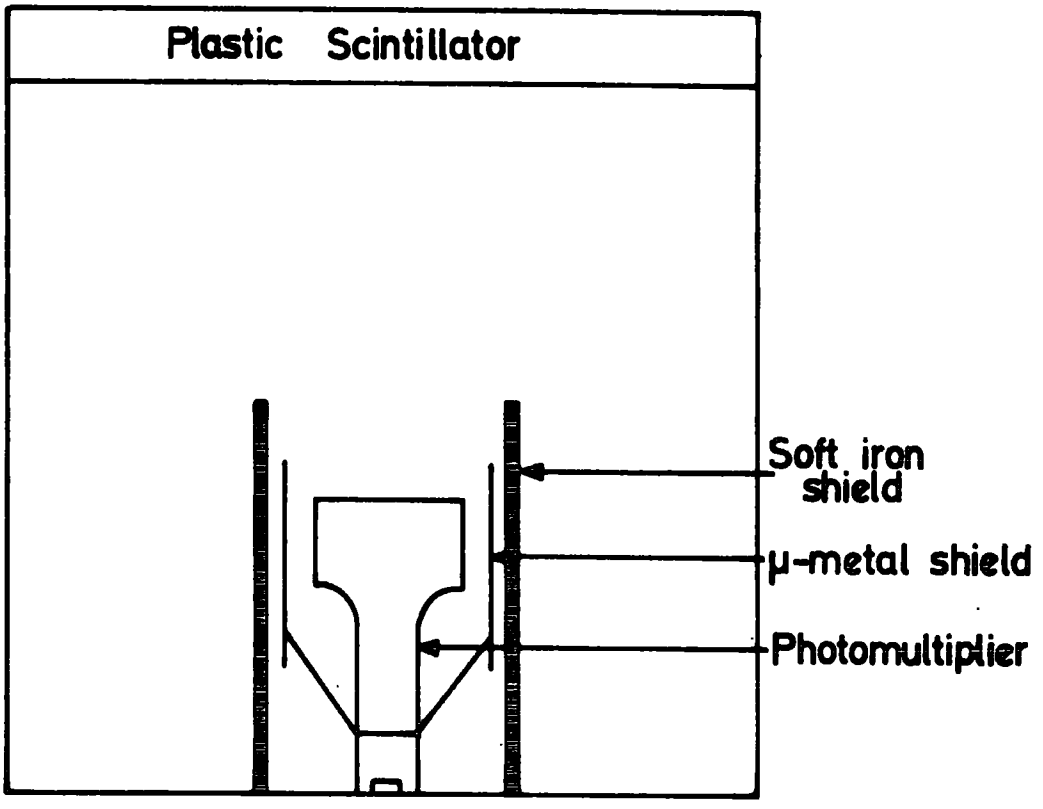

Figure 3.4 : Shielding system of a photomultiplier tube.

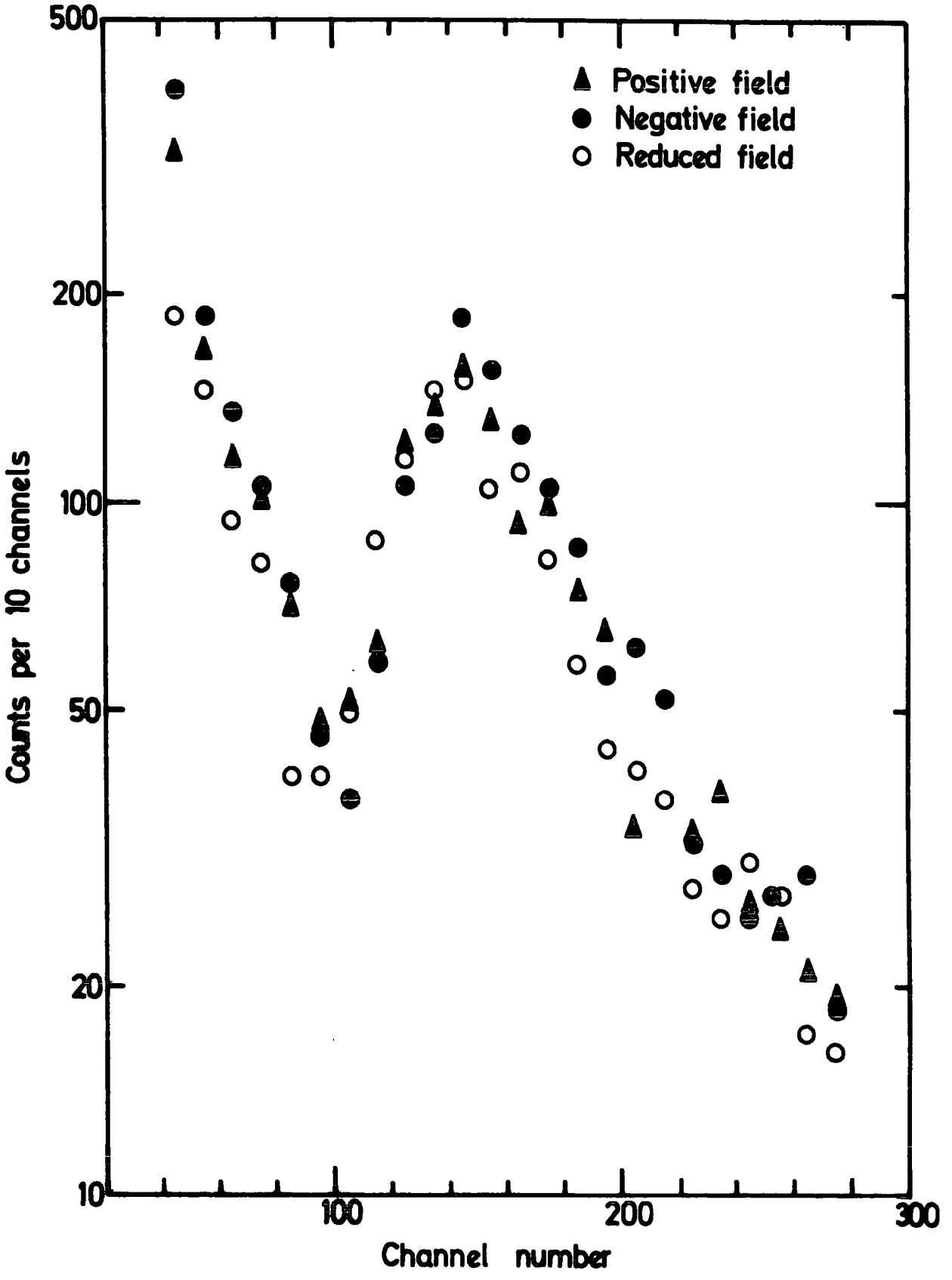

FIGURE 3.5 Pulse height spectra obtained with positive, negative and reduced magnetic fields.

3.4 THE ARRAY ASSOCIATED ELECTRONICS

3.4.1 The Power Supplies

The high voltage required for the dynode chains of the photomultipliers was obtained from a highly stable positive power supply. The E.H.T. was fed initially into a potential divider box which comprised of 10 parallel connections of resistors, each connection consisting of 32 resistors of value 100 k Ω in series, as shown in Figure 3.3. The potential divider box served as a variable resistor for the control of the E.H.T. to individual photomultipliers. The low voltage supply to the amplifiers was obtained from a stabilised D.C. power supply of +17 volts.

3.4.2 The Head Amplifiers

Output pulses from the photomultiplier tubes on leaving the light tight box were fed to a two transistor head amplifier. Two head amplifiers per detector were placed together inside a grounded aluminium box contained within the detector. The head amplifiers were simply emitter-followers, (Figure 3.6) with a gain of approximately unity, providing sufficient power to drive the linear output signals into $\sim$ 10 m of coaxial cable of 75 Ω impedance. The saturation voltage of the emitter-follower was typically 16 volts as shown in Figure 3.7 where the output gain is plotted against the input voltage. The gain stability of the amplifiers was checked periodically during the course of operation of the experiment and no significant changes were found. Pulses from the head units were then sent via coaxial cables to discriminators. Thus, each main detector (consisting of two scintillation counters) had five cables connected, these being two high voltage cables each supplying one photomultiplier, a cable supplying power to the head amplifiers and two cables carrying the output pulses from the detector to the discriminators.

The discriminators have a fixed threshold level of 250 $\pm$ 30 mV. The setting of the threshold levels will be discussed in Section 3.6.

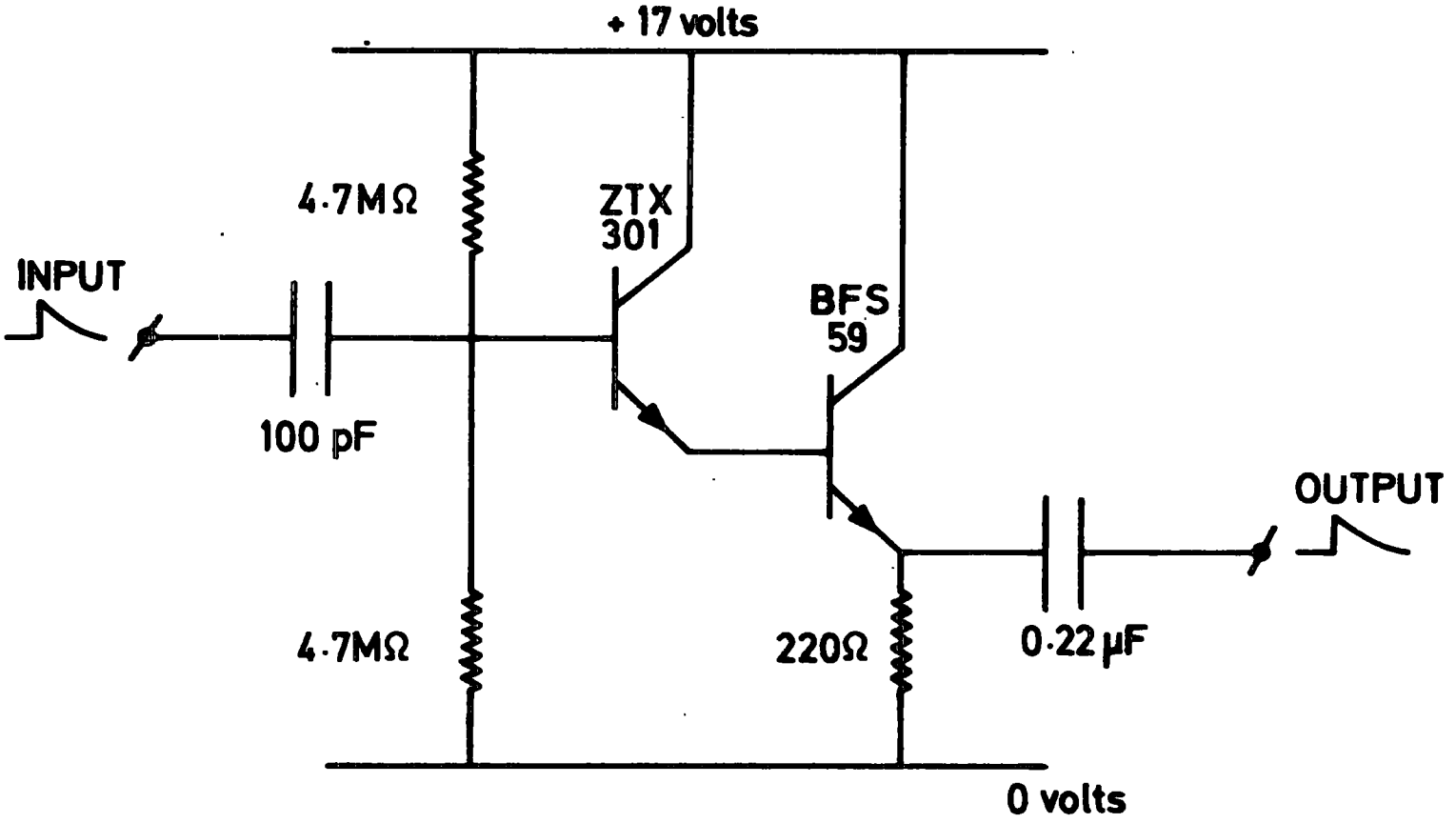

Figure 3.6: A head amplifier unit.

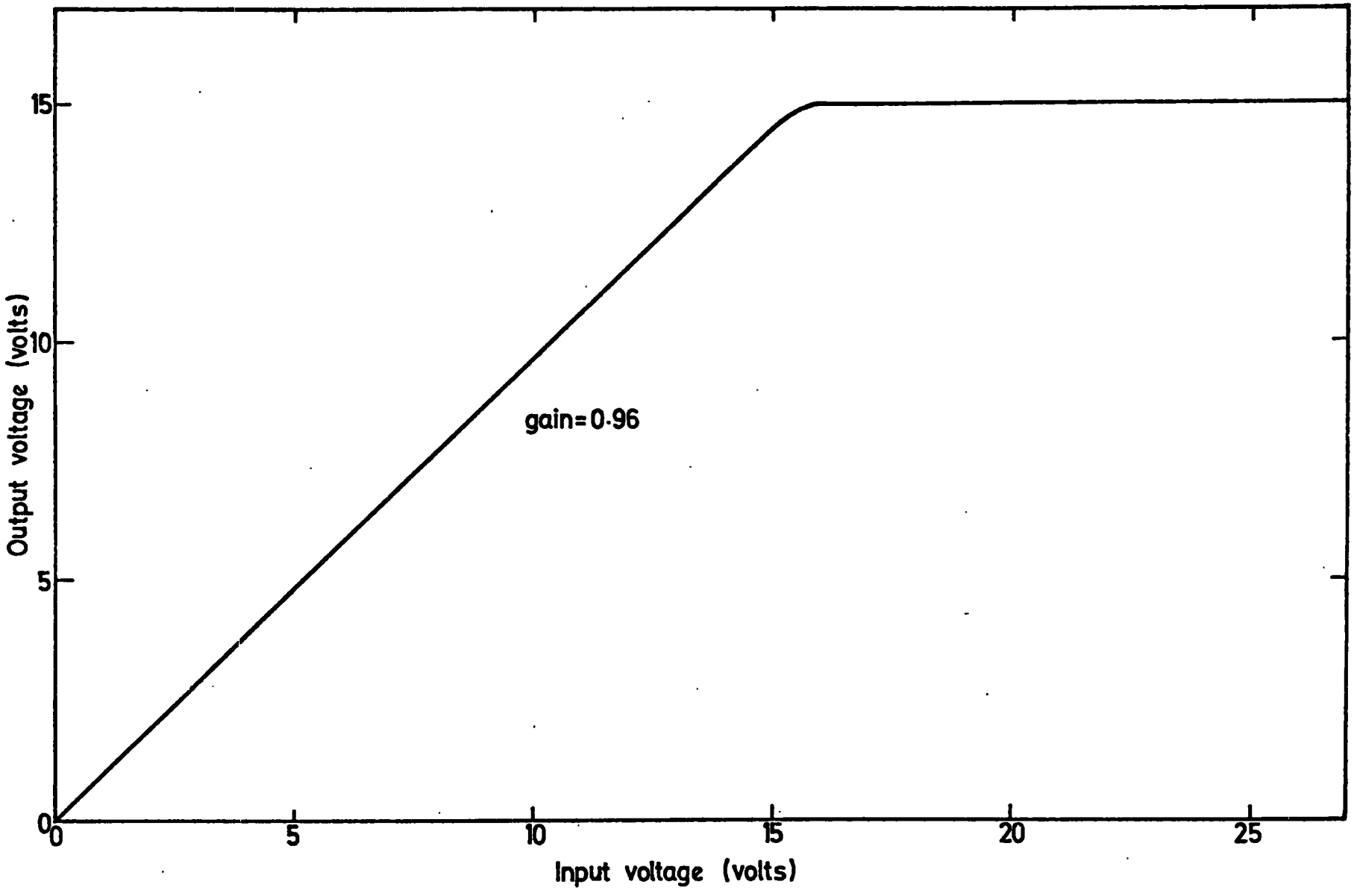

FIGURE 3.7 The dynamic range of the head amplifiers

3.5 THE AIR SHOWER COINCIDENCE-COUNTING SYSTEM

3.5.1 The Coincidence Unit

Output pulses from the discriminators (3 volts positive logic) were fed to a coincidence and anticoincidence unit.

The coincidence unit, Figure 3.8, incorporated four OR gates at the input which served to add the pulses from two adjacent counters. The added pulses were inverted, delayed slightly and shaped to 1 μs, and then fed into an eight input NAND gate. The resolving time of the coincidence circuits was 1 μs. The 3-fold coincidence pulse from the spectrograph was gated to the 5-input NAND coincidence gate without delay.

Air showers are defined by 2, 3 or 4-fold coincidences and the resultant coincidence pulses are recorded on a scalar. A further coincidence of the E.A.S. coincidence pulse with a M.A.R.S. pulse, which defines an E.A.S. muon event, was also registered on a scalar.

3.5.2 The Coincidence Scalar Counter

Figure 3.9 shows the circuit diagram of the multi scalar designed for the purpose of counting the number of showers registered during the experiment. It comprises three individual scalars, each scalar consisting of four BCD counters. The specification of the scalar is that it accepts negative or positive logic pulses with a duration of $\geq$ 500 nsec. The scalar information could be displayed on the display tubes, it being possible to read from any of the three scalars in turn.

3.6 BALANCE AND CALIBRATION OF DETECTORS

Initially, the working voltage of an individual scintillation counter was obtained by measuring the most probable pulse height, h, for various values of the high voltage, V, applied to the photomultiplier tube. The dependence of the output voltage on the E.H.T. is shown in Figure 3.10. Typically, the gain of the photomultiplier tube varies as $V^{6.2 \pm 0.6}$. In

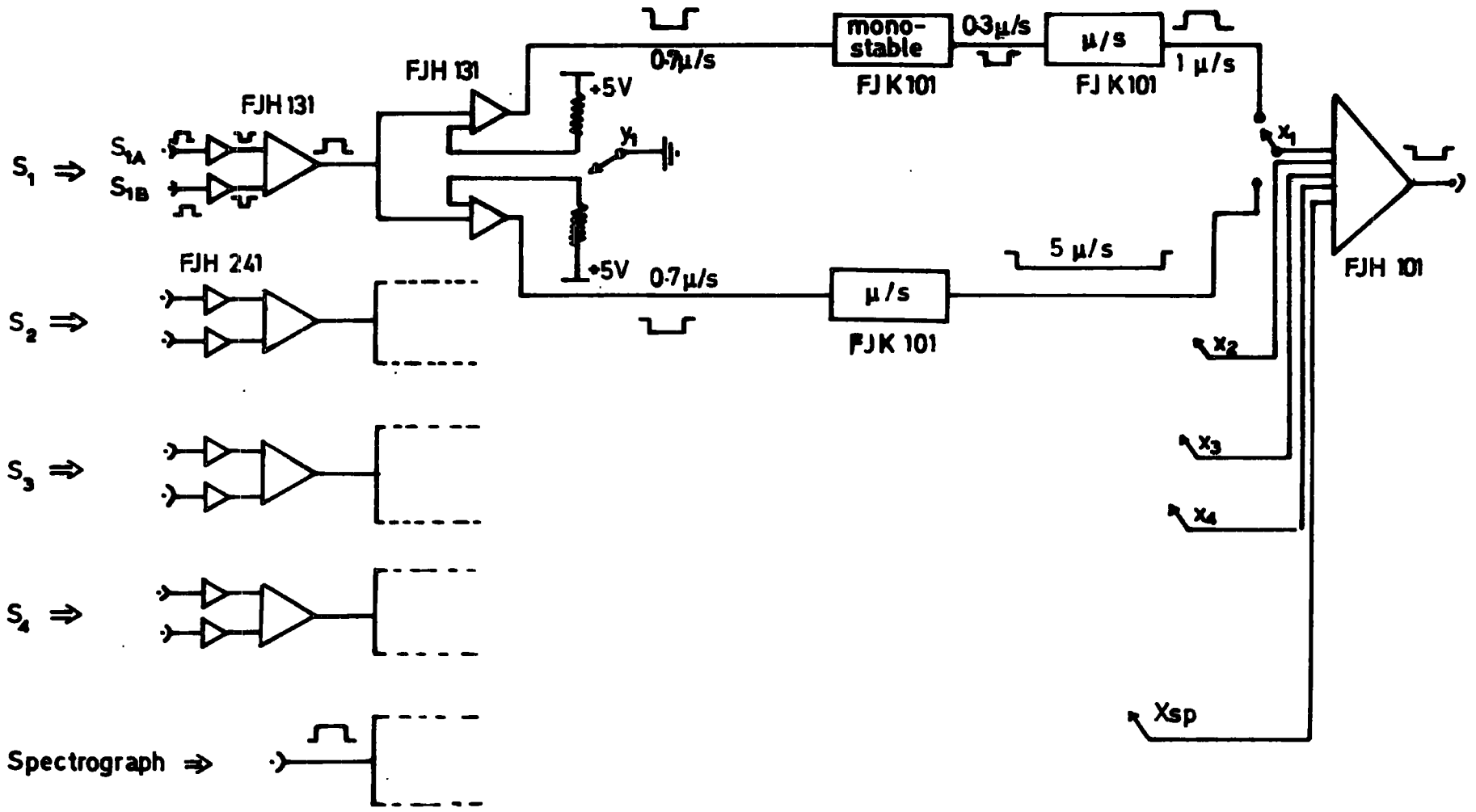

FIGURE 3.8 COINCIDENCE AND ANTICOINCIDENCE UNIT

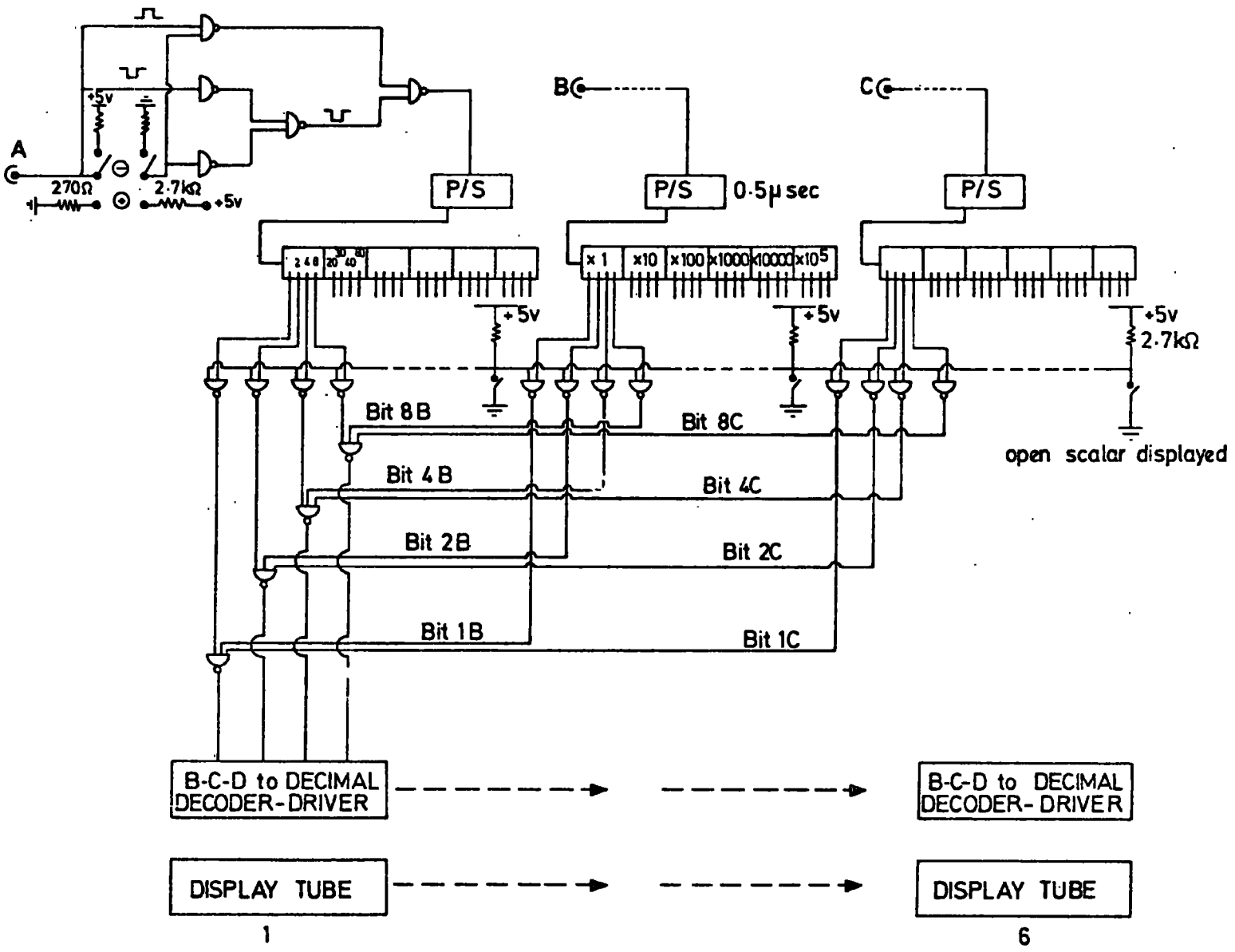

Figure 3.9: The Counter Coincidence Scalars.

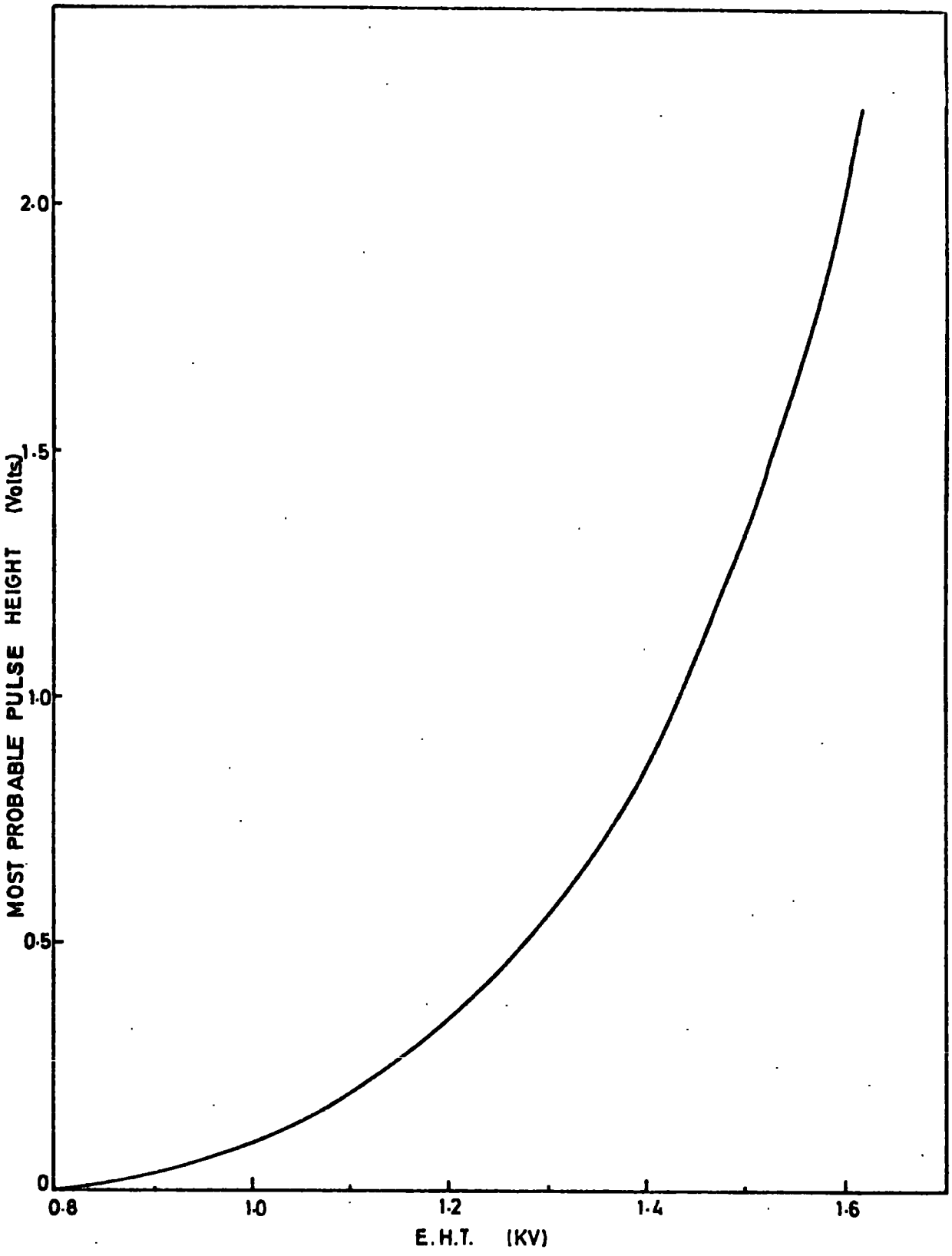

FIGURE 3.10 Variation of the P.M. gain voltage with E.H.T.

order that the output pulses from the scintillation counter be meaningfully interpreted, it is necessary that they be calibrated in terms of the pulse height produced by the vertical traversal of single cosmic ray particles through the sensitive area of the detector. This calibration was accomplished using a small scintillator telescope of sensitive area 9" x 9" (Figure 3.11) to select cosmic ray particles passing through the scintillation counter, the telescope being placed above the scintillator to be calibrated. A differential pulse height spectrum of the pulses from the detector under test was obtained by simply gating detector pulses using the telescope into a 400 channel pulse height analyser (P.H.A.). A typical calibrated pulse height distribution is shown in Figure 3.12 a. The mode of this distribution was taken to be proportional to the mean output pulse height produced by a single shower particle crossing the central region of the counter. By adjusting the high voltage applied to each photomultiplier tube, the gains of the tubes were altered such that the modes of the observed distributions were the same to within $\pm$ 10%. The method used to set the discriminator was to feed the discriminator output pulses into the coincidence gate of the P.H.A. to trigger the undiscriminated output pulses of the same photomultiplier. In this way the differential pulse height spectrum of the cosmic ray particles above a certain threshold was obtained, and the position of the discrimination level could be seen. The discrimination threshold levels were set within the region of minimum noise level of the pulse height distribution which was obtained to be at the 250 $\pm$ 30 mV level. The procedure was repeated for positive, negative and 'reduced' magnetic field of the spectrograph and it was found that there were no significant differences between the calibrations corresponding to each magnetic field direction. The count rate of a single photomultiplier scintillation counter was typically 40-50 sec^{-1}. The integral particle density spectrum for a typical scintillation counter is shown in Figure 3.12 b.

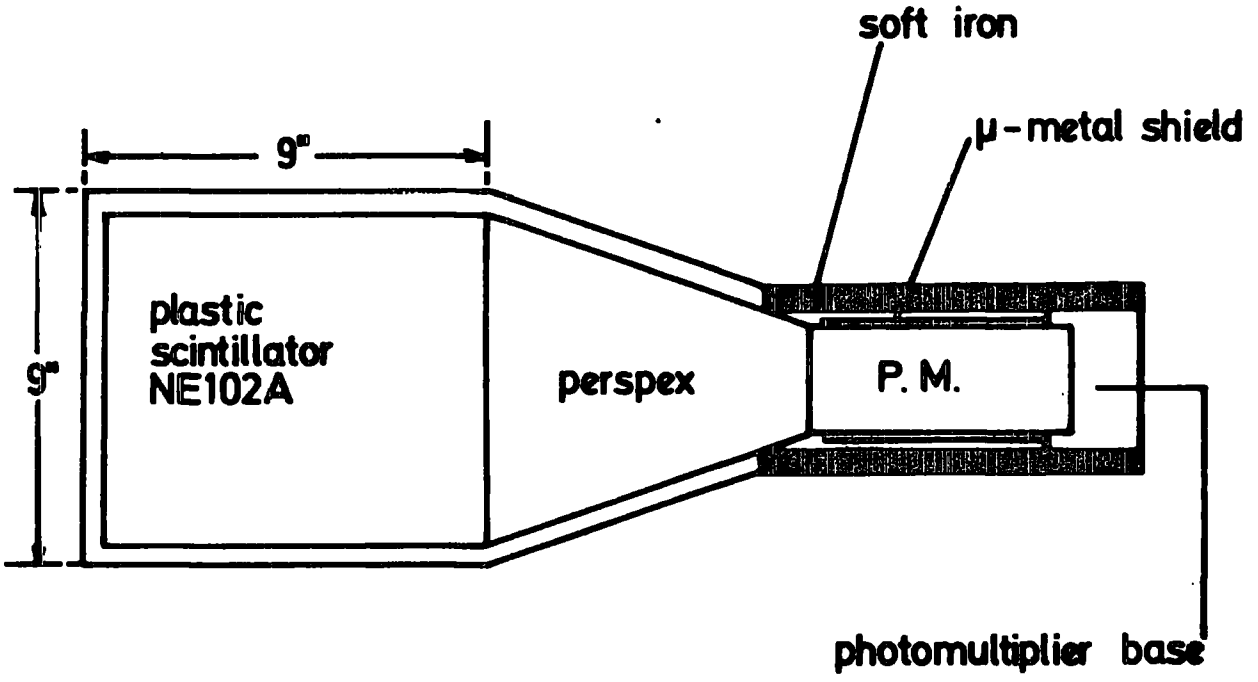

FIGURE 3.11 The Telescope

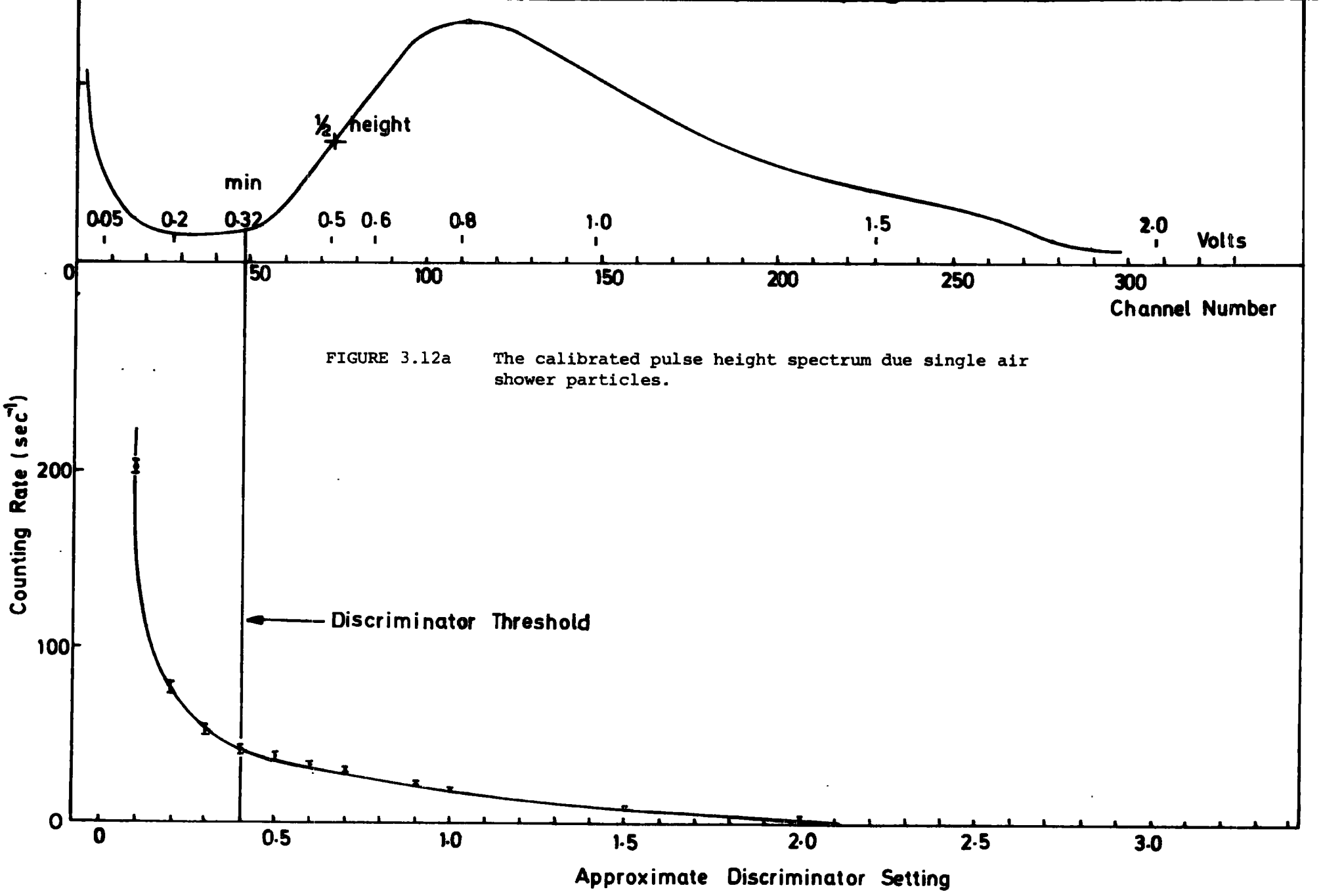

FIGURE 3.12a The calibrated pulse height spectrum due single air shower particles.

FIGURE 3.12b The integral density spectrum of particles in a single scintillation counter.

3.6.1 The Uniformity of the Detectors

The response of the detector to single particles crossing various regions was determined in a preliminary experiment using a scintillator telescope (Figure 3.11) in coincidence with the detector under test. A 400 channel P.H.A. was used to measure the differential pulse height spectrum due to single shower particles traversing the detectors at various places. Figure 3.13 shows a least squares fit to the most probable pulse heights obtained, corresponding to various positions of the telescope, and the detector is seen to have quite a uniform response.

3.6.2 Performance of the Array Detectors

It is essential in air shower experiments to have some knowledge of the response of the arrays to showers that fall around the array detectors. Since each single scintillation counter has been calibrated to give a pulse height equivalent to one or more particle per scintillator area, then the minimum number of particles that can be detected is 2 p/m^2 (the area of one detector is 0.5 m^2). This corresponds to a minimum shower size of $\sim 1 \times 10^3$ particles falling at about one meter from the detector. Showers as large as 10^6 particles could trigger the array if their cores fall closer than 150m from the detector S_4. The median shower size detected by the array depends on the number of detectors employed ; for instance, for 2-fold, 3-fold and 4-fold, coincidence, the median shower sizes that the array responds to are 8.5×10^3, 2×10^4 and 4×10^4 particles respectively. Detailed calculations on the contribution of showers to the measured rate are given in Chapter 4. It is found that for showers in the range $8 \times 10^2 - 10^7$ particles, the main contribution to the observed rates comes from showers which fell with their cores in the region 10-40m from the detector S_4.

3.7 THE EFFICIENCY OF THE SCINTILLATION COUNTERS

In order to obtain the absolute rate of occurrence of air showers

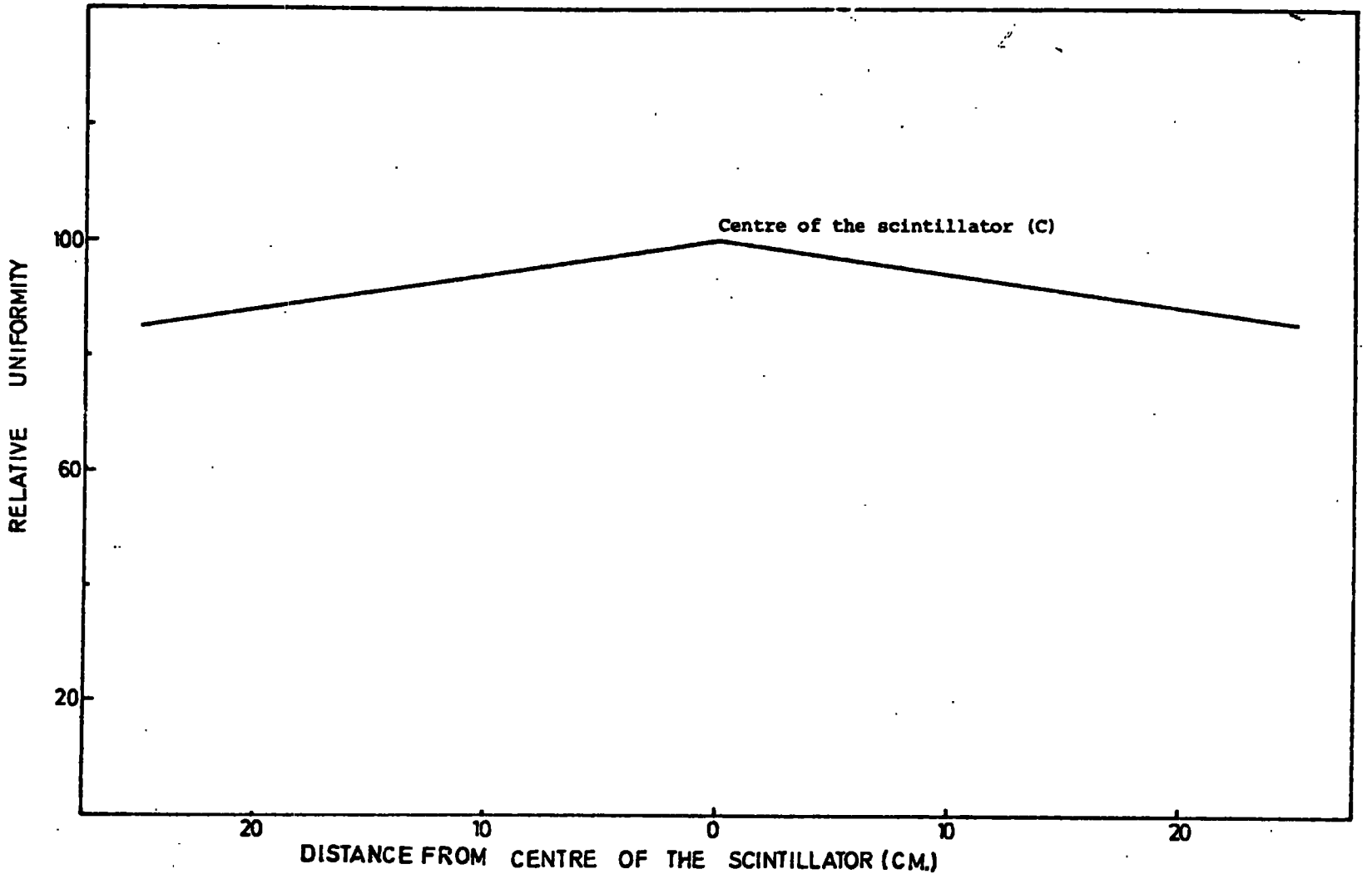

FIGURE 3.13 The uniformity curve of one scintillation counter

detected by the present experiment, the efficiency of the detecting elements of the array must be known. The scintillation counters' efficiencies were obtained by examining the pulse height distributions due to cosmic ray particles traversing the whole scintillation counter and estimating the ratio of the count rate of the detector due to particles producing pulses equal to or greater than the discriminator level to the total count rate expected due to charged particles falling on the counter. The experimental procedure used to obtain the efficiency of the individual scintillation counters was similar to that used for the counters calibration. The small 9" x 9" scintillator telescope was used to select cosmic ray particles passing through the regions $\overline{A}$, $\overline{B}$ and $\overline{C}$ of the plastic scintillator as indicated in Figure 3.14. Then a composite pulse height distribution for the whole area of the counters was obtained by adding the individual pulse height distributions. Table 3.2 shows the efficiencies of the individual counters of the arrays, and also of the combined adjacent scintillators that form one air shower detector level. The detection efficiencies for various detectors' coincidence modes are listed in Table 3.3.

3.8 THE MAGNETIC AUTOMATED RESEARCH SPECTROGRAPH (M.A.R.S.)

3.8.1 General Description

This instrument has been designed and assembled at Durham for the purpose of measuring the vertical cosmic ray muon momentum spectrum up to 5000 GeV/c (Whalley,1974, Piggott, 1975) and the muon charge ratio at sea level (Hume, 1975). The spectrograph has been described in detail in several publications (Ayre, et al, 1969; Ayre, 1971, and Thompson and Wells, 1972). The important characteristics of the spectrograph are listed in Table 3.4. In this section a brief description of the spectrograph is given with particular attention to the parts that are essential or related to the work done in this thesis.

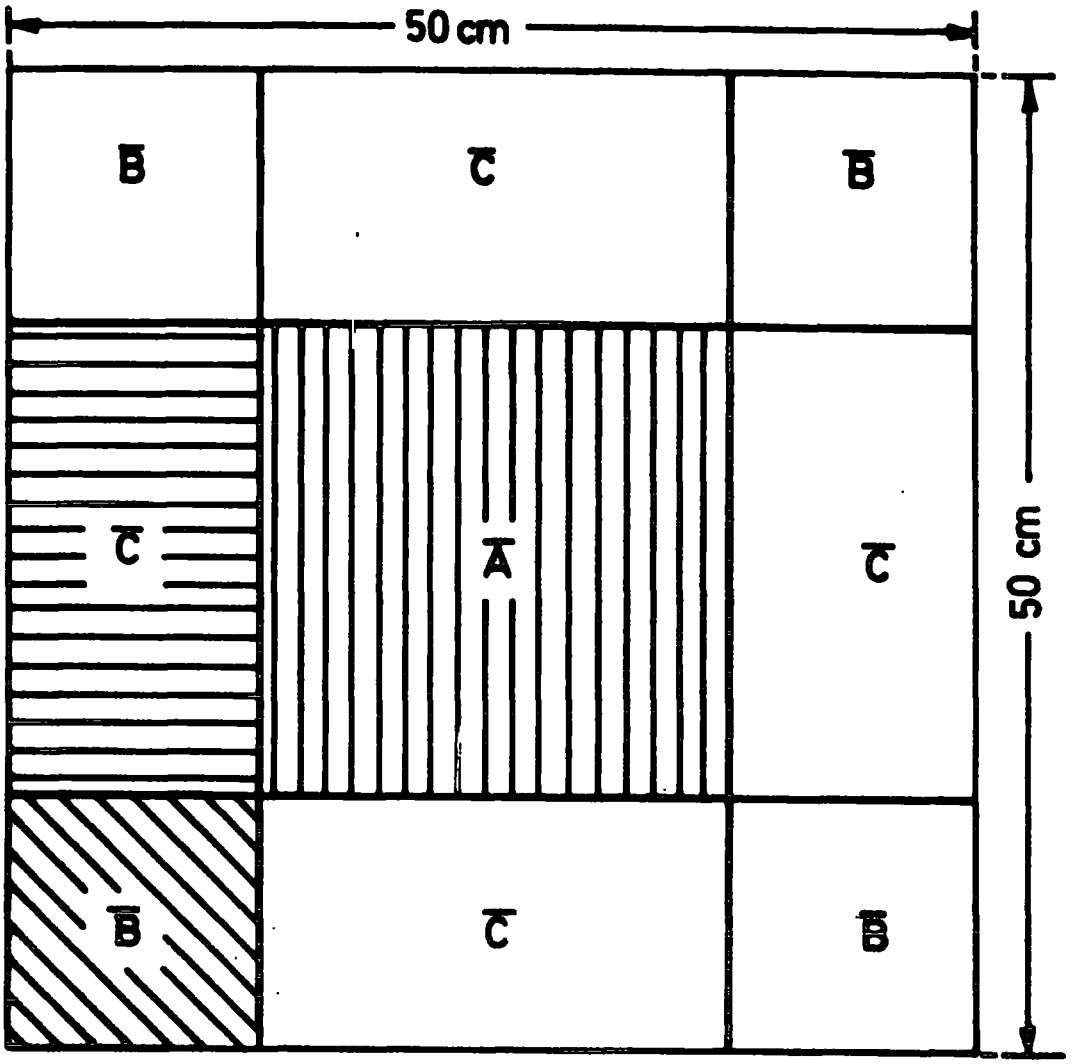

FIGURE 3.14 Schematic diagram shows the shaded regions $\bar{A}$, $\bar{B}$ & $\bar{C}$ which have been used to obtain the compositepulse height distribution curve.

Detector	S_1		S_2		S_3		S_4	
Individual Scintillators	S_1A	S_1B	S_2A	S_2B	S_3A	S_3B	S_4A	S_4B
	98.4 ±1.1	95.9 ±1.0	98.1 ±1.1	96.9 ±1.1	96.2 ±1.1	93.3 ±1.1	97.9 ±1.1	98.4 ±1.1
	97.2 ± 0.8		97.5 ± 0.8		94.8 ± 0.8		98.2 ± 0.8	

TABLE 3.2: The measured efficiencies of the air shower detectors (individual scintillators and the whole detector)

TABLE 3.3

THE MEASURED EFFICIENCIES OF EACH FOLD OF COINCIDENCE COUNTERS WITH AND WITHOUT SPECTROGRAPH

Fold of coincidence	% efficiency	Fold of coincidence with spectrograph	% efficiency
$S_3 + S_4$	93.01 ± 1.03	$S_3 + S_4 + S_p$	83.063 ± 0.94
$S_2 + S_4$	95.67 ± 1.05	$S_2 + S_4 + S_p$	85.43 ± 0.96
$S_1 + S_2$	94.71 ± 1.05	$S_1 + S_2 + S_p$	84.58 ± 0.96
$S_1 + S_4$	95.37 ± 1.05	$S_1 + S_4 + S_p$	85.65 ± 0.96
$S_2 + S_3$	92.37 ± 1.03	$S_2 + S_3 + S_p$	82.49 ± 0.94
$S_1 + S_3$	92.07 ± 1.03	$S_1 + S_3 + S_p$	82.22 ± 0.94
$S_1 + S_3 + S_4$	90.37 ± 1.22	$S_1+S_3+S_4+S_p$	80.7 ± 1.1
$S_2 + S_3 + S_4$	90.67 ± 1.22	$S_2+S_3+S_4+S_p$	80.97 ± 1.11
$S_1 + S_2 + S_4$	92.95 ± 1.25	$S_1+S_2+S_4+S_p$	83.01 ± 1.13
$S_1 + S_2 + S_3$	89.75 ± 1.21	$S_1+S_2+S_3+S_p$	80.14 ± 1.1
$S_1+S_2+S_3+S_4$	88.1 ± 1.37	$S_1+S_2+S_3+S_4+S_p$	78.67 ± 1.23
Spectrograph	89.3 ± 0.2		

$\int Bdl$		$= 8\ wm^{-1}$
Acceptance (single muons)	:	$= 0.0408\ m^2\ sr$
Magnet: weight	:	= 284 tons
overall height	:	= 7.6 metres
width	:	= 2.16 metres
depth	:	= 3.66 metres
Power consumption	:	= 100 A at 100 V
Maximum detectable momentum	:	= 5,000 GeV/c
Minimum momentum required to traverse spectrograph	:	= 7 GeV/c
Momentum selector	:	50% cut off low momentum particles at 200 GeV/c full acceptance above 310 GeV/c.
Three-fold trigger rate (7 GeV/c)		$\simeq 28\ min^{-1}$

TABLE 3.4: The main characteristics of the spectrograph.

The principle of operation of the spectrograph is to observe the deflection of a charged particle that is subjected to a magnetic field, and to relate this deflection to the momentum of the particle. Essentially, M.A.R.S. is a multi-layer type spectrograph, consisting of four rectangular iron blocks providing four regions of magnetic field which deflect the penetrating charged particles. There are two similar sides of the spectrograph (these being called the blue and red-sides) shown in Figure 3.15. In this diagram the front and the back planes of the spectrograph are shown. The blue-side of the spectrograph has been used in both the experiments described in the present work to study some aspects of muons associated with E.A.S.

3.8.2 The Detecting Elements of the Spectrograph

The detecting elements are the following :-

a) The scintillation counters. In both sides of the spectrograph scintillation counters are placed at the so called levels 5, 3 and 1, effectively at the top, middle and bottom of the magnet. The scintillators detect the passage of a muon through the spectrograph, and they are each of size 133 x 75 x 2.5 cm^3, being NE 102a plastic scintillator material. Each scintillator slab is viewed by four photomultiplier tubes (type 53 AVP), two photomultipliers viewing each end via a triangular shaped Perspex light guide (see Figure 3.16). The two resulting added pulses from each diagonally opposite pair are amplified, discriminated and fed to a 2-input coincidence gate. The resulting pulses from the detectors in the three levels of the magnet are then fed into a 3-input coincidence gate, whose output pulse indicates the passage of a particle through the spectrograph. This pulse is the main trigger pulse of the spectrograph and has been used to link the air shower experiments with the blue-side of the spectrograph.

The efficiency of the scintillation counters of the spectrograph has been measured by Whalley (1974), and the overall efficiency of the system is (0.894 $\pm$ 0.002)%.

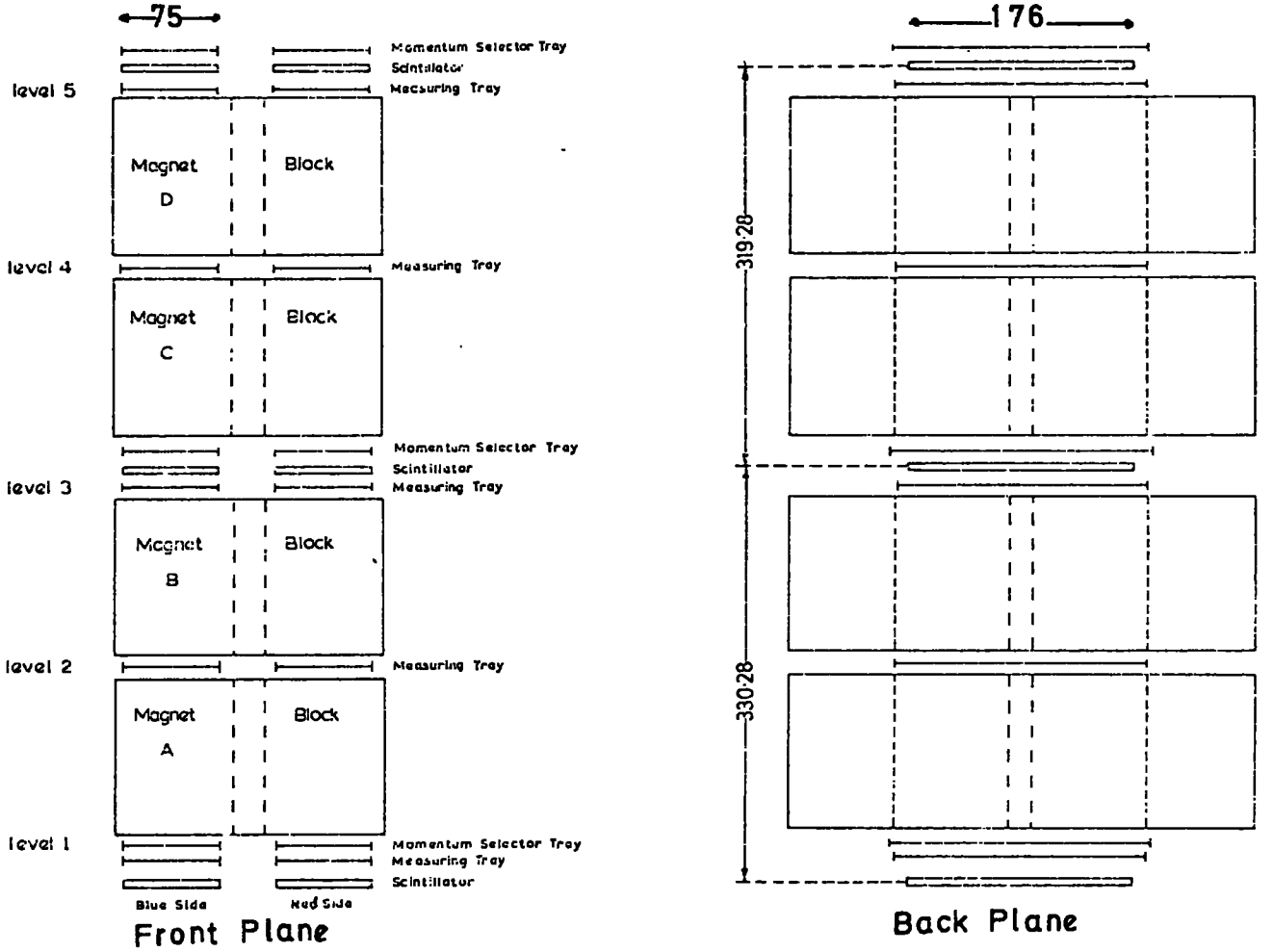

FIGURE 3.15 The M.A.R.S. Spectrograph, dimensions between scintillators are given in cm.

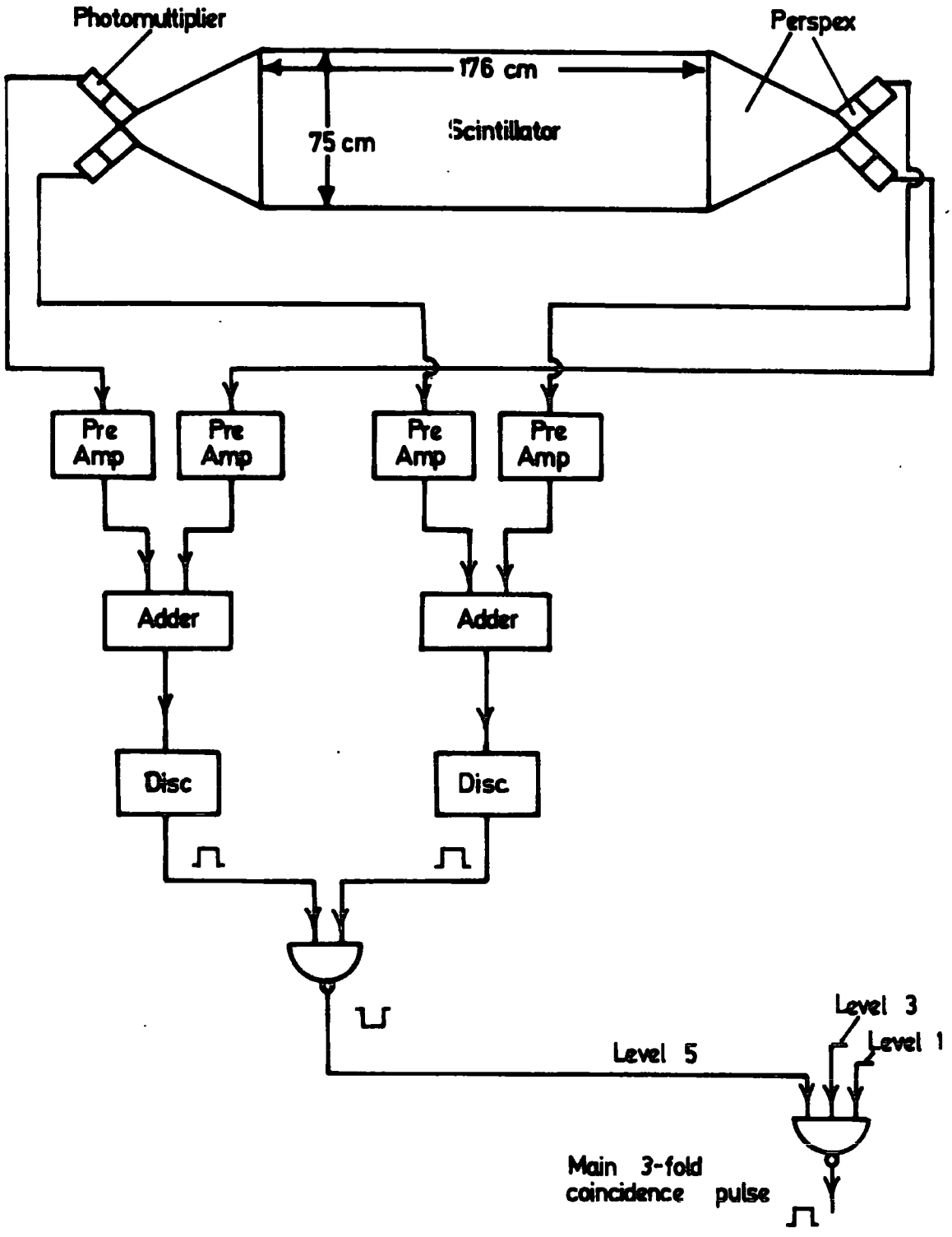

FIGURE 3.16 Schematic diagram of the spectrographs 3-fold scintillator system (After Hume, 1975).

b) The neon flash tube arrays. The second type of detecting elements are the trays of neon flash tubes that define the muon trajectories. In one side (the blue-side) of the spectrograph two types of flash tubes are used. The first type are in the momentum selector trays, each tray containing 204 tubes in four layers (each tube has an internal diameter of 1.53 cm. filled with commercial neon gas at 0.8 atmosphere).

The second type of flash tube used are in the measuring trays which contain tubes of diameter 0.55 cm. and each tray consists of 712 flash tubes arranged in eight layers. The neon flash tubes are digitised according to the method of Ayre and Thompson (1969). Digitised information is sent to an on-line IBM 1130 Computer for storage and subsequent analysis.

3.8.3 The Triggering and Pulsing Systems of the Spectrograph

The passage of a muon through the spectrograph is detected by the three scintillation counters in the top, middle and bottom levels of the magnet. Within 2 μsec. of the particles traversal of the spectrograph a high voltage pulse ($\sim$5 kV) is applied to the neon flash tube trays in the spectrograph using a high voltage spark-gap and a constant delay line. Since there are two types of flash tube trays, two spark gaps are used, one to pulse each type.

3.8.4 The Momentum Selector System

This system has been designed (Ayre et al, 1972) for the purpose of selecting particles of high momentum ($\gtrsim$ 70 GeV/c). It consists of trays of neon flash tubes (momentum selector trays) and probes to provide the digitisation for the pulses. The points across the width of trays where the particle traversed each of the trays in the spectrograph are determined using electronic circuitry and subsequent circuitry decides whether or not the particle was of high momentum. When a high momentum event has been detected the system initiates the storing of data from the flash tubes in

the measuring trays. The data from the trays consists of the column numbers of the discharged tubes, the discharged tubes themselves and other subsidiary information such as the number and time of the event, the magnetic field direction and atmospheric pressure. All these data are fed into a memory core store. After storage of one event has been completed in the core store, the on-line computer is interrupted and the data are transferred to a magnetic disc for subsequent analysis. A detailed description of the procedure of selecting high momentum particles using this system is given in Hume (1975) and Piggott (1975).

For the purpose of measuring the muon lateral distribution in E.A.S. at various muon energies which is described in the second part of this thesis, muon events of low momenta (7-100 GeV/c) have been transferred to the computer and also stored.

3.8.5 The Acceptance of the Spectrograph for Muons Accompanied By Air Showers

The acceptance of an instrument exposed to a certain flux of particles is defined as the ratio of the observed rate (R) of particles traversing the instrument to the incident flux (I_o). Simply, this relation can be written as follows :

$$\text{Acceptance} = \frac{R(\sec^{-1})}{I_o(m^{-2}\ \sec^{-1}\ sr^{-1})} \quad m^2.\ sr. \qquad (3.1)$$

In the case of M.A.R.S., as a consequence of the muon trajectory having been bent by the spectrograph magnetic field, this acceptance will become a function of momentum and hence of the incident zenith (θ) and azimuthal (ϕ) angles in the bending and side planes of the spectrograph. Two methods have been employed to work out the acceptance of the spectrograph. The first is analytical (Whalley, 1974, and Hume, 1975) in which the acceptance of the spectrograph for single associated muons has been obtained, and the

second is a Monte Carlo technique (Hawkes, 1977) which is used to give a solution for the acceptance of the spectrograph that satisfies the experimental conditions considered in Chapters 3 and 5.

In both of the experiments described in this thesis, the muon is always accompanied by a shower and hence the muon traverses either trays 1 - 4 or the detecting elements in levels 1 - 3 of the blue-side of the spectrograph as explained in Chapters 3 and 6. Figure 3.17a,b, shows the two categories of triggering requirements for the spectrograph used in the present work, shown in both bending and back planes. From the figure it can be seen that the muon trajectories that are defined as being within the measuring tray at level 4 and the scintillation counter at level 1,when projected back to the plane of the measuring tray at level 5 in both the bending and the back plane of the blue-side of the spectrograph (as is demonstrated in Figure 3.17a), lead to an increase in the sensitive area of the top measuring tray. A similar fact is illustrated in Figure 3.17b for muon trajectories that are defined to be within the scintillation counters at levels 3 and 1. An allowance for the increase of both categories of acceptance was made to the computer model of the spectrograph following the work of Hawkes (1977). The Monte Carlo technique was used to simulate particles over this increased area for both categories. In the above mentioned technique a computer random number generator was used to simulate the air shower particle flux modulated by $\cos^n\theta$ (where θ is the shower's zenith angle of incidence and n is the shower's angular exponent).

The acceptance of one side of the spectrograph at a particular value of muon momentum is obtained as follows :-

$$\text{Acceptance} = 2\pi A \times \frac{S}{T} \int_0^{30} \cos^{n+1}\theta \sin\theta \, d\theta \qquad (3.2)$$

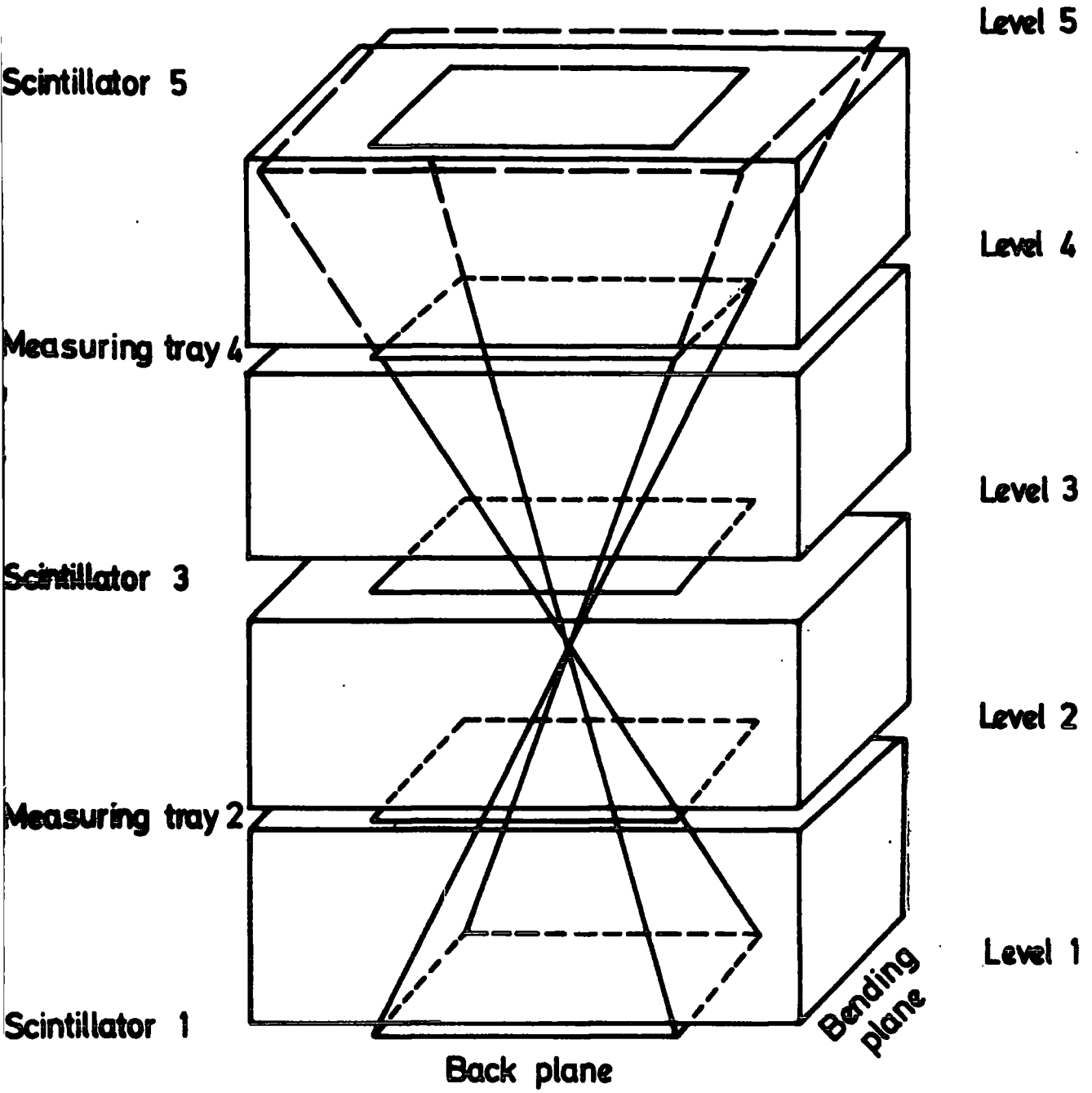

FIGURE 3.17a Illustration of the 1-4 tray category acceptance of the blue-side of M.A.R.S.

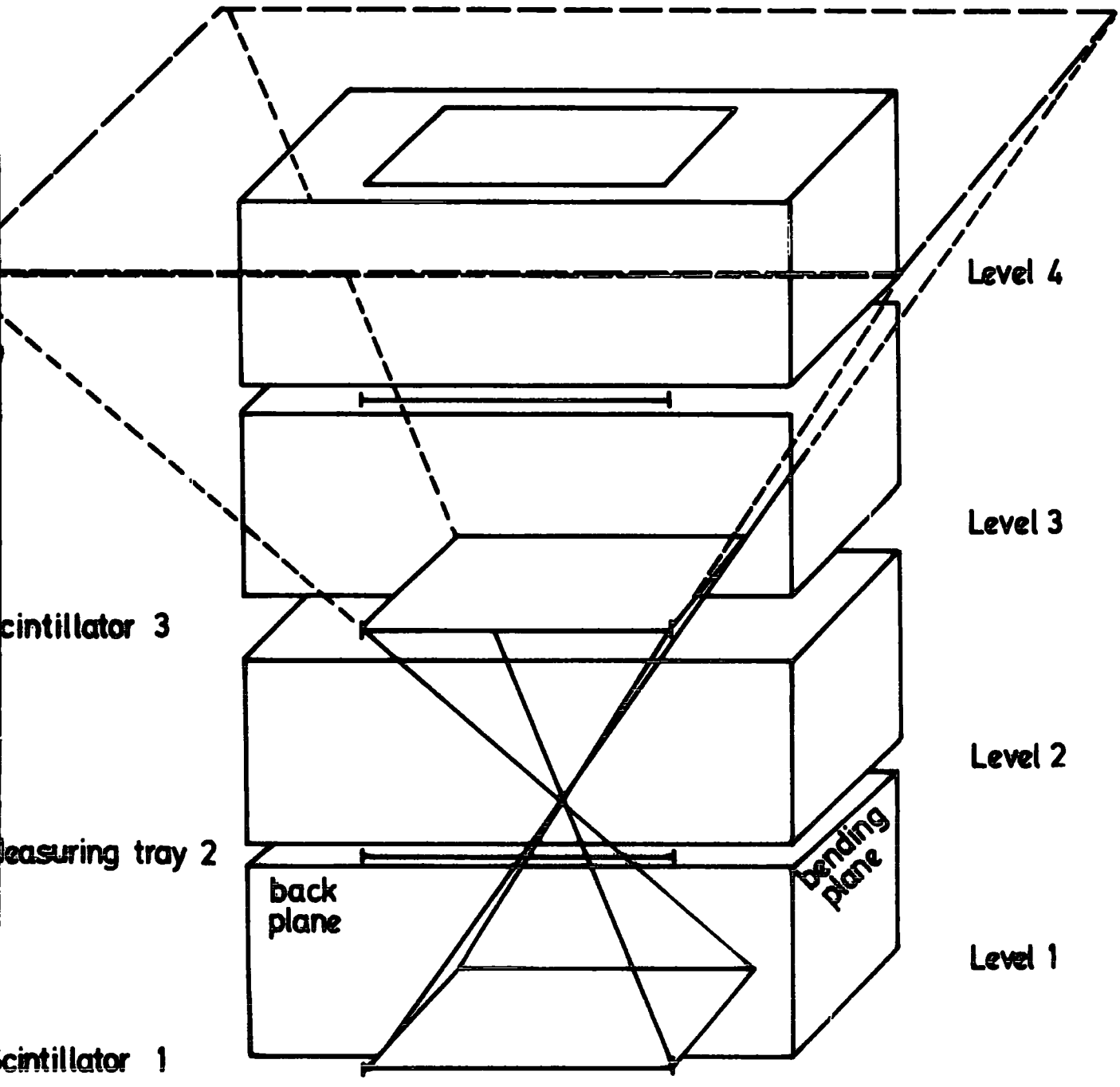

FIGURE 3.17b Illustration of the 1-3 tray category acceptance of the blue-side of the spectrograph.

where S is the number of particles which pass through the spectrograph successfully out of T incident particles, and A is the geometrical area of the spectrograph detecting elements for vertically incident particles.

Solving the integral in equation 3.2 for θ gives :-

$$\text{Acceptance} = 2\pi A \times \frac{S}{T} \quad \frac{1 - \cos^{n+2} 30}{n + 2} \tag{3.3}$$

and substituting the value of A = 1.32 m^2 and n = 10 which correspond to showers detected by the present array (Smith, 1977) gives :-

$$\text{Acceptance} = 0.57 \times \frac{S}{T} \ m^2 sr \tag{3.4}$$

In the computer simulations of the particle trajectories, the deflections of the muons are considered along with the energy loss of the muons as they traverse the iron. The particles are required to remain within the defining trays and detectors of the spectrograph. Figure 3.18 shows the calculated acceptance for the two categories used in the present work (1 - 4 and 1 - 3 tray acceptances). It can be seen from this figure that the acceptance levels off at around 20 GeV/c and 10 GeV/c for the 4-tray and 3-tray acceptance categories respectively. It has also been found that the variation of the absolute value of the acceptance in each category with values of n ranging from 8 to 12 is smaller than the statistical error obtained.

3.9 OPERATIONAL DETAILS OF THE EXPERIMENT

The design and the final setting of the experiment ensure that variations in the supply voltages and temperature changes of the equipment would not affect the proper operation of the experiment. Daily checks on the counting rate of individual detectors and the counting rate of the

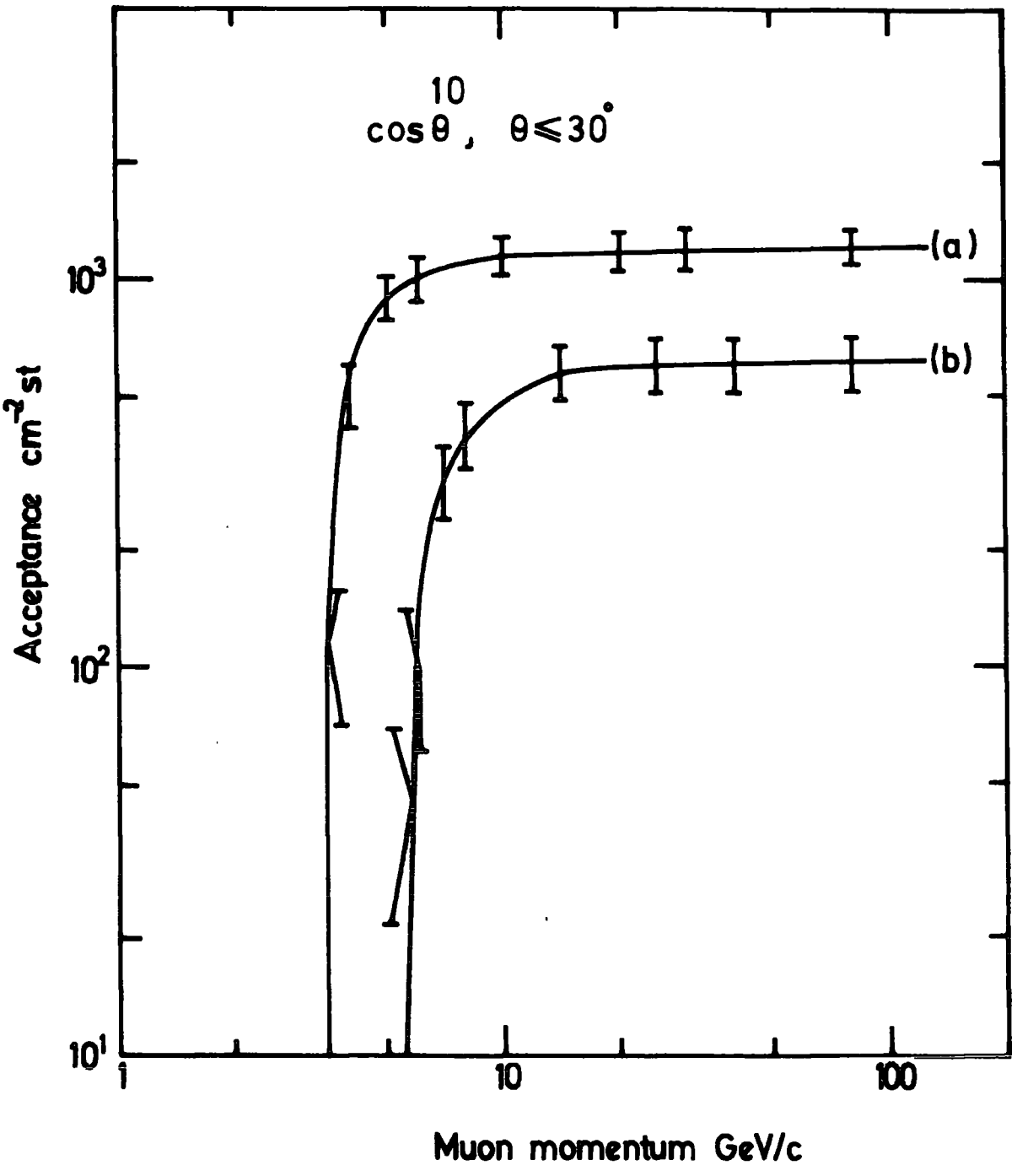

FIGURE 3.18 The spectrograph acceptance obtained by employing the Monte Carlo technique.
Category (a) is for 1-3 tray acceptance and (b) for 1-4 tray acceptance.

detectors in various coincidence arrangements were made every morning during the period of operation.

Initially some electrical pick-up was encountered during the operations of the experiment from October to December 1972 and this was due to electrical interference arising from one of the M.A.R.S. triggering spark gaps. So, during this period the experiment was run only when the spark gap was out of action. Eventually the pick-up problem was solved by a proper shielding of all cables around the spark gap region.

During the operation of the experiment the daily variation of the coincidence counting rates of the detectors of the apparatus were checked, due allowance being made for the variation of the rate with atmospheric pressure.

The experiment has two main data sets, the first one containing the shower coincidence rates, and the second constitutes the observed rates of muons of energies $\geq$ 5 GeV/c accompanied by showers.

CHAPTER FOUR

THE RATES OF MUONS AND AIR SHOWERS

4.1 INTRODUCTION

The running of the M.A.R.S. spectrograph in coincidence with the simple arrangement of the array of air shower detectors described in Chapter 3, was basically aimed at determining the rate of muons traversing the spectrograph (under the conditions of a full magnetic field) in association with air showers and carrying out some investigations on small air showers of sizes 10^3 - 3 x 10^5 particles at sea level using the same array of air shower counters. Determination of the expected rate of muons was achieved making use of the sea level shower size spectrum and two empirical functions describing the lateral structure of the electrons and muon componentsof E.A.S.

Besides the muon rate experiment, investigations of small air showers recorded by the counter arrangement involved measurements of the shower rates, the shower density spectrum, the"decoherence curve" and the exponent of the zenith angle distributions of the recorded showers. Consequently, an attempt was made to produce the integral shower size spectrum in the size range 10^3 - 3 x 10^5 particles. Theoretical considerations and predictions of the rates of registered showers are presented in this chapter.

4.2 DATA COLLECTION

The present experiment was operated for a period of six months during which time showers of varous sizes having particle densities ≥ 2 p/m^2 at each detector were recorded using two modes of operation

of the apparatus. One mode involved the running of the shower array in conjunction with the blue-side of the M.A.R.S. spectrograph, the other mode involved the recording of showers alone. Two major sets of data were thus collected, the first concerned with the measurements of the rate of E.A.S. muons having energies $\gtrsim$ 5 GeV and the second concerned with the measurements of air shower rates. Table 4.1 gives a summary of the total number of events collected in each set and the total sensitive time of the apparatus. Details of the individual numbers of recorded showers for various coincidence arrangements of the air shower detectors with and without the spectrograph are given in Section 4.7.

4.3 SYSTEMATIC AND STATISTICAL CORRECTIONS OF DATA

4.3.1 E.A.S. Muon Events

The spectrograph was not designed originally to study air shower muons or to be used in air shower experiments. As a consequence considerable difficulty was experienced in interpreting the data which are contaminated in many ways, for example, by side showers and bursts. The rate of side showers and other contaminating events is expected to be significantly high compared with the rate of genuine muon events. This can be seen from the computer "pictures" of the spectrograph events recorded with a simple coincidence between air shower detectors and the spectrograph. Since there were no computer "pictures" of the present data, study of the spectrograph shower events were made using former coincidence experiments performed with the spectrograph. The first of these experiments was a coincidence between the central detector C (of the air shower array to be described in Chapter 5) and the spectrograph while the second involved a coincidence of M.A.R.S. and detectors

TABLE 4.1 : Summary of the total number of events collected by the experimental set up.

	Mode of Operation	Total Number of Events	Total Running Time (h)
Muons in E.A.S.	Coincidence of shower counter and M.A.R.S.	12386	864.9
Showers	Coincidence of shower counters only	306946	903.4

C + 12 + 32 + 61 (See Chapter 5). The selection criteria applied to the data was that, for a genuine muon shower event, the muon must pass through at least three flash tube trays in levels 3, 2 and 1 and a shower triggers the top flash tube tray (level 5). The results of the examination of the two test runs are presented in Table 4.2. It is clear from the table that the events not satisfying the selection criteria (i.e. unresolved events) amount to ∿ 71% of the data. The percentage does not vary according as a single shower counter or a group of counters is used in the coincidence arrangement. The total error on this contribution is estimated to be ∿ 11% which is greater than the statistical errors due to an additional error arising as a result of the judgement of some events. The effect of accidental counting rates in the above triggers is calculated and found to be negligible.

4.3.2 Accidental Coincidences

In coincidence experiments, it is important to minimize the effect of accidental coincidences such that the rate of spurious events recorded as genuine ones will be negligible. An array of n detectors feeding pulses into a coincidence unit of a resolving time τ μsec, and having rates for each detector $R_1, R_2, R_3 \ldots R_n$, has an accidental coincidence rate given approximately by

$$R_{acc}(n) = n! R_1 R_2 R_3 \ldots R_n \tau^{n+1} \quad \text{sec}^{-1} \qquad (4.1)$$

Since the average rate of a single counter ranges from 80-100 counts/sec. and the resolving time of the coincidence unit used is nearly 1μsec., the accidental counting rates of various sets of coincidences can be estimated from equation 4.1 and the results are tabulated in Table 4.3.

TABLE 4.2 : Examination of the M.A.R.S. computer plots of 854 Muon Events selected from two modes of coincidence with air shower detectors.

Coincidence Mode	C + M.A.R.S.	C + 32 + 12 + 61 + M.A.R.S.
Number of muon events crossing the lower half of the spectrograph	143	106
Number of unresolved events	351	254
Total	494	360
Unresolved events (percentage of the total)	71.05 $\pm$ 3.8%	70.56 $\pm$ 4.4%

TABLE 4.3

The estimated rate of chance coincidences calculated for three orders of coincidence assuming a mean rate of 90 counts/sec. per detector.

Order of Coincidence	Accidental Rate $R_{acc}(n)$ min^{-1}
2-fold	9.7×10^{-1}
3-fold	1.32×10^{-4}
4-fold	1.58×10^{-8}

It can be seen from Table 4.3 that the accidental rate in case of two-fold coincidence counters is larger than that predicted for three-fold or four-fold coincidence and it amounts to (7-12) % of the measured two-fold coincidence rate ; the latter has been corrected for this effect. The estimated three-fold and four-fold accidental counting rates are 1.32×10^{-4} and 1.58×10^{-8} per min : since the slowest three-fold rate was 3.1/min, accidental counts were always negligible.

4.3.3 The Barometric Effect

It is well known that the cosmic ray intensity varies with atmospheric pressure at the level of observation, this variation can be expressed as follows:

$$I = I_o \exp - \beta (P-P_o) \quad m^{-2}.sec^{-1}.st^{-1} \qquad (4.2)$$

where I is the cosmic ray intensity at pressure P, I_o is the intensity at standard atmospheric pressure P_o (76 cm.Hg) and β is the barometric

pressure coefficient. A mean value of β of $\sim$ 10% per cm.Hg (Galibraith, 1958 and Murdoch, 1958) has been used to correct the measured air shower rates to a standard atmospheric pressure by employing equation 4.2. Figure 4.1 shows the pressure variation of the four-fold coincidence rates obtained from a series of independent observations.

4.3.4 Detector Efficiency

The efficiency of each detector was obtained experimentally as explained in Section 3.7. Correcting the measured rates for the detector efficiencies requires the knowledge of the number of detectors struck by the shower simultaneously, thus the corrected rate in this case can be obtained as follows :

$$R_c(n) = \frac{R(n)}{E_1 \times E_2 \,..\, E_n} \quad \text{sec}^{-1} \qquad (4.3)$$

where R(n) is the observed rate of the n-fold coincidence detectors whose efficiencies are E_1, E_2 .... E_n. In a similar manner the E.A.S. muon rates have been corrected by considering the three-fold detectors efficiency of the blue-side of the spectrograph.

4.4 PREDICTIONS OF THE COINCIDENCE RATE OF MUONS ASSOCIATED WITH AIR SHOWERS

The rate of muons in E.A.S. can be calculated from the knowledge of the sea level shower size spectrum and the probability of a muon passing through the spectrograph in association with an air shower. As has been explained in Chapter 3, for an E.A.S. muon event to be recorded by the apparatus a muon must penetrate the spectrograph (i.e. trigger the scintillation counters at levels 3 and 1) while a shower triggers the scintillation counter in level 5. Thus, it is always

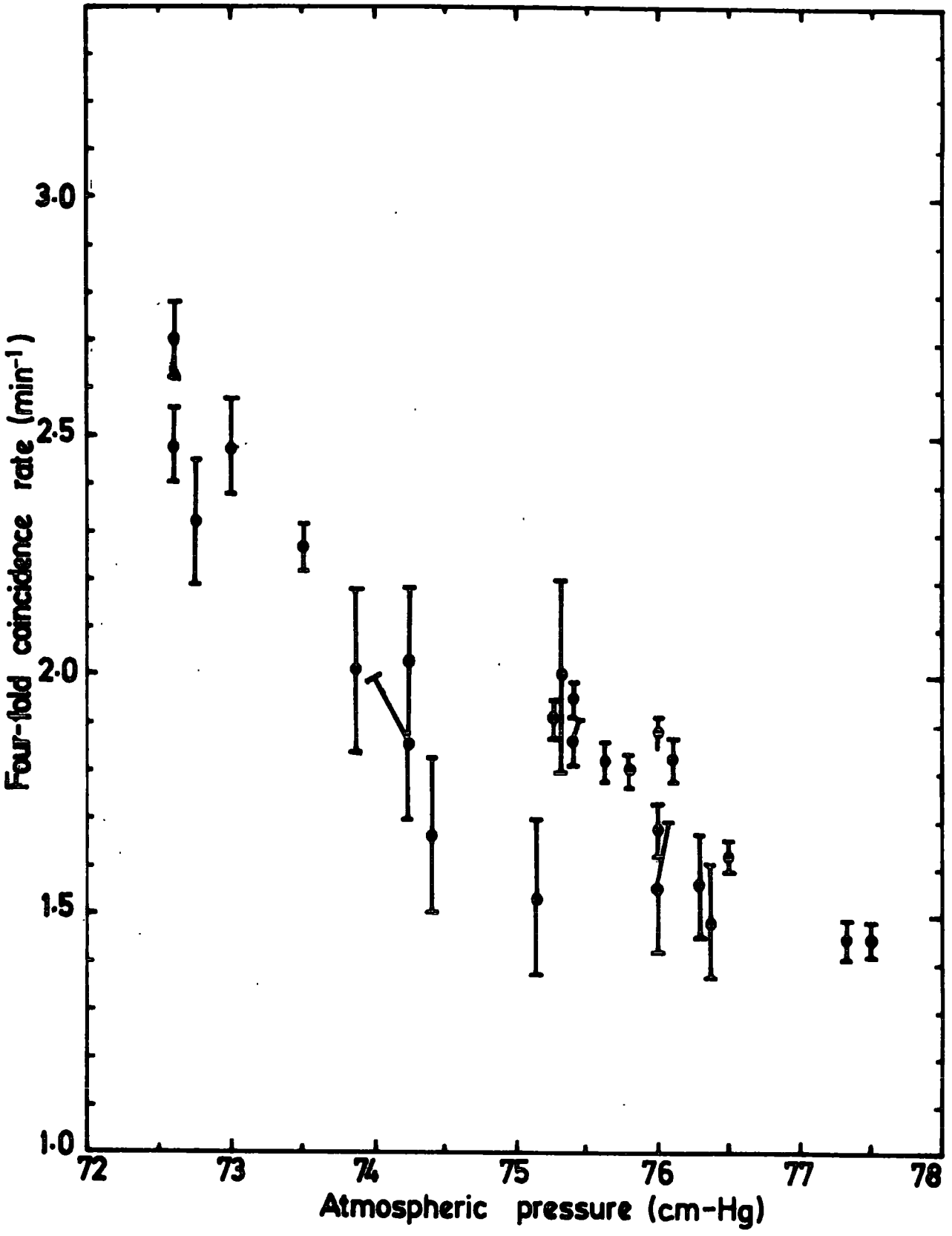

FIGURE 4.1 The pressure variations of observed showers.

required that the counter in level 5 is struck by shower particles. This is shown schematically in Figure 3.17b. The acceptance of the spectrograph in this case is that explained in section 3.8.5. The estimated value of the acceptance at muon energy > 5 GeV is 0.09 $\pm$ 10% $m^2 sr$. The sea level shower size spectrum employed is that derived from the sea level survey of Bell (1974) (See Figure 2.7). According to the survey the integral shower size spectrum is as follows :

$$F\ (>N) = 63.0 \times N^{-1.50} \quad \text{for} \quad N<7\times10^5 \tag{4.4}$$

and

$$F\ (>N) = 8.50\times10^4 \times N^{-2.034} \quad \text{for} \quad N>7\times10^5 \tag{4.5}$$

where F (>N) is units of $m^{-2}\ sec^{-1}\ sr^{-1}$.

The errors on the constant were estimated to be 6%. The differential shower size spectrum, F(N), can then be expressed as follows :

$$F(N)dN = 94.5 \times N^{-2.5} \quad \text{for} \quad N<7\times10^5 \tag{4.6}$$

and

$$F(N)dN = 1.725 \times 10^5 \times N^{-3.034} \quad \text{for} \quad N>7\times10^5 \tag{4.7}$$

To estimate the detection probabilities of E.A.S. muons empirical formula are used to represent the lateral structure of the electrons and muons in E.A.S. at sea level as suggested by Greisen (1960). These expressions are given in equations 2.4 and 2.10 respectively. Evaluation of the detection probability can be explained as follows :

The probability of detecting an air shower $P_e(n)$ by a number (n) of detectors can be written as :

$$P_e(n) = \left(1 - \exp\left\{ - \rho_i(r_i, N_e)\ S_i \right\} \right)^n \tag{4.8}$$

where $\rho_i(r_i, N_e)$ is the density (m^{-2}) of a shower of size N_e particles falling at a distance r (m) from the ith detector whose sensitive area $S_i(m^2)$. The probability of detecting a muon passing through the spectrograph is given by

$$P_\mu\ (\geq E_\mu \text{GeV}) = \left\{ 1 - \exp \left\{ - \rho_\mu(r_\mu, Ne, \geq E_\mu \text{GeV}) S_\mu \right\} \right\} \qquad (4.9)$$

where $\rho_\mu(r_\mu, Ne, > E_\mu)$ is the density of muons with energies not less than E_μ(GeV) in a shower of size N_e falling at a distance r_μ(meter) from the spectrograph and S_μ is the geometrical detecting area of the spectrograph which is simply the area of a scintillation counter (1·33 m^2).

The intensity of muon events ($sec^{-1}\ sr^{-1}$) with energies not less than E_μ(GeV) passing through the lower half of the spectrograph (i.e. traversing at least levels 3 and 1) and accompanied by a shower triggering the scintillation counters at the top of the spectrograph is then

$$I_\mu(n, \geq E_\mu \text{GeV}) = \int_N \int_r 2\pi r\ P_\mu(\geq E_\mu \text{GeV}) P_e(n) F(N)\, dN dr \qquad (4.10)$$

$$(sec^{-1}\ sr^{-1})$$

In a computer programme showers of sizes in the range 5×10^2 - 7×10^7 particles were allowed to fall on a plane. For a shower of size N particles falling on the plane at a point (r,θ) from detector S_4, the distance between the shower axis and other detectors (ri), including the spectrograph, can be obtained from the geometry of Figure 4.2 as follows :

$$r_i = \left\{ r^2 + a_i^2 - 2\, a_i\, r \cos(\phi_i - \theta) \right\}^{\frac{1}{2}} \quad \text{meter} \qquad (4.11)$$

where a_i & ϕ_i are the locations of the ith detector from the centre of detector S_4. Calculations of muon and electron densities follows from

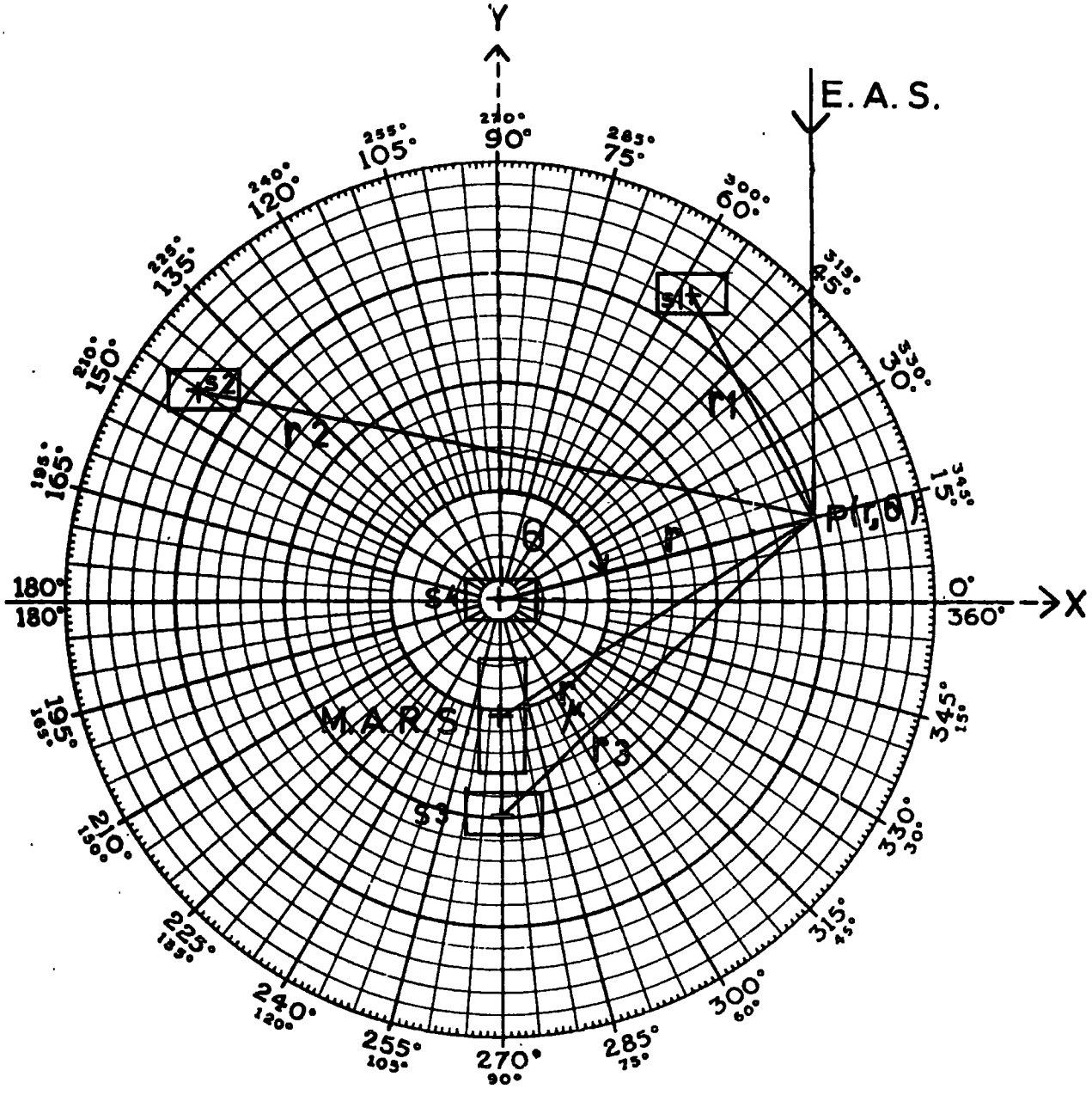

FIGURE 4.2 Determination of the core distances for various counters and the spectrograph in the plane polar co-ordinate system of the array.

the determination of r_is at a particular value of θ which varies from 0-2π in the plane polar system, the detection probabilities $P_e(n)$ and $P_\mu(\geq E_\mu)$ were then calculated for specified values of r_i and θ. The resultant probability $P_e(n) \times P_\mu(\geq E_\mu)$ was then obtained and averaged over all the values of θ at a particular value of r. The same procedure was then repeated for other values of r. Thus for a certain value of shower size N, the detection probabilities of a muon associated with an air shower triggering the present arrangement were calculated for a range of shower core distances of 0.1 - 800 m. According to equation 4.10 the first integration procedure was performed over this range of core distance. By selecting various shower sizes a second integration is performed over the shower size range used (5×10^2-7×10^7 particles). The resultant of both integrations gives an estimate of the sea level vertical intensity of muons with energies $>E_\mu$ passing through the spectrograph in association with an E.A.S. triggering a number n of shower counters on top of the spectrograph. The contribution to the rate of muons from different shower sizes can be obtained by evaluating the following expression

$$I_\mu(N,\geq E_\mu) = 2\pi F(N) \int_{0.1}^{800} P_e(n) P_\mu(\geq E_\mu) 2\pi r dr \quad \text{sec}^{-1}\text{sr}^{-1} \quad (4.12)$$

Figure 4.3 shows a plot of $I_\mu(N,\geq 5$ GeV) versus shower size for a coincidence between the spectrograph and 2, 3 and 4 shower counters for showers falling at distances in the range 0.1 - 800 metres from the detector S4. The median shower sizes for each counter combination with the spectrograph are given in the figure ; it is found that there is no appreciable contribution to the muon rates from showers of sizes $7 \times 10^3 \geq N_e$ and $N_e \geq 1 \times 10^6$ particles. To obtain the contribution to the rates of muons at various radial distances from showers of all

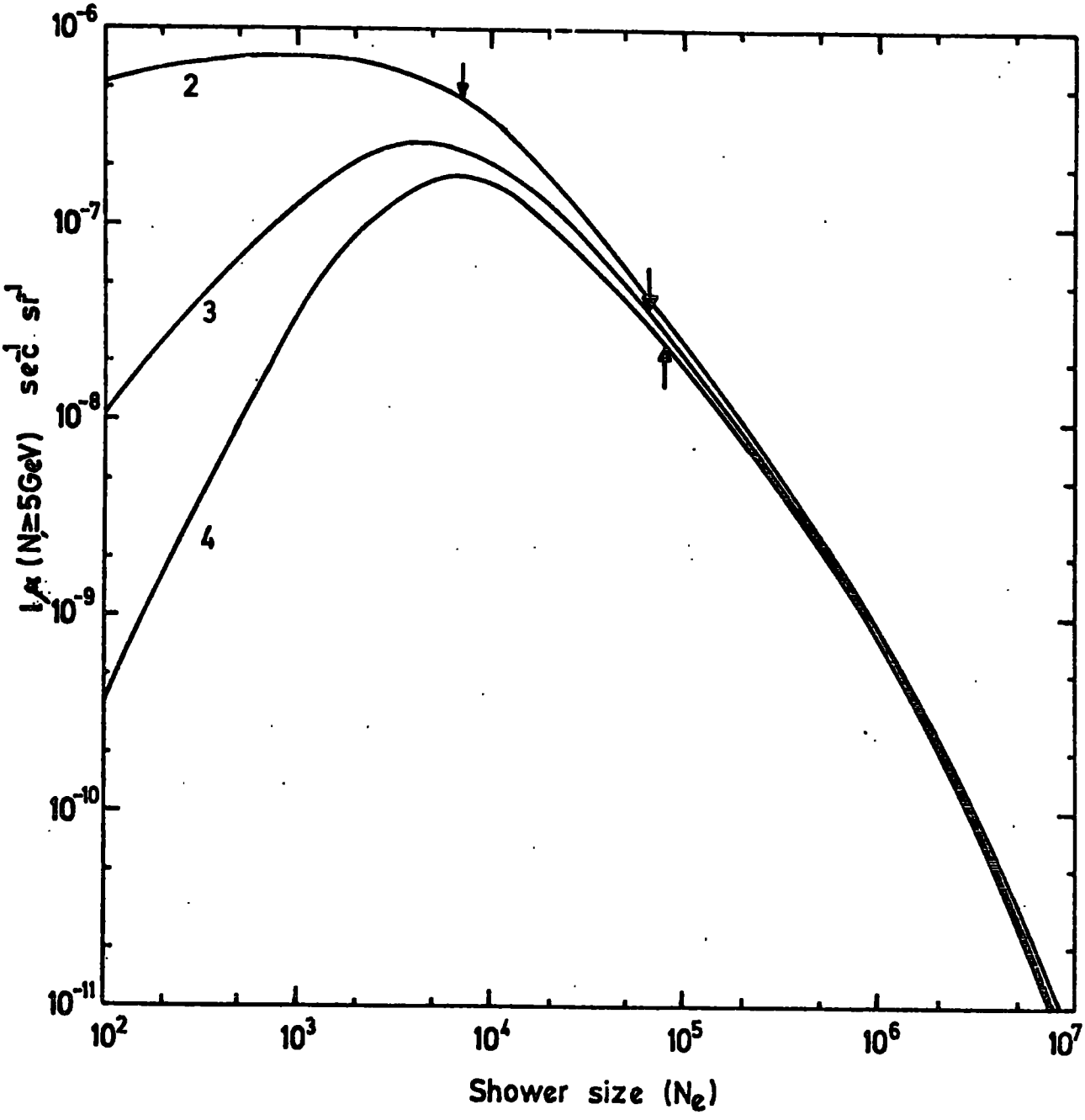

FIGURE 4.3 Contribution in shower size to the muon rates as predicted for the coincidence between M.A.R.S. and the three orders of counter combinations (2,3 and 4). The arrows indicate median shower sizes.

sizes the expression 4.10 has been evaluated for certain intervals of radial distance such that the resultant integral represents the intensity of muons $I_\mu(\leqslant r, \geqslant E_\mu)$ due to showers of all sizes falling at distance <r from the detector S4. Value of $I_\mu(\leqslant r, \geqslant 5$ GeV) are shown in Figure 4.4 and plotted versus the limit of integration on the radial distance. It is evident from the figure that showers of any size falling at distances 2.0$\geqslant$ r or r $\geqslant$100 metres make a negligible contribution to the rate of muons. Table 4.4 summarises the values of the median sizes and core distances for showers accompanied by muons traversing the spectrograph for a combination of 2, 3 and 4-fold coincidence detectors. The ranges of radial distance and shower size for all showers that contribute $\sim$ 80% to the muon rates are also given. In order to enable the theoretical calculations of the muon rates to be made, it is essential to have the knowledge of particles threshold energy and the acceptance of the spectrograph. As part of the coincidence mode used in this experiment a muon must pass through the lower half of the spectrograph (total thickness of 1985 gm/cm^2). For vertical incidence from the theory of energy loss a muon needs in this case an energy of not less than 3.5 GeV (Ayre, et al 1971) to traverse the apparatus. The amount of absorber increases for inclined trajectories to the vertical where the particles can traverse the spectrograph anywhere from the side and front planes of the spectrograph within an angle of $\leqslant 30^\circ$. The presence of a full magnetic field in the spectrograph causes the particles trajectories to be extremely curved and this effect is very effective at low muon energies, in particular near the value of the cut-off energy for the spectrograph. Thus, the magnetic field will give a small overall increase to the value of the muon cut-off energy. The effects of the iron absorber of the upper half of the spectrograph and that of the magnetic field results in an increase in the cut-off energy of the lower half of

TABLE 4.4 : Radial and size contributions of showers to the rate of muons ($E_\mu \geq 5.0$ GeV) in association with showers triggering 2, 3 and 4-fold coincidence detectors and M.A.R.S.

Order of Coincidence	Limits for 80% contribution in radial distance (meter)	Limits for 80% contribution in shower size (particles)	Median core distance (meter)	Median shower size $\bar{N}$ (particles)
2-fold	2.0 - 70	$3.0 \times 10^3 - 6 \times 10^5$	14.0	7.0×10^3
3-fold	2.2 - 70	$6.5 \times 10^3 - 8 \times 10^5$	14.5	6.5×10^4
4-fold	3.2 - 60	$8.0 \times 10^3 - 10^6$	16.0	8.0×10^4

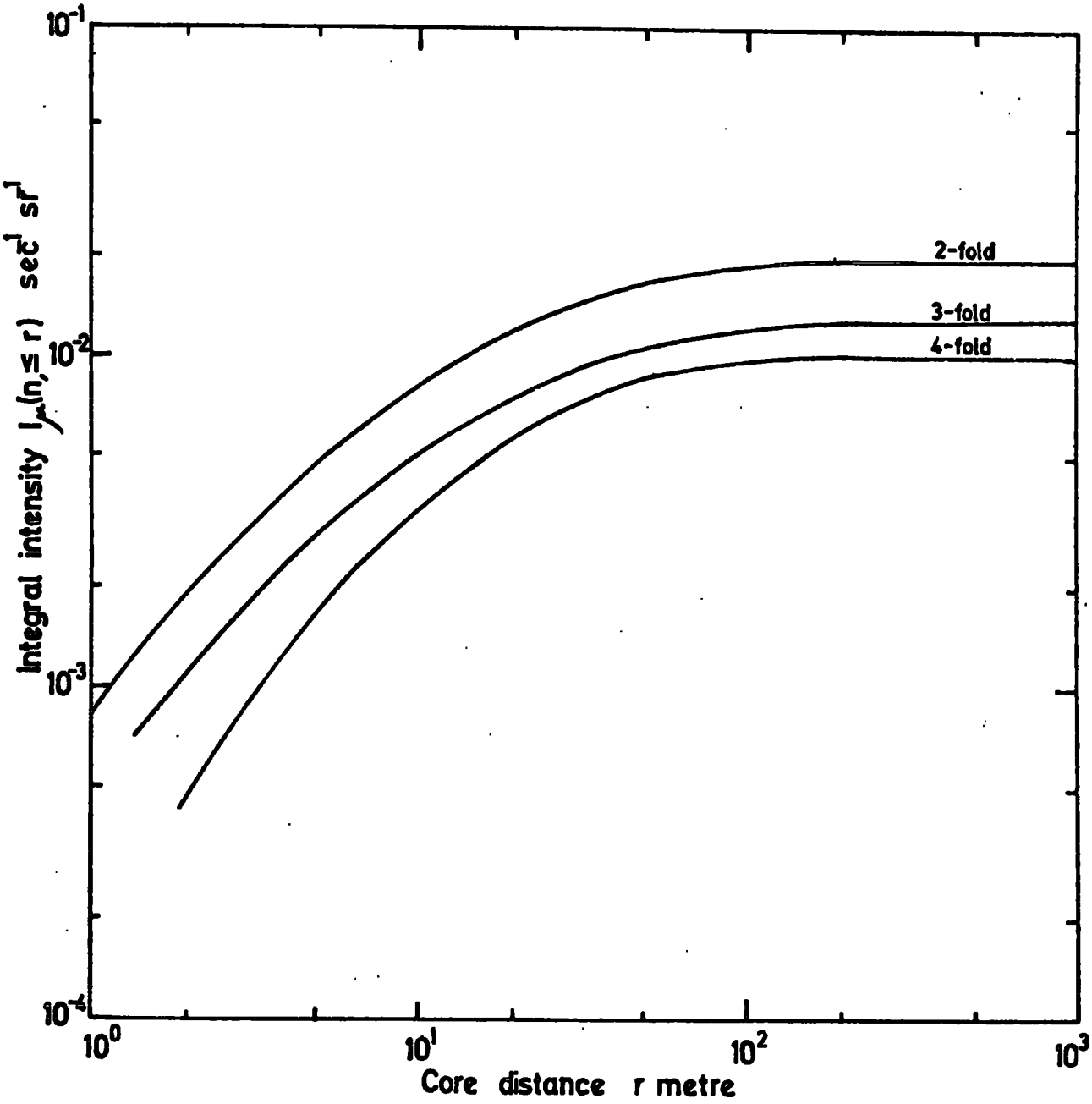

FIGURE 4.4 Radial distance contribution of all shower size to the total rate of muons for 2, 3 and 4 counters in coincidence with M.A.R.S.

the instrument to an effective value lying in the range 3.5 GeV to 7 GeV. The results of calculations of the muon intensities $I_\mu(n, \geq E_\mu)$ for muons of energy thresholds 4 and 5 GeV are given in Table 4.5. It is also seen that the mean integral intensities above both energies are sensitive to the number of counters used in coincidence with the spectrograph.

The vertical intensities of E.A.S. muons predicted by a coincidence of two counters and M.A.R.S. seems to decrease by $\sim$ 32% when a third counter is employed and $\sim$ 44% when all the four counters of the array are used. It is also evident from Table 4.5 that there are no detectable differences in the calculated muon intensities above 4 or 5 GeV when calculated for a particular number of counters in coincidence with the spectrograph.

In order to predict the coincidence counting rates of air shower counters with the spectrograph $R_\mu(n, \geq E_\mu)$, the acceptance functions of the spectrograph must be folded in to the calculated intensities of the main expression 4.10, such that

$$R_\mu(n, \geq E_\mu) = I_\mu(n, \geq E_\mu) \times A_{cc}(E_\mu) \quad \text{sec}^{-1} \tag{4.13}$$

where $A_{cc}(E_\mu)$ in this case is the acceptance function of the lower half of the spectrograph in m^2.sr. as defined by the scintillation counters in levels 3 and 1 of the spectrograph. In Section 3.8.5, it is explained that this acceptance is a function of muon energy and the angular distribution of the incidence flux. Values of A_{cc} used in this work are those obtained from Figure 3.18. Muon rates have been computed from expression 4.13 and then used in comparison with observations in Section 4.12.

TABLE 4.5 : Calculations of the intensities of muons with energies $\geq$ 4, 5 GeV, for various order of coincidences of counters with M.A.R.S.

Order of coincidence	Counter combination	$I_\mu(\geq 4\ GeV) \times 10^{-2}$ $sec^{-1}sr^{-1}$	$I_\mu(\geq 5\ GeV) \times 10^{-2}$ $sec^{-1}sr^{-1}$
2	S_3+S_4	2.00	1.85
	S_2+S_4	1.89	1.75
	S_1+S_2	1.84	1.71
	S_1+S_4	1.88	1.74
	S_2+S_3	1.85	1.70
	S_1+S_3	1.83	1.71
	mean intensity	1.88	1.74
3	$S_1+S_2+S_4$	1.26	1.18
	$S_2+S_3+S_4$	1.29	1.20
	$S_1+S_3+S_4$	1.28	1.19
	$S_1+S_3+S_2$	1.24	1.15
	mean intensity	1.27	1.18
4	$S_1+S_2+S_3+S_4$	1.01	0.996

4.5 PREDICTIONS OF SHOWER COINCIDENCE RATES FROM THE SEA LEVEL DENSITY SPECTRUM

The concept of an air shower density spectrum enables the results to be interpreted in a manner which does not depend very strongly on the dimension of the apparatus. The concept of the shower density spectrum can be meaningful if the shower density is assumed almost constant over the dimensions of the experimental set up. In the present experiment the area occupied by the shower detectors is small in comparison to the area covered by a shower and the detector spacings are large enough to assure no detection of narrow showers that originate in the vicinity of the detectors. Thus, the assumption of a uniform density over all the area covered by the small array is subject only to statistical fluctuations which are represented by the Poissonian triggering probabilities for one or more detectors to be struck by a shower. Considering a detector of sensitive area $S(m^2)$, then the probability of m particles crossing this area in a shower of mean density $\Delta(m^{-2})$ is

$$P\ (\Delta,S) = (\Delta S)^m \frac{e^{-\Delta S}}{m\ !} \qquad (4.14)$$

The probability of no particle going through that detector will be

$$P_o\ (\Delta,S) = e^{-\Delta S} \qquad (4.15)$$

Thus, the probability for a detector to be hit by one or more particles is

$$P\ (\Delta,S) = 1 - \exp\ (-\Delta S) \qquad (4.16)$$

For an array of n detectors of areas S_i, the probability that these detectors will be triggered by a shower of mean density Δ at the location

of the detectors is the product of the independent probabilities such that

$$P_n(\Delta,S_i) = \prod_{i=1}^{n} \left\{ 1 - \exp(-\Delta S_i) \right\} \tag{4.17}$$

for detectors of a similar area the above expression will be reduced as follows

$$P_n(\Delta,S) = \left\{ 1 - \exp(-\Delta S) \right\}^n \tag{4.18}$$

If the number of showers per unit time whose densities lie within the range Δ and $\Delta + d\Delta$ is $F(\Delta)d\Delta$ then the coincidence counting rate between n number of detectors is given as

$$C_n = \int_0^\infty P_n(\Delta,S) \; F(\Delta) \, d\Delta \quad \text{sec}^{-1} \tag{4.19}$$

where $F(\Delta)\, d\Delta$ is the differential density spectrum. The frequency of showers of densities $>\Delta$ (m^{-2}) can be expressed as a power law of the form :

$$F(\geq\Delta) = K \Delta^{-\gamma} \quad \text{sec}^{-1} \tag{4.20}$$

where γ is the exponent of the integral density spectrum which varies slowly with density and altitude, then the differential spectrum of equation 4.20 can be derived as follows

$$F(\Delta)\, d\Delta = K\gamma \; \Delta^{-\gamma-1} \quad d\Delta \quad \text{sec}^{-1} \tag{4.21a}$$

The contribution for showers of density between Δ and $\Delta + d\Delta$ to the

coincidence rates is proportional to the following expression

$$B(\Delta)\, d\Delta = \left\{ 1 - e^{-\Delta S} \right\}^{n} F(\Delta)\, d\Delta \qquad \text{sec}^{-1} \qquad (4.21\ b)$$

Figure 4.5 shows the contribution B (Δ) plotted against values of Δ ranging from 2×10^{-2} to 100 p/m^2 for γ of the form given by Murdoch (1958) as follows

$$\gamma = 1.34 \pm 0.018 \ \ell n \Delta$$

Justifications for using this value of γ stems from the fact that this measurement is applicable for showers in the low density range of the shower density spectrum, whose mean densities are ≈ 1 p/m^2 ; furthermore, the exponent γ in this case was derived from a sea level experiment of similar size to the present one. It is apparent from Figure 4.5 that showers whose densities in the range $0.3 \lesssim \Delta \lesssim 70$ p/m^2 contribute strongly to the coincidence rates. In Equation 4.18 the function $P_n(\Delta,S)$ varies from zero to unity over a small range of densities while F(Δ) is found to be rapidly decreasing with Δ , thus, the integrand of equation 4.19 shows a sharp maximum occurring at a shower density of approximately $1/S$ (m^{-2}), see Figure 4.5. Therefore, most of the contribution to the shower rates come from comparatively narrow range of densities. The density spectrum need be valid only over this range of densities. The integral in equation 4.19 has been evaluated by a computer programme using the shower density spectra of Murdoch (1958) and Greisen,(1960) respectively. In both predictions the limit of the integration was taken from 0.01 - 500 p/m^2. The predicted rates of the 2, 3 and 4-fold counter coincidences are shown in Table 4.6.

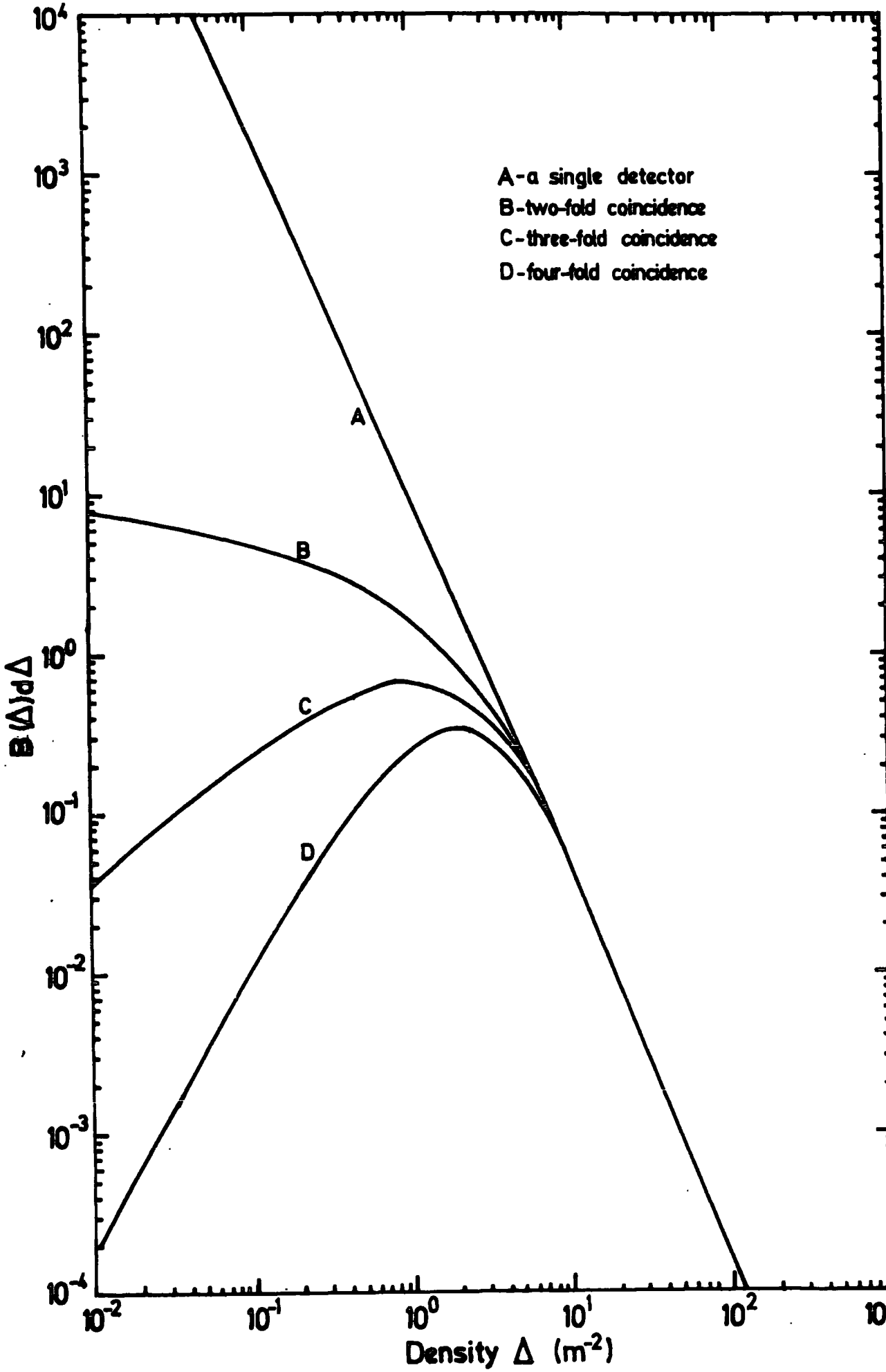

FIGURE 4.5 The contribution of all showers in particle density (p/m^2) to the coincidence counting rate between the detectors.

TABLE 4.6 : Predictions of the showers coincidence counting rate on the basis of the shower density spectrum.

Author	Coincidence Rate (≥ 2 p/m^2) min^{-1}		
	2-fold	3-fold	4-fold
Murdoch (1958)	6.05 $\pm$ 0.11	2.76 $\pm$ 0.07	1.87 $\pm$ 0.06
Greisen (1960)	6.59	3.14	2.16
Present work	9.55 $\pm$ 0.10	2.94 $\pm$ 0.12	1.95 $\pm$ 0.034

4.6 PREDICTIONS OF THE COINCIDENCE RATE OF SHOWERS FROM THE STRUCTURE FUNCTION OF PARTICLES IN E.A.S.

The predictions of the coincidence counting rates of showers by employing an empirical formula for the lateral structure functions of air shower particles and a known shower size spectrum represent a simple and satisfactory method that yields various information on the character of the showers recorded, for example, their intensities, lateral spread and angular distributions. The method of calculation is similar to that for the muon rate predictions described in Section 4.4. In order to interpret the observed measurements it is always essential to calculate the probability that a particular shower of size N will cause an n-fold coincidence if it hits with an axis through the point (r,θ) on the plane of the shower detectors to give at least one particle through each detector. This probability $P_e(n)$ is well represented by equation 4.8. If the number of showers of size N particles be F (N) m^{-2} sec^{-1} sr^{-1}, then the coincidence rate of the n-fold counter combinations is

$$C(n) = \int_{\substack{\text{plane} \\ (r,\theta)}} r\,dr\,d\theta \int_{N} P_e(n)\ F(N)\ dN \quad sec^{-1} \qquad (4.22)$$

θ being the angle in the plane of the array as shown in Figure 4.2. The integration in Equations 4.22 have been performed numerically employing the lateral electron structure functions of showers given by Greisen(1960) for an age parameter of 1.3 and using the shower size spectrum obtained from the survey of Bell (1974) and following the method of calculations

given in Section 4.4, the limits of radial distance r and shower size N were the same used in this prediction as for the evaluation of Equation 4.10. The contribution in shower size to the rate of showers for three orders of coincidence counters(2,3 and 4) are evaluated from the following expression

$$I_e(N,n) = 2\pi F(N) \int_{0.1}^{800} r \times P_e(n)\, dr \quad \text{sec}^{-1}\ \text{sr}^{-1} \qquad (4.23)$$

Plots of $I_e(N,n)$ are shown in Figure 4.6. Inspection of the figure shows the effect of the change in slope of the employed shower size spectrum in the region of $\sim 7 \times 10^5$ particles. The contributions in radial distance to the shower rates was obtained by evaluating Equation 4.22 for all shower sizes and then carrying the integration of radial distance over certain intervals of r, the resultant contribution for the three orders of coincidence is presented in an integral form in Figure 4.7. It is clear from the figure that showers at distances $\geq r \geq 100$ metres have a negligible contribution to the rate of showers. Table 4.7 summarises some properties of the showers recorded by various orders of coincidence. The effect of varying the age parameter on the predicted intensities was also investigated. Since most of the showers recorded by the present arrangement are past their maximum development they can be regarded as "old showers". The relation between the calculated integral intensities and age parameter is that shown in Figure 4.8 where it is seen that the intensity of showers decreases slowly with increasing age parameter. The value selected for the comparison of shower rates is that at an age parameter of 1·3 for all orders of coincidence. The expected values of shower intensities as obtained by integrating over all the ranges of shower sizes and radial distance in Equation 4.22 are

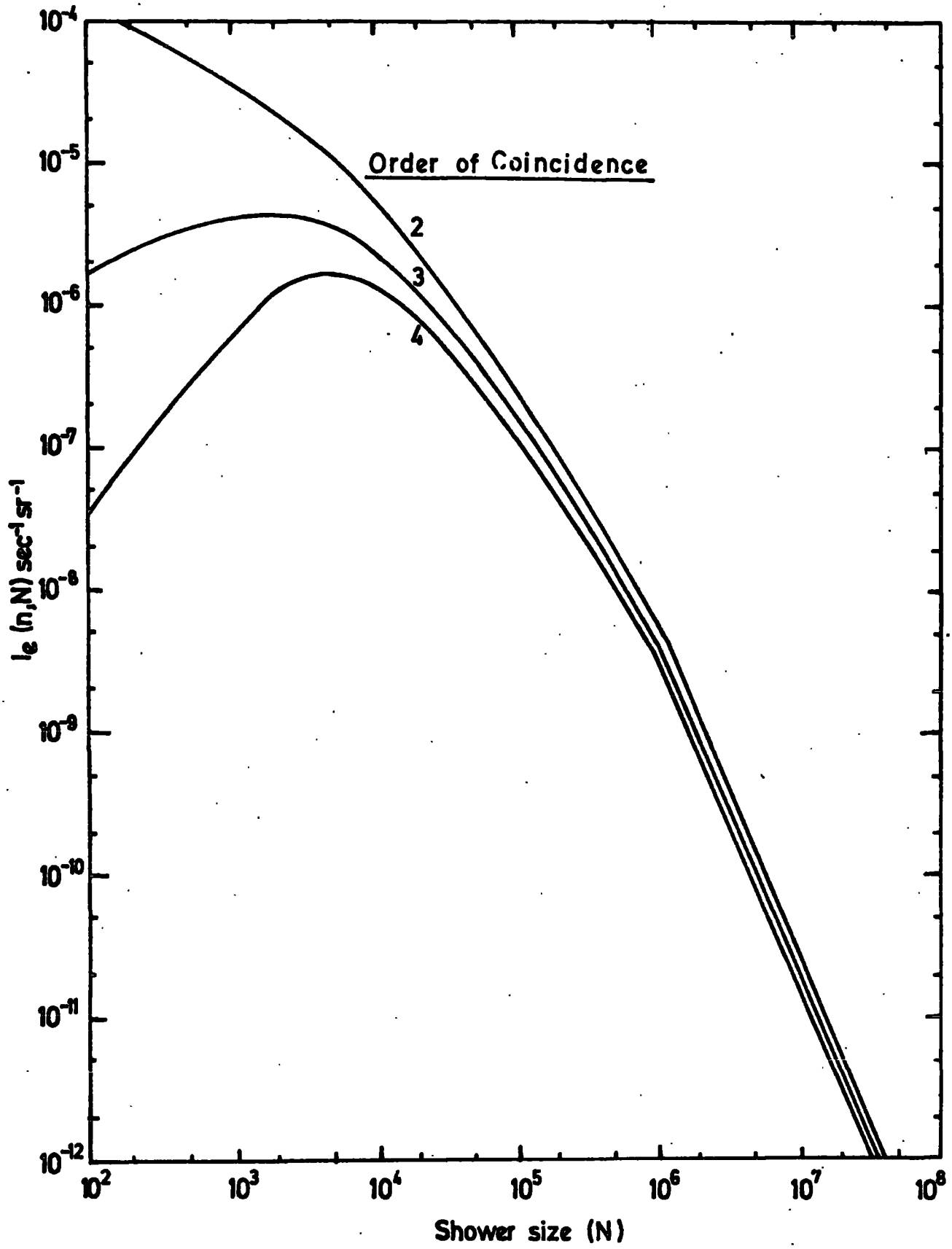

FIGURE 4.6 Size contribution to the rate of showers falling at distance 0.1-800 metres from the centre of detector S4 detected by the 2,3 and 4-fold coincidences.

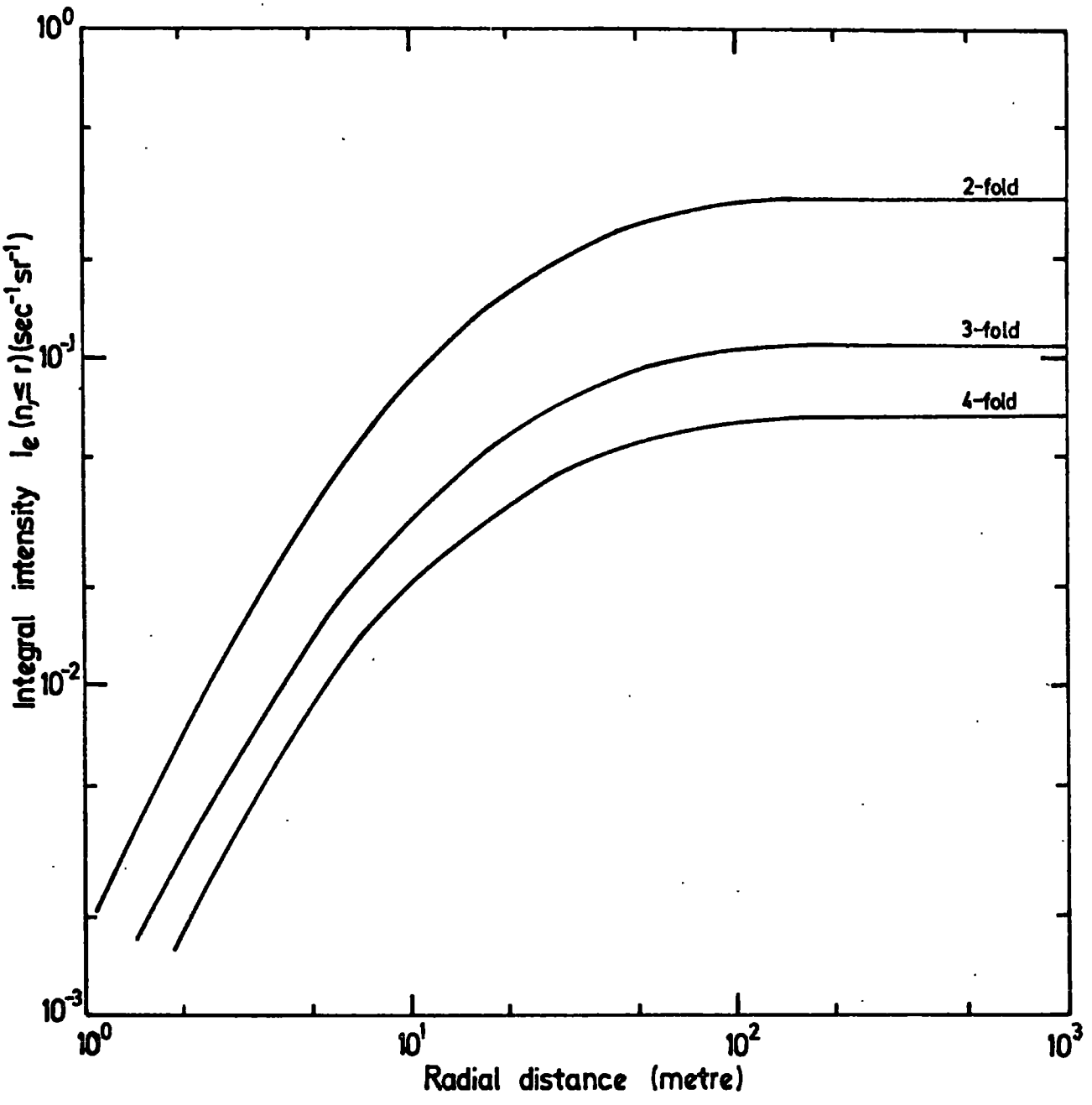

FIGURE 4.7 Contribution in radial distance to the shower rates from all showers falling at distances $\leq$ r(m) from the detector S4.

TABLE 4.7 : The radial distance and size contribution of showers to the coincidence rates of 2, 3 and 4-fold coincidences.

Order of Coincidence	Limits of 80% radial contributions (meter)	Limits of 80% size contributions (particles)	Median core distance (meter)	Median shower size (particles)
2-fold	4.5 - 70	$6x10^2$-$2x10^5$	20	9×10^3
3-fold	4.0 - 70	$4x10^3$-$4x10^5$	19	$3.3x10^4$
4-fold	4.0 - 60	$6x10^3$-$6x10^5$	18	5×10^4

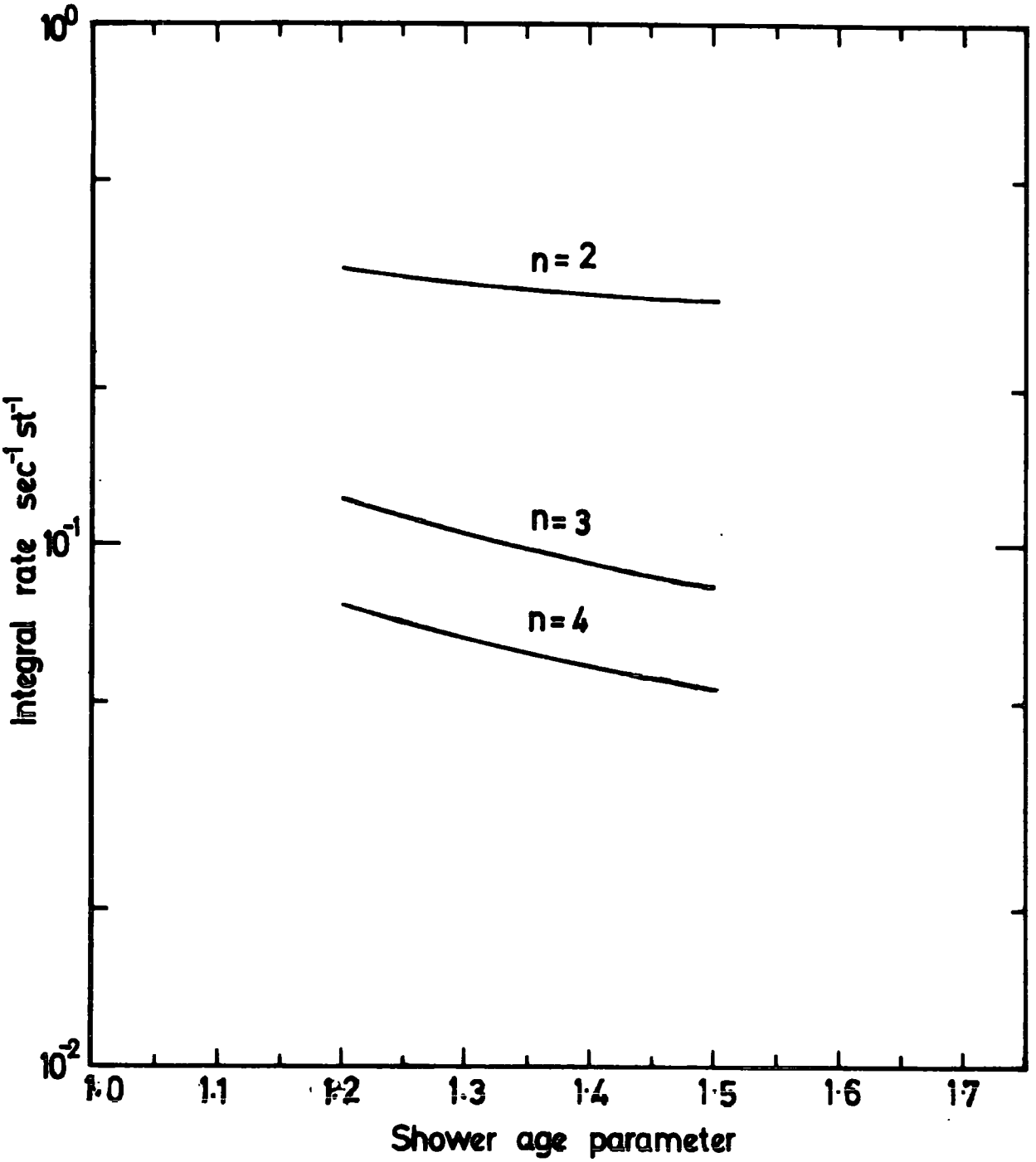

FIGURE 4.8 The effect of varying age parameter on the theoretical rates.

presented in Table 4.8 and for all orders of coincidence and counter combinations used within each order. For the case of the two-fold coincidence rate it is apparent that the calculated intensities do not differ significantly from one combination to the other. Another similarity in the predicted shower intensities can be seen for the case of the four sets of the three-fold coincidence. However, it is evident that the mean densities of showers responsible for the triggering in both orders of coincidence do not vary significantly over the whole detecting area and can be assumed to be independent of the combined counter varying geometries. The total rate of air showers can be obtained by integrating the shower intensity in the vertical direction I_o (sec^{-1} sr^{-1}) over all directions in the hemisphere about the zenith such that

$$R_T = \frac{2 \pi I_o}{m + 1} \quad (sec^{-1}) \tag{4.24}$$

where m is the exponent of the angular distribution of showers at sea level assumed to follow a $I_\theta = I_o \cos^m \theta$ law. The derivation of the relation 4.24 is shown in Appendix 1. By folding the measured rates into Equation 4.24 and knowing the values of I_o, it is possible to obtain estimates of the exponent m in an indirect way. The results of these estimations are discussed in Section 4.10. A comparison of the predicted shower rates and observations is given in Section 4.12.

4.7 EXPERIMENTAL RESULTS

Besides the data summary given in Table 4.1, about 3.3% of the total air shower data have been rejected and 41 muon events were also removed from the analysis. The reason for the rejections is that

TABLE 4.8 : Predicted Intensities of shower in the vertical direction for an age parameter of 1.3.

Order of Coincidence (n)	Counter Combination	C(n) sec^{-1} sr^{-1}
2-fold	$S_3 + S_4$	3.18×10^{-1}
	$S_2 + S_4$	3.14×10^{-1}
	$S_1 + S_2$	3.14×10^{-1}
	$S_1 + S_4$	3.13×10^{-1}
	$S_2 + S_3$	3.00×10^{-1}
	$S_1 + S_3$	3.00×10^{-1}
3-fold	$S_1 + S_2 + S_4$	1.13×10^{-1}
	$S_2 + S_3 + S_4$	1.09×10^{-1}
	$S_1 + S_3 + S_4$	1.08×10^{-1}
	$S_1 + S_3 + S_2$	1.07×10^{-1}
4-fold	$S_1 + S_2 + S_3 + S_4$	6.66×10^{-2}

the observed rate of recording these data deviates from the mean rate of the specified coincidence by at least three standard deviations. Table 4.9 A presents the measured number of the spectrograph events collected from various runs of the air shower counters in coincidence with the spectrograph. For a certain order of coincidence and for all possible combinations of counters in that coincidence the measured rates of spectrograph events are given. The measured rates of muons are given in Table 4.9 B, the column "corrected rate of events" represents the rate of events after being corrected for the efficiency of the particular triggering mode of coincidence. It can be seen from Table 4.9 B that the measured rate of the spectrograph events show no variation with varying combination of either two-fold or three-fold coincidence. Corrections to the measured rate of the spectrograph events for the effects of the unresolved events will be given in Section 4.12. In a similar way air showers data have been presented in Table 4.10 A,B). Shower rates presented in Table 4.10 B show evidence for a slight dependence of detector separation in the case of the two-fold coincidence. Comparing the rate of showers as measured by the three-fold coincidence it is seen that these measurements are not highly sensitive to variations in the counter combinations and consequently counter separations. It is, therefore, believed that at sea level a large proportion of the recorded showers do not exhibit strong variations of particle density in the vicinity of the area occupied by the present counter arrangement. In the following sections, it is shown how the experimental measurements presented in Tables 4.9 A and 4.10 B , are used to produce an estimate of true muon rates and to deduce the density and size spectra of E.A.S. respectively.

TABLE 4.9 A : A summary table of the total number of muon events observed with various coincidence combinations of scintillation counters with the spectrograph, the corrected number column represents the number of muon events, after being corrected for the triggering efficiencies of the specified modes.

Coincidence	Observed Number of muon events	Corrected Number	Total Running time (min)
$S_3 S_4$	1202	1446	5087
$S_2 S_4$	727	851	3053
$S_1 S_2$	830	981	3549
$S_1 S_4$	701	824	3431
$S_2 S_3$	181	220	844
$S_1 S_3$	408	496	1930
$S_2S_3S_4$	2917	3601	13750
$S_1S_3S_4$	1108	1368	4560
$S_1S_2S_4$	1061	1278	4865
$S_1S_2S_3$	565	705	2600
$S_1S_2S_3S_4$	1471	1869	8225

TABLE 4.9 B : The observed rates of muon events corrected for the triggering efficiencies of coincidence modes between the showers scintillation counters and the spectrograph. The presented rates are weighted over the total number of runs of the particular coincidence mode.

Coincidence	Weighted Mean of Corrected rate min^{-1}	Standard Error of Weighted Mean	Standard Deviation of the Data
S_3S_4	2.81×10^{-1}	8.15×10^{-3}	3.46×10^{-2}
S_2S_4	2.79×10^{-1}	1.03×10^{-2}	3.57×10^{-2}
S_1S_2	2.76×10^{-1}	9.6×10^{-3}	3.59×10^{-2}
S_1S_4	2.40×10^{-1}	9.1×10^{-3}	3.40×10^{-2}
S_2S_3	2.55×10^{-1}	1.91×10^{-2}	6.62×10^{-2}
S_1S_3	2.54×10^{-1}	1.26×10^{-2}	4.00×10^{-2}
	Weighted mean =	0.2664 ± 0.0042	
$S_2S_3S_1$	2.61×10^{-1}	4.8×10^{-3}	1.86×10^{-2}
$S_1S_2S_4$	2.98×10^{-1}	8.9×10^{-3}	3.33×10^{-2}
$S_1S_3S_4$	2.58×10^{-1}	8.0×10^{-3}	3.30×10^{-2}
S S S	2.69×10^{-1}	1.1×10^{-2}	3.65×10^{-2}
	Weighted mean =	0.267 ± 0.0035	
$S_1S_2S_3S_4$	2.26×10^{-1}	5.9×10^{-3}	3.12×10^{-2}

TABLE 4.10 A : A summary of the number of shower events observed. The second column represents the total number of shower events corrected for pressure variation during a certain number of runs of the data collection whose total running time is given in the third column.

Observed No. of showers	Corrected No. of showers	Total Running time (min)	Counter Combination	Order of Coincidence
55014	51012	4032	$S_3 + S_4$	2-fold
52270	52856	5344	$S_2 + S_4$	
39369	37511	3885	$S_1 + S_2$	
26531	27512	2563	$S_1 + S_4$	
14122	13832	1795	$S_2 + S_3$	
14082	14270	1632	$S_1 + S_3$	
16574	16343	6686	$S_1S_2S_3$	3-fold
10329	11073	4030	$S_1S_2S_4$	
12593	12429	4457	$S_2S_3S_4$	
13813	12661	4709	$S_1S_3S_4$	
27493	26482	15071	$S_1+S_2+S_3+S_4$	4-fold

TABLE 4.10 B: The integral coincidence rates of showers having densities of $\geq 2 p/m^2$ obtained by various coincidences between air shower detectors. The presented rates are corrected for pressure variations and the triggering efficiencies of the specified coincidence modes.

Coincidence	Corrected rate min^{-1}	Standard Error	Standard Deviation
$S_3 + S_4$	12.30	0.16	1.20
$S_2 + S_4$	9.64	0.14	0.91
$S_1 + S_2$	9.39	0.13	0.82
$S_1 + S_4$	10.06	0.15	1.00
$S_2 + S_3$	8.43	0.14	0.84
$S_1 + S_3$	7.45	0.13	0.78
	Weighted mean = 10.44 ± 0.057 min^{-1}		
$S_2+S_3+S_4$	3.02	0.060	0.22
$S_1+S_3+S_4$	3.10	0.068	0.23
$S_1+S_2+S_4$	3.00	0.066	0.26
$S_1+S_2+S_3$	2.66	0.050	0.19
	Weighted mean = 2.90 ± 0.03 min^{-1}		
$S_1+S_2+S_3+S_4$	1.95	0.034	0.18

4.8 MEASUREMENTS OF THE 'DECOHERENCE' CURVE FOR SHOWERS

4.8.1 Introduction

Measurements of the coincidence counting rate of two detectors as a function of the separation between them was first measured by Auger et al, (1939). For detector separations 1-1000 metres the lateral spread of measured showers by this "decoherence" curve agree well with the theoretical predictions of the electron-photon cascade. A well defined plateau occurs in the "decoherence" curve for distances between about 1-10 meter separation (Wei and Montgomery, 1949). The theoretical calculations of Moliere (Wei and Montgomery,1949) have shown only a negligible increase in the counting rate of two detectors as their separation decreases to zero. This behaviour is never fulfilled in practice ; observations deviate from theory and a sharp rise in counting rate is found at less than one metre. The discrepancy at this small separation is believed to be due to local showers. In the present experiment, the separation of the shower detectors, 3-7.5 m, ensures that no local showers that originate in the vicinity of the detectors are detected. In an experiment of this kind where the lateral separation of the detector is of the same order as the dimensions of the detector it is difficult to locate the shower axes, consequently precise measurements of the lateral distributions of E.A.S. are precluded. Instead a study of the frequency of showers as a function of the horizontal separation between two detectors could offer some knowledge on the lateral spread of air showers at small distance from the core of the shower.

4.8.2.The 'Decoherence' Curve

The two-fold coincidence rates, $R(d, \geqslant 2\ p/m^2)$ for six counter combinations were simultaneously recorded as a function of the detector separation d(m). Following the procedures outlined in Section 4.3, corrections to the counting rates were made due to pressure variations,

combined detector efficiencies and accidental coincidences. The "decoherence" curve obtained is shown in Figure 4.8. A least squares fit to the data points in the figure has been made and it is found that the counting rate R (min^{-1}) can be represented by a negative power law as a function of detector separation as follows

$$R(d, \geq 2p/m^2) \alpha \quad d^{-0.72 \pm 0.25} \tag{4.25}$$

predictions of the "decoherence" curve can be made from the calculated shower rates in Section 4.6. Comparison of the theoretical predictions with measured data will be discussed in Section 4.12.

4.9 THE DENSITY SPECTRUM OF E.A.S.

4.9.1 Introduction

The density spectrum of charged particles in E.A.S. is the frequency distribution of the occurrence of a particle density at a particular place, irrespective of information concerning the size and location of the axis of the showers responsible to the particles. The density spectrum is usually analysed with the intention of deducing the size spectrum of E.A.S. Under the assumption of a fixed lateral distribution of charged particles around the axis of the shower the exponent of the density spectrum can be shown to be equal to that of size spectrum (Cocconi, 1961, and Greisen, 1956). This is a relatively simple way to determine the size spectrum which finally reflects a knowledge of primary cosmic radiation. To study the density spectrum of E.A.S, the rate of occurrence of small air showers has been observed in this experiment. The character of showers which contribute to the density spectrum have been studied, the observed rates of E.A.S. were first analysed with respect to the sea level density spectrum reported

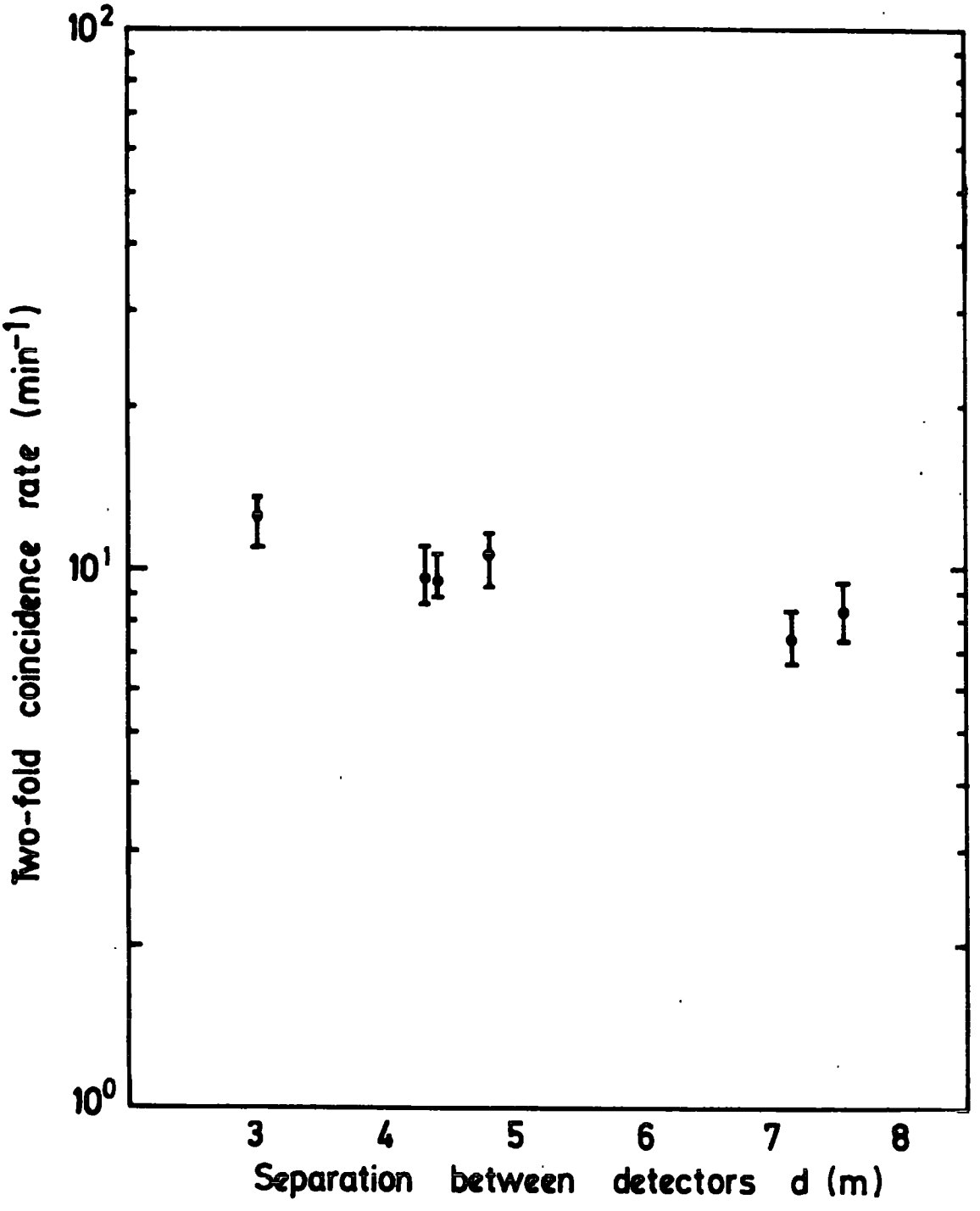

FIGURE 4.9 The "decoherence" curve of recorded showers.

by various authors, and then analysed using the measured size spectrum and the lateral distribution of E.A.S. at sea level. It is expected that both methods of calculation will yield no difference in the predicted rates of showers and thus provide a test on the validity of the assumption of a fixed density for all charged particles in the shower over the area occupied by the array detectors.

4.9.2 Previous Measurements of the Sea Level Density Spectrum

The density spectrum of cosmic ray air showers has been studied by many workers. Experiments covering a limited range of particle densities have been found to be consistent with a power law integral density distribution of the form

$$N\ (>\Delta) \;=\; K\ \Delta^{-\gamma} \qquad \text{sec}^{-1} \tag{4.26}$$

where K is a constant, the exponent γ is not strictly constant, but increases with density. Experiments conducted over a wide range of particle densities have shown a departure from this power law, up to densities of 500 p/m^2 the number of showers in all the range of density is nearly proportional to $\Delta^{-1.5}$ at sea level. Norman (1956) produced a good evidence for a steeper spectrum for densities greater than 500 p/m^2. The steepening in the spectrum was first confirmed by Prescott (1956) using proportional chambers and later by Reid et al (1961) using cloud chambers. At the low density range ($\Delta \simeq 1\ p/m^2$) early measurements have shown that the sea level density spectrum can be approximated by a single power law (for example, Murdoch (1958)). The present experiment enables the measurements of sea level density spectrum at low densities to be made and examined. In order to make a comparison of the experimental results with other workers a survey

of the sea level density spectrum has been made and is given in Table 4.11.

4.9.3 Measurement of the Sea Level Shower Density Spectrum

It has been shown in Section 4.7 that the three-fold coincidence rates of showers are not highly sensitive to variations in detector spread, it is therefore believed that in the present experimental arrangement, most of the showers do not exhibit significant variations of particle density over the area occupied by the counter arrangement. However, if the sea level integral density spectrum of showers falling at a certain point is a power law of the form $K\,\Delta^{-\gamma}$ where K is a constant and Δ is the particle density, it is then possible to determine the exponent of the spectrum γ from the ratio of the n-fold coincidence rate to (n-1)-fold coincidence rate by assuming that the separation between the detectors is negligible, so that the same density Δ may occur at each detector. If the counting rate of the n-fold coincidence counters is given by

$$C(n) = \int_0^\infty (1-e^{-\Delta s})^n \; K\gamma \; \bar{\Delta}^{\gamma-1} \; d\Delta \qquad \text{sec}^{-1} \tag{4.27}$$

where s is the area of a detector in m^2. An integration of this form can be solved by parts (Galibraith, 1958 and Cocconi, 1961) to give

$$C(n) = K\,S^{-\gamma}\,(-\gamma-1)\,!\;\; I(n,\gamma) \tag{4.28}$$

where $I(n,\gamma) = ({}^nC_1) - ({}^nC_2)\,2^\gamma + ({}^nC_3)\,3^\gamma \ldots + ({}^nC_n)\,n^\gamma$

This method has been applied to calculate the exponent γ from the ratio of the 4-fold to 3-fold rates. Thus, for n = 4, 3 expression

TABLE 4.11 : Survey of early measurements of the sea level integral shower density spectrum.

Reference	Density Range (p/m^2)	Exponent (γ)	K(min^{-1})	Detector Type
Murdoch (1958)	1 - 500	$1.34 \pm 0.018 \ln\Delta$	7.90	Giegers
Greisen (1960)	1 - 10^4	$1.3 \pm 0.55 \log\Delta$	9.00	see references
Galibraith (1958)	15 - 10^3	1.4	9.37	see references
Miyake et al, (1962)	15 - 800	1.55 ± 0.1	-	Scintillators
Chatterji et al, (1965)	2 - 100	1.40 ± 0.07	-	Scintillators
Cocconi et al (1949)	0.3-2x10^4	$1.29 \pm 0.02 \log\Delta$	-	Giegers
Broadbent and Hakeem (1950)	5 - 500	1.425 ± 0.022	10.33	Giegers
McCaughan et al (1965)	40 - 500	1.491 ± 0.036	-	Cloud Chamber
Ashton et al (1973)	40 - 10^3	1.50	6.85	Neon Flash Tubes Chamber
Hayakawa (1969)	1 - 10^4	$1.32 \pm 0.019 \ln\Delta$	12.6	See references

4.28 has been reduced to the following

$$I(4,\gamma) = 4^{\gamma} - 4 \times 3^{\gamma} + 6 \times 2^{\gamma} - 4 \qquad (4.29)$$

and

$$I(3,\gamma) = -3^{\gamma} + 4 \times 2^{\gamma} - 3 \qquad (4.30)$$

The calculated values of γ are plotted in Figure 4.10 for an assumed ratio of $C4/C3$. Plotted on the same figure are the experimental ratios of $C4/C3$ taken from the data in Table 4.10 B ; the values of γ obtained from the experimental ratios are presented in Table 4.12. The actual statistical error on γ are significantly smaller than those given in the table. The experimental values of γ are then considered to determine an average exponent for the present arrangement, the average value of γ obtained is $\gamma = 1.43 \pm 0.03$. The value of the constant K of the spectrum has been determined according to the following formula

$$K(n) = \frac{C(n)}{S^{\gamma} \times \Gamma(-\gamma) \times I(n,r)} \qquad (4.31)$$

where $\Gamma(-\gamma)$ is the well known gamma function and S(n) is the coincidence counting rate of the n-fold counter combination, the mean experimental value of K obtained from the 3-fold measurements is

$$K = 12.5 \pm 2.0 \text{ min}^{-1}$$

and the value of K obtained from the 4-fold rate is

$$K = 11.9 \pm 1.6 \text{ min}^{-1}$$

Hence there is no significant difference in the experimental determination of K by either coincidence rate. By using the last estimate of K

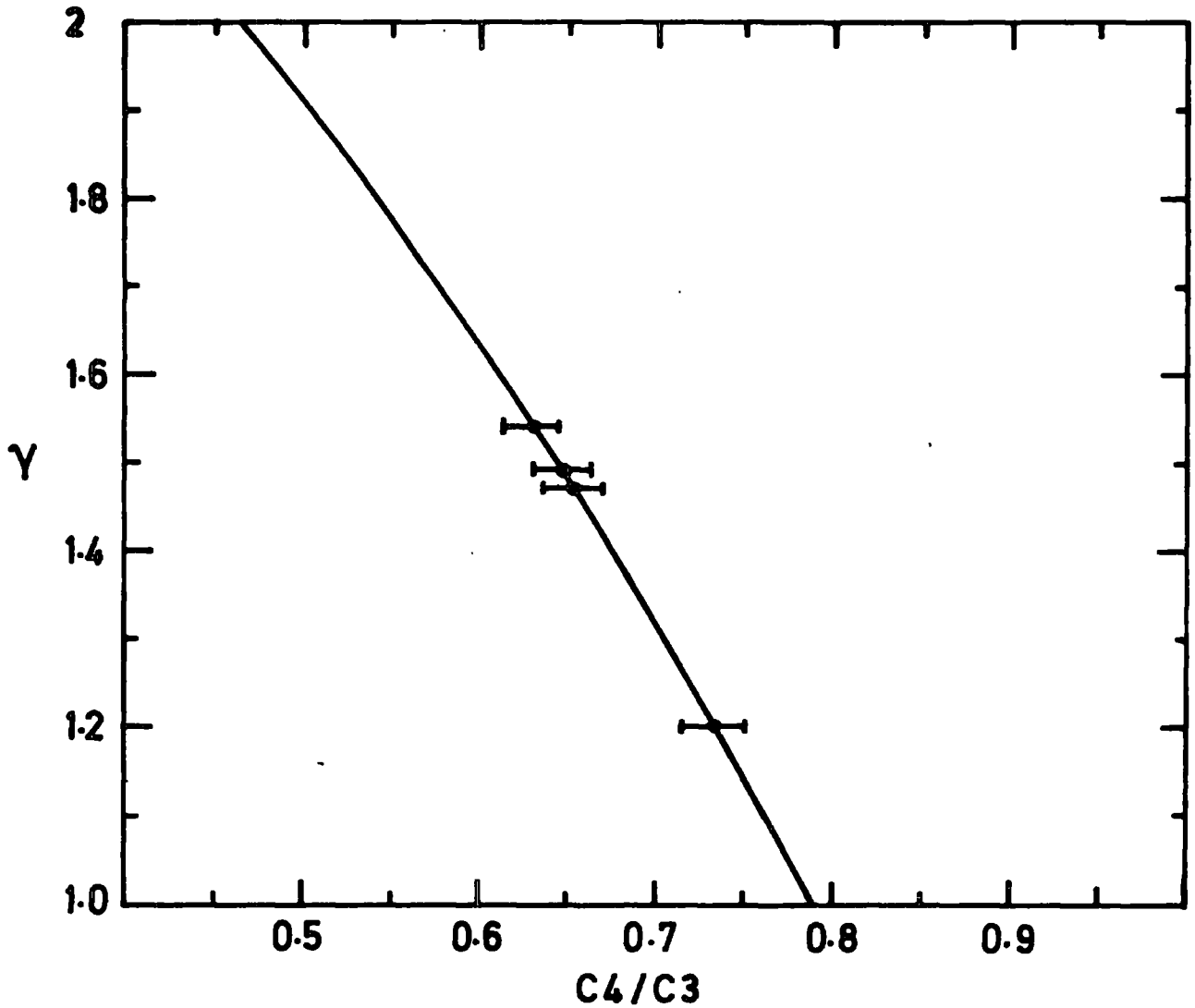

FIGURE 4.10 The experimental values of the ratio of the 4-fold to 3-fold coincidence rates, obtained by comparison ; the solid line represents the theoretical predicted values of γ.

TABLE 4.12 : The values of the integral exponent γ of the density spectrum of showers observed as obtained from equation 4.28 by comparing the 4-fold and 3-fold measured rates.

Counter Combination	Value of the Exponent (γ)
$S_1 + S_2 + S_4$	1.47 ± 0.065
$S_1 + S_3 + S_4$	1.54 ± 0.050
$S_2 + S_3 + S_4$	1.50 ± 0.050
$S_1 + S_2 + S_3$	1.20 ± 0.060
Weighted mean	$= 1.43 \pm 0.03$

the measured sea level density spectrum for showers with density ≥ 2 p/m^2 can be represented by a power law of the form

$$F\ (\geq 2\ p/m^2) = (11.9 \pm 1.6)\Delta^{-(1.43 \pm 0.03)} \quad min^{-1} \qquad (4.32)$$

The errors on γ and K are considerably larger than those predicted on the basis of statistics alone. The spectrum obtained in Equation 4.32 is confined to densities in the range 0.3 - 80 p/m^2.

4.10 THE EXPONENT OF THE ANGULAR VARIATION OF E.A.S.

It is well known that the intensity of cosmic ray particles observed at a certain zenith angle θ can be assumed of the form

$$I\ (\theta) = I\ (o)\ \cos^m\theta \qquad m^{-2}sec^{-1}sr^{-1} \qquad (4.33)$$

where I (θ) is the intensity of shower particles falling at sea level with an angle θ to the vertical, I (o) is the vertical intensity (i.e at $\theta = o^o$) and m is the exponent of the angular distribution. The measurement of m could give direct information on the attenuation of showers through the atmosphere. As has been mentioned in Section 4.6, the value of m can be simply derived from expression 4.24, by folding the observed shower rates and the calculated vertical intensities. The results of this estimation are shown in Table 4.13. Measurements obtained by the two-fold coincidence rates have not been used due to the fact that showers are not well defined by two detectors. Only three and four-fold measurements are selected for the derivation of m. The uncertainty in this determination comes mainly from statistics and the errors given in the calculated shower vertical intensities. It was

TABLE 4.13 : Measurements of the exponent m of the angular distribution of small showers (10^3 - 10^5 particles)

Order of Coincidence	Counter Combination	m
2-fold	$S_3 + S_4$	8.75 $\pm$ 0.95
	$S_2 + S_4$	11.3 $\pm$ 1.2
	$S_1 + S_2$	11.8 $\pm$ 1.2
	$S_1 + S_4$	10.7 $\pm$ 1.2
	$S_2 + S_3$	14.2 $\pm$ 1.8
	$S_1 + S_3$	12.4 $\pm$ 1.4
3-fold	$S_2 + S_3 + S_4$	12.1 $\pm$ 1.0
	$S_1 + S_3 + S_4$	12.6 $\pm$ 1.0
	$S_1 + S_2 + S_4$	13.4 $\pm$ 1.1
	$S_1 + S_2 + S_3$	14.2 $\pm$ 1.2
	mean exponent	13.08 $\pm$ 2.16
4-fold	$S_1 + S_2 + S_3 + S_4$	11.9 $\pm$ 1.2
	mean 3 & 4-folds	12.20 $\pm$ 0.95

found that the value of m is

$$m = 12.20 \pm 0.95$$

This value indicates a rather steep angular distribution, thus the angular variations of showers in the range 10^3 - 10^5 particles may be expressed as

$$I(\theta) \alpha \cos^{12.20 \pm 0.95} \theta$$

It is considered that the general interpretation of this relatively larger value of m is that these showers originate at greater heights than those most frequently observed in other experiments, for example, the sea level value observed by MacLeod (1956) and Ashton et al. (1973) are $m = 6.5 \pm 0.5$ and $m = 8.0 \begin{smallmatrix} + 1.4 \\ - 1.2 \end{smallmatrix}$ for median shower sizes of 3×10^6 particles and 1.5×10^5 particles respectively.

4.11 MEASUREMENTS OF THE INTEGRAL SIZE SPECTRUM OF SMALL AIR SHOWERS

Measurements of the showers size spectrum are most accurately made through studying individual showers. For showers of size less than about 10^5 particles, this method is difficult to apply due to the considerable difficulties connected with the measurement of a small number of particles crossing the detecting elements of an experimental air shower arrangement. This is mainly due to the uncontrollable fluctuations in the measured densities of particles and consequently the core of the showers will not be determined accurately. For this reason, in this experiment, the determination of the size spectrum of showers is studied through statistical observations of the frequency of showers in a method similar to that of Kulikov et al. (1960). By

assuming that the slope of the size spectrum and the lateral density distribution of all charged particles in E.A.S. is independent of shower size, it is possible to deduce the shower size spectrum in an indirect way from the measured showers density spectrum, (see Section 4.9). It is well known that both size and density spectra of showers follow a power law of the form :

$$F\ (>N) \;=\; A\ N^{-\beta} \qquad m^{-2}\ sec^{-1}\ sr^{-1} \qquad (4.34)$$

and

$$J\ (>\Delta) \;=\; K\ \Delta^{-\gamma} \qquad sec^{-1} \qquad (4.35)$$

respectively, where β and γ are the spectral exponents and A, K are constants. As has been mentioned earlier in Section 4.9, the exponent γ of the density spectrum is approximately the same as that of shower size spectrum (i.e. $\gamma \approx \beta$). The method adopted to calculate the integral intensity of showers was to assume the exponent γ to be constant over all shower size ranges recorded by this experiment such that the size spectrum can be represented as

$$F\ (>N) \;=\; A\ N^{-1.43\ \pm\ 0.03} \qquad m^{-2}\ sec^{-1}\ sr^{-1} \qquad (4.36)$$

By folding this spectrum in a differential form into relation 4.22, the following relationship was obtained

$$I\ (n) \;=\; 2\pi A \int_r \int_N r \times P_e(n)\, \gamma\, N^{-\gamma-1}\ drdN \qquad sec^{-1}\ sr^{-1} \qquad (4.37)$$

Hence,

$$I\ (n) \;=\; A \times J\ (n) \qquad sec^{-1}\ sr^{-1} \qquad (4.38)$$

where J (n) is the effective area of detection for showers of all sizes falling at various radial distances from the detector S_4 for a certain number (n) of coincidence combination of the counters, A has the units of $m^{-2}sec^{-1}sr^{-1}$. The evaluations of the constant A in this method may introduce some inaccuracy at the highest shower sizes (where the term $N^{-1.43}$ is not applicable), however, the differential size spectrum itself decreases with increasing size so that the effect is negligible. The value of the constant A is then obtained from the comparison of the measured rates with those calculated. After performing the integration of Equation 4.22, relation 4.24 was then used to give the values of A as follows

$$R\ (n) = \frac{2\pi\ A\ J\ (n)}{(m + 1) \times 60} \quad sec^{-1} \tag{4.39}$$

Thus for m = 12

$$A = 0.034\ \frac{R\ (n)}{J\ (n)} \quad m^{-2}sec^{-1}sr^{-1} \tag{4.40}$$

The resulting shower intensities are shown in Figure 4.11 plotted against the median shower sizes of each of the 2, 3 and 4-fold orders of coincidence. The errors on the measured intensities are due to the error on the exponent of the spectrum. Since the size of the errors are all of the same order of magnitude, an average value for the spectrum has been obtained from the figure and can be represented as follows

$$F\ (>N) = 35.3 \pm 6.5\ N^{-1.43 \pm 0.03} \quad m^{-2}sec^{-1}sr^{-1} \tag{4.41}$$

This spectrum is applicable for shower sizes in the range 10^3-3×10^5 particles, and is set by one standard deviation limit from the median

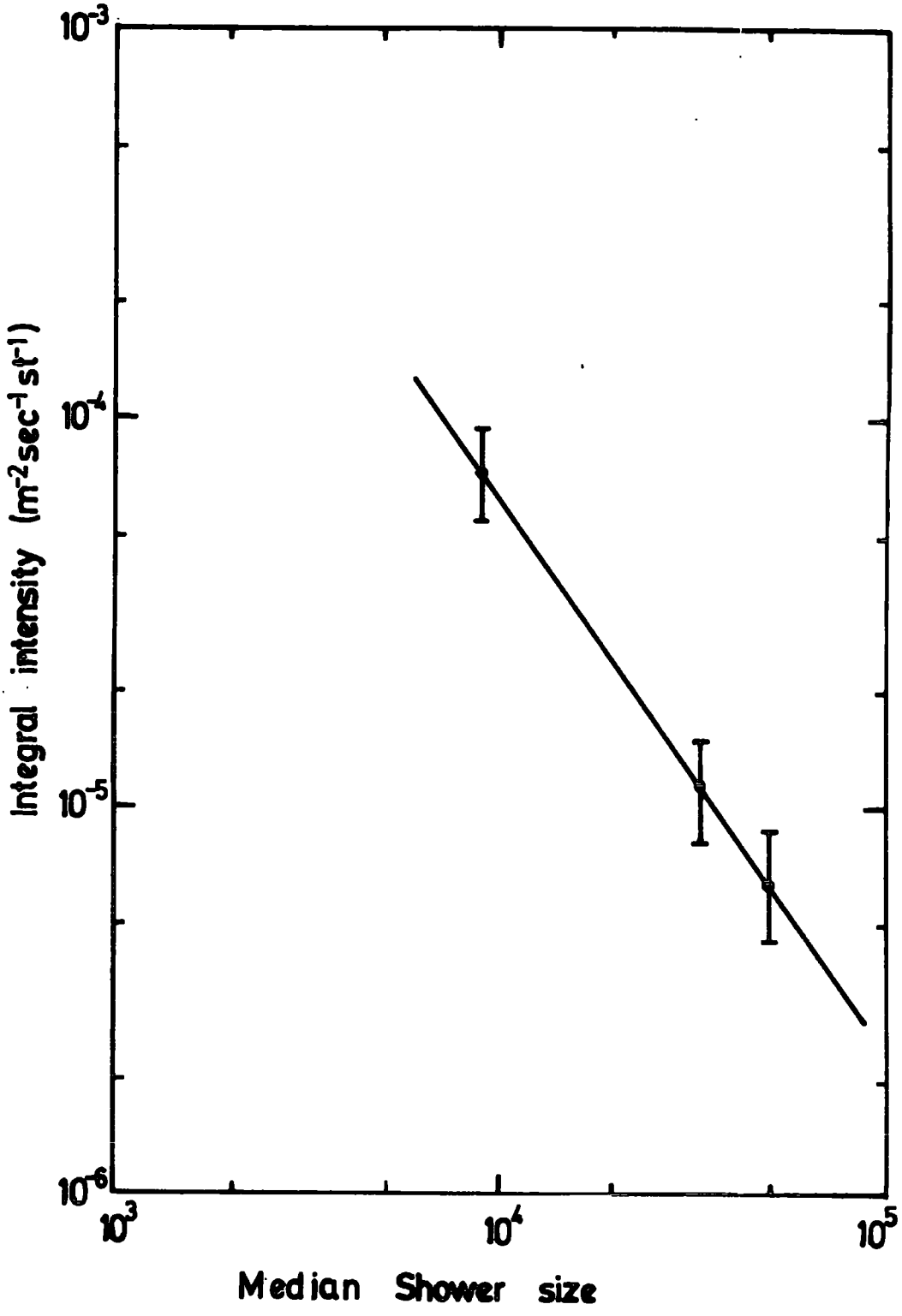

FIGURE 4.11 The integral shower spectrum of showers recorded by the present experiment.

shower sizes to which 2, 3 and 4-fold coincidence counters respond. Although, the present spectrum is subject to a considerable degree of uncertainty, particularly the estimation of shower sizes and the effect of the counter threshold for shower particles, it still gives an approximate representation of the actual spectrum at the lower end of the shower size spectrum at sea level. The accuracy of the points presented in Figure 4.11 could be improved by a more elaborate calculation in which a better estimate of the angular distribution exponent m and age parameter of the recorded showers is considered.

4.12 COMPARISON OF THE EXPERIMENTAL RATES WITH THEORETICAL PREDICTIONS

Direct comparison can now be made between the experimental results on the muon and air shower rates analysed earlier in this chapter and the theoretical predictions of the rates as follows :-

A. Muon Rates

Figures 4.12 and 4.13 show the experimental rates of muons associated with air showers obtained by various coincidences of the counters with the spectrograph. In order to make a comparison with the experimental results the predicted muon intensities for energies $\geq$ 4 and 5 GeV are corrected for the acceptance of the lower half of the spectrograph. The results are shown on Figure 4.12 (A,B). The theoretical predictions for two and three counters in coincidence with the spectrograph appear as solid lines. Unlike the muon intensities calculated in Section 4.4, which show only a slight sensitivity towards the number of counters used in coincidence with the spectrograph, the predicted muon rates above energies 4 and 5 GeV show marked differences throughout all orders of coincidence. Besides these differences the

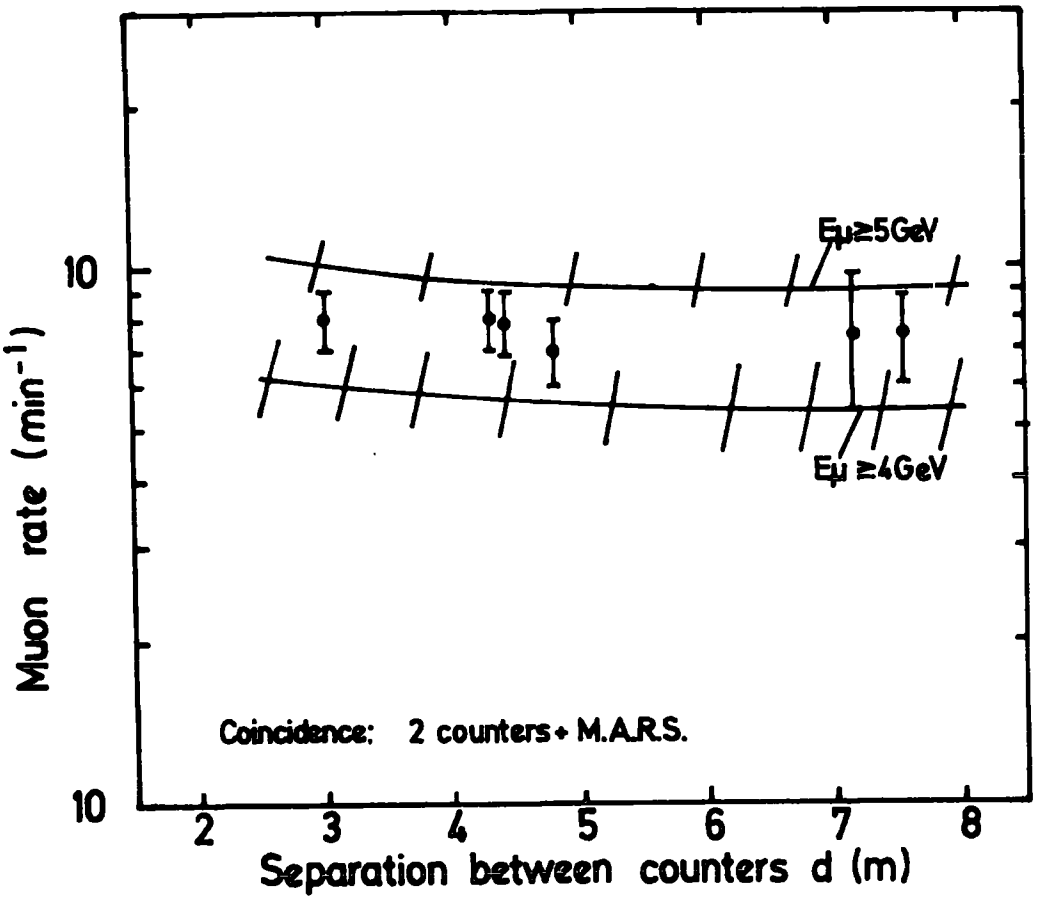

FIGURE 4.12.a Comparison of the measured rates of muons with theoretical predictions as obtained for muons having energies $\geq$ 4 GeV and $\geq$ 5 GeV.

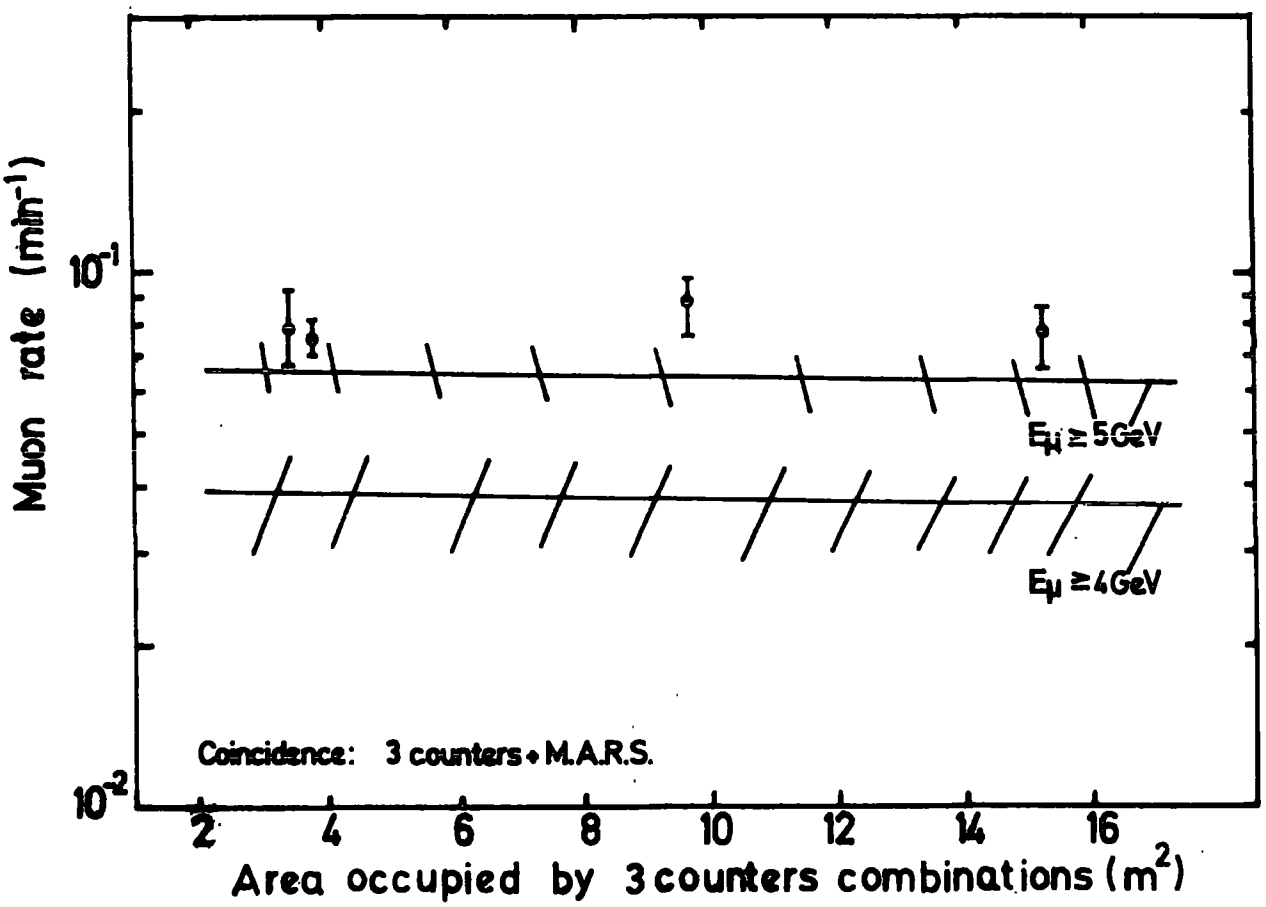

FIGURE 4.12.b Comparison of muon rates measured by a combination of three counters and M.A.R.S. with theoretical predictions.

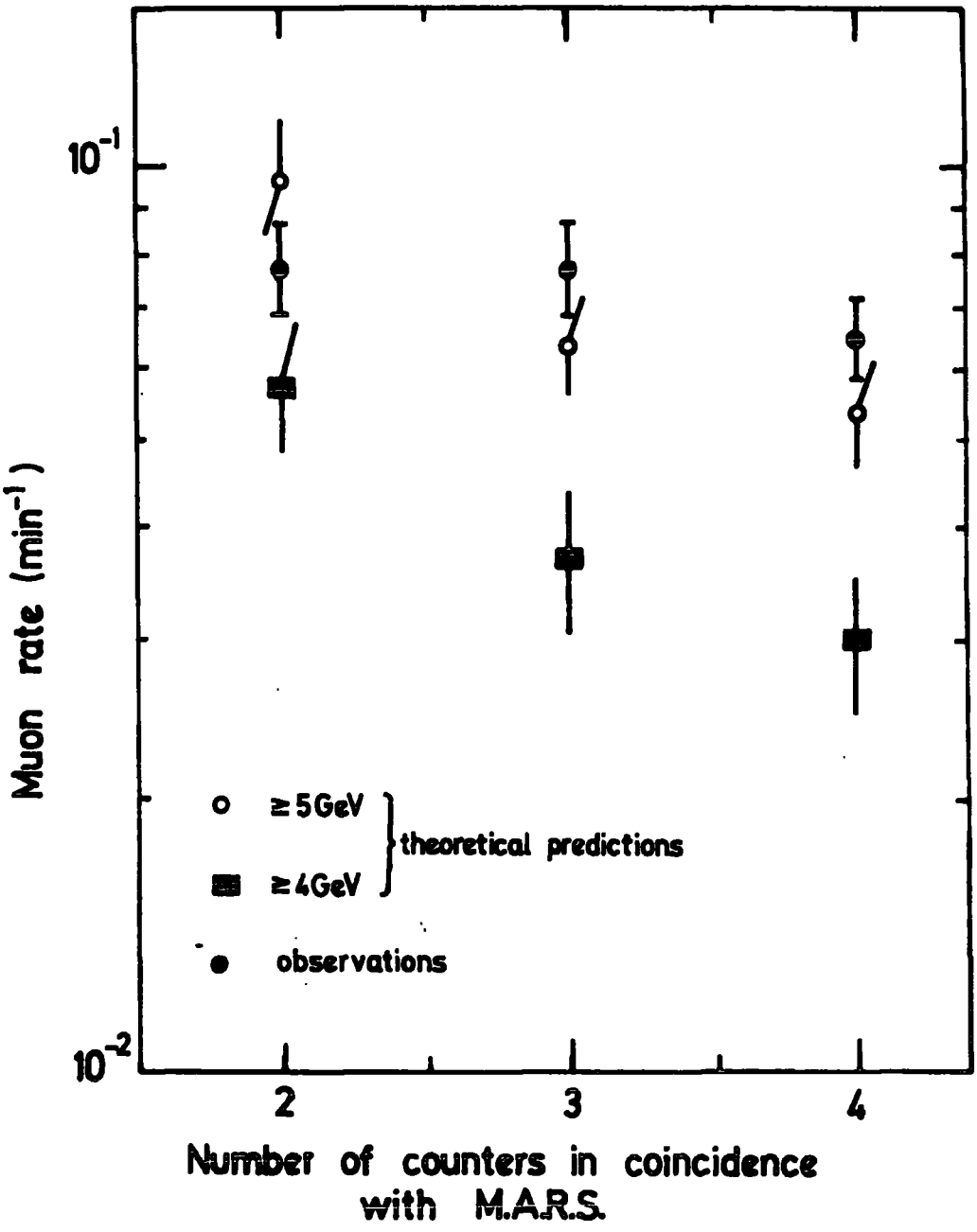

FIGURE 4.13 Mean muon rates as a function A the number of counters used in coincidence with the spectrograph. The theoretical calculations are also shown for muons having energies ⩾ 4 GeV and ⩾ 5 GeV.

rate corresponding to muons with energies $\geq$ 5 GeV appears to be higher than that for muons with energies $\geq$ 4 GeV. Both differences arise entirely from the combined effects of the spectrograph geometry (Acceptance) and the magnetic field in the spectrograph (effective cut-off energy for the muons) on the flux of particles passing through the instrument. The agreement between measured rates and the predictions for $E_\mu \geq 5$ GeV is acceptable. Thus, it is concluded that the adopted input parameters of the calculation are fairly correct.

B. Air Shower Counting Rates

In order to enable a comparison to be made between predicted and measured shower coincidence rates, the vertical calculated intensities of Table 4.8 have been folded into relation 4.24 with an assumed angular distribution of the $\cos^m \theta$ type where $m = 12 \pm 2$. Figure 4.14 (A,B) shows a comparison between measured and predicted rates for all the coincidence counter combination used in recording the showers. In the case of the two-fold coincidence rate (Fig. 4.14 A) the agreement between measured and predicted values is good, which can be regarded as an evidence on the validity of the theoretical calculations and confirms the use and validity of the presented shower size spectrum of Section 4.11 and the considered structure function of shower particles (Greisen 1960). These facts are well emphasised by the remarkable agreements obtained by comparing the three and four-fold coincidence rates presented in the same figure. Theoretical predictions of the two-fold coincidence rates show almost no variation with detector separation in the range 3-7.5 metres. This can be taken as an evidence for a plateau in the "decoherence" curve which agrees with early calculations of Moleire (see Section 4.8). Since the detector separation of the present arrangement lies within the plateau range, then it is to be expected that the observed two-fold

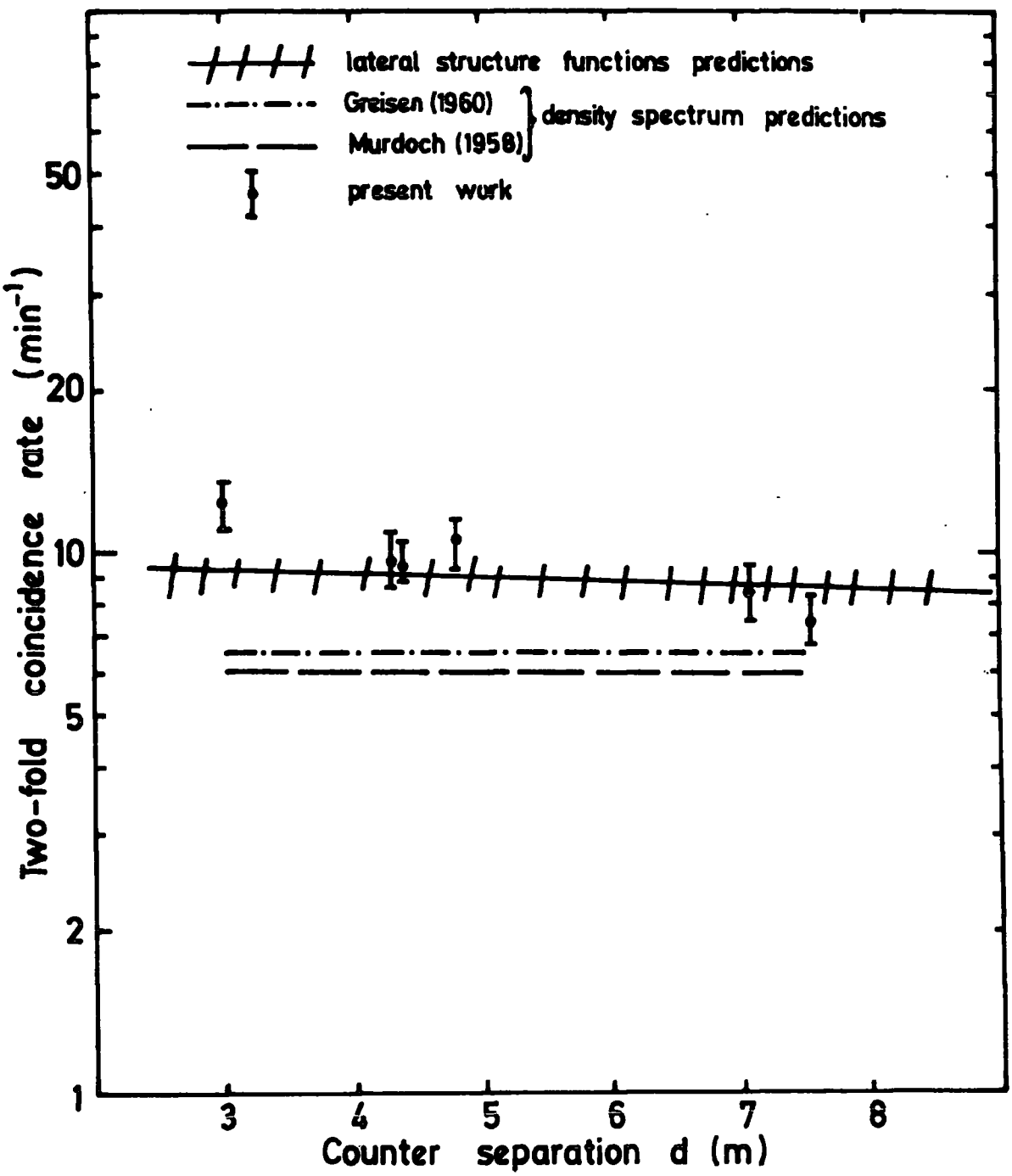

FIGURE 4.14 a The two-fold coincidence rate as a function of counter separation compared with the theoretical calculation.

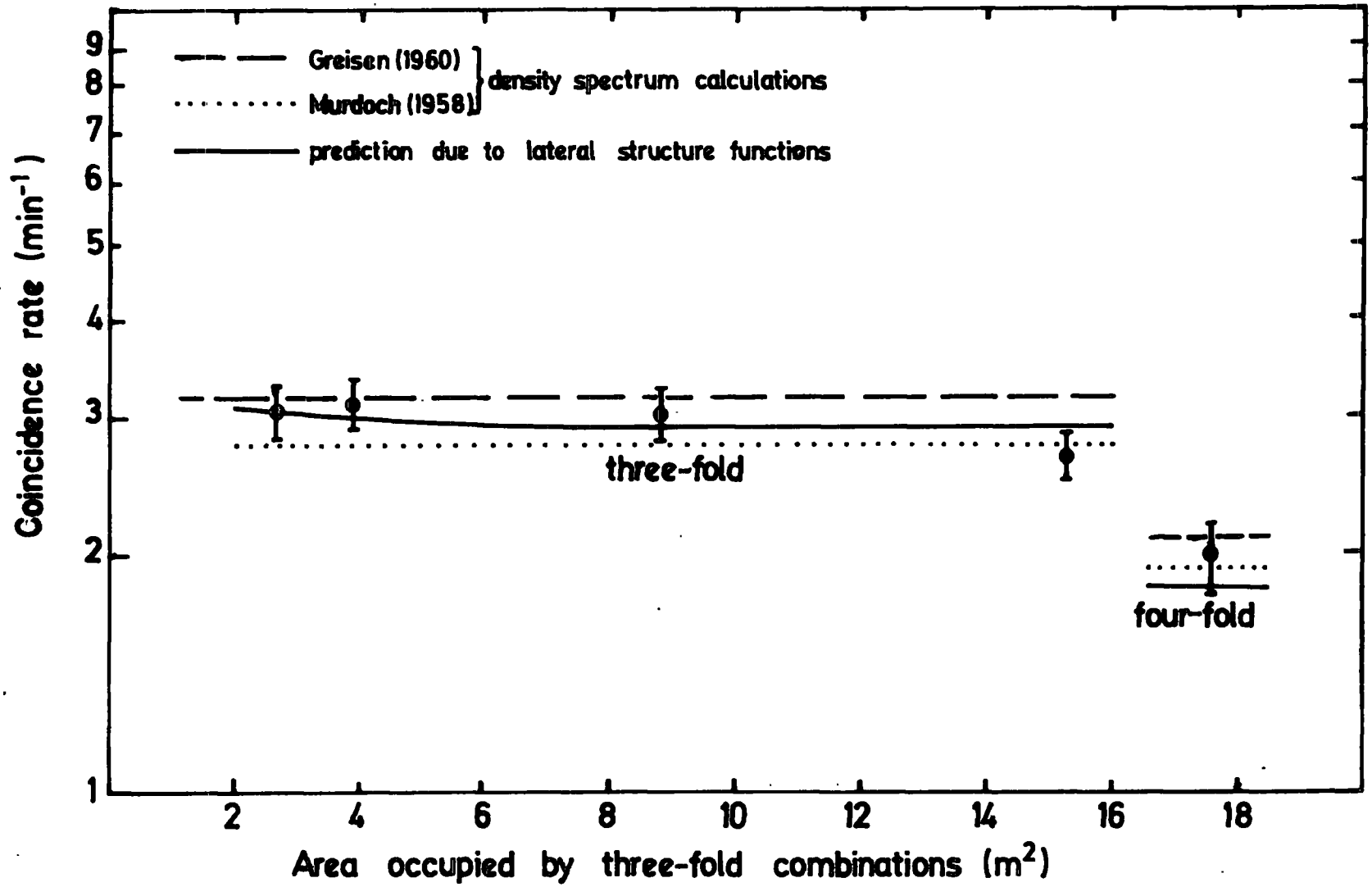

FIGURE 4.14b Comparison of the mean shower rates of three and four fold coincidence rates with the theoretical predictions.

coincidence rate would be constant if the detected particles resulted entirely from air showers. However, the observed rates deviate slightly from the theory and a slowly decreasing trend in the rate is observed with increasing separation. It is also believed that some of the discrepancy may be some additional counts due to local showers generated in the 4 gm/cm^2 of the laboratory roof. Since the roof is $\sim$ 2 m above the apparatus, the particles produced could diverge and separate sufficiently to trigger at least detectors which have the closest separation, i.e. S_3 and S_4. In the same section of Figure (4.14 A) the predicted coincidence rate of two counters has been plotted as obtained from the sea level density spectrum of air showers (see Section 4.5). The predicted two-fold rates due to the spectra of Greisen (1960) and Mordoch (1958) as applied to this case, seem to underestimate the measured values by an average of $\simeq$ 35%. As will be seen in Figure 4.14 B a good agreement with these spectra has been found in the case of three and four-fold coincidences, therefore, the discrepancy in the case of the two-fold coincidence rates could be attributed to either a partial contribution from local showers or to an erroneous assumption that the average shower densities are constant over the recording apparatus. This assumption is clearly never fulfilled, especially near the core of showers where the density changes very rapidly with radial distance. Figure 4.15 shows a comparison between the measured and predicted rates of coincidence as a function of the order of coincidence. The experimental rates plotted are the weighted means of the counter combination within each order of coincidence and the theoretical values are the vertical intensity averages of the values predicted for each combination, the total rate of each average value has been calculated for several values of the exponent of angular distribution m. It is seen from the comparison that there is good agreement between observation

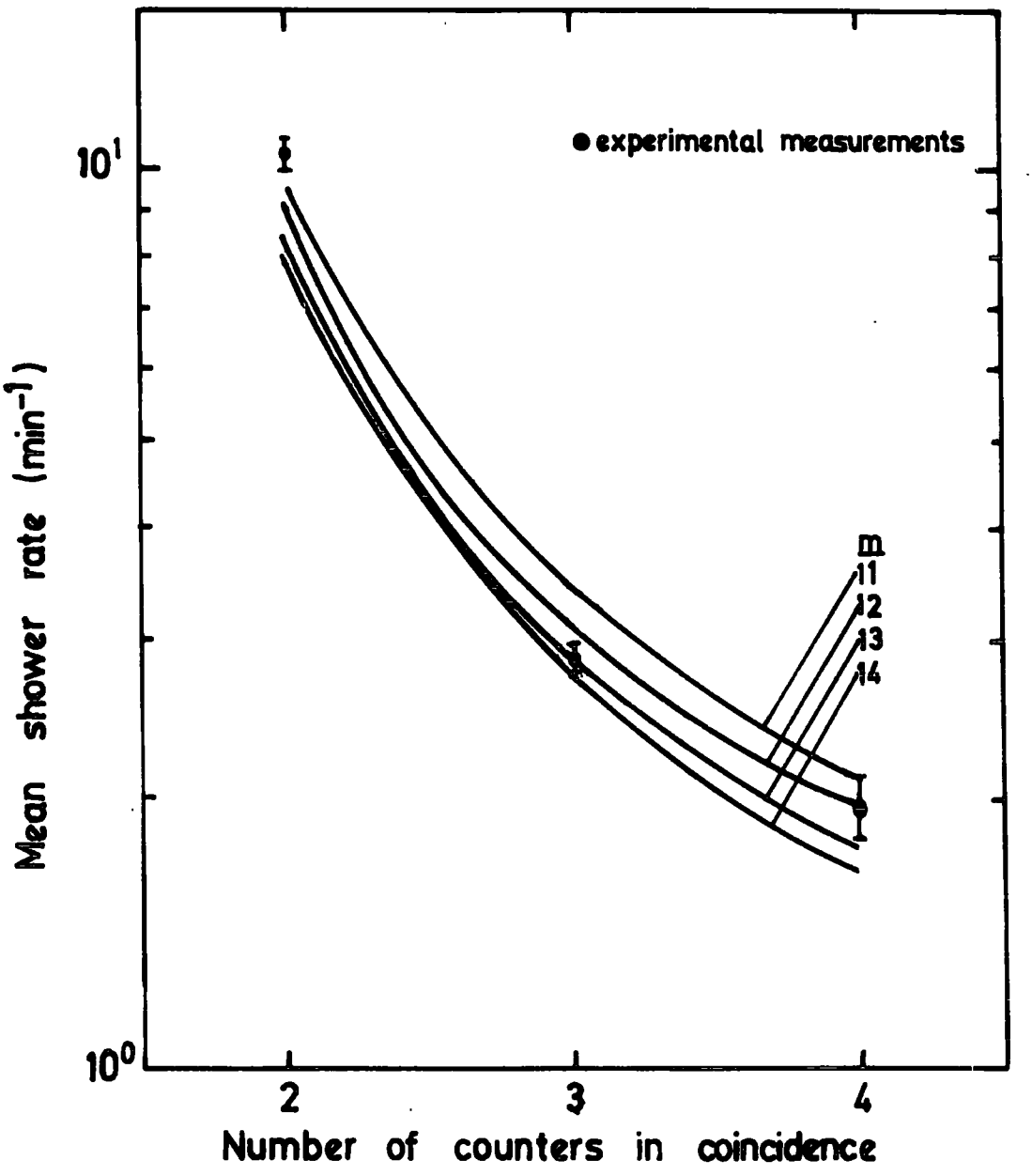

FIGURE 4.15 Mean showers coincidence rate for 2, 3 and 4 orders of coincidence counters.

and the theoretical predictions based on the lateral structure functions of showers for different orders of coincidence. The relation between the counting rates of the three and four-fold coincidence is in agreement with a power law density spectrum for showers with a constant exponent. The discrepancy in the two-fold rates when predicted by the density spectrum concept has been explained earlier. The present experimental data agree with a value $\sim$ 12.0 $\pm$ 1.0 for the exponent of the angular distribution of showers.

4.13 COMPARISON OF MEASURED DENSITY SPECTRUM WITH THE RESULTS OF OTHER WORKERS

The most important aspect of the measured density spectrum is its slope at densities $\geq$ 10 p/m^2 where the detection of showers by the four-fold coincidence is 100% efficient. Thus, there are no experimental biases due to the apparatus on the measured spectrum above that limit of particles density. Figure 4.16 shows a comparison between the density spectrum obtained from this experiment and that of other workers. It is evident from the figure that the observed slope and rate of the spectrum are in reasonable agreement with spectra obtained by other workers. In particular a very close agreement in the shape of the spectrum is obtained with the early measurements of Murdoch (1958). At densities $\leq$ 10 p/m^2, the observed spectrum steepens slightly in comparison to that given by Greisen (1960) and Hyakawa (1969). However, at low densities the measurements are subject to fluctuation of the showers densities. Thus the steepening in the density range 0.3 - 10.0 p/m^2 is not considered significant.

4.14 COMPARISON OF THE MEASURED SHOWER SIZE SPECTRUM WITH THE RESULTS OF OTHER WORKERS

The survey of the sea level shower size spectrum of Figure 2.6

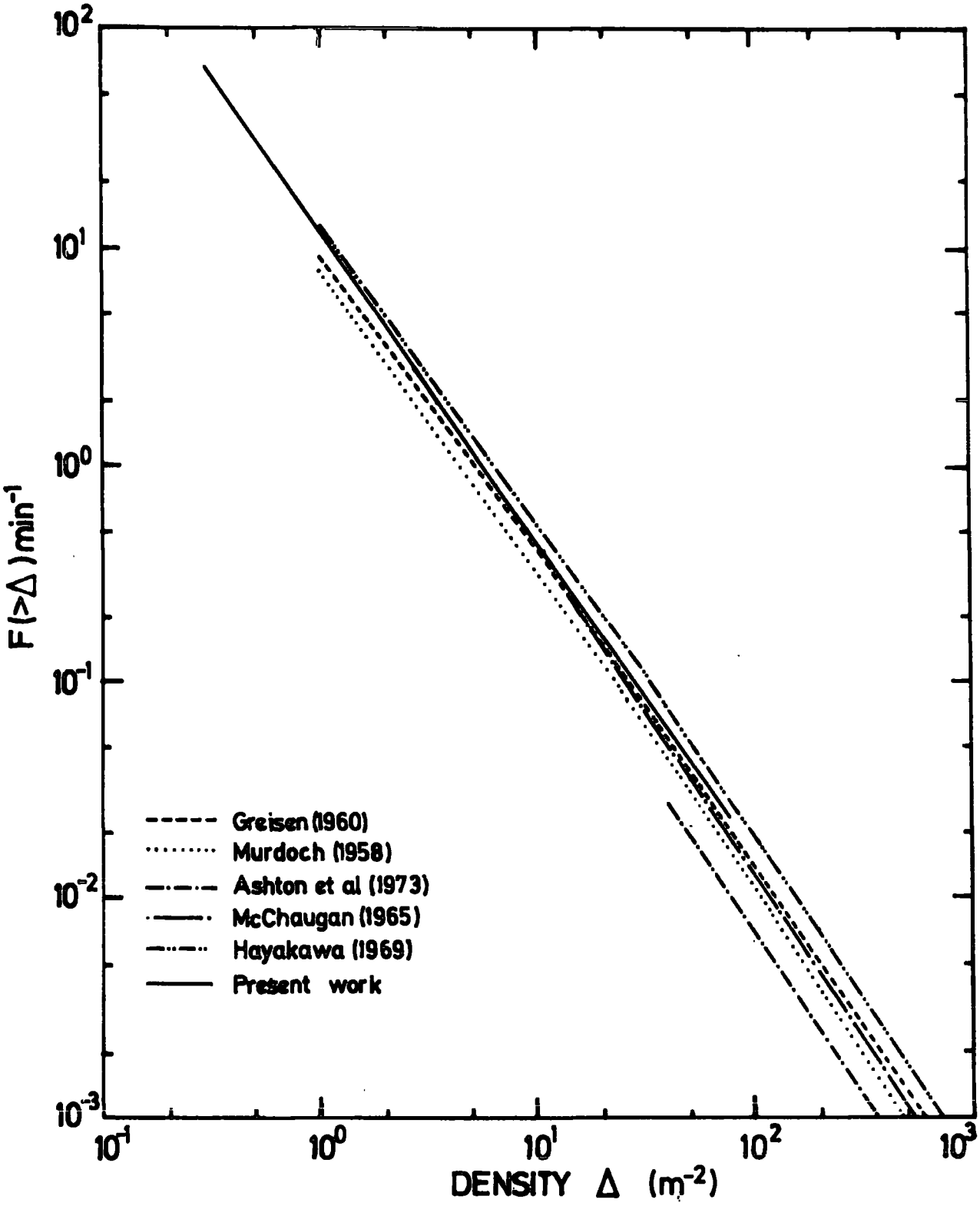

FIGURE 4.16 Comparison of the present measurement of the shower density spectrum with other spectra measured at sea level.

has been reproduced in Figure 4.17. The present experimental points are plotted in the figure. Although the accuracy of the present experimental data points is poor in comparison to other experimental results, it can be seen that within the statistical limits, the results are in general agreement with those of other workers in both shape and absolute value. It is also clear that the present experimental points which extended the measured shower size spectrum to the region of 10^4 - 10^5 particles do not show any marked deviation from an extrapolation down the spectrum in the size range 10^5 - 7 x 10^5 particles.

4.15 CONCLUSIONS

The present investigations have been concerned with some average properties of the muon and electron components of small air showers. Measurements have been made of the sea level rates of muons with energies $\geqslant$ 5 GeV in showers, and it is believed that the approach has succeeded in eliminating most of the spurious events detected alongside the 'real' events. The mean muon rates obtained are shown in Figure 4.12. In the investigation of the electron component, the "decoherence" curve of showers recorded shows a dependence of shower rates on detector separation which is in contradiction with theoretical predictions based on the lateral structure function of E.A.S. This discrepancy is believed to be due to the detection of local showers generated in the vicinity of the apparatus. It has been found that the measured rate of three-fold coincidence detectors is almost independent of the geometry and area occupied by various combinations of detectors. A good agreement has been obtained between the observed three and four-fold shower coincidence rates and theoretical predictions based on both the density spectrum concept and the lateral structure of air showers. It has been found that the experimental results in this case, taken in conjunction with theoretical predictions, indicate that the densities of the showers

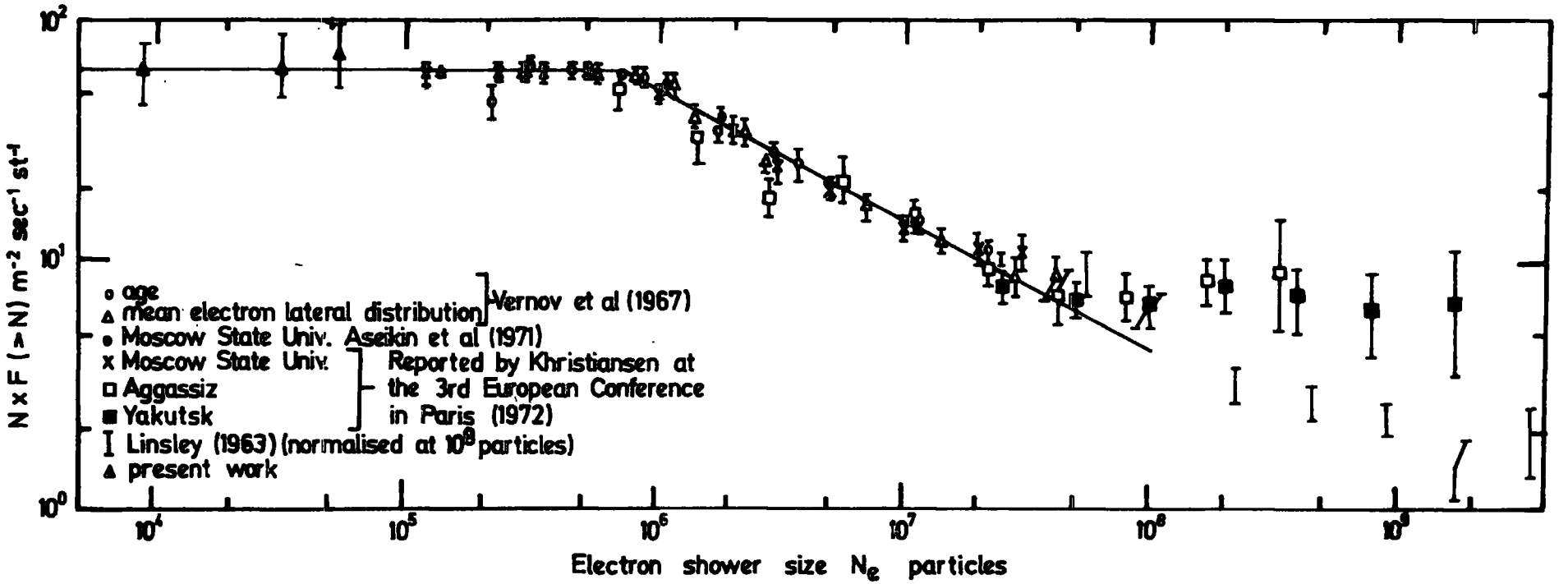

FIGURE 4.17 Comparison of present shower size spectrum with various sea level measurements.

recorded were uniform over the experimental detecting area and it is also concluded that the shower coincidence rates can be represented by a single power law. Measurements of the sea level shower size spectrum has been established in the region 10^3 - 3 x 10^5 particles. Reasonable agreement has been found between present measurements of the absolute intensity and shape of the spectrum, and other measurements for showers of size 10^5 - 7 x 10^5 particles. Measurements of the shower density spectrum have been found to agree well with the results of earlier workers. Indirect determination of the angular distribution exponent (m) of the showers recorded in the size range 10^3 - 3 x 10^5 particles have shown that the intensity of these showers at a particular angle θ to the zenith varies as $\cos \theta^{12.0 \pm 1.0}$. The high value of the exponent m indicates a steep angular distribution which is expected for such showers. However, the measurements made of the rate of the three-fold and four-fold coincidences show no evidence of a considerable contribution from local showers that may cause the steepening.

CHAPTER 5

THE DURHAM EXTENSIVE AIR SHOWER AUTOMATED ARRAY

5.1 INTRODUCTION

It was decided to build a small air shower array in the vicinity of the Physics Department of Durham University, around the M.A.R.S. spectrograph. Hence it would be possible to carry out a comprehensive study of the muon component of Extensive Air Showers. In addition, information on the Hadron component of showers could be obtained in conjunction with the Hadron flash tube chamber that exist near M.A.R.S.

In general,the array provides information on showers in the size range $5 \times 10^4 - 5 \times 10^6$ particles, corresponding to a particle density range of from 1 - 80 p/m^2 at the detectors. Using the fast timing technique it is possible to determine the arrival directions of the recorded air showers.

The detecting elements of the array form a triangular arrangement with detector C at the centre of the array, as shown in Figure 5.1.

5.2 THE AIR SHOWER AUTOMATED ARRAY (GENERAL DESCRIPTION)

It has already been stated that the array, in general, forms a triangular arrangement of scintillation detectors. The first stage of the array contained eleven detectors, four of which were for fast timing and shower density determination, while the rest were for shower density measurements only.

All the density data and fast timing data from the array is digitised and controlled using a "digital unit for storage and transfer" (D.U.S.T.) (see Smith, 1976, for details of D.U.S.T.). The data are stored in a Mullard MM1501 memory core store, and transferred in a predetermined order to an on-line IBM 1130 computer for analysis at a later date.

For the daily check on the operation of the array detectors, a scalar monitor system was designed to give the counting rate of single detectors, as well as various coincidence counting rates between two or more specific detectors in the array.

The array extends over an area of 11,300m^2 with a maximum radius of 60m from the central detector. Figure 5.1 shows the relative positions of the array detectors in respect to the Physics Department ; the M.A.R.S. spectrograph and the Hadron Chamber are included in the map. Detectors 33, 32, 31, C, 51 and 52 are installed on the roof of the building at a mean height of 15m above ground level, while the rest of the detectors are at ground level, except detector 61 which is on the top of the gallery inside the departmental cosmic ray laboratory 10m above ground level. "During this work detectors 31, 11, and 51 are not operational, but the other eleven detectors are all operating as stated."

5.3 THE ARRAY DETECTING ELEMENTS

5.3.1 Introduction

As was mentioned at the beginning of this Chapter, the detecting elements of the array are scintillation counters. The array's fourteen detectors are classified according to the purpose each has been designed to perform :-

a) the timing and shower density detectors,

b) the shower density detectors.

In general, every detector consists of four photomultiplier tubes viewing plastic scintillator. All output pulses from the photomultipliers are sent to a four input linear adder, which sends the summed output pulse via 50Ω coaxial cable to the cosmic ray laboratory.

5.3.2 Timing and Shower Density Detectors

a) The $2m^2$ detectors. The array contains a triangular arrangement of three detectors each having a $2m^2$ sensitive area, and each detector is

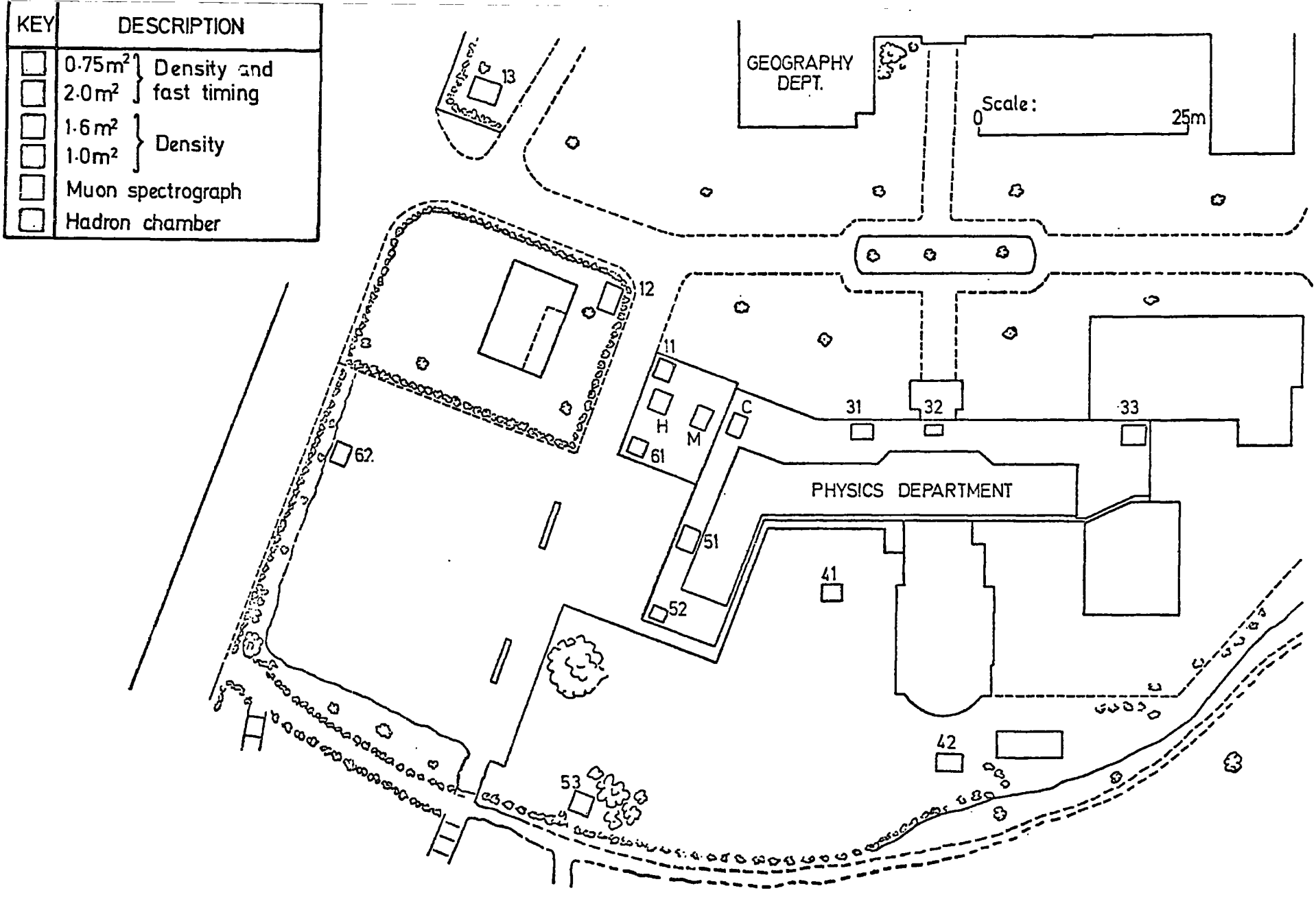

FIGURE 5.1 THE DURHAM EXTENSIVE AIR SHOWER AUTOMATED RESEARCH ARRAY.

installed at the corner of an equilateral triangle forming the main array design. The three detectors are on the circumference of a circle of radius 60m.

Each individual detector consists of a sheet of plastic scintillator coplanar with four photomultiplier tubes (Mullard 9759), having five inch diameters. Two of the tubes are placed at one side of the plastic scintillator and the other two at the opposite side, 1.5m apart and 24 inches from the scintillator surface (see Figure 5.2b). In each detector a fast photomultiplier tube is attached to one side of the plastic scintillator, half way between two five inch tubes. Pulses from the fast photomultipliers are transmitted via 50Ω cable, 100m in length, to the laboratory, and hence a time delay of 500 nsec. occurs before the pulses are received at the cosmic ray laboratory. The linearity map for this type of detector is shown in Figure 5.3a.

b) The Central Detector. The central detector C consists of two identical halves of NE102a plastic scintillator, each of an area 0.38 m^2 and thickness 5 cm. Figure 5.2a shows each half of the detector and the relative position of the density measuring phototubes (Phillips 53 AVP) that have been attached via perspex light guides. Also a fast timing tube (Phillips 56 AVP) is attached to the perspex light guide and gives the zero timing pulse with which the fast timing pulses from other detectors are referenced. These pulses are sent to the laboratory via a 50Ω cable, 30m.in length which ensures that the fast timing signals from the central detector arrive at the recording equipment before the fast timing pulses from the other detectors.

The linearity contour map of the central detector is shown in Figure 5.3b.

5.3.3 The Shower Density Detectors

Seven detectors have been constructed to measure the particle density

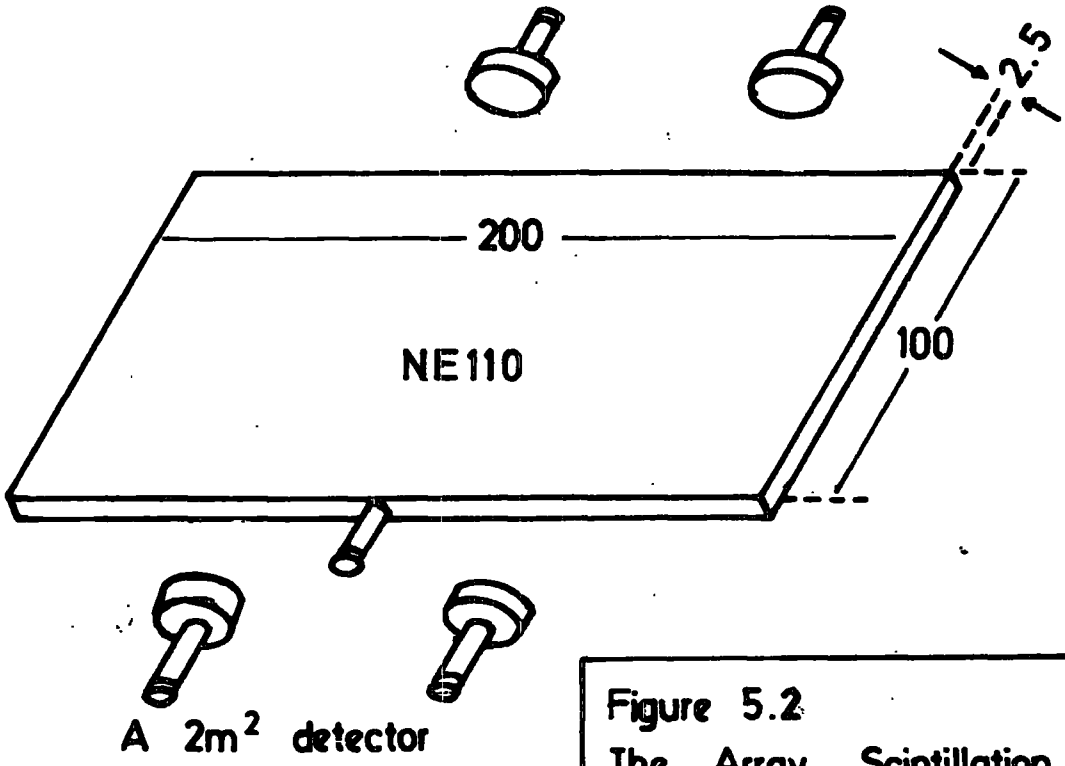

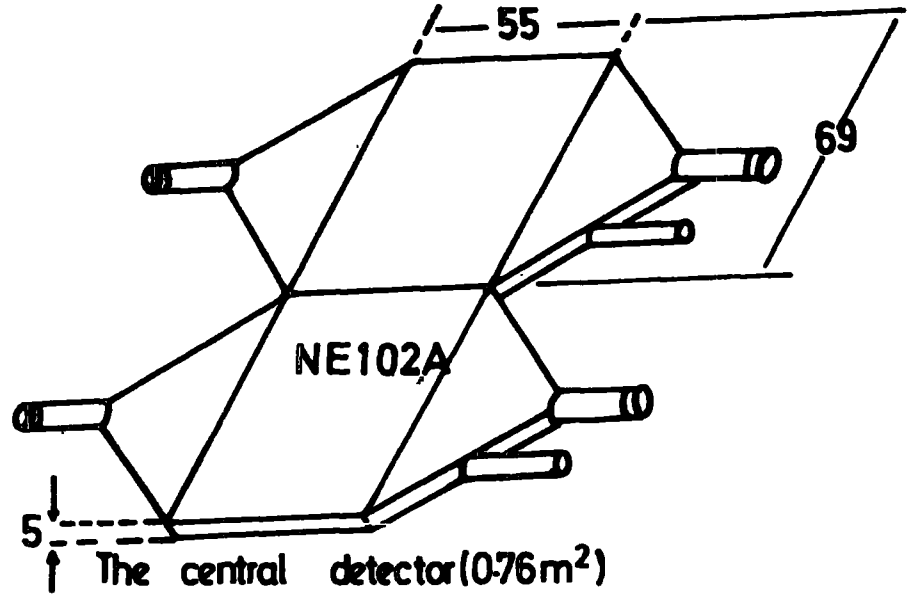

Figure 5.2
The Array Scintillation Detectors
(All Dimensions in cm.)

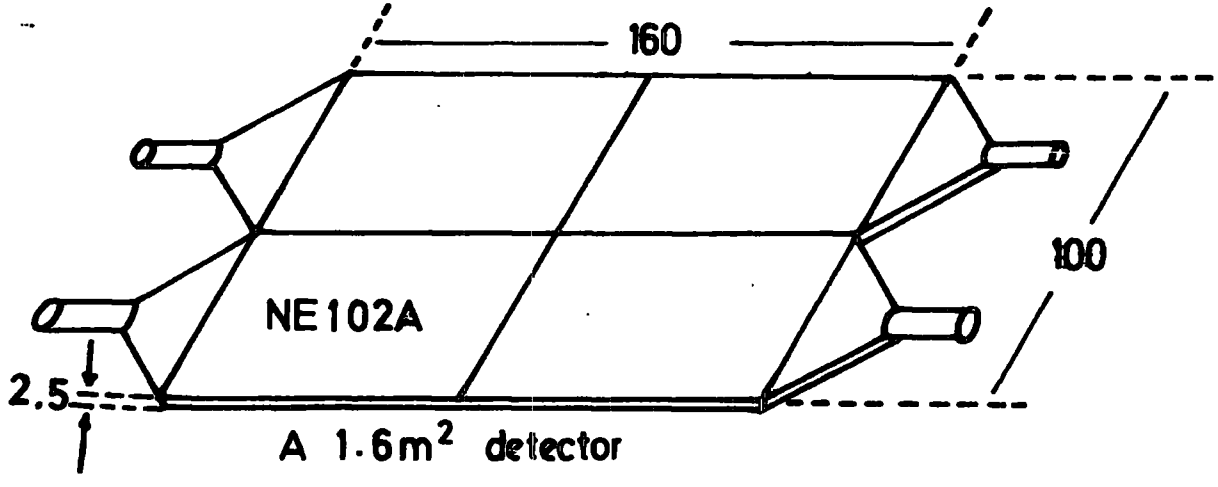

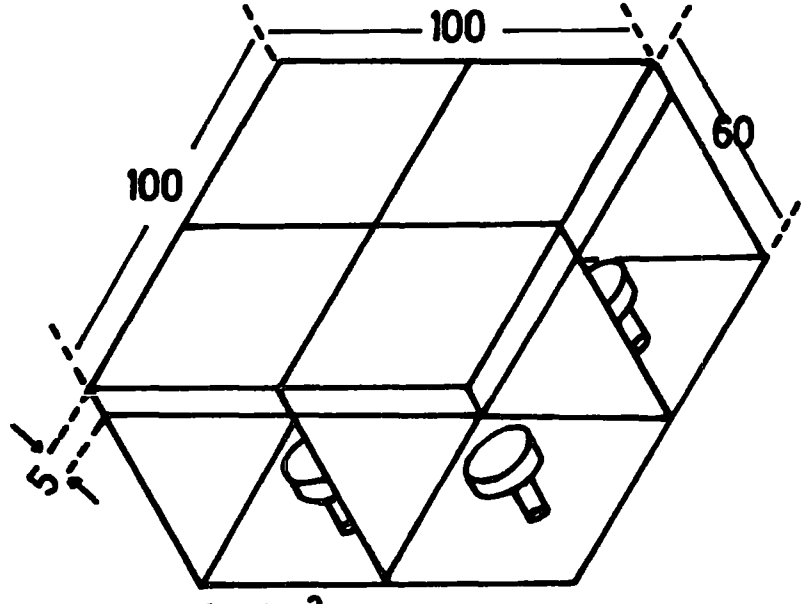

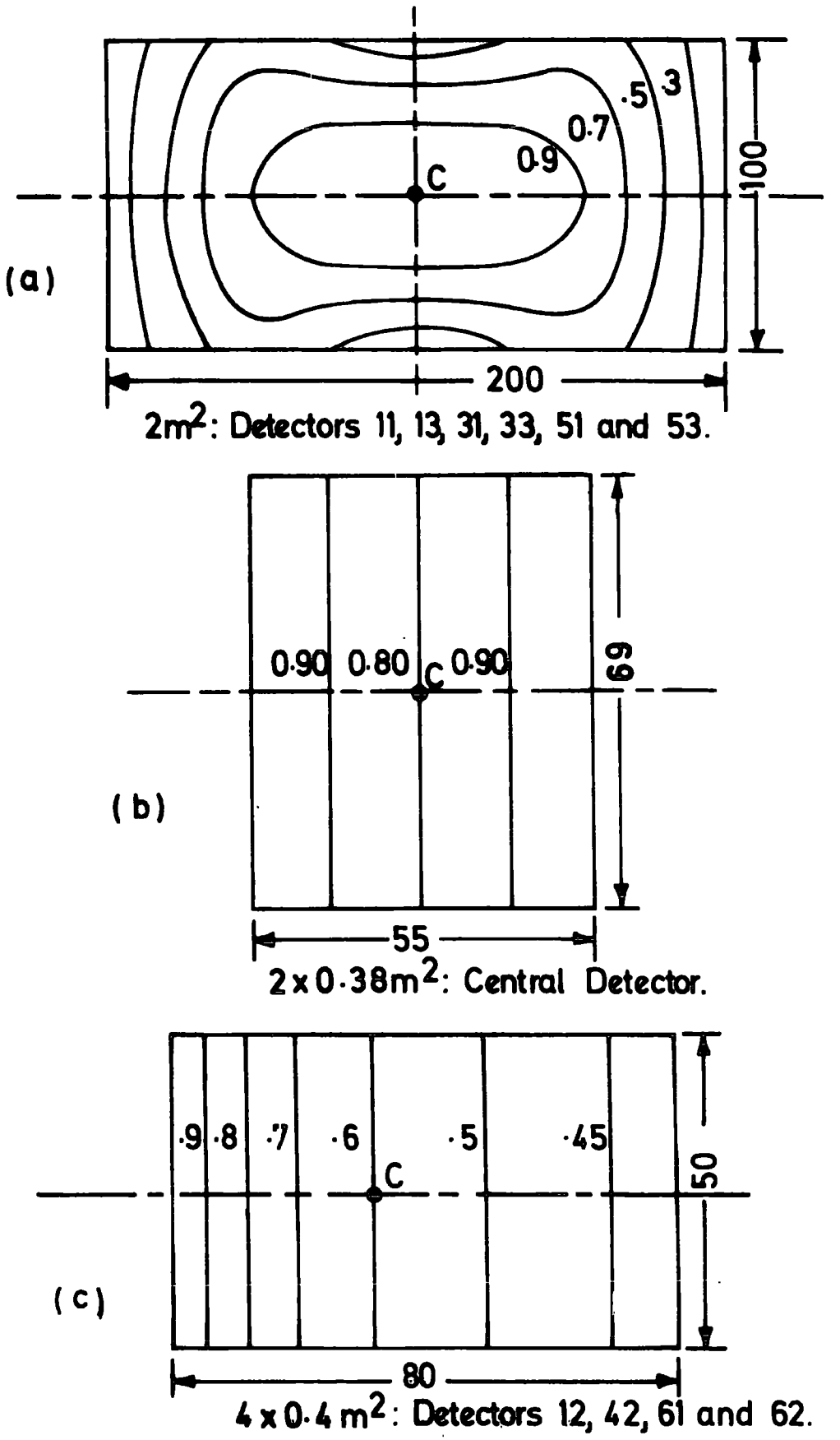

Figure: 5.3 Pulse height contour map of the Array's Scintillators.
Dimensions in centimetres.
C represents the calibration points.
(After Smith, 1976)

only at points in showers. Three of the seven shower density measuring detectors have an area of 1 m^2 each, the other four having an area of 1.6 m^2.

a) The 1 m^2 Detectors (41, 52, 32). The particular location of the 1 m^2 detectors can be seen from Figure 5.1. Each of the detectors 52 and 32 is at a distance of 30m from the central detector C. Each detector consists of four individual quarters (as shown in Figure 5.2d), each quarter being designed in a similar manner to the individual scintillation counters that were used in the previous experiment (Chapter 3). The differences are that the cylindrical iron shield has been removed and the photomultiplier base (see Figure 5.4) has been changed to give a negative output pulse from the anode with $\geq$ 30 μsec pulse duration to meet the requirement of the present experiment. Figure 5.3d shows a contour map of the linearity of one quarter of the detector. By evaluating the average pulse height output at every point on the linearity map over the whole area of the quarter, it was found that the region A can specify the mean pulse height given by that detector to within 10% ; this can be normalised to the central region where calibration measurements take place. A calibration factor was introduced (f), which is the ratio of the mean pulse height of shower particles in regions A and C (see Figure 5.3d).

b) The 1.6 m^2 Detectors. There are four detectors of this type represented by the numbers 42, 12, 62 and 61. The first three of these detectors are located outside the building, while the last one is on the roof of the gallery inside the cosmic ray laboratory. Individual quarters of this type of detector consist of a rectangular slab of plastic scintillator, with a photomultiplier tube (Phillips 53 AVP) joined to the NE102a scintillator plastic by way of a perspex light guide, (see Figure 5.2c). The linearity contour map is shown in Fig. 5.3c.

The dynode resistor circuits of the photomultipliers used in the detectors are shown in Figure 5.4.

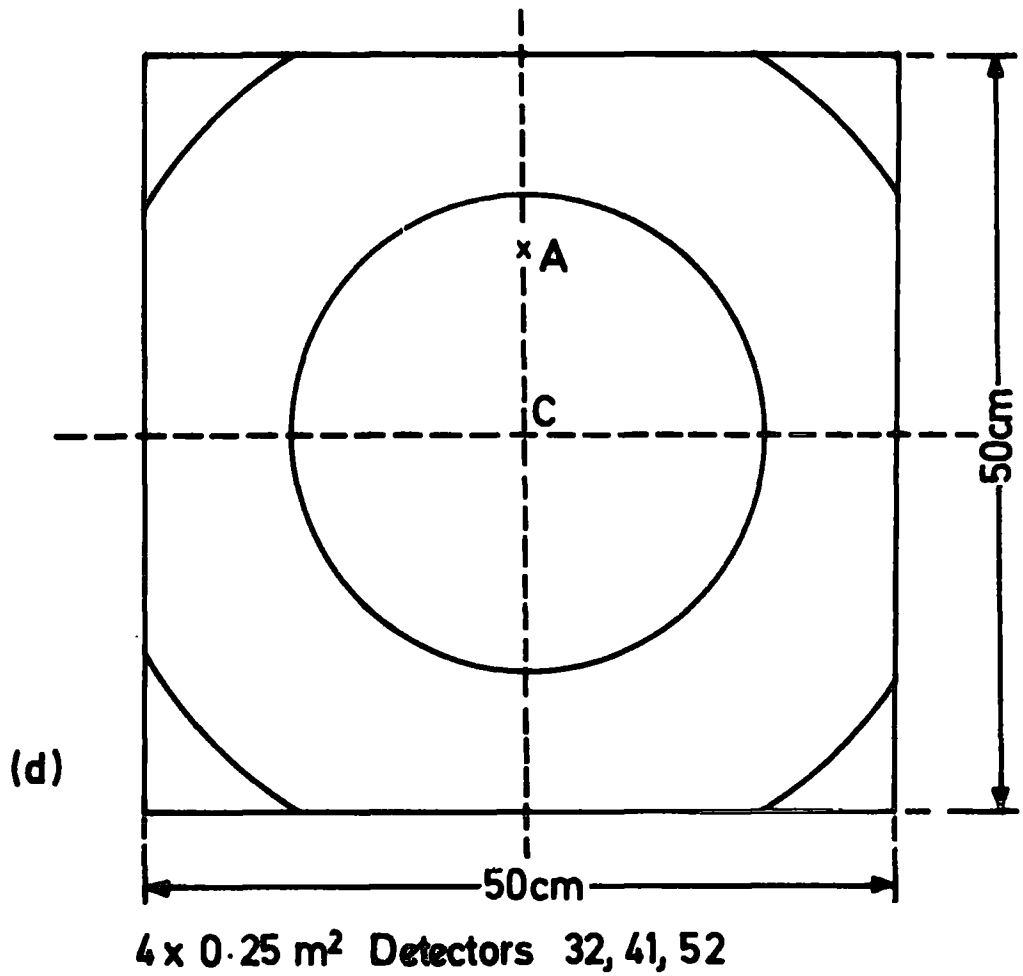

FIGURE 5.3d Pulse height contour map of one quarter of the $1m^2$ density measuring detector. C represents the calibration point.

Base circuit for EMI 9579B PMT

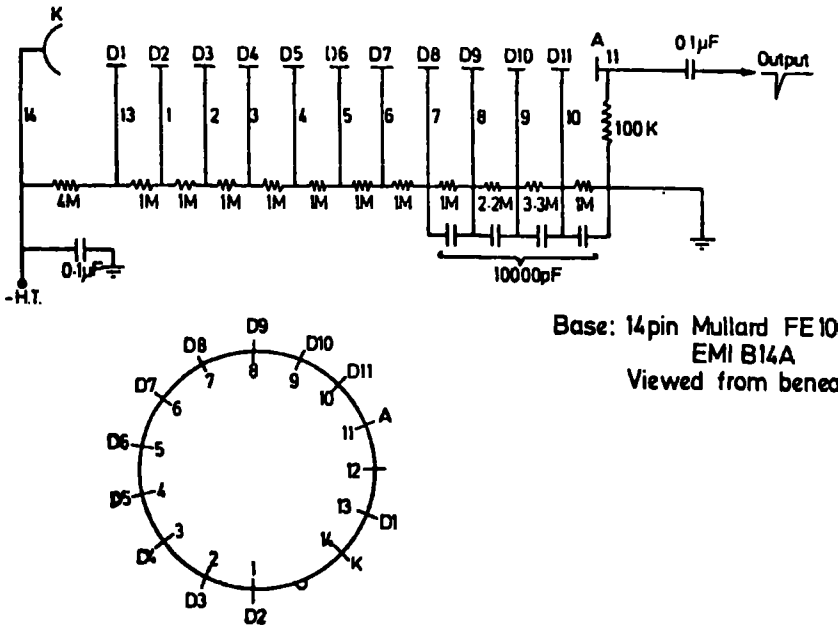

Base: 14pin Mullard FE1001
EMI B14A
Viewed from beneath.

Base circuit for PHILIPS 53 AVP P.M.T.

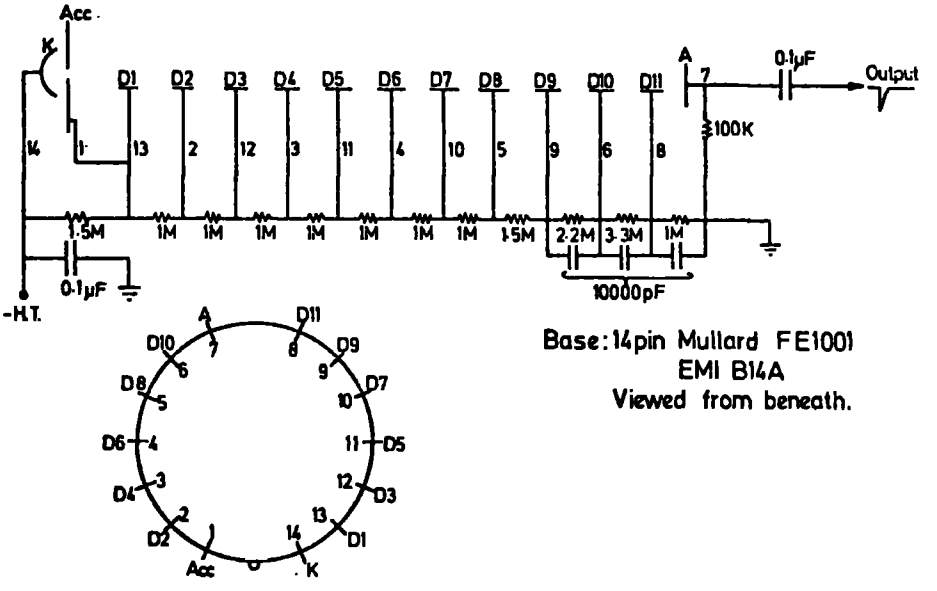

Base: 14pin Mullard FE1001
EMI B14A
Viewed from beneath.

Base circuit for PHILIPS 56 AVP P.M.T.

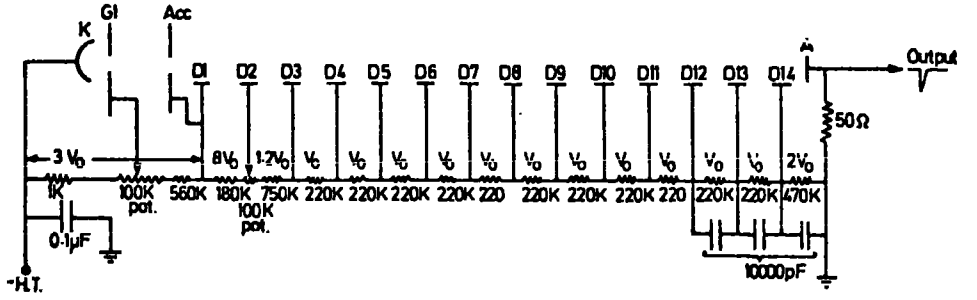

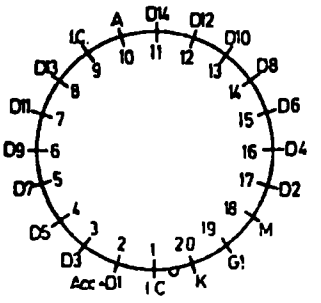

Base: 20pin Mullard FE1003
Viewed from beneath.

Figure 5.4. The Array photomultiplier base circuits.

5.4 THE ARRAY CABLE AND VOLTAGE SUPPLY DISTRIBUTION

5.4.1 The Array Cable Distribution

A cable distribution of 50Ω impedance coaxial cable was used to carry the high voltage output pulses to and from the individual stations in the array. The low voltage supply to the amplifiers was carried through a multiwire screened cable. Twin flex wires supply the service box to every station, including the telephone and soldering iron. A spare coaxial cable connects every station to the laboratory for general use.

5.4.2 E.H.T. Supply Units

There are two types of power supply units. The first is an Ortec 456 high voltage supply unit that supplies the voltage to the photomultipliers used for the density measuring detectors, and it is set at 2.4 kV. The other power supply unit is a NE4646 that supplies the fast timing photomultiplier tubes, and this is set at 2.5 kV.

Due to the different values of working voltage needed by each photomultiplier the voltage supplies were fixed at the above mentioned values, and these values were reduced at each photomultiplier tube by using a potential divider of resistors, each containing initially a row of 23x(100 kΩ) series resistances and a subminiature potential divider of 100 kΩ in value (see Figure 5.5).

5.4.3. Low Voltage Supply

The low voltage supply for the detector head amplifier units was a 24 V unit with a good stabilization against changes in mains voltage.

5.5 THE AMPLIFIERS

The amplifiers are similar to that designed by Hansen (1975) which consists of four emitter followers with their outputs connected to an operational amplifier set to give a gain of 5 $\pm$ 0.1 for each individual input.

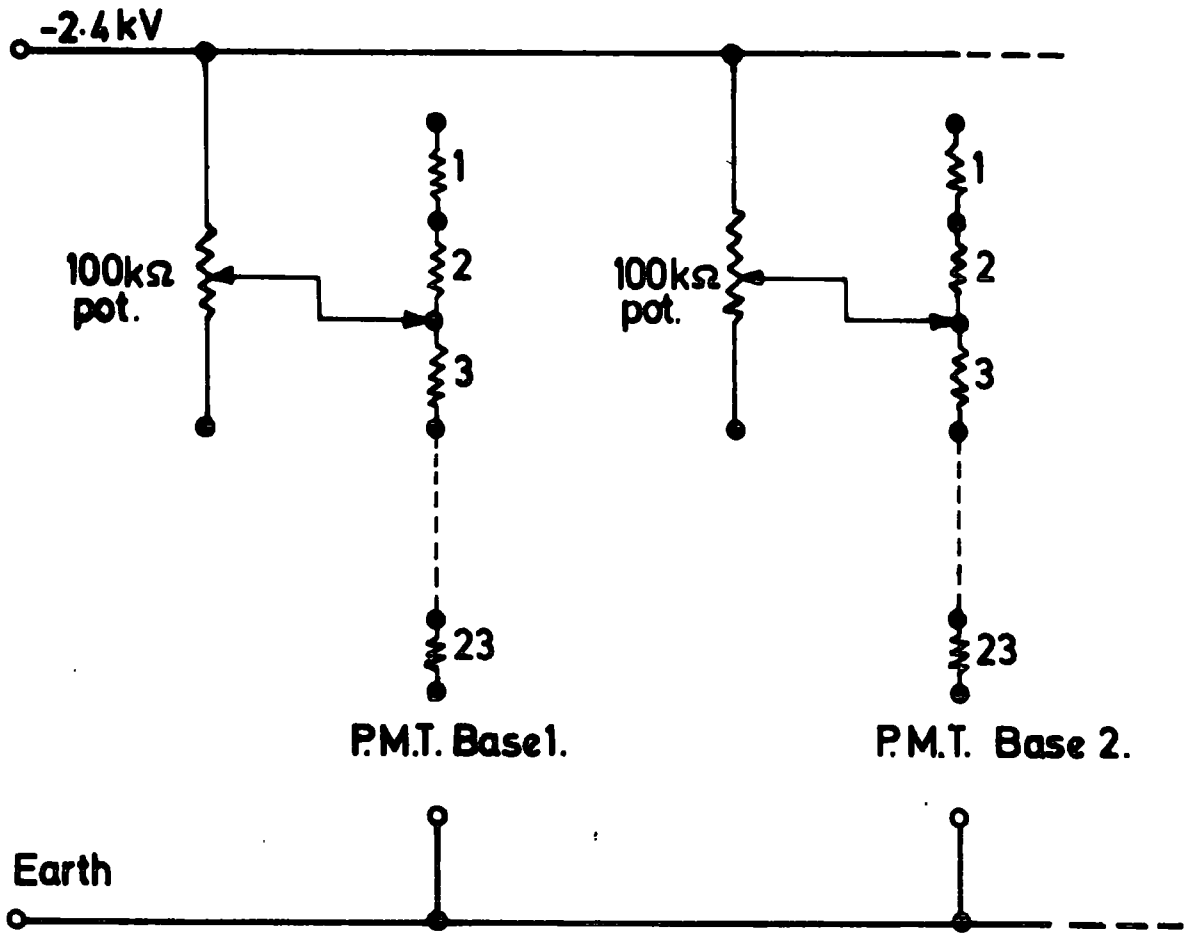

Figure 5·5. The sections of the four E.H.T. distributions at each detector. All resistors are 100kΩ.

The amplifier has an output impedance of 50Ω, and sums the pulses from the four inputs. Output pulses from the photomultiplier anode are negative with a mean duration of 30 μsec, and rise time of 100 nsec. The output pulses from the amplifier are positive. The temperature stabilization coefficient of the amplifiers was 0.1%/^{o}C in the range -40 to +40^{o}C. Figure 5.6 shows the amplifier circuit ; Figure 5.7 shows the gain-temperature variation curve.

5.6 CALIBRATION OF THE DENSITY MEASURING DETECTORS

The density detectors were calibrated so that they had a standard response to the passage of a single cosmic ray particle. The calibration procedure was carried out on individual scintillation detectors since all the detectors differ in design, geometry, and consequently in their response towards cosmic ray particles. Regions of calibration were assessed by studying the linearity contour map of each type of the detectors. The detectors were calibrated to register a mean pulse height of 100 mV per particle per square metre. Since every detector consists of a number of individual scintillators, each of area A, the calibration could be done for a mean pulse height of (100 mV)/A per particle per m^2.

For detectors that consist of a single piece of plastic scintillator of sensitive area S viewed by a number of photomultipliers n, the calibration will be on a mean pulse height of (100 mV)/(n x S) per particle per m^2. For practical reasons it is quicker to measure the peak (mode) of the pulse height distribution obtained rather than the mean, this required the introduction of a factor (R) into the calibration of the detectors. This factor is the ratio of the value of the mean/mode of the measured pulse height distributions averaged over the sensitive area of the detector. Measurements of R for all detectors in the array have shown that R varies only weakly with detector design, and it varies by 5% over the sensitive area of

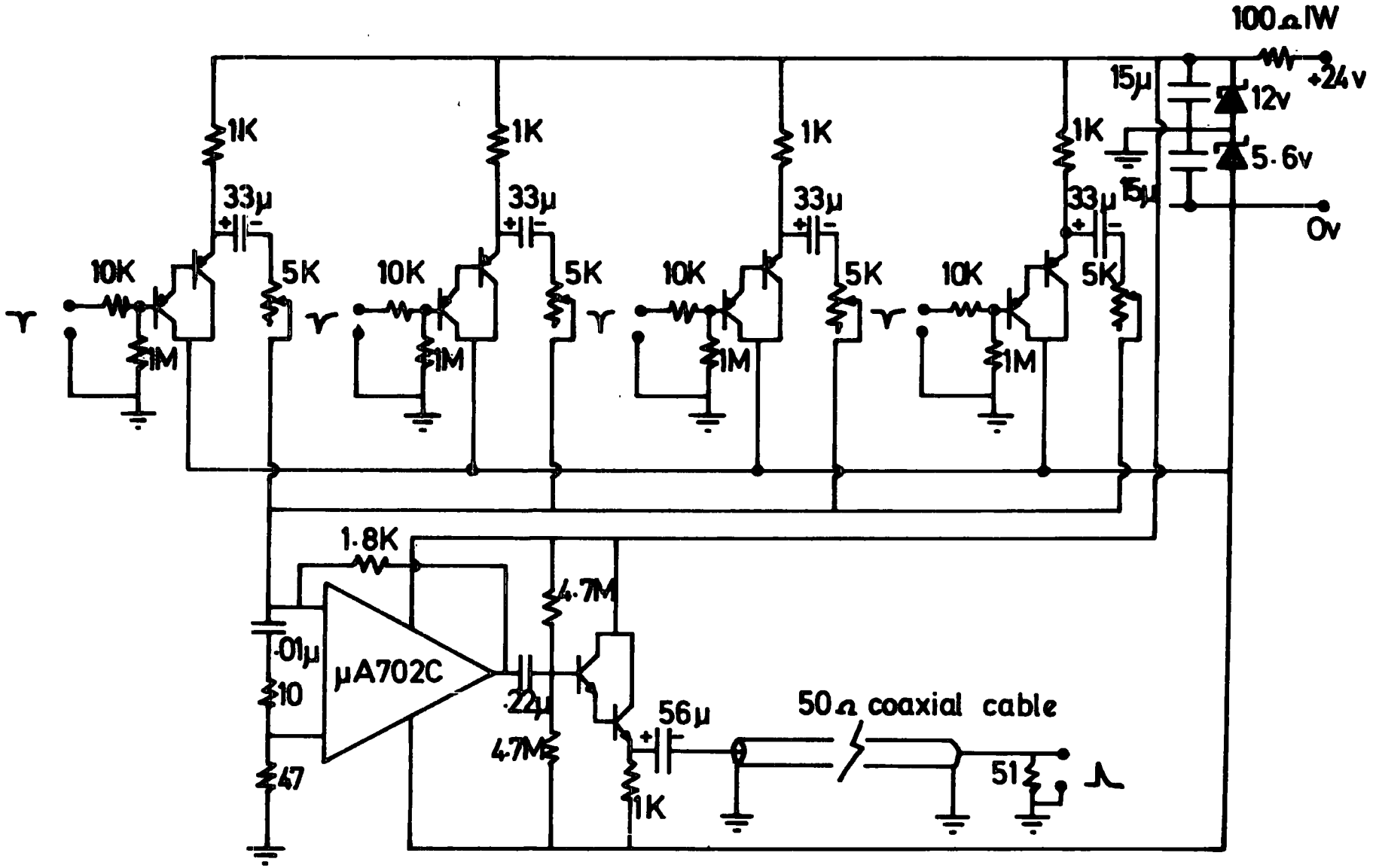

Figure 5·6. Four input gain five mixer-amplifier.
(Transistors: PNP ZTX501, NPN ZTX301)

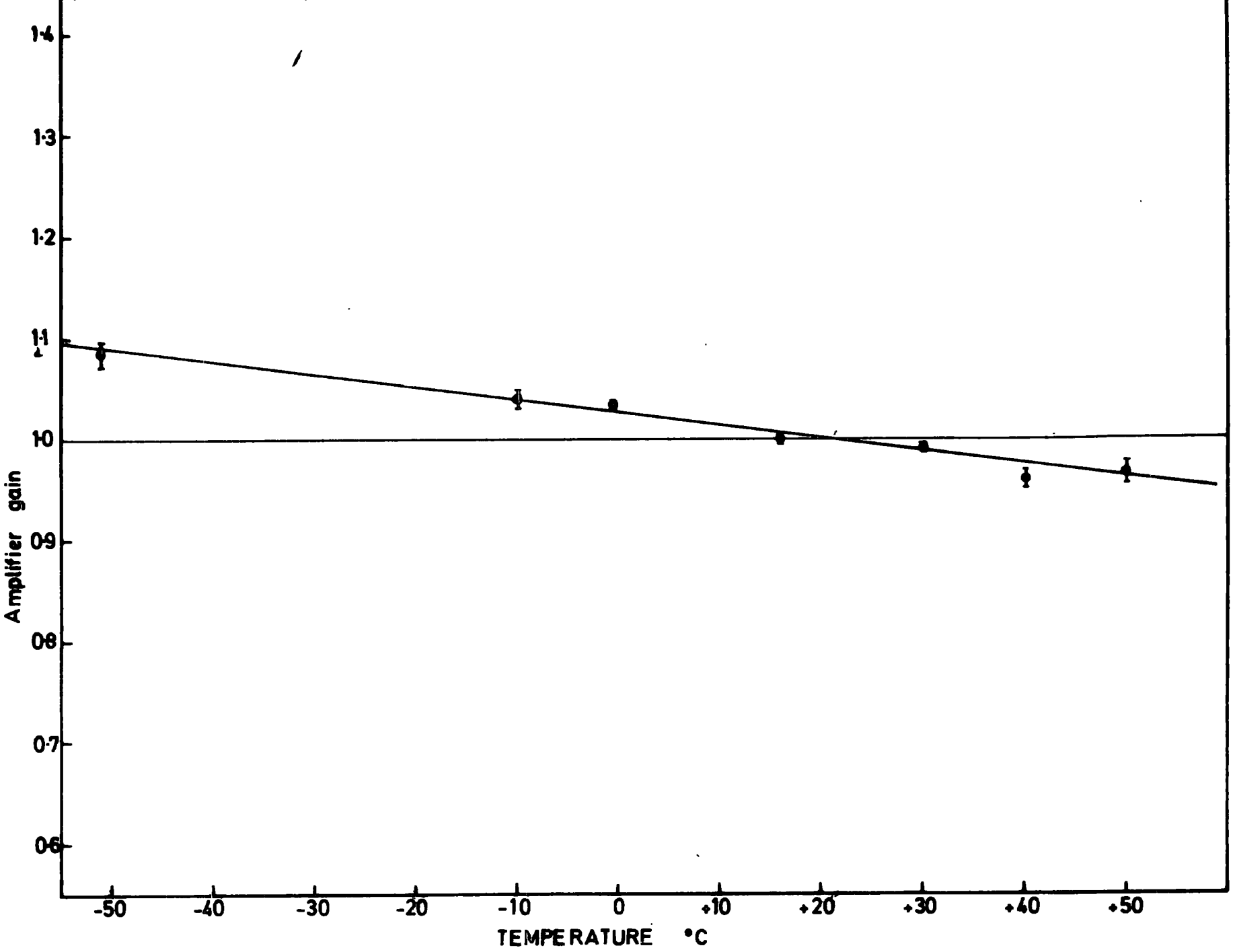

FIGURE 5.7 The temperature gain variation of a Head Amplifier.

various detectors. Another parameter has been included in the calibration procedure, this parameter (F) allows for the non-uniformity of the responses of the various detectors to single cosmic ray particles. Thus the calibration of a specified detector in the array has been modified as follows :

$$\frac{F \times 100\ mV}{n \times S \times R}$$

where n x S = A for a detector that consists of one piéce of plastic scintillator viewed by n photomultipliers. Table 5.1 shows the measured values of the parameters R and F, and also the calibrated pulse heights of the detectors in the array.

5.6.1 The Telescope

In order to calibrate individual detectors, regions of calibration of the air shower detectors are defined by a scintillator telescope which consisted of a 23 x 23 x 3 cm. plastic scintillator viewed by two photo-multipliers (Phillips 53 AVP) as shown in Figure 5.8. The procedure was to open the gate of the M.C.A. by the coincidence positive logic pulse from the telescope phototubes. The telescope counting rate was 6 sec^{-1}.

5.6.2 The Calibration Procedure

The telescope just described was used for the calibration of the density measuring tubes. Positive logic pulses produced by the telescope due to the detection of particles, opened the gate of the Analogue to Digital Converter (A.D.C.) in the Multichannel Analyser (M.C.A.) and enabled the particle pulse height distribution from the region of the detector selected by the telescope to be stored. In order to calibrate the photomultiplier the E.H.T. on the tube was adjusted using the potential divider across the specified photomultipliers such that the peak of the distribution coincided with the chosen calibration value. This procedure was done for all the tubes used in the array density measuring detectors. Figure 5.9 shows a

TABLE 5.1

THE CALIBRATION MEASUREMENT PARAMETERS FOR THE DENSITY TUBES

Detector	Total area in m^2 (A)	Number of scintillators in a detector	Number of photomultipliers		Mean/mode (R)	F	Calibration pulse height	Scintillator calibration coordinates
			No. per piece (n)	Total				
C	0.76	2	2	4	1.53 ± 0.01	0.89	38.3	0,0
32, 41, 52	1.0	4	1	4	1.40 ± 0.01	1.00	71.4	0,0
12, 42, 61, 62	1.6	4	1	4	1.60 ± 0.01	1.00	39.1	-7,0
11, 31, 51, 13, 33, 53	2.0	1	4	4	1.83 ± 0.01	1.41	9.6	0,0

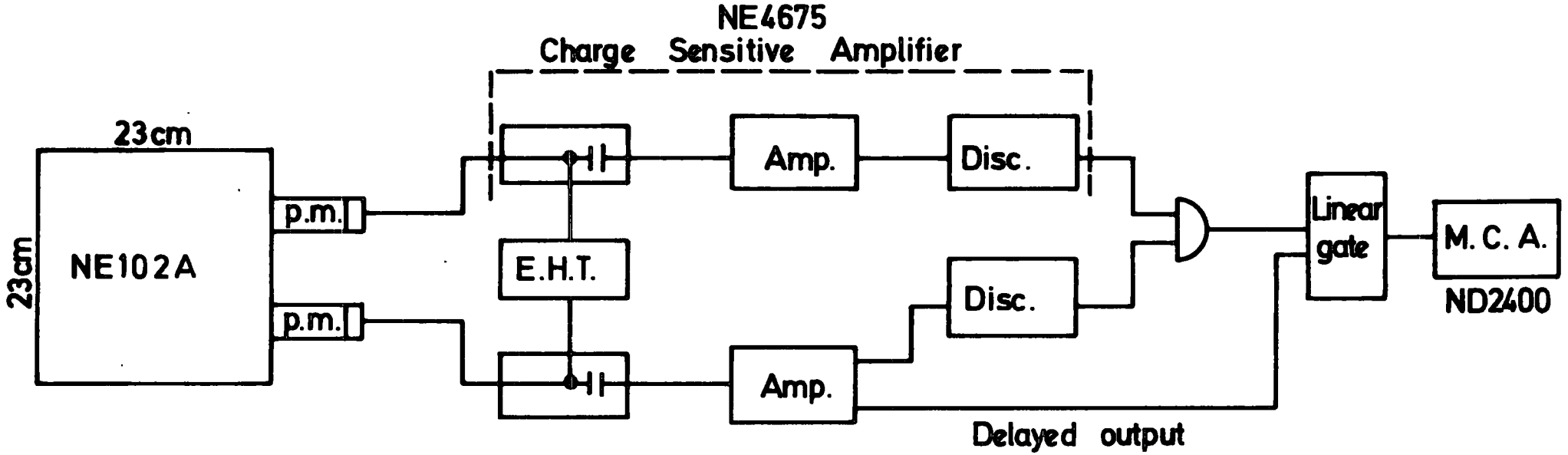

FIGURE 5.8 The telescope electronics block diagram.

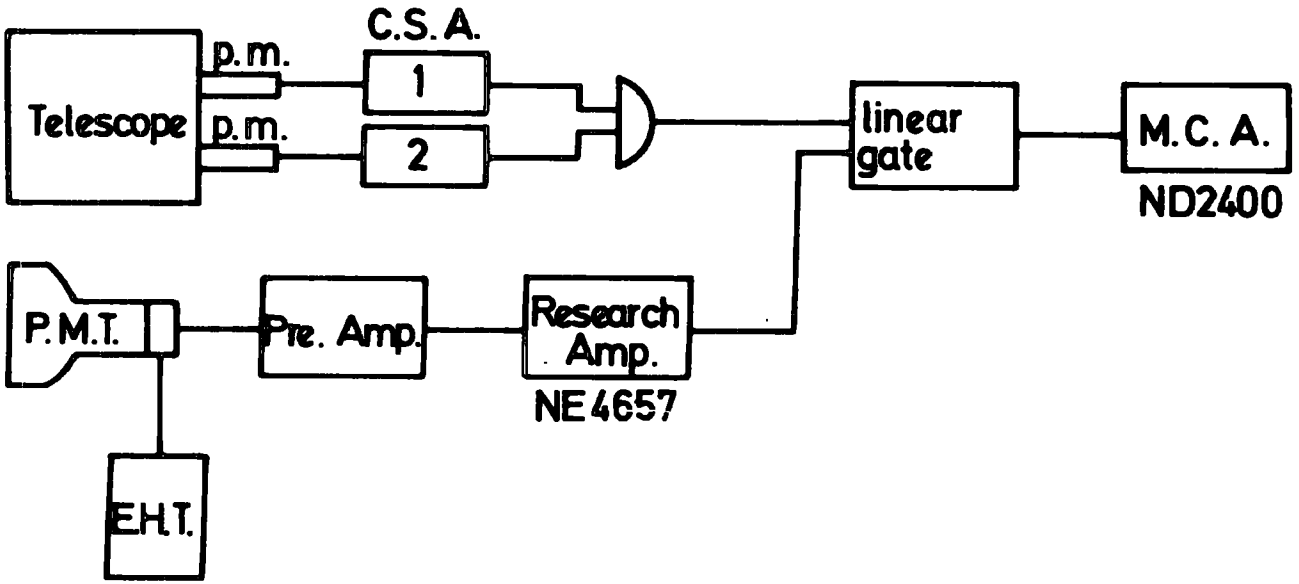

FIGURE 5.9 The calibration electronics block diagram.

block diagram of the electronic set-up.

5.6.3 Calibration of Fast Timing Phototubes

Output signals from fast photomultipliers are rather short (∿5 nsec.) compared with those of the density pulses at the FWHM. In the present experiment these tubes were set up so that the probability of there being a fast timing pulse generated when the discriminators on the density measuring tubes were triggered was high, typically > 95%. The counting rate of the fast timing tubes was noted and maintained constant throughout the experiment. The rates were checked for all fast tubes before the start of a run as part of the daily checking procedure of the data handling electronics. The typical fast tube counting rate was 500 sec^{-1}.

5.7 THE COINCIDENCE SCALAR MONITOR

This serves to measure the daily counting rates of single detectors at certain discriminator levels. As has already been stated, output pulses from the head units are brought to the laboratory, via 50 Ω coaxial cables of different lengths varying from 20 m to 150 m ; pulses are positive with a duration of ≳ 30 μsec. and a rise time of ∿ 100 nsec., which are then fed into a discriminator preset to discriminate at the 2 particle m^{-2} level. After the pulses have been discriminated they are fed into a coincidence unit which is designed to give fourteen single output pulses and fourteen multiple coincidence pulses (≳ 2-fold coincidence). Output pulses from the coincidence unit were fed into a scalar and the various rates monitored.

Figure 5.10 shows the coincidence scalar monitor system used. In this way it was possible to monitor the rates of single detectors at the same time, the period of counting usually being 120 sec. Rates of single detectors were of the order of 2,000 - 8,000/2 mins. Table 5.2 shows the integral rates per sec. for each detector (≳ 2 p/m^2). This rate remained

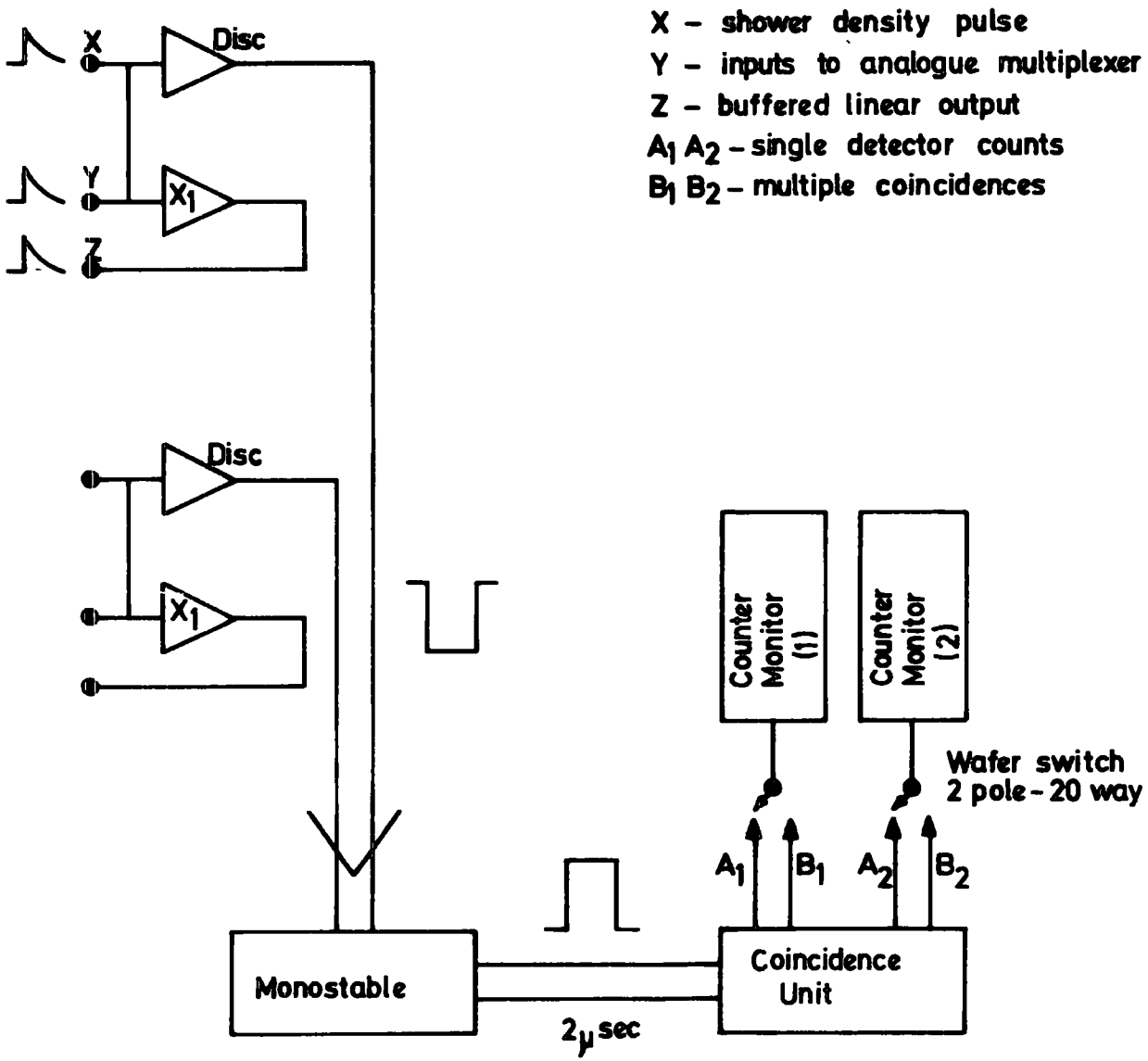

Figure 5·10 The array coincidence monitoring system.

TABLE 5.2

THE INTEGRAL SINGLE COUNTING RATES OF THE OPERATIONAL ARRAY DETECTORS ABOVE THE DENSITY LEVEL OF $2p/m^2$

Detector area (m^2)	Detector number	Integral rate (sec^{-1})
$1m^2$	32	14.0 ± 0.3
	41	22.3 ± 0.4
	52	19.5 ± 0.4
$1.6m^2$	12	52.2 ± 0.66
	42	40.3 ± 0.6
	61	58.5 ± 0.7
	62	51.4 ± 0.7
$2m^2$	13	44.6 ± 0.6
	33	66.4 ± 0.7
	53	20.4 ± 0.4
Central detector	C	63.6 ± 0.7

constant, except for barometric variations, to within 2%. Sixteen multiple coincidence arrangements were used, consisting of eleven 2-fold, three 3-fold and two 4-fold coincidences.

5.8 THE LINEARITY OF THE ARRAY PHOTOMULTIPLIERS

Photomultiplier tubes in all the detectors serve to convert the light output of the scintillator into electrical signals which can be interpreted in terms of particle densities at the detectors. Three types of photomultipliers have been used in the array detectors ; E.M.I. 9579B having a 5 inch diameter photocathode, and Phillips 53 AVP and Phillips 56 AVP, both having 2 inch diameter photocathodes. In order to check the linearity of the photomultiplier tubes light pulses were provided by a pulsed light emitting diode which was set up to give light pulses similar to those obtained from the scintillator. The intensity of the light from the diode could be reduced by using crossed polarizing filters. The output signals from a photomultiplier anode were taken to an oscilloscope and measured as a function of the intensity of light falling on the tubes. Figure 5.11 shows the results of these measurements on the E.M.I. 9579B and and the 53 AVP respectively, and shows that the phototubes were linear over the range of applied voltages used in the present experiment.

5.9 THE DATA HANDLING ELECTRONICS

The array data handling electronics (Figure 5.12) processes two sets of data for every air shower event. One set comprises the analogue signals representing the air shower density information from the array density detectors. The second set comprises information from seven timing markers. One of these markers defines the origin of the timing co-ordinate system (zero time) and the other time markers are related to this, such that the relative time differences can be used to determine the zenith and azimuthal angles of the shower. This section describes briefly how the

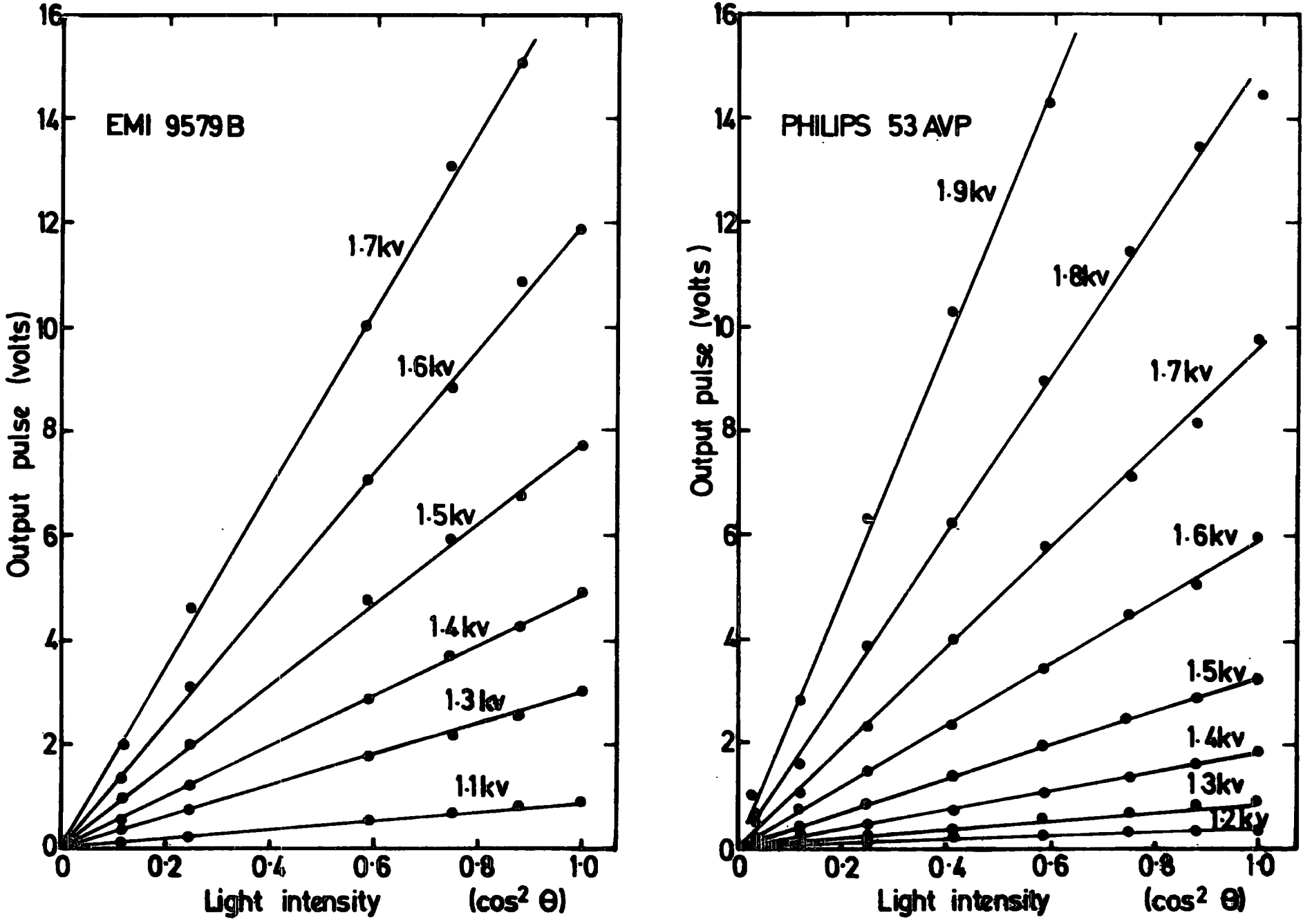

Figure: 5.11 The linearity of the Array particle density measuring photomultiplier tubes.

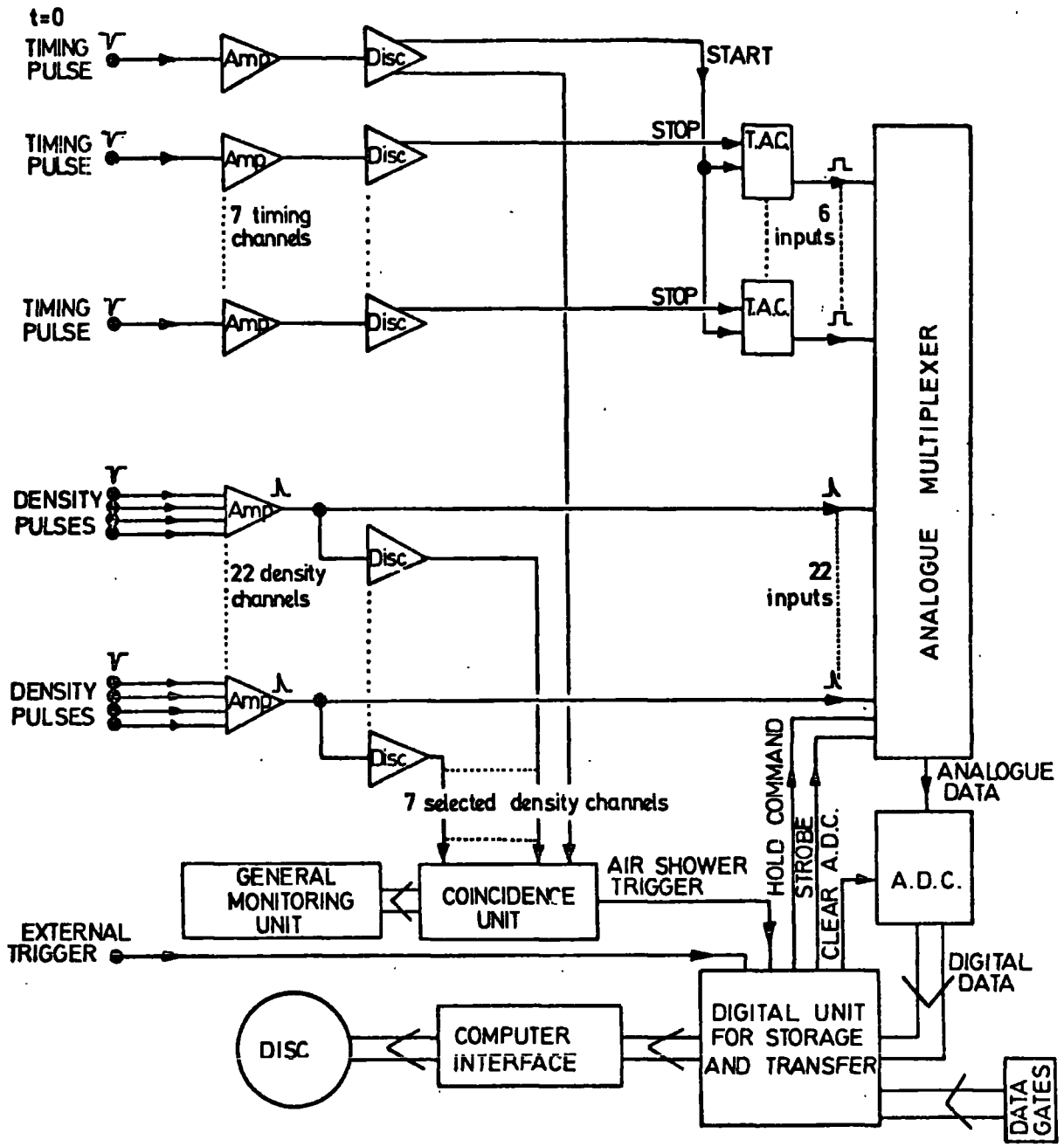

FIGURE 5.12 The shower event handling circuitry.

data are initially produced, and then follows the progress of these data to the point where they are ready for processing inside the laboratory. It is from these data that the parameters of the air shower are eventually evaluated, specifically the size, core location and arrival direction of the showers.

5.9.1 The Timing Pulses

Timing pulses, on their entrance to the laboratory, are fed into fast discriminators. From the relationship between the timing pulses the angular direction of the shower axis is determined. The time differences between the pulses are converted into analogue voltages using time to amplitude converters (T.A.C's). The central detector timing pulse is used to 'start' all the T.A.C's, and the pulses from individual detectors 'stop' each T.A.C. The T.A.C's outputs are then fed to the analogue multiplexers and also to linear buffers and discriminators for monitoring purposes.

5.9.2 The Density Pulses

For each of the phototubes in a detector the density pulses are added, amplified and calibrated before they reach the laboratory. At the laboratory the pulses pass via buffer gates to the analogue multiplexer, and also to discriminators for event selection and monitoring purposes. The discriminators are used to monitor the counting rate of each detector (Section 5.7) and also provide logical signals for the coincidence unit which may trigger the air shower array or other external devices.

5.9.3 The Analogue Multiplexers

This device serves to store a shower's data for a short period of time after an event has been established. In this time the data are digitised using an analogue to digital converter ; each analogue pulse is processed sequentially by the same converter.

5.9.4 Digitisation

The above mentioned analogue to digital converter (A.D.C.) is a device that accepts analogue signals in the range 0-5 V and converts them

into binary digits in the range 0 to 1023. The A.D.C. typically takes 100 μsec. to process a single analogue pulse. In order to identify an air shower a certain amount of "book-keeping" information is required. This information is initially assembled in devices called the data gates and consists of the following :-

1 The event header

2 The run number

3 The event number

4 The event trigger mode

5 The operational units

6 The time of the event

7 The event ender

The event number, (i.e. item 3) is supplied by the M.A.R.S. general scalar that is described in the work of Hansen (1975). Shower events that are associated with muons traversing the spectrograph have identical event numbers.

5.9.5 Data Unit for Storage and Transfer (D.U.S.T.)

This important device controls the acquisition and transfer of the air shower data from the memory core store in which it is initially held to the IBM 1130 computer. It supplies all the appropriate commands that ensure that the data are written in the correct location in the memory core store. It instructs the on-line IBM 1130 to read out all of the stored data when the core store becomes full. The transferred data are stored on magnetic disc where it remains for a few days before being sent to the IBM 370/168 for subsequent analysis.

5.10 THE RESPONSE OF THE E.A.S. ARRAY

In order to interpret and understand the experimental results it is necessary to have a knowledge of how the array responds to showers of

a certain size. The array's response to showers can be estimated using the established electron lateral distribution function. Limits on the minimum radial distance and measured densities can be set by considering the smallest air shower detector used in the array. Since the smallest detector used in the array is of area $1m^2$, the electron lateral distribution cannot be measured below 1 metre from the shower core, and the minimum detectable density is limited to a value of 0.5 particles per square meter since the largest detector used is 2 square meters. The array will detect showers that fall at large distances from the central detector C, but showers that fall more than 50m from the array's centre are not used in any analysis. The maximum detectable shower density is determined by the saturation voltage of the shower density measuring electronics which corresponds to a value of 80 p/m^2 at the present time.

Figure 5.13 shows simply the above mentioned features of the array for showers in the size range 10^3 - 10^7 p/m^2. This range in shower size is further reduced by folding in the shower probabilities.

In the present work the detectors used for triggering purposes are the central detector and the 2 m^2. detectors. Although this criteria is not the most useful (see Chapter 7) it was the only one that could be used when the experiment commenced since these detectors were the only available detectors that initially possessed the fast timing facilities.

5.11 THE TRIGGERING REQUIREMENTS FOR THE EXPERIMENT

The experimental objective was to obtain a number of associated events between M.A.R.S. and the array which could yield information on the muon lateral distribution, energy spectra and other aspects of muons in E.A.S. An electronic circuit was designed to trigger both sets of apparatus (M.A.R.S. and the Array). The normal triggering requirements which are

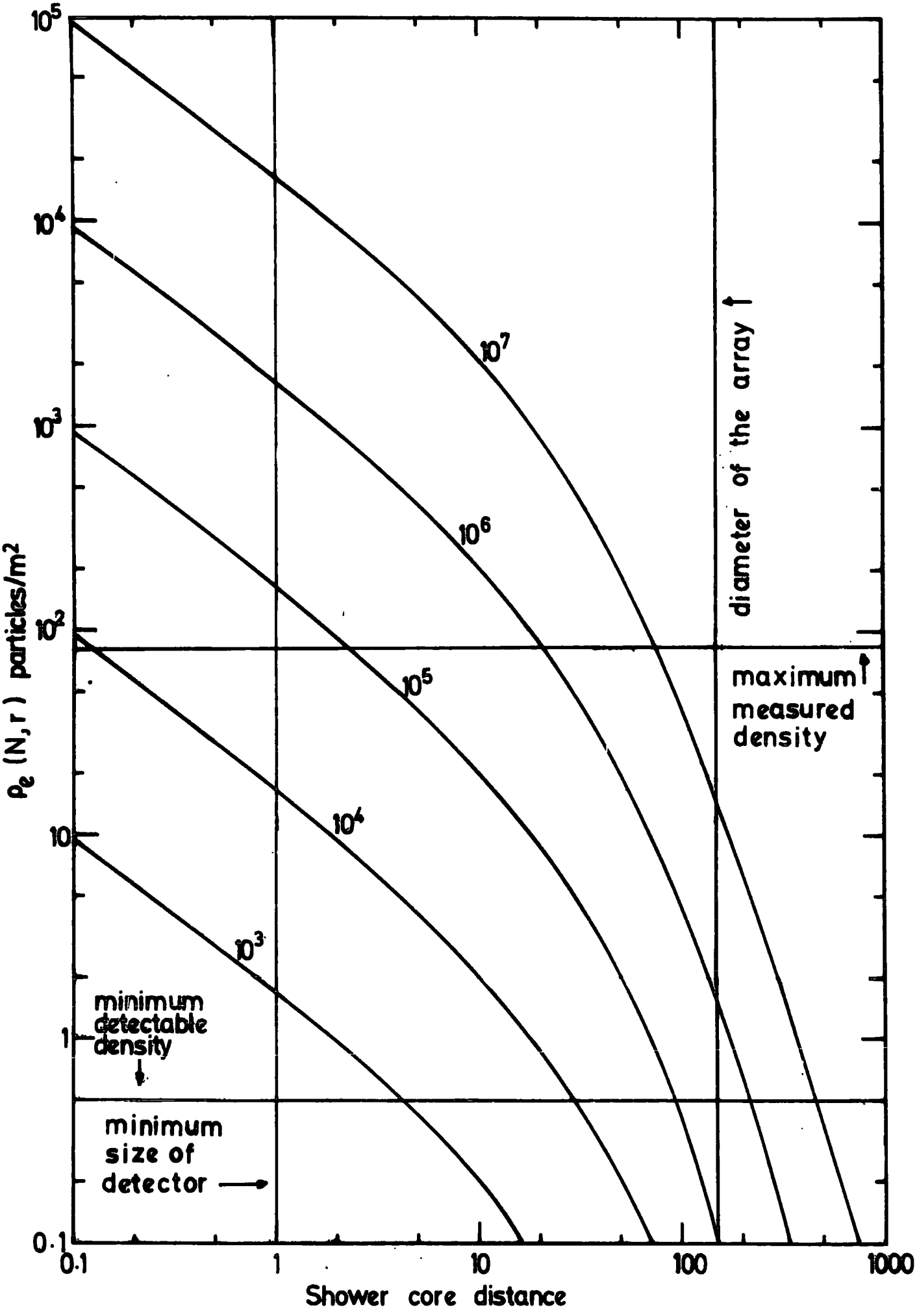

FIGURE 5.13 The general response of the air shower array.

designated as C + M.A.R.S. is that a pulse from the central detector (C) corresponding to a density of more than 4 p/m^2 coincided with a master pulse from the spectrograph due to it having been traversed by a muon (i.e. the 3-fold coincidence pulse of the blue-side scintillators).

When both M.A.R.S. and the Array are triggered in coincidence, flags specifying the coincidence are recorded with each set of recorded data. This arrangement made it possible to identify events that contained muons associated with air showers from amongst all the other classes of event that were being recorded on the equipment.

The counting rates of the coincidences were checked every day to ensure the correct functioning of the apparatus.

In addition to the C + M.A.R.S. triggering requirement, the apparatus was operational under the triggering requirement of a normal array trigger and M.A.R.S. i.e. C + 13 + 33 + 53 + M.A.R.S.; such a criterion generally provided timing information connected with the detected showers which frequency allowed the determination of the shower arrival direction to be made.

5.12 RUNNING DETAILS AND MAINTENANCE OF THE APPARATUS

Various daily checks were carried out on the performance of all the array detectors and the data handling electronics. The integral counting rates of the array detectors above a preset discriminator threshold was measured every day. These rates were then plotted and any significant change in the rates of one of the detectors was easily noticed. Also, a daily plot of the multiple coincidence rates between various detectors (two, three and four fold coincidence rates) was made.

Before the start of a new run, the data storage cycle was checked, and this test ensured that all the data gates were operating correctly, and that the analogue data were being stored, digitised and read correctly into the buffer memory. For each detector and Time to Amplitude Converter a

pulse height distribution was obtained daily and the consistency of the distribution examined. Figure 5.14 (a,b) shows a typical daily histogram that was obtained during the running of the experiment. The analogue multiplexer and the A.D.C. gains were continuously monitored with each event. This was achieved by presenting a standard pulse to one of the analogue signals of the multiplexer. The histogram of the standard pulse was also plotted in the same way as the density and the T.A.C's histograms were plotted. It was found that the analogue multiplexer and the A.D.C. gains were satisfactorily constant and no noticeable change was found from run to run.

5.13 DISCUSSION

This Chapter has described the elements of the air shower array and the standard method of the calibration of the detectors, and given also a brief description of the data acquisition procedure and the data storage and transfer system. The next chapter deals with the array and M.A.R.S. data analysis programmes and their function with a special reference to the muon data collection in this work.

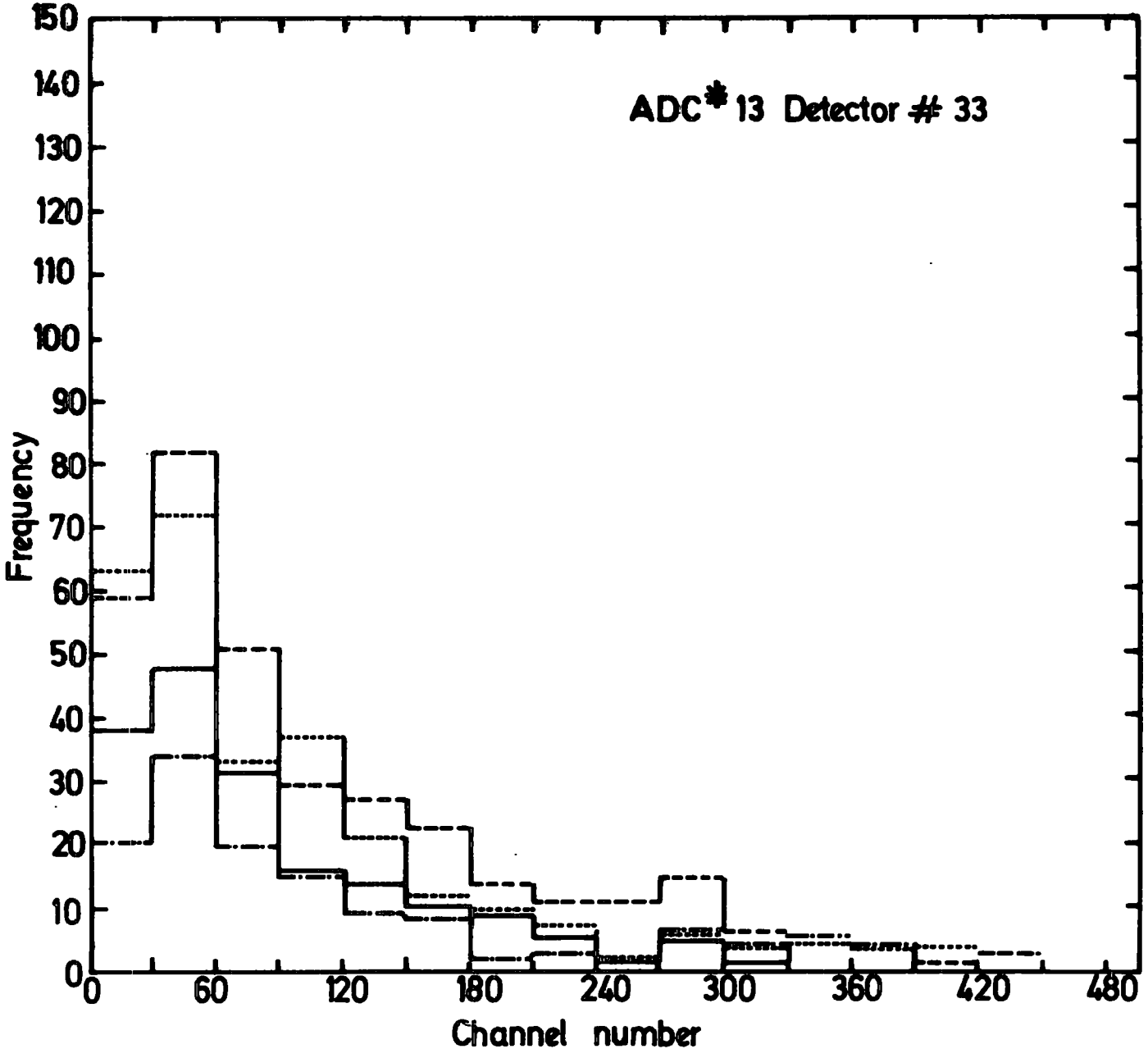

FIGURE 5.14a A typical pulse height histogram for detector # 33

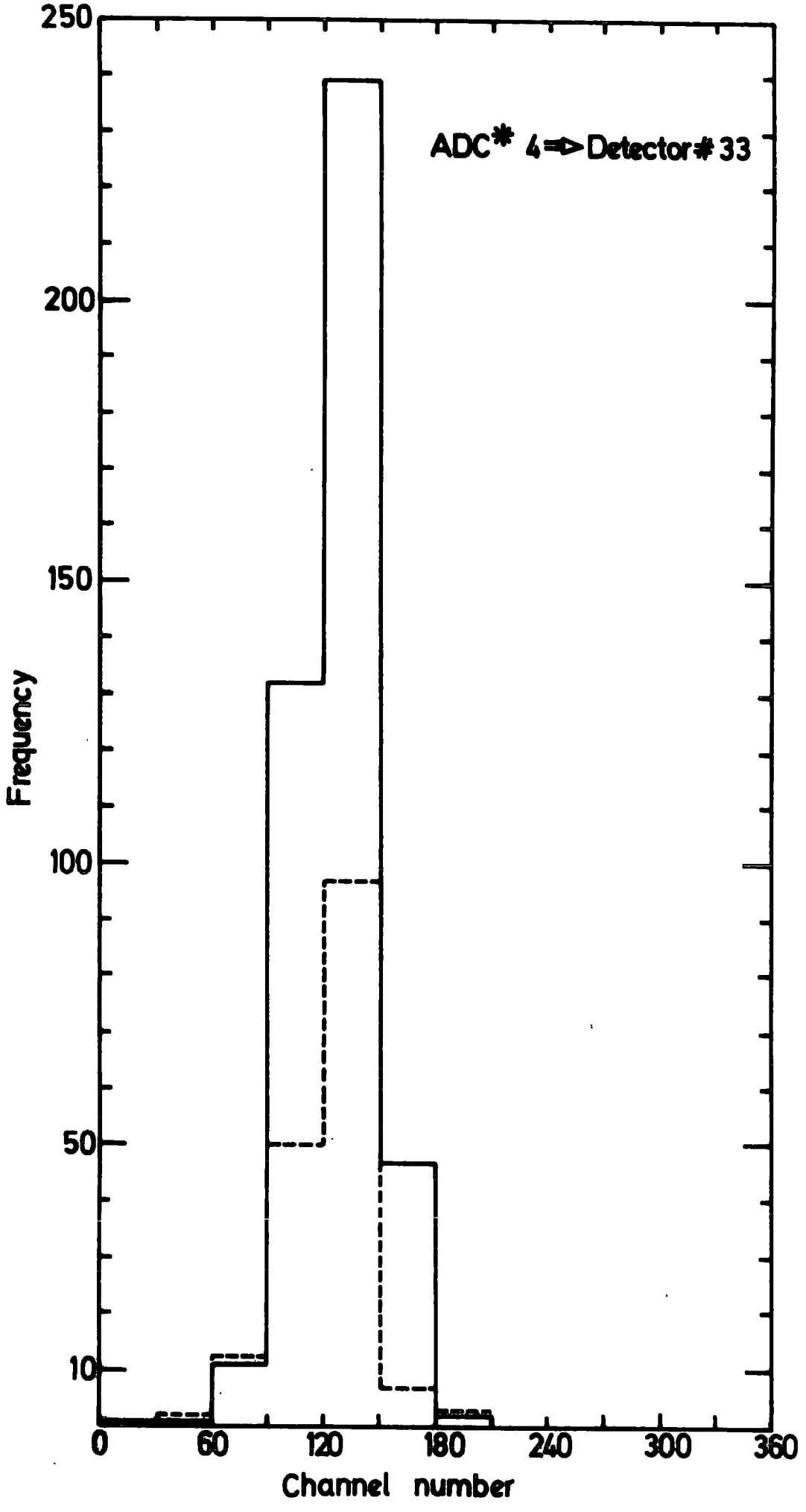

FIGURE 5.14b A typical T.A.C. histogram for fast timing tube in detector ## 33.

CHAPTER 6

THE DATA HANDLING AND ANALYSIS

6.1 INTRODUCTION

It is important for experiments such as M.A.R.S. and the Air Shower array that acquire large amounts of data to use automatic methods for data collection and the subsequent analysis. The raw data of both the present experiments are coded and stored on a magnetic disk attached to an IBM 1130 computer. Before being analysed, the data is converted into a compatible form that can be handled by the IBM 370/168. The data, after being analysed, are then stored in the Northumbrian Universities Multiple Access Computer (N.U.M.A.C.) on either a private disk or a magnetic tape where it remains until required for more analysis. The computer analysis programme of the muon data relevant to M.A.R.S. is described in detail by Wells (1972) and Piggott (1975) and that of air showers is described by Smith (1976) and Smith and Thompson (1977). In this chapter a brief description of both analysis programmes is given together with the handling procedures of the raw and analysed data. In the course of the development of the M.A.R.S. analysis programme, presentation of a visual display of the flash tube trays of the spectrograph for each event is provided such that events that failed the analysis could be examined in more detail. As would be expected with an apparatus of the size and complexity of M.A.R.S. and the air shower array, corrections for systematic effects must be taken into consideration. In the case of the spectrograph data, effects that might be of a magnetic field dependent nature have been reduced by reversing the fields of the magnets regularly, typically once a day. The array systematic biases or any temperature dependent drifts are corrected for automatically in the analysis of that

specified data through obtaining new calibration parameters that are used to adjust the data for such systematic effects. Chapter 7 discusses the experimental results, their interpretation and comparison with other experimental work, and model predictions of high energy nuclear interactions.

6.2 THE DATA HANDLING PROCEDURE

During normal operation of both the spectrograph and the array, M.A.R.S. and D.U.S.T. are triggered simultaneously when a coincidence occurs between the array triggering detectors and M.A.R.S. Information from various detectors in the array and the digitised information from the spectrograph detecting elements together with their corresponding flags, are stored in a magnetic disk via the online IBM 1130 computer. The handling of experimental data aims to form two main sets of raw data files, the first for muons and the second for their associated air showers, and eventually aims to manipulate and match the analysed data of both files according to specified selection conditions to be imposed on both muon and air shower analysed data. The programmes for the interpretation of the M.A.R.S. data were developed by Wells and Thompson (1972) and Daniel (internal report), and those for the EAS data by Davidson, by Smith (private communications) and by the author. Figure 6.1a shows the first stages of the raw data handling procedure. During the preliminary analysis stage the array and the spectrograph data are separated into two main files in which the data can be matched according to event numbers. These two files are the main source data files that are used in estimating the muon lateral distributions. The total number of matched events is 5479 collected over a period of approximately eight months. The analysis of the raw data, their treatment and data file manipulation and handling on

the IBM 370/168 are shown in Figures 6.1b, c and d.

6.3 AIR SHOWER ANALYSIS

6.3.1 Introduction

Although E.A.S. analyses vary from one experiment to another, in general they pursue the same aim, which is to find the best estimates of the parameters characterising an air shower from the available observed data.

In air shower experiments, the accuracy of the measured shower parameters such as the shower size, core location, arrival direction, etc., is largely affected by the nature of the raw data and the calibrations concerned with the correcting of the data to the actual situations at the detecting elements of the array. In the present air shower analysis, the technique of a function fitting by least squares minimisation has been employed. The proposed function is defined by certain measured quantities (timing and density data). In this technique the calibrated raw data are fitted to a theoretical expression that describes the air shower, such as the shower front curvature and lateral structure functions. By feeding the raw data to the theoretical expression and varying the shower parameters the value of the function can be found. The minimum value of this function will correspond to the best fit values of the shower parameters.

6.3.2 The Air Shower Analysis Programme

The analysis programme of the air shower data acquired by this array has been described by Smith and Thompson (1977).

A short review of its functions and features is given here. The analysis programme comprises a collection of subroutines which are called and manipulated by the main programme according to a specified analysis code. Various degrees of analysis can be allowed for by using these

FIGURE 6.1 a

A FLOW CHART OF THE DATA HANDLING PROCEDURES

ON THE IBM 1130 AND IBM 370/168

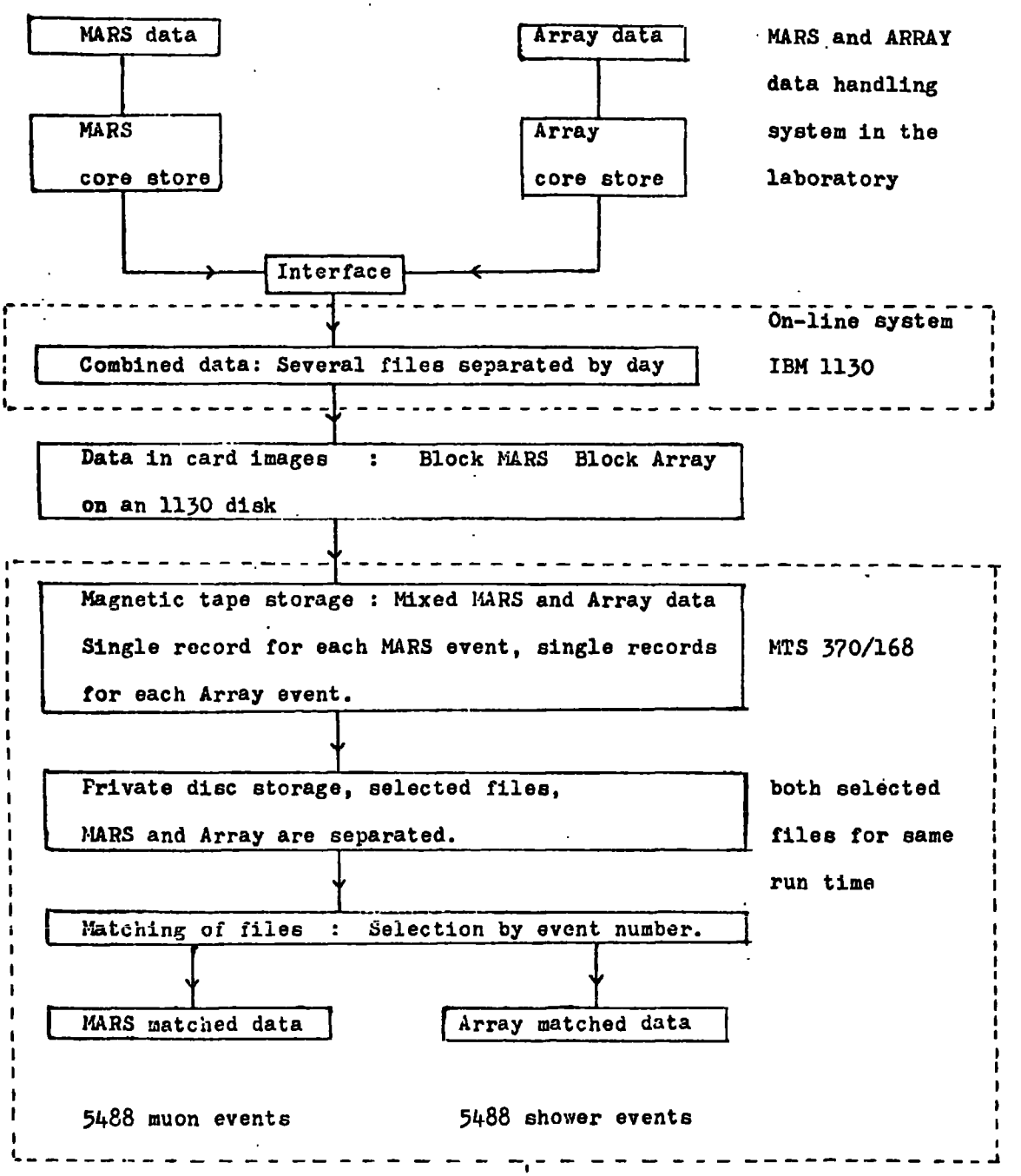

FIGURE 6.1 b

THE ANALYSIS OF MUONS AND AIR SHOWER DATA

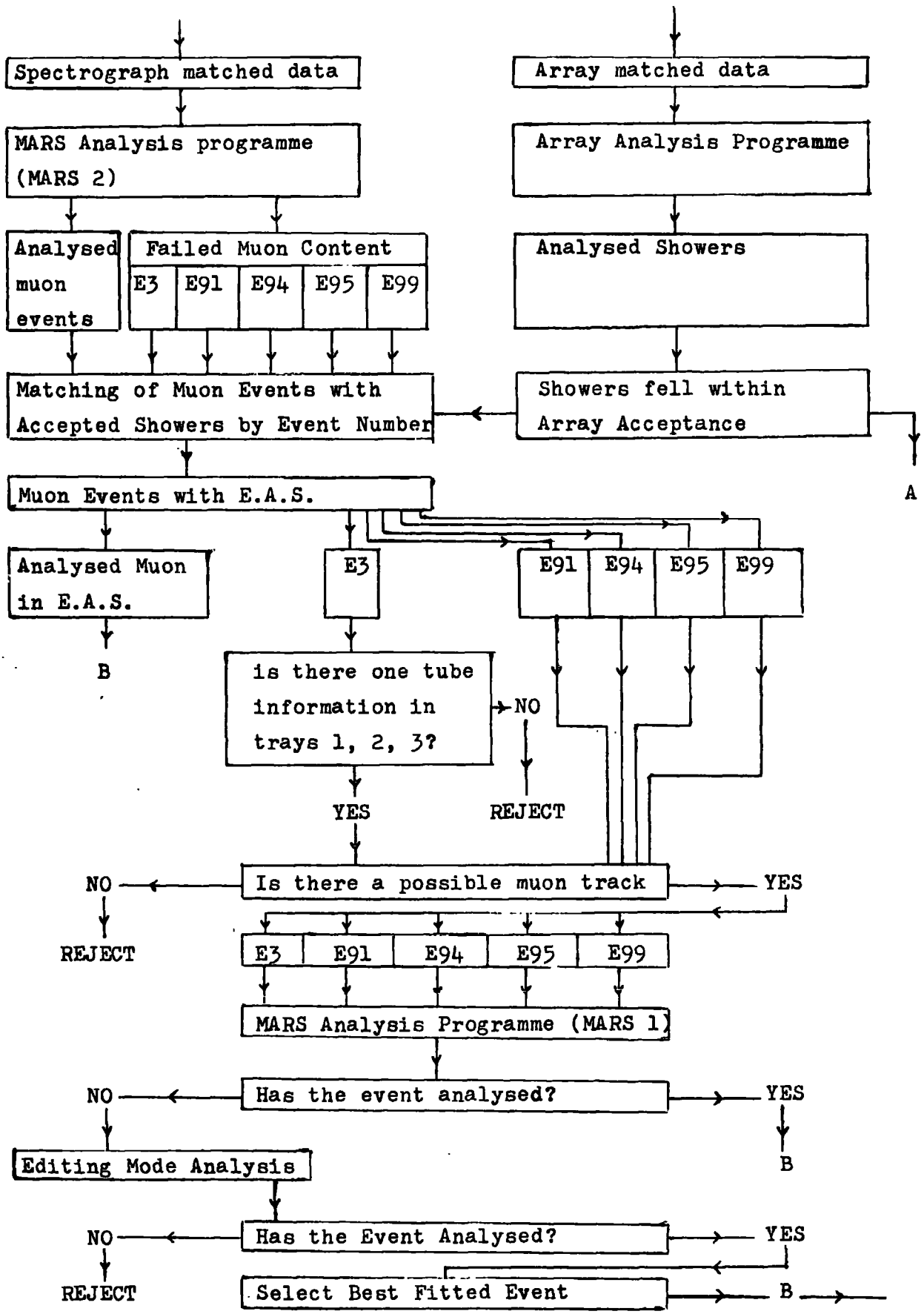

FIGURE 6.1 C

THE TREATMENT OF AIR SHOWER ANALYSED DATA

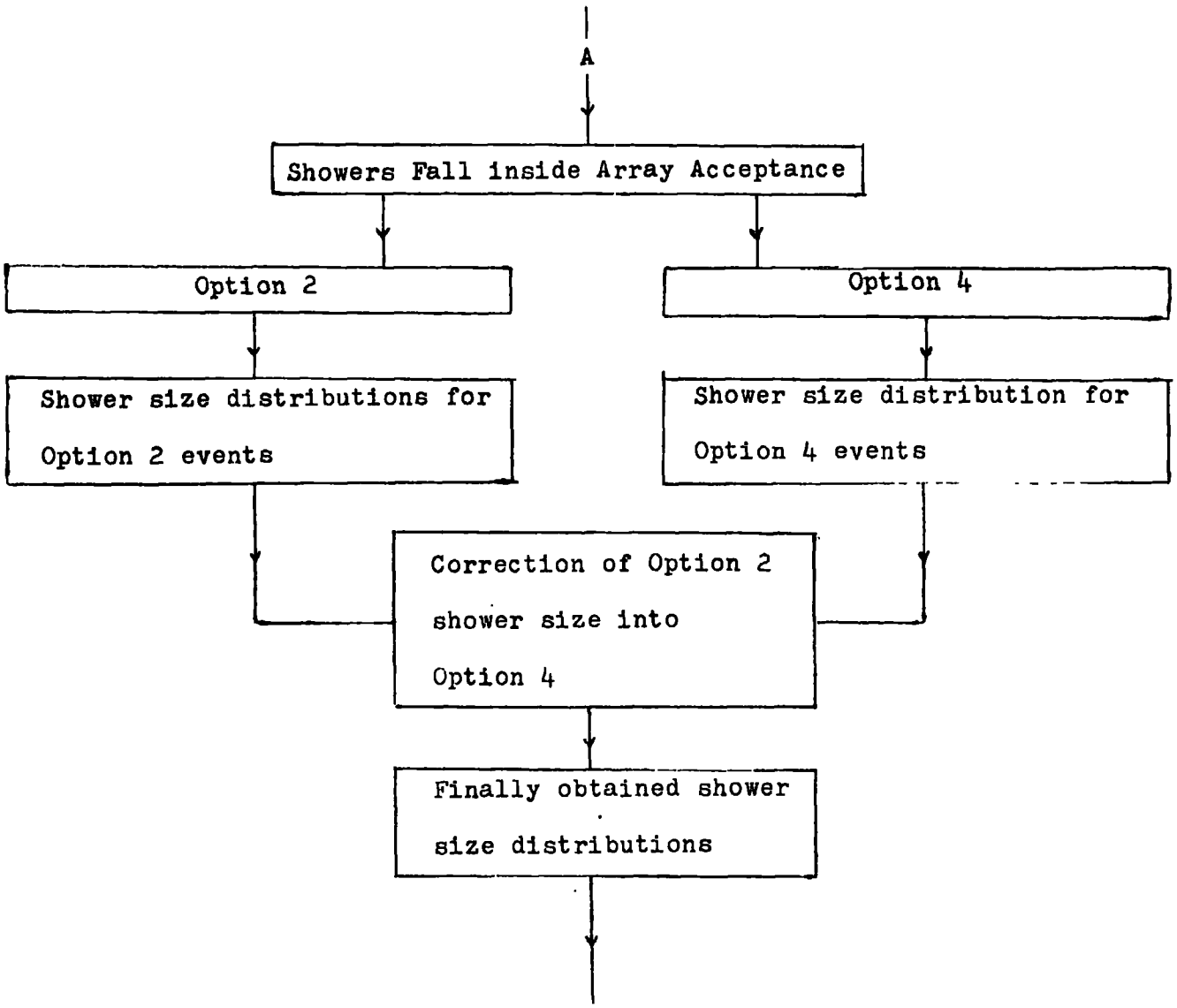

FIGURE 6.1 d

THE TREATMENT OF THE SPECTROGRAPH ANALYSED DATA

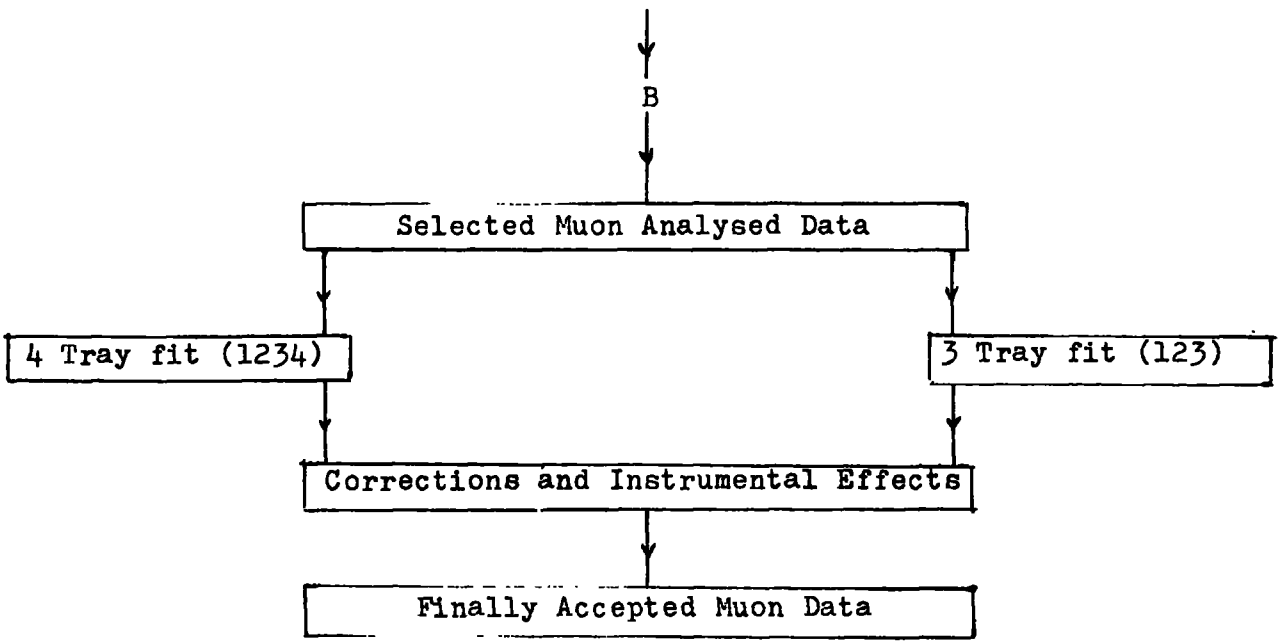

codes, also, facilities are available in the routines for data simulation to test the programme and analysis procedures. In the course of a full analysis of an input data file, the summarising subroutines produce a summary table of the data which includes the run numbers contained in the input file and the number of events that each run contains. This table is also used by other sub-routines to assist in their manipulation of the available data, and in the execution of the analysis. The summarising subroutines also perform tests for spurious and incomplete runs (i.e. runs that contain less than eleven events which represent one D.U.S.T. core load).

The next step in the analysis is to decode all the information that is sent from the laboratory, such as the timing information, density information, trigger mode data, operational units, etc. In this stage a check is provided on the purity of the input data, the sequence of events in each run, the incorrect transfer of data, or any inefficiencies in the data acquisition electronics.

Following the data summary, the mode, mean and standard deviation of the mean of the histograms of each analogue Multiplexer input are calculated. These statistical quantities serve to monitor the state of the analogue multiplexer data and also provide parameters that may be used for internal calibration. After this stage the analysis programme proceeds in two main sections as follows :-

(1) Calibration of observed data.

(2) The analysis of the calibrated data.

In the first section the relative times of arrival of the shower front are produced as well as the particle densities in terms of vertical calibration particles. These calibrated times and densities are then considered to give the arrival directions, core locations and size of the

shower. For a certain event there are four possible ways of analysis, each depends on the availability of the amount of timing and density information. These are called the event analysis options and are explained in Table 6.1.

It can be seen from the table that in option 4 analysis showers are fully analysed, whereas in options 2 and 3 showers are only partially analysed. It is expected that the shower parameters obtained in the option 2 analysis would be similar to those obtained when analysed as option 4 events with sufficient timing information.

6.3.3 The Minimisation Procedure

The minimisation subroutines are the most important features upon which the analysis programme is based. This package of subroutines is efficient and versatile ; it is contained in the CERN programme MINUIT (James and Roose, 1971). In this procedure the technique of least squares fitting to a three-dimensional plane is employed in minimising the timing and density data. In order to determine the arrival direction of the shower, the fast timing data are fitted to a plane shower front using the least squares technique. The following function is minimised ; the summation is over all operational timing detectors.

$$\Phi = \sum_{\text{all timing detectors}} (t_{i_{obs}} - t_{i_{calc}})^2 \qquad (6.1)$$

where $t_{i_{obs}}$ is the observed time of arrival measured by one i^{th} timing detector relative to the central detector ($t_c = 0$) and $t_{i_{calc}}$ is the predicted time at the i^{th} detector calculated on by assuming a shower incident on the array at Zenith angle (θ) and azimuthal angle (ϕ). The most significant values of θ and ϕ are those when the function Φ is minimum. Minimisation of the shower density data will then be proceeded

Analysis Options	Description	Available Data	
		No.of timing values	No. of density values
1	Insufficient timing and density data.	≤ 2	≤ 5
2	Insufficient timing data and density data used to calculate N_o, X_c, and Y_c, θ is assumed to be 0^o.	≤ 2	≥ 5
3	Insufficient density information.	≥ 3	≤ 5
4	Sufficient timing and density data, θ ,ϕ , N, X_c, Y_c are calculated.	≥ 3	≥ 5

TABLE 6.1 : The shower analysis options.

with if there are sufficient density measurements. A shower structure function is fitted to the density data by minimising the following function :-

$$L^2 = \sum_{\substack{\text{(all density} \\ \text{detectors)}}} \frac{(n_{i_{calc}} - n_{i_{obs}})^2}{\delta_i^2} \qquad (6.2)$$

where $n_{i_{calc}}$ is the calculated number of particles at the i^{th} detector ; the predictions of n_i were based on employing a known structure function. $n_{i_{obs}}$ is the measured number of particles at the i^{th} detector and δ_i represents an error estimate on the measured number of particles at the i^{th} detector. In the present analysis of air shower data used in this experiment the shower structure function used is that of Catz, et al (1975) which has been obtained by employing scintillation detectors in an array of similar dimensions to the present array at sea level.

6.3.4 The Measured Shower Parameters

The most significant parameters that can be obtained for each shower recorded by the array by utilising the analysis programme are the following :-

(1) The zenith and azimuthal angles of the arrival direction of the shower.

(2) The core distance from the central detector, measured in the plane of the shower front, and consequently the core distance from the top of the spectrograph and also along the shower front as explained in Figure 6.2.

(3) The shower size (N).

Measurements of the radius of curvature of the shower front cannot be obtained due to the inaccuracy in the time difference and the lack in number of timing detectors.

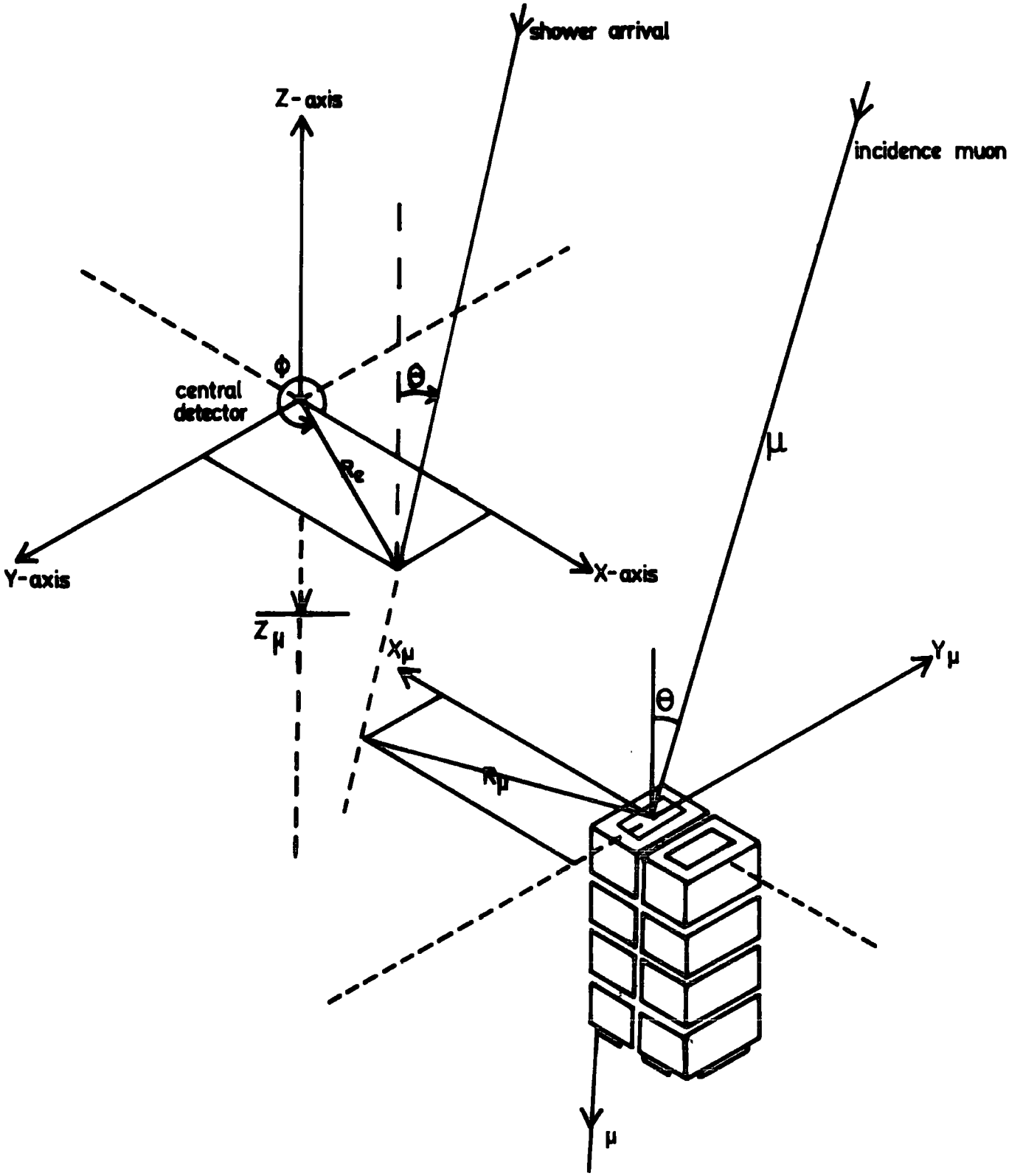

$$R_\mu^2 = (X_c - X_\mu)^2 + (Y_c - Y_\mu)^2 + (Z_\mu)^2 - \{\sin\theta\cos\theta(X_\mu - X_c) + \sin\theta\sin\phi(Y_\mu - Y_c) + \cos\theta Z_\mu\}^2 \text{ and, } R_\mu^2 = (X_c - X_\mu)^2 + (Y_c - Y_\mu)^2 + Z_\mu^2 \text{ for } \theta = 0^o.$$

FIGURE 6.2 The relative positionSof the central detector of the array and the spectrograph.

6.4 THE M.A.R.S. COMPUTER ANALYSIS PROGRAMME

6.4.1 The Main Programme

The M.A.R.S. analysis programme has been developed by Wells (1972), Thompson, et al (1972) and Daniel (Internal Report). Although the analysis programme is used in converting the basic binary information into a form that could be used on the IBM 370/168 or in the handling procedures, its main aim lies in the determination of the momenta of muons that traverse the spectrograph, their sign of charge and the determination of the angles of incidence of incoming muons. From the knowledge of the motion of a charge particle in a uniform magnetic field B (Gauss), (its trajectory will be a circle with a radius of curvature R (cm)), the relation between the particle momentum p (eV/c) and the radius of curvature R (cm) is namely :-

$$P = 300 \; B \times R \qquad (6.3)$$

In practice a parabola is fitted to the muon trajectories rather than a circle to take into account the energy loss of the muons while traversing the spectrograph. The computer programme uses the least squares method to fit a parabola to a set of three, four, or five flashed tube co-ordinates along the observed muon track in the flash tube trays of the spectrograph. A parabola of the form $y = ax^2 + bx + c$ can give the best fit to the co-ordinates of the track in each flash tube tray. The standard deviation of the experimental data points around the fitted trajectories are minimised and the momentum of the smaller standard deviation of the fitted trajectories is then chosen as the apparent momentum of the muon. By using the equation 6.3 and substituting for the characteristics of M.A.R.S. the result is that the mean momentum, P, of a muon traversing the spectrograph

can be written as :-

$$P = \frac{0.1949}{a} \quad GeV/c \tag{6.4}$$

where a is the first coefficient of the best fitted parabola and related to the radius of curvature by the relation :-

$$a = \frac{1}{2R} \quad m^{-1} \tag{6.5}$$

The effect of the gaps between the magnet blocks is taken into consideration in equation 6.4.

6.4.2 Track Identification and Trajectory Fitting

It is mentioned in the previous section that the M.A.R.S. analysis programme tries to fit a parabolic curve to either a set of five, four or three muon track co-ordinates in the spectrograph flash tube trays. Thus, to locate a track in a tray (a tray consists of 712 tubes arranged in 8 rows of 89 columns), the programme searches for groups of more than or equal to two discharged tubes in one column or in adjacent columns of flash tubes.

In the present work, for trays that contain more than one group in a tray, the analysis programme has been set to try 30 possible combinations of groups besides a special treatment that splits the numbers of groups to allow the programme to fit better tracks for combined groups. Ideally, flash tubes that are traversed by the particle are discharged, but this is not the case in practice, since flash tubes are not absolutely 100% efficient and it is quite possible that some of the tubes traversed by the particle do not discharge ; also, it is possible that knock-on electrons may discharge tubes in adjacent columns. For the above cases

the analysis programme has been provided with a specified option such that the flash tubes in a tray can be switched ON or OFF. Figure 6.3 shows the track fitting options that are available to the programme, and a description of each option is given in Table 6.2. In general these options enable the programme to fit a track through the flash tube information in a particular tray by taking into consideration tube inefficiencies or knock-on electrons. From Figure 6.3 options with the lower order are more likely to occur and thus the programme will use them in the track fitting procedure instead of using those options of higher order.

The co-ordinates of the tracks of the lowest option orders in the trays are then used for initial fitting of the parabola. A group of only two tubes is not used in the fitting procedure because of the difficulty in providing an option that fits this very clearly. Bursts (groups containing more than ten discharged tubes or occupying more than five adjacent columns) are also not included in the fitting of the parabolic trajectory of the particle. Flash tube information in groups that consist of 4-5 columns of data are used three columns at a time, this number of columns represents the maximum number that a muon can discharge when traversing a tray at the largest acceptable angle.

After the tracks in each tray have been defined a parabolic curve is fitted to the located co-ordinates in the flash tube trays. If the angle of the fitted parabola at each tray correlates with the angle of the actual track as obtained from the flash tube information and the fitted option to that tray, that option will be used, otherwise another option is considered. If the programme failed to find any correlation between the two angles, then the track is not used in determining the particle momentum. When the above conditions are fulfilled then a second parabola is used to fit the new co-ordinates of the particle trajectory, this parabola has a

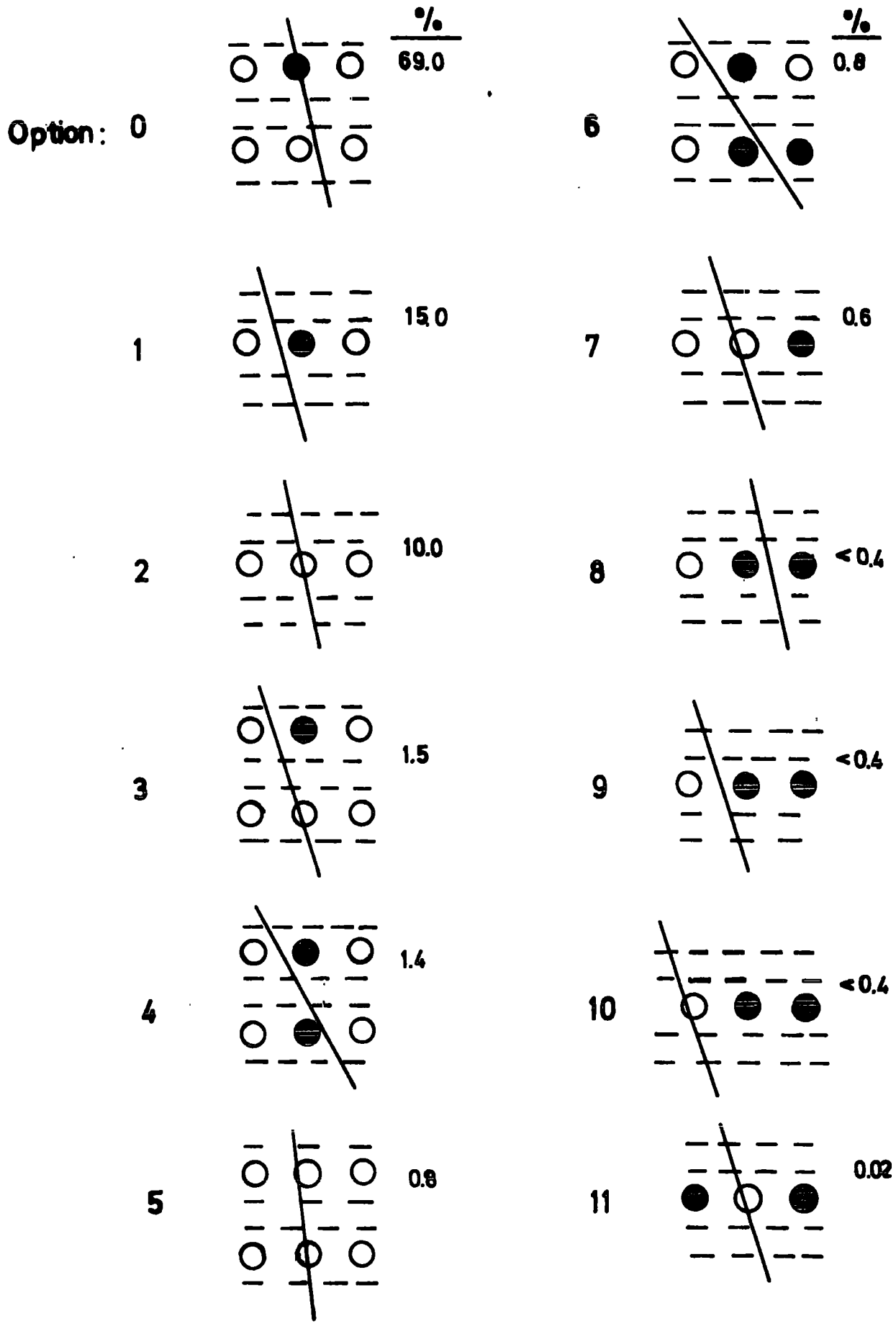

FIGURE 6.3 Illustration of Track Fitting Options ; the percentages given represent the frequency of using each option by the analysis programme (After Wells, 1972).

TABLE 6.2 The track fitting options (After Wells, 1972)

Option	Description
0	Good fit - no information has to be assumed.
1	A knock-on electron is assumed (a discharged tube is neglected).
2	A tube inefficiency is assumed (an undischarged tube is assumed to have discharged).
3	A knock-on electron and a tube inefficiency in different layers are assumed.
4	Two knock-on electrons in different layers are assumed.
5	Two inefficiencies in different layers are assumed.
6	One single knock-on and one double knock-on are assumed in different layers.
7	A tube inefficiency and a knock-on in the same layer are assumed.
8	Two knock-ons in the same layer are assumed (muon passed between them).
9	Two knock-ons in the same layer are assumed (muon passed to one side of them).
10	An inefficiency and a double knock-on are assumed in the same layer.
11	Assumes an inefficient tube between two knock-ons.

better and more accurately fitted co-ordinate than the first.

Data in a tray are not used for various reasons ; an explanation of the error codes and their causes is given by Piggott (1975). The momentum of the particle and the standard deviation of the fitted trajectory are calculated. If there are other groups in any of the trays the analysis programme tries further group combinations while storing the results of the first analysed trajectory. After trying all possible group combinations the programme selects the fit that contains the greatest number of trays used in the trajectory fitting. Having done this, the programme searches for the trajectory that gives the lowest standard deviation.

In the case of a double muon event, after finalising the first muon trajectory the programme considers the possible second muon trajectory in the same manner. Events that contain more than two muons are flagged as a multiple muon event ;these type of events are generally due to showers whose cores fall near the spectrograph. The analysis of these events was carried out by employing the editing mode of MARS1 as explained in Section 6.5.4.

6.4.3. Features of the M.A.R.S. Analysis Programmes

Besides the fact that the M.A.R.S. spectrograph has not been essentially designed to study muons associated with air showers, the M.A.R.S. analysis programme MARS 1 (Daniel, private communication) and its new version MARS 2 are established to interpret single muon events rather than muon events that are associated with an air shower which triggers the top tray of the spectrograph (Tray 5).

The presence of the shower flash tubes information in tray 5 makes it almost impossible to tell whether the muon has passed through that tray or not. For the above reasons some modifications have been introduced to the analysis programme (MARS 2) to overcome the difficulty

arising in the analysis of muons accompanied by air shower events. By employing these modifications within the analysis programme it is hoped that as many as possible muon events can be analysed such that the particles will be assigned a certain value of momentum using only trays 1 - 4 or trays 1 - 3.

Concerning the spectrograph analysis programmes, the original programme (MARS 1) has been modified by Daniel (internal report) and is referred to as MARS 2. Both MARS 1 and MARS 2 programmes with the shower modification introduced have been used in the analysis of the spectrograph data. It is of interest to this work to mention some important features that led to the use of both programmes on the muon data in an attempt to obtain the actual number of muons traversing the spectrograph during the acquisition time of the data collected in this experiment.

The main aim of the MARS 2 analysis programme is to identify a group of discharged flash tubes associated with a given muon trajectory in each of the five measuring trays and to analyse these particular groups using the original programme MARS 1. A group is defined by MARS 1 as three or more discharged flash tubes contained within a column or a sequence of columns that are separated from another group by one column of undischarged tubes. This definition has been altered by MARS 2 to two or more discharged tubes contained within a column or a sequence of columns that is separated from another group by either one column of undischarged tubes or two columns each containing only one discharged tube. As a result of the latter definition of the group in MARS 2, this programme will have the following specifications when applied to the spectrograph data :-

(a) The ability to correctly interpret events having more than

one group of more than, or equal to, three tubes per tray.

(b) Its usage of any tray that contains more than, or equal to, two groups, while MARS 1 will not use a tray if more than two groups are present.

It is also important to mention that the MARS 2 programme can handle as many as 25 specified groups in any tray (default to 10). In this context the MARS 2 programme provides further discrimination against events that contain one or more flash tube information in a tray (either error 3 or error 91, see Table 6.3), in particular those trajectories that are outside the spectrograph acceptance in the back plane, but on the other hand this will lead also to the rejection of muon shower events in which tray 4 is either inefficient or contains a single discharged flash tube. This type of event is selected and reclaimed by using MARS 1 (only trays 1-3). In both programmes the flash tubes in the top tray have been effectively switched ON, thus the whole tray is completely removed from the analysis. Hence, only trays 1, 2, 3 and 4 are used for momentum determination.

The number of flash tubes discharged in tray 5 may give an estimate of the density of electrons in showers falling on top of the spectrograph. In an attempt to correlate between the shower density at the central detector of the array (c) and the number of discharged tubes in that tray, Hawkes, et al (1976) found that tray 5 can be used as a shower measuring density detector.

6.5 THE DATA ANALYSIS

6.5.1 Introduction

The analysis falls into two parts, the analysis of air shower data and that of the muons accompanying it. Section 6.5.2 will deal with the air shower data analysed, while the analysis of the spectrograph

data is described in Section 6.5.3.

6.5.2. The Analysis of Air Shower Data

The "raw" air shower data collected in this experiment are subdivided into 24 "runs". These data are collected under the triggering of the air shower array corresponding to four-fold coincidence between the central detector (C) and the $2m^2$ detectors 55, 33 and 13. In the initial period of operation of the apparatus the array data acquisition electronics could not distinguish between a zero recorded density or a detector saturation. Since the particle density triggering detectors were calibrated at low particle density levels (4 p/m^2 for the central detector and 2 p/m^2 for $2m^2$ detectors), it is found that about 56% of the acquired data has insufficient timing information for timing analysis and these showers are assumed to be vertical.

A correction was made to the intensity of these showers to correspond to a 30° zenith angle cut. Figure 6.4 shows the correction factor obtained from the analysis of 672 real shcwers with and without timing information, an overall correction factor of 0.65 was allowed for in the shower size range $1 \times 10^5 - 3 \times 10^6$ particles over the radial distance range (0 - 50)m from the shower core to the muon spectrograph. Once all shower data had been analysed, they were stored on a magnetic disc. The selection criteria imposed on the air shower data are the following :-

(1) Shower cores must fall within 50m from the central detector.

(2) Showers (Option 4 analysed events only) must have a zenith angle of less than or equal to 30°.

After imposing these selection criteria, the accepted shower events are then extracted from the main answer file and transferred into another file such that it will be matched with the spectrograph data as

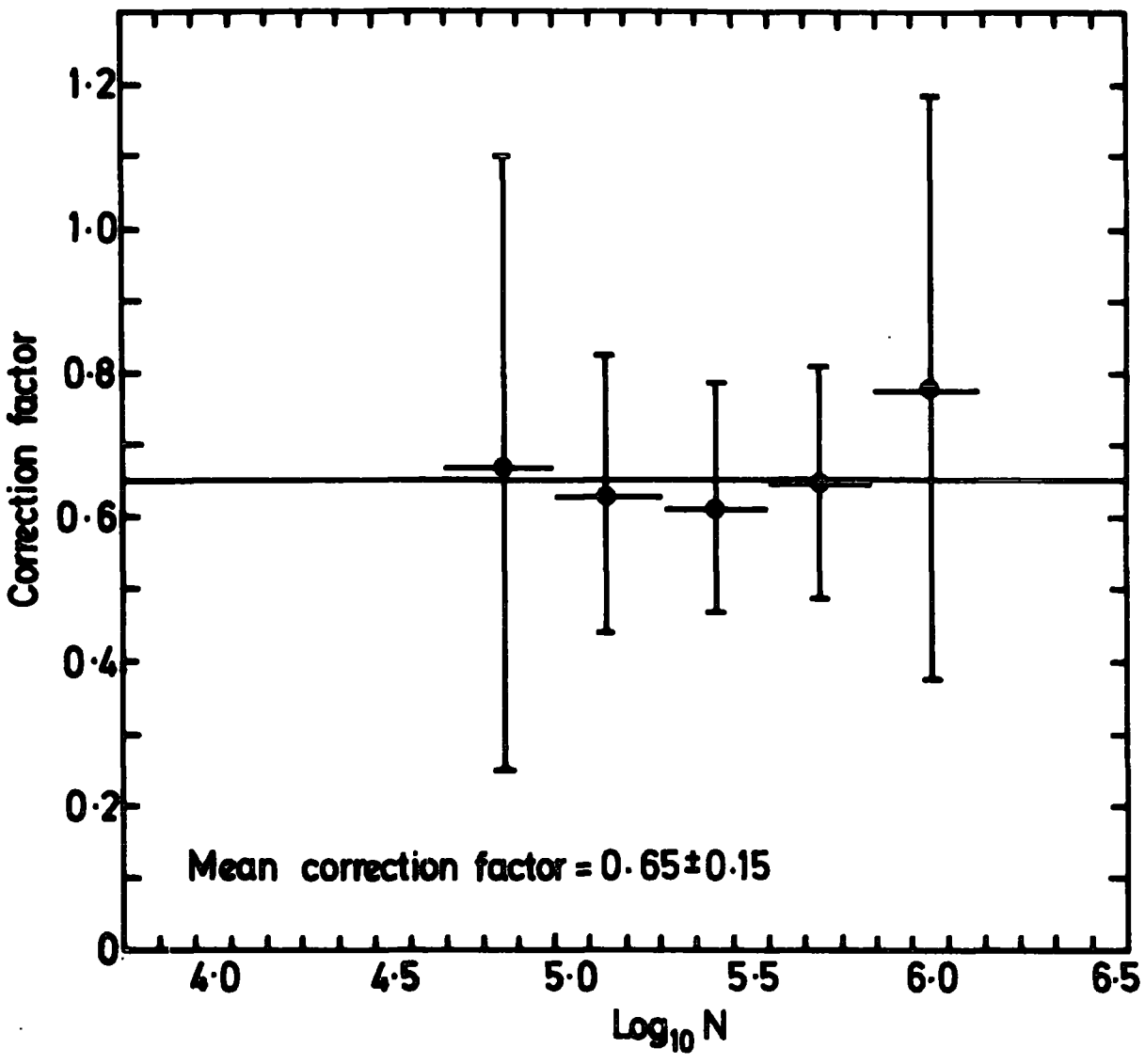

FIGURE 6.4 The correction to be applied to option 2 analyzed shower events falling at distances ≤ 50 m from the bending plane of the spectrograph.

shown in Figure 6.1b.

6.5.3 The Analysis of the Spectrograph Data

It has been stated earlier that the M.A.R.S. spectrograph in its present design is not the ideal muon detecting instrument that operates with the present air shower array. It is essential to remove various instrumental biases and detector inefficiencies from the observations. This will be explained in detail in Chapter 7.

In order to speed up the analysis of muon events, muon data are matched with the air shower analysed data that have satisfied the shower selection criteria. Computer plots of matched muon events are then produced and studied by eye. Muon events that do contain a muon trajectory or a multiple muon event were selected. Figure 6.5 shows various categories of muon events that have been accepted in this data analysis such that muon trajectories are either assigned a 1 - 4 tray or 1 - 3 tray fit.

The following criteria were set for data rejection :-

(1) There is no possible muon trajectory in the specified event.

(2) Side showers.

(3) No flash tube information in either trays 1, 2 or 3.

(4) Large standard deviation of the points used to fit the muon parabolic trajectory ($\gtrsim 2.5 \times 10^{-3}$ m).

Figure 6.6 shows the standard deviation distribution of all muon events that are assigned a 4 tray fit momenta ; a cut at a standard deviation value of 2.5×10^{-3}m was imposed on muon events. In selecting 3 tray fit momentum events no standard deviation test has been introduced. The only checks on the validity of a 3 tray fit muon event is to have a very clear muon trajectory in trays 1, 2 and 3. An example of an event is shown in Figure 6.7. Figures 6.8 and 6.9 are examples of events having a burst or inefficient tubes.

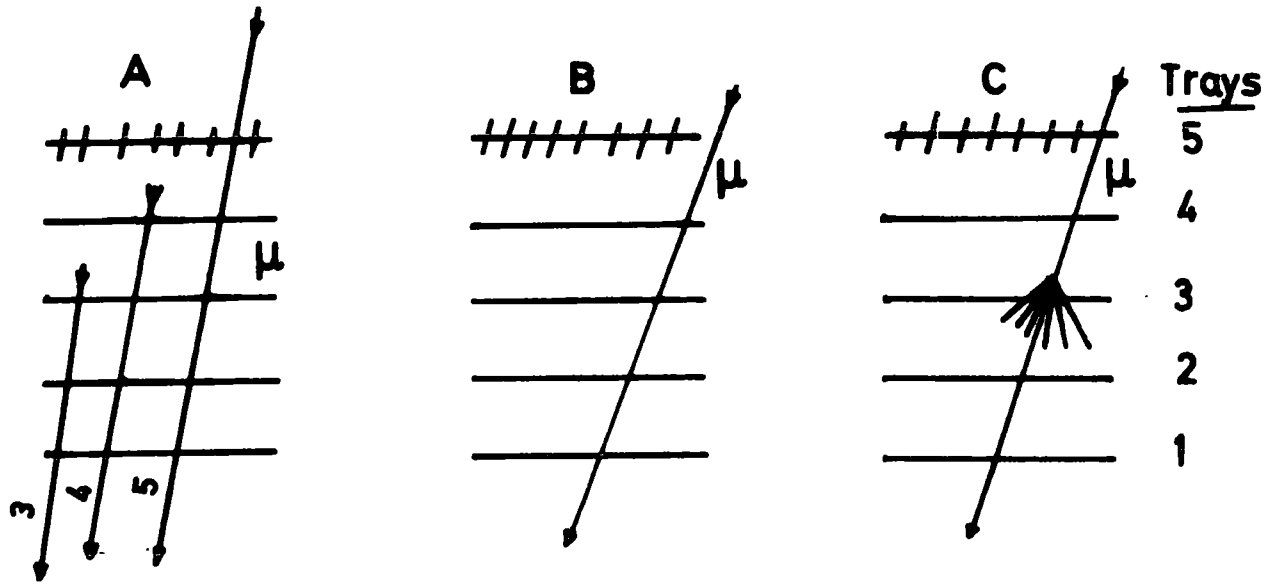

A - Muon trajectories are within 3 and 4 tray acceptance

B - A 4-tray fit muon event with trajectory outside the 5-tray acceptance

C - A 3-tray fit muon event with a burst in tray 3.

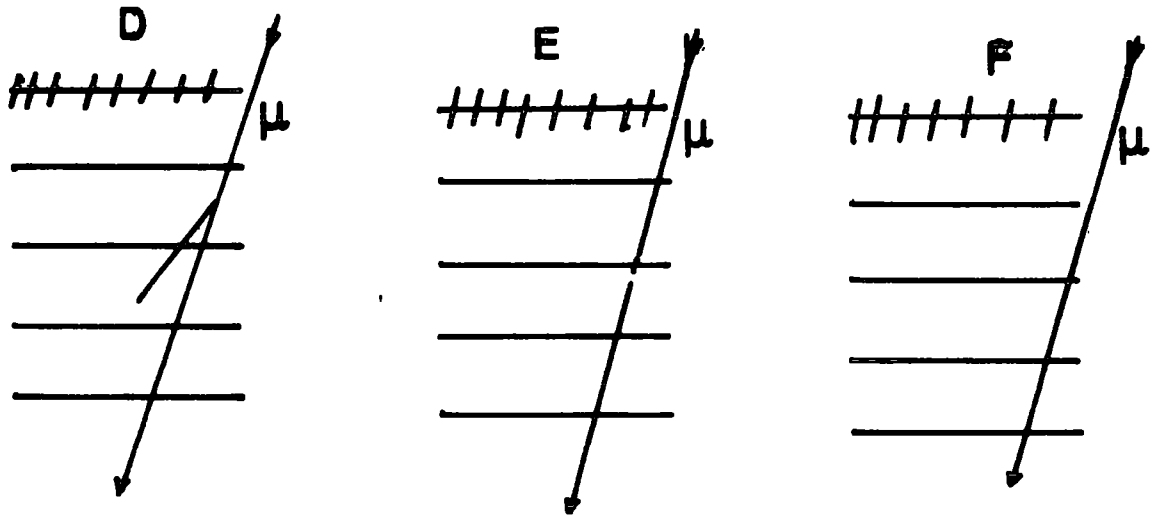

D - A muon event with a knock-on in tray -3.

E - A muon event with an inefficiency in tray -3.

F - A 3-tray fit muon event with trajectory outside tray -4.

FIGURE 6.5 Illustration of the accepted muon events.

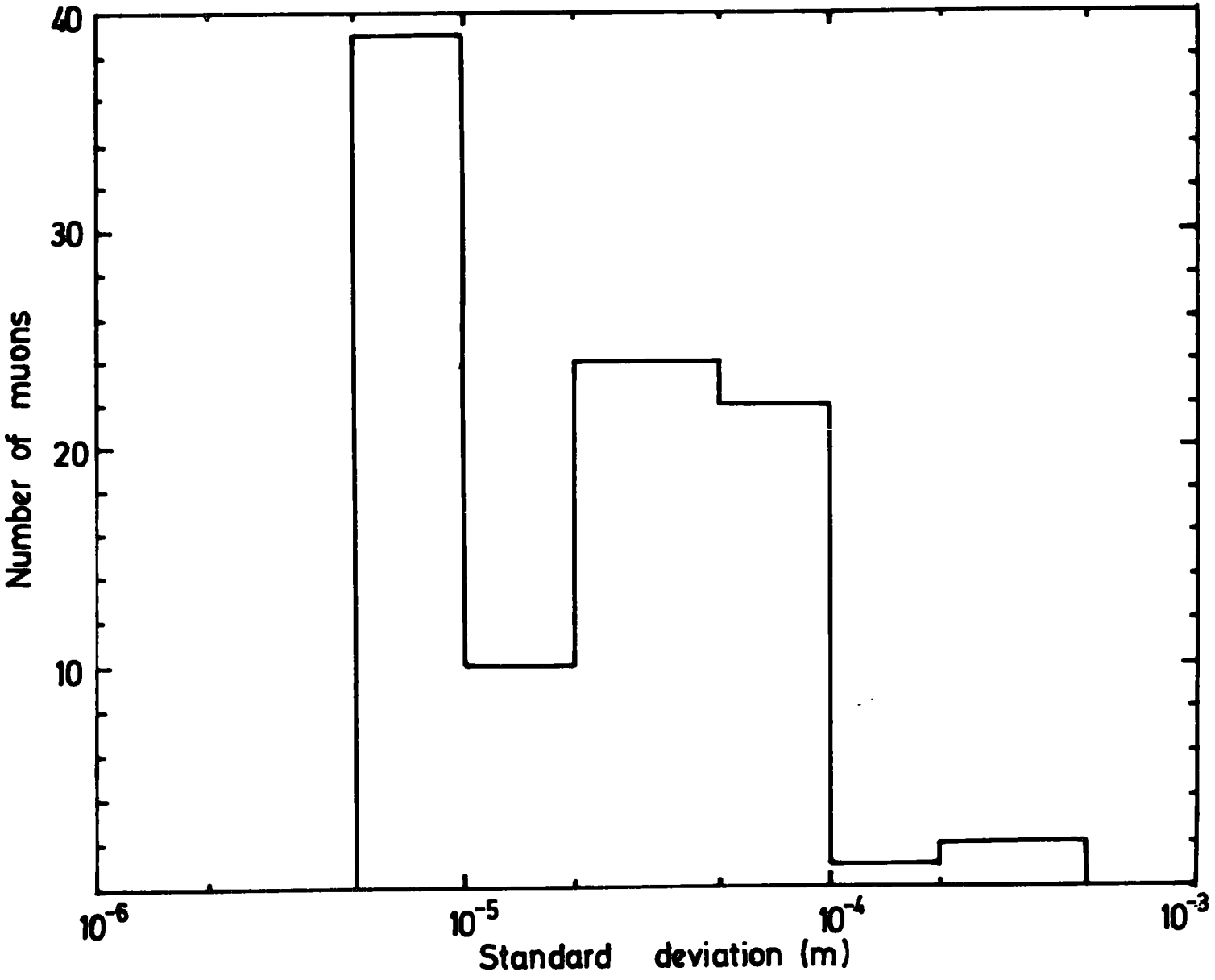

FIGURE 6.6 The standard deviation distributions of all 1-4 tray fit muon events with energies $\geq$ 50 GeV.

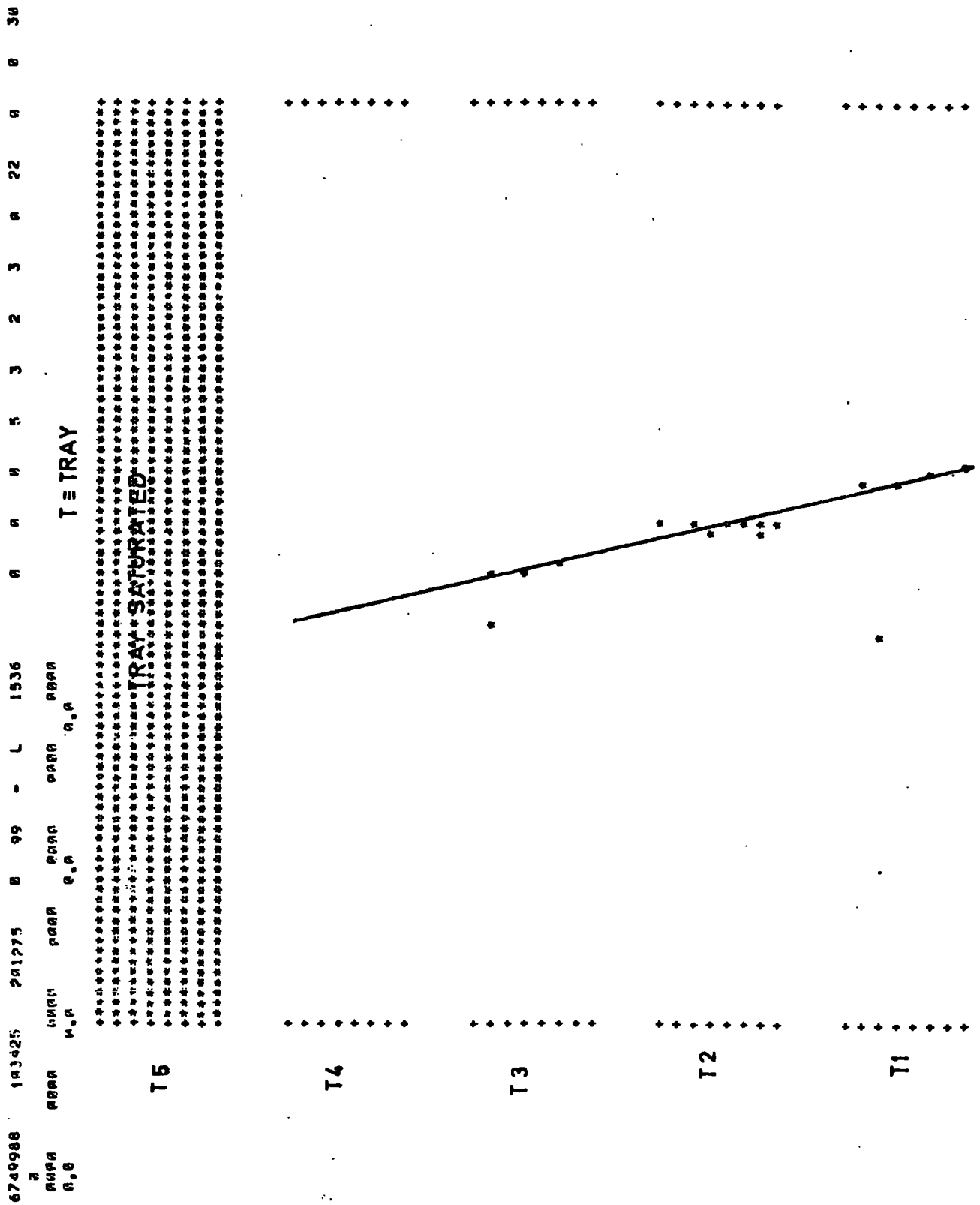

FIGURE 6.7 A typical error 3 event (rejected by MARS 2) and analyzed by MARS 1 Programme.

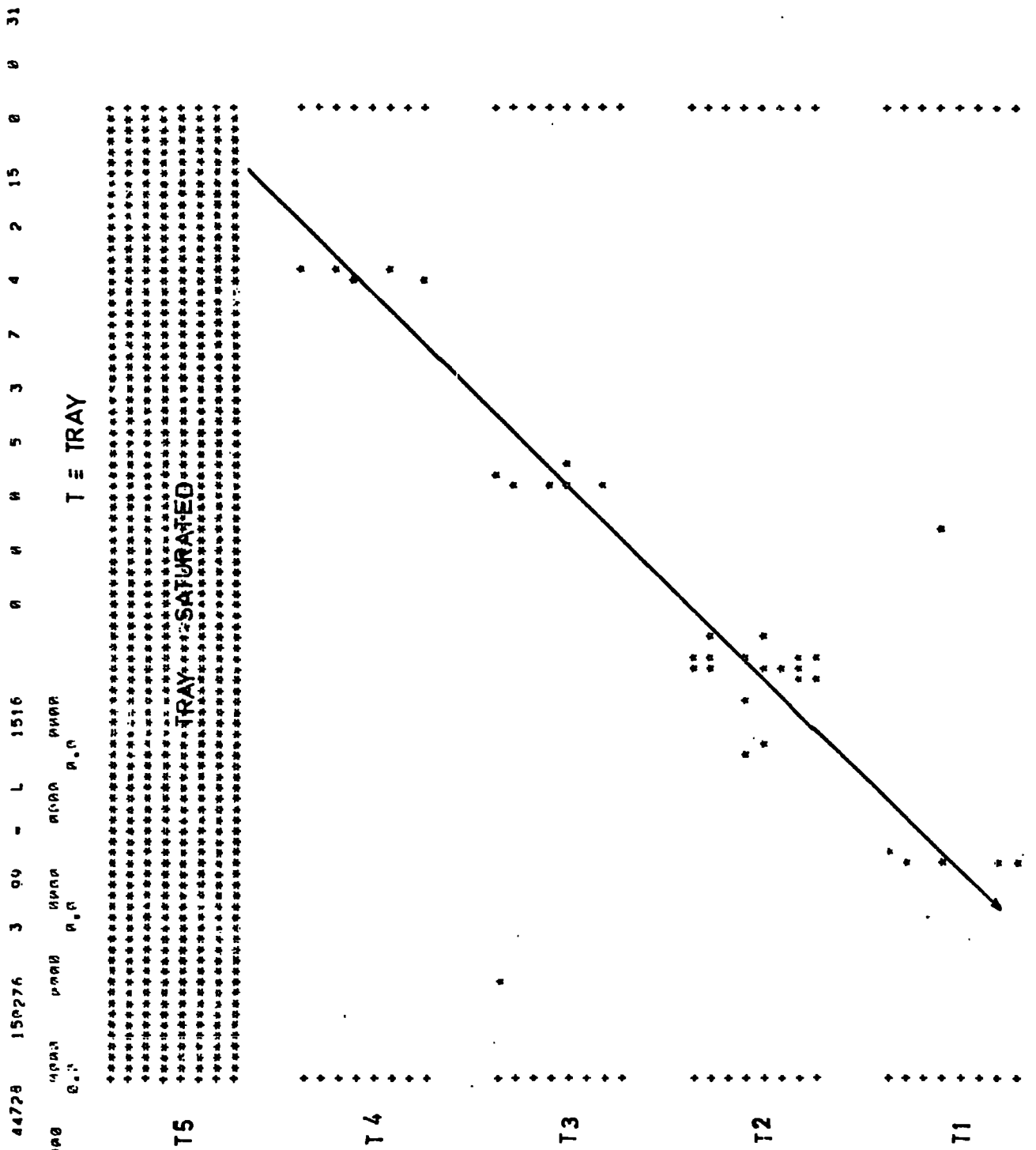

FIGURE 6.8 A computer plot of a 3-tray fit muon momentum with a burst in tray -2.

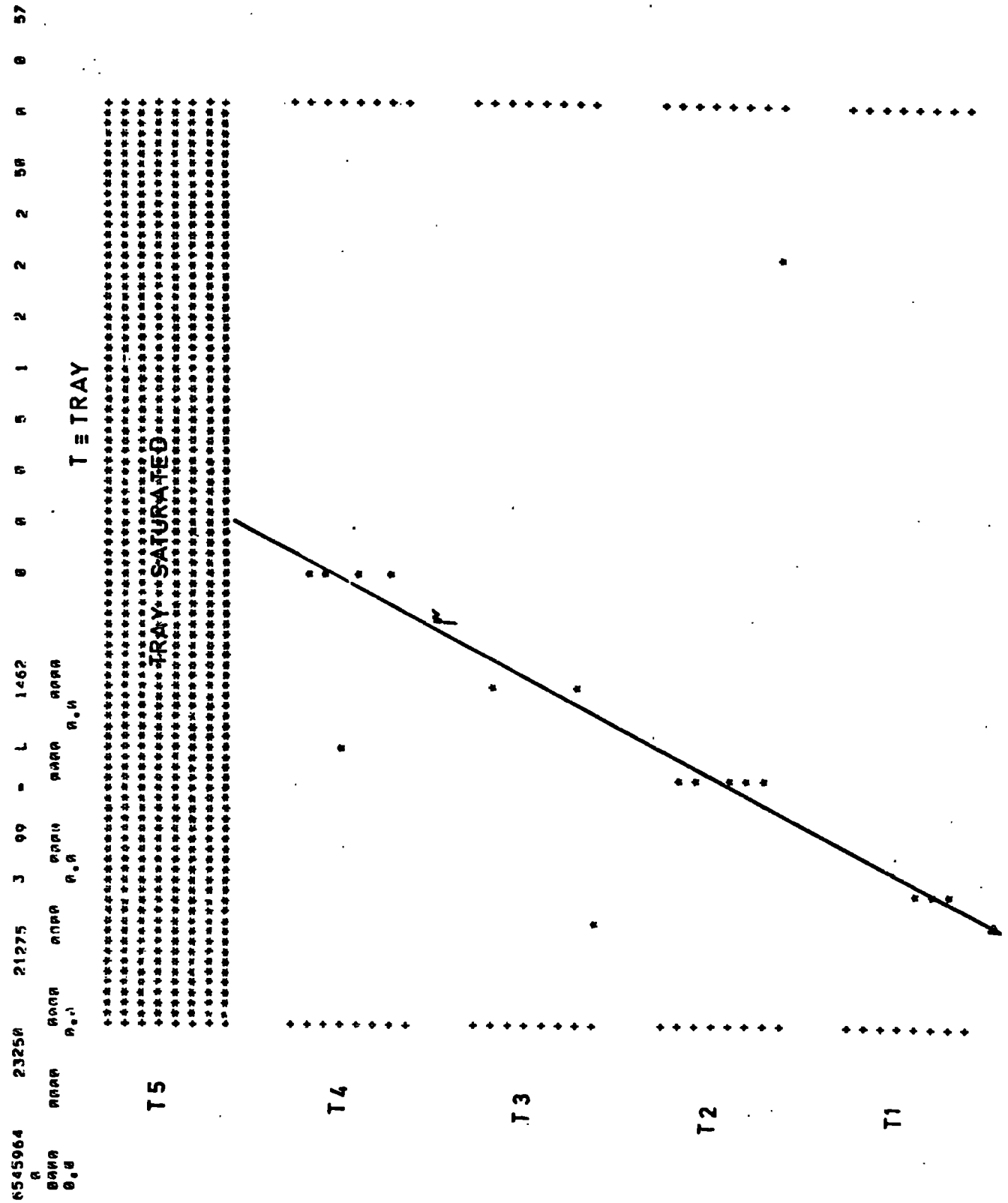

FIGURE 6.9 A computer plot of an accepted muon event assigned a 3-tray fit momentum with an inefficiency in tray -3.

After the first analysis (using MARS 2 programme), the failed events are transferred into a separate file according to their error codes that they have been given by the analysis programme (see Figure 6.1b).

An explanation of these error codes and the treatment of muon failed events are given in section 6.5.4. The data are then analysed by the MARS 1 programme, and the data that failed this analysis were analysed manually on the computer using an editing mode of the programme. Data that failed the editing mode analysis are rejected.

6.5.4 Muon Failed Events

In the first attempt of the spectrograph data analysis (using the MARS 2 programme) only about 7% of the data was assigned a momentum. It has been found about 34% of these data have their shower cores satisfying the array acceptance, thus the majority of muon events have failed the analysis. The error codes associated with the failed events are listed in Table 6.3.

It has been stated earlier that the aim in analysing the muon data is to obtain the actual number of muons above a certain energy that are detected during the period of operation of the apparatus. Thus it is important to reclaim muon events that initially fail but which do contain a muon.

The MARS 1 programme has been used such that the limitations due to spectrograph acceptance are not imposed on the data analysis. Muon events with the following error codes have been reclaimed :-

(1) Error codes 3 and 91 ; these events contain no information or no groups with > 2 flash tubes in tray 4 such that the muon trajectory is assigned a 1-3 tray fit momentum. A typical reclaimed event of error 3 type is shown in Figure 6.7 while Figure 6.10 shows a reclaimed event of error code 91.

Error Codes	Explanation
3	No data in a tray
91	No group of $\geq$ 2 tubes in a tray
94	All possible group combinations have failed
95	All possible group combinations have failed either the standard deviations or the acceptance test or the group trajectory.
99	Too many group combinations

TABLE 6.3 : Error codes given to muon events that failed M.A.R.S. 2 Programme.

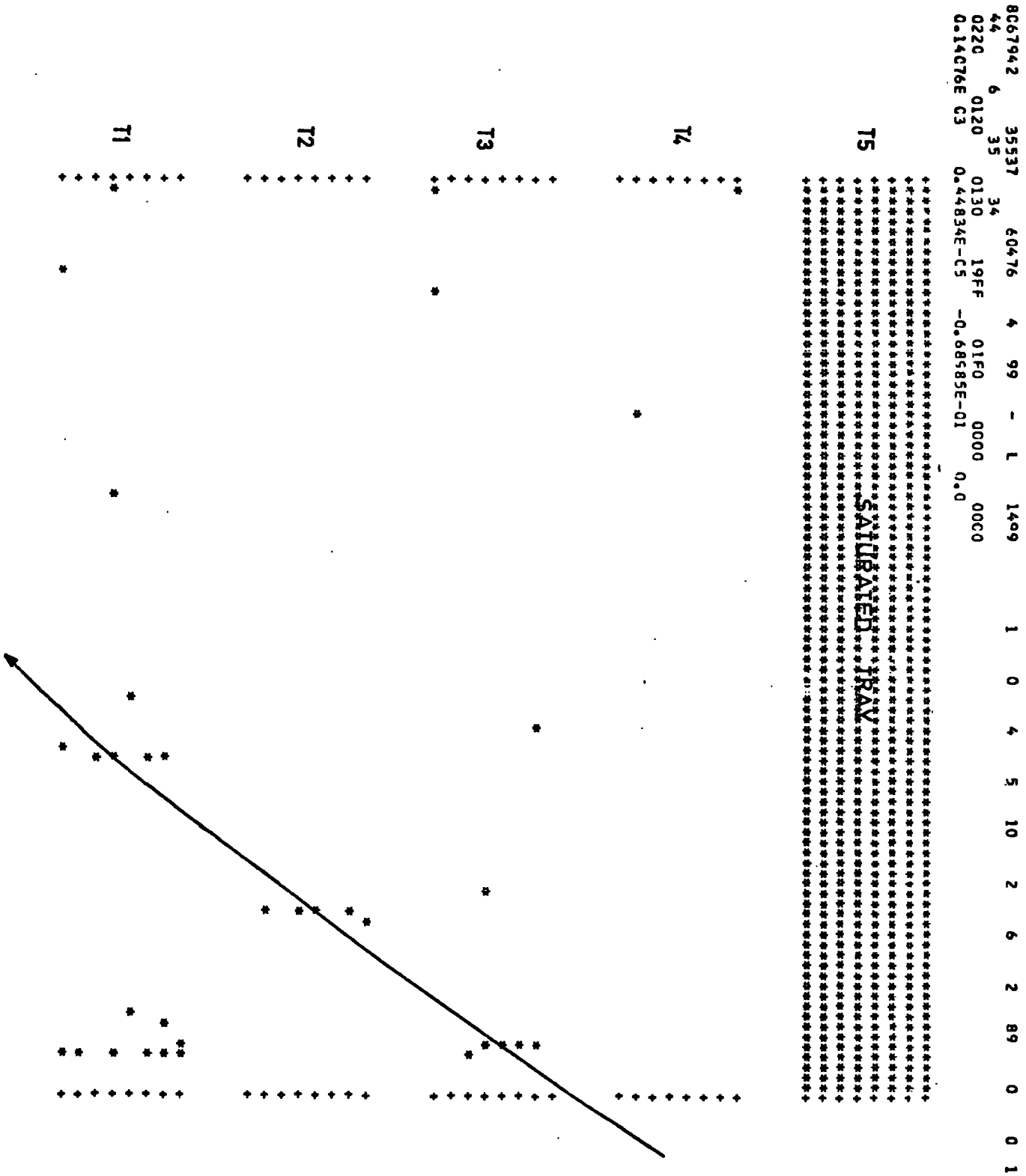

FIGURE 6.10 A 3-tray muon event with only one tube information in tray -4 (error code 91).

(2) Error 95 ; muon events with trajectories or extrapolations of their trajectories falling outside the 1 - 5 or 1 - 4 tray acceptance ; Figure 6.11 (a, b) shows examples of such events.

Other than these events the remaining data that failed this MARS 1 analysis have been investigated carefully through a study of their "computer pictures". Events that contain confused muon trajectories have been plotted on a precise diagram of the flash tube trays. The majority of the events are those of error code 99. Figure 6.12 (a, b) shows a multiple muon event that has been plotted on the reduced trays diagram, each trajectory has been edited individually. The air shower associated is also presented in part b of the Figure 6.12.

6.6 ARRAY TRIGGERING PROBABILITY

In E.A.S. experiments it is essential to have a knowledge of the response of the E.A.S. triggering elements towards detecting showers of various sizes and core locations. This response may be described as the probability of detecting an air shower of a certain size falling at a particular distance from a fixed point on the E.A.S. array. This probability depends mainly upon the triggering conditions and the geometry of the array. In calculating the detection probability of the array the method of Smith and Thompson (1977) has been used. Showers of a particular size, core location (measured from the top of bending plane of the spectrograph along the shower front) and zenith angle are fired at the array. The densities at the triggering detectors are calculated and used to obtain the detection probabilities. By making use of the assumption that the number of shower particles detected follow Poisson statistics then the detection probability P_i at the i^{th} triggering detector can be represented as follows :-

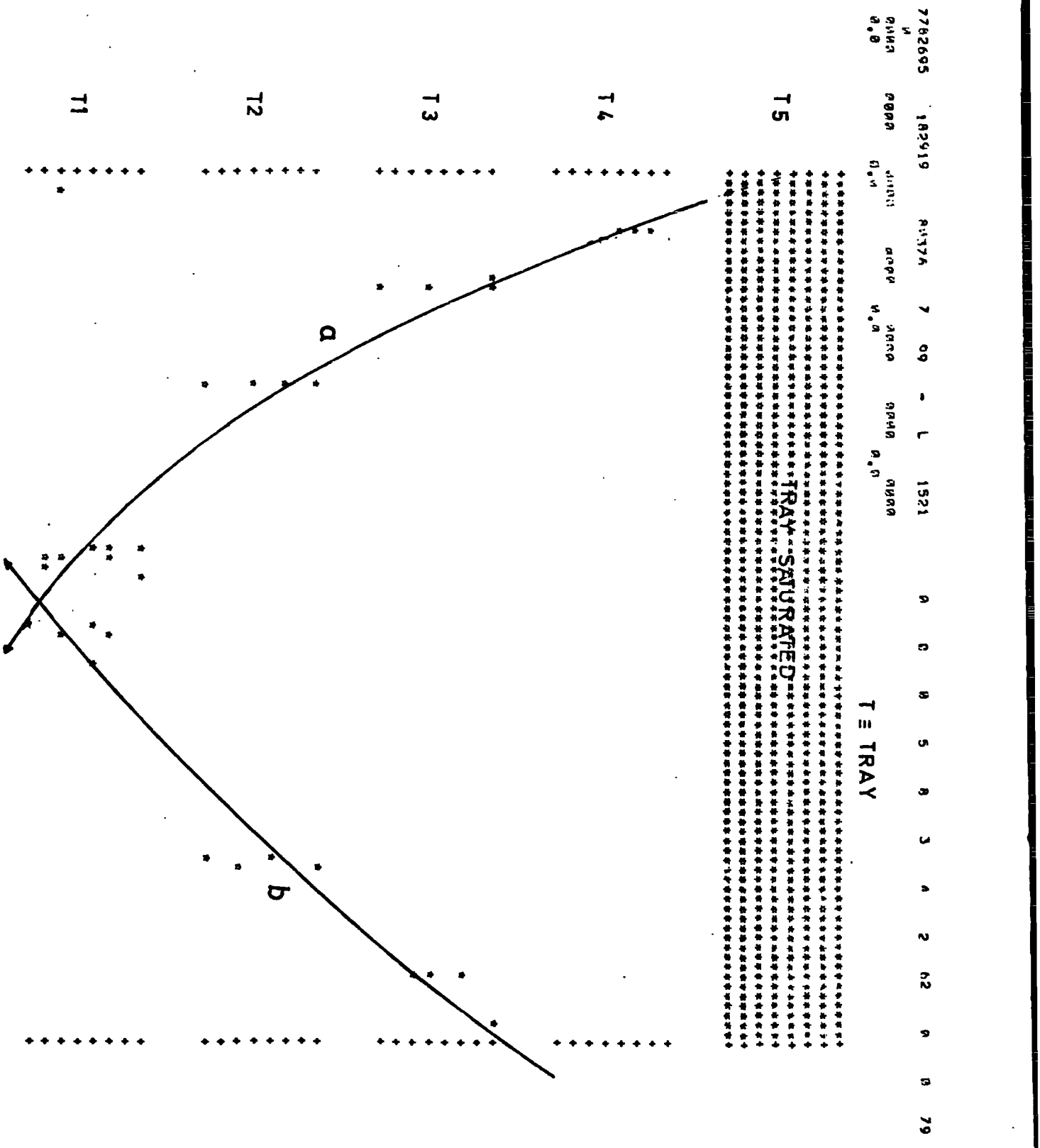

FIGURE 6.11 A double muon event with the extrapolation of muons trajectories falling outside the 1-5 tray acceptance (muon a) and outside the 1-4 tray acceptance (muon b)

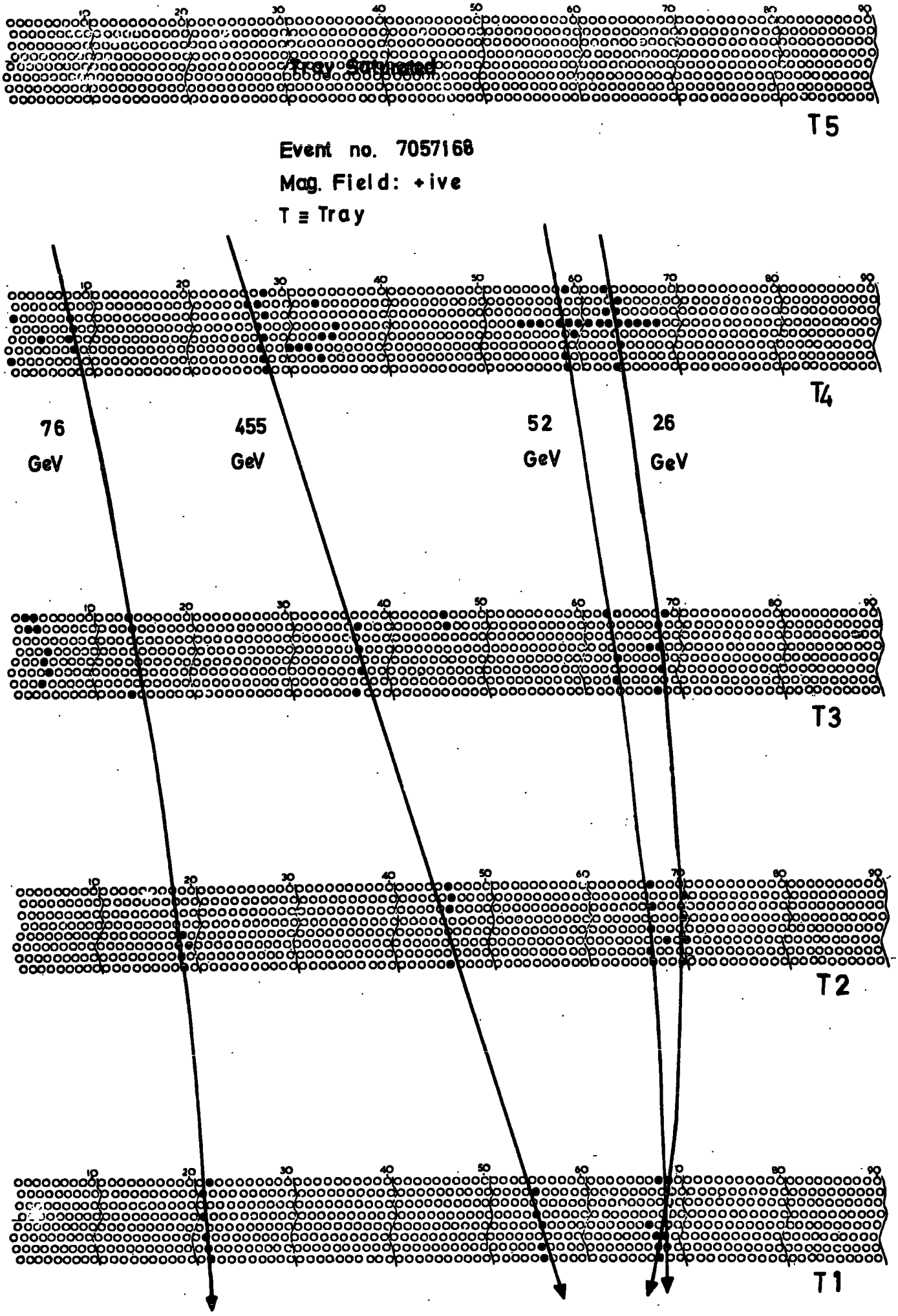

FIGURE 6.12a A multiple muon event (error Code 99).

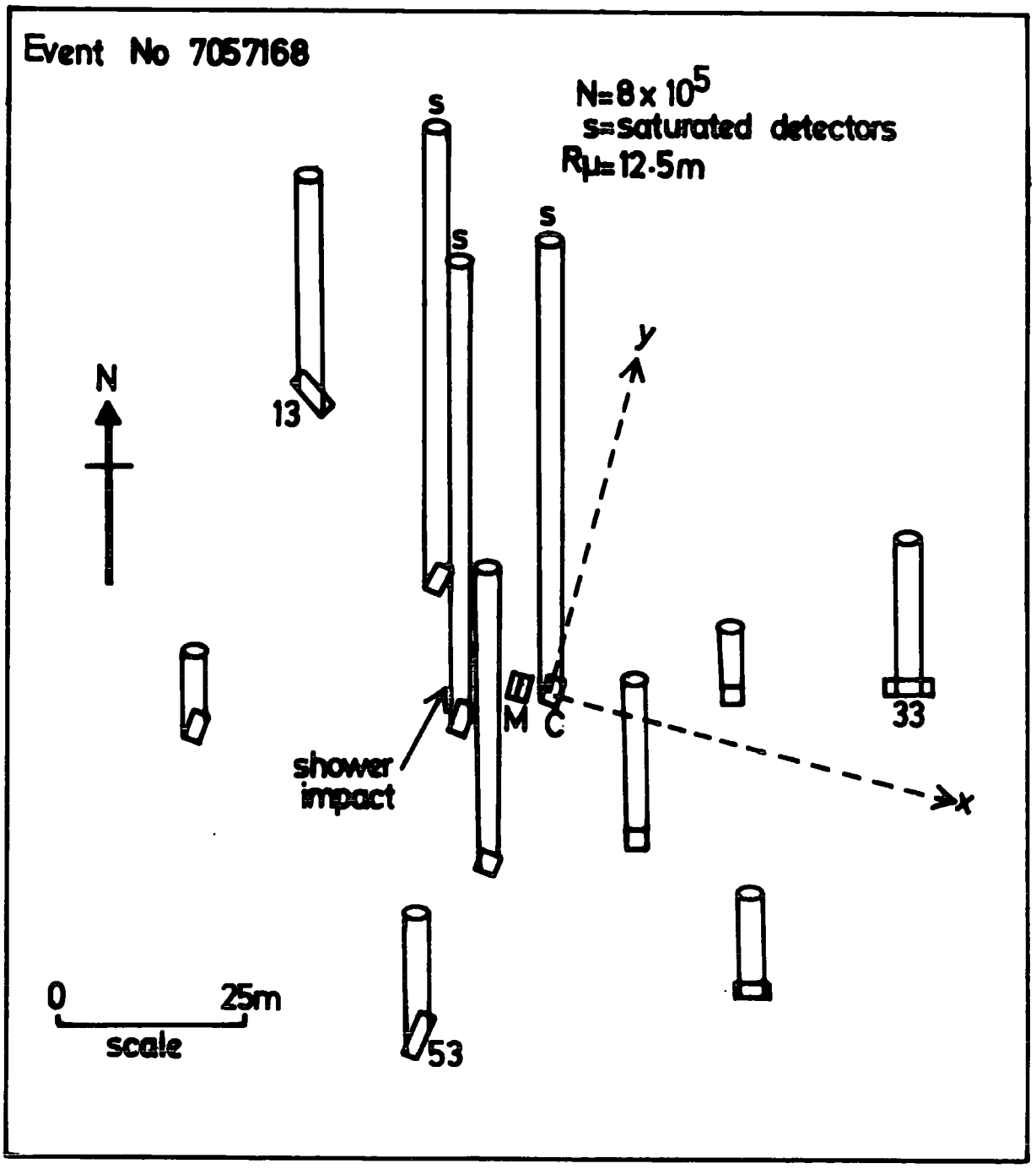

FIGURE 6.12b The air shower event accompanied the multiple muon event in Figure 6.12a, detectors C, 12 and 61 are all saturated hence only eight detectors are used in the shower analysis.

$$P_i(\Delta_i, S_i, \geq m) = e^{-\Delta_i S_i} \sum_{n=0}^{\infty} \frac{(\Delta_i S_i)^n}{n!} E_i(n, m) \qquad (6.6)$$

where Δ_i is the particle density at a detector of area S_i and whose particle detector's threshold is m, E_i (n, m) is a detector efficiency term which depends on the number of particles n incident on a detector above the detection threshold m. In calculating the densities, the lateral structure function used by Griesen (1960) with an age parameter of 1.25 was employed. Figure 6.13 shows the normalized detection probabilities which are calculated using equation 6.6. These probabilities have been obtained by integrating over a core location region ($r_2 - r_1$) as shown in the figure, and a pre-defined arrival direction modulated by $\cos^{10}\theta$. The probabilities that are plotted are the average probability over a certain core distance region for different shower sizes. For showers of size $\geq 10^6$ particles the probability is unity and becomes independent of core location.

6.7 EXPERIMENTAL RESULTS

The spectrograph data yielded 441 muons with energies $\geq$ 10 GeV from a total of 2300 showers that triggered the air shower array and satisfied the shower criteria of acceptance. Table 6.4 shows the number of showers involved according to their analysis option. The number of muons above 20 GeV are also listed and grouped according to the number of trays used in determining the muon momentum. The muon numbers presented in this table represent the total number of useful muon events including 29 multiple muon events. It was found that about 2.9% of the muon data have a standard deviation of $\geq 2.5 \times 10^{-3}$ m ; these events have been rejected. No restrictions due to the array detection efficiency have been imposed on the air shower data presented in this table.

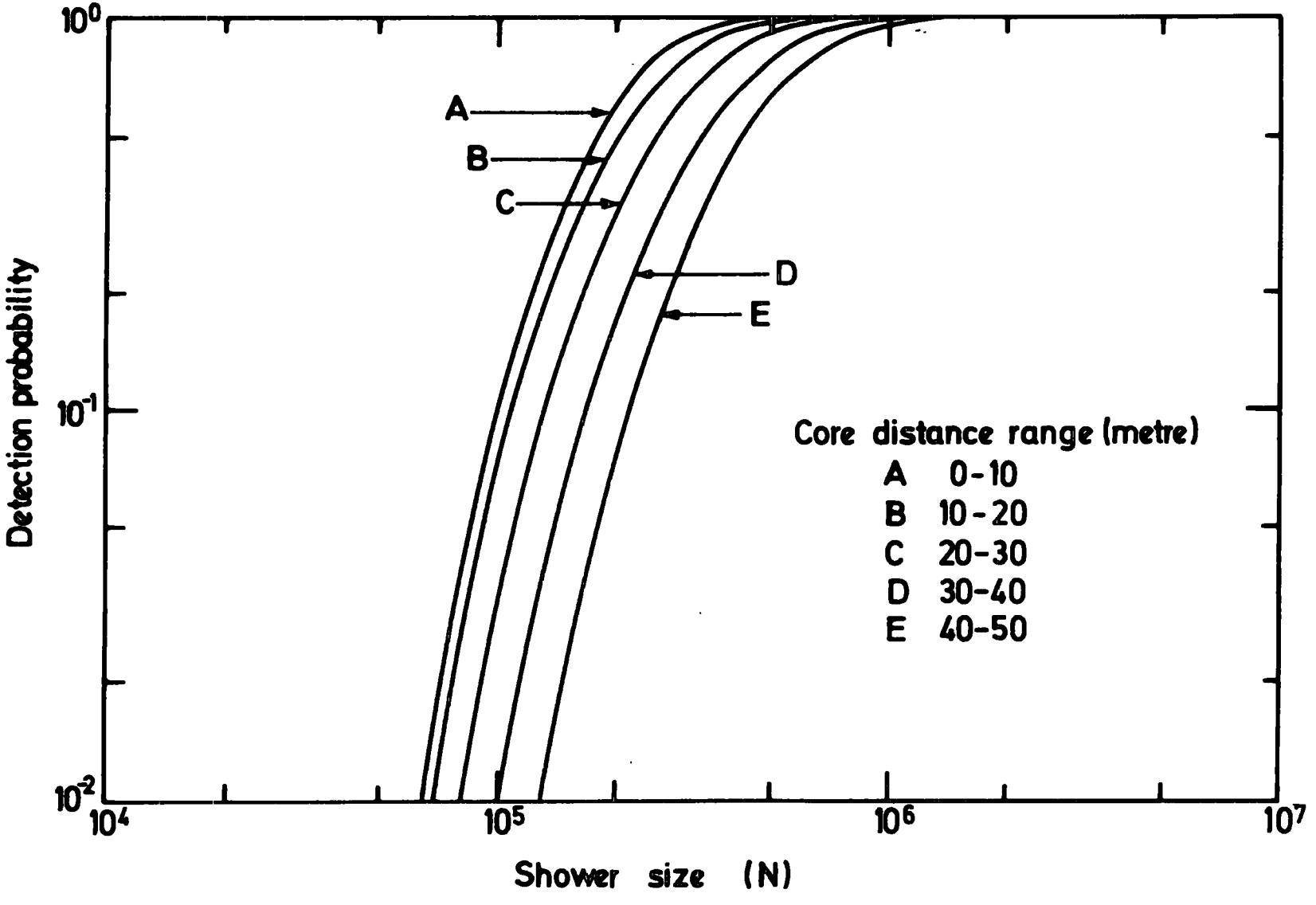

FIGURE 6.13 The array detection probability for shower falling within 30° of the zenith and various core distance ranges from the muon spectrograph.

Muon analysed data			Shower analysed data	
Muon threshold energy (GeV)	Tray fit		Core distance (m)	Number of showers
	3	4		
20	158	186	$\leq$ 50	2031
50	85	133	$\leq$ 40	1823
100	45	57	$\leq$ 30	1488
200	13	27	$\leq$ 20	1058
300	7	11	$\leq$ 10	477

TABLE 6.4 : The data collected in this experiment.
Muon and air shower data satisfying the muon and air shower selection criteria.

6.8 ACCURACY OF MEASURED PARAMETERS

In order to have any confidence in the estimated muon lateral distributions and other results obtained in this work it is important to determine the input parameters to a degree of accuracy which makes the errors of these parameters too small to markedly affect the final results. A detailed Monte Carlo analysis on the accuracy of the measured air shower parameters has been carried out by Smith (1977). Showers have been simulated and fired at the array with random core location, shower size, zenith and azimuthal angles.
It is concluded that for 800 showers triggering the array at zenith angles $\leq 30^{\circ}$ falling within 50 metres from the central detector, the accuracy of each shower parameter measured in the present work is as follows :-

(a) Core Location Accuracy

The error in core location is represented by calculation of the difference in the radial distances of the simulated input and the output shower axes from the central detector. It is concluded that there is an overall uncertainty of $\pm$ 4m in core distance for showers in the size range $3 \times 10^5 - 5 \times 10^6$ particles falling at distances of $\leq$ 50 metres from the central detector.

(b) Shower Size Accuracy

The error in shower size determination has been estimated by measuring the bias in the output shower size spectrum from a simulated input spectrum. It is found that for showers whose zenith angles are $\leq 30^{\circ}$ and whose cores are at $\leq$ 50 metres from the central detector, a suitable correction of the following form may be applied in the size range $3 \times 10^5 - 3 \times 10^6$ particles (Smith, 1977) :-

$$(N_i \times 10^{-6}) = (1.20 \pm 0.12)\ (N_o \times 10^{-6})^{(0.95 \pm 0.14)} \qquad (6.7)$$

for $2 \times 10^5 < N < 3 \times 10^6$.

(c) Accuracy of Arrival Directions

In working out the error in the arrival directions of the showers, the simulated showers are assumed to have timing measurements with standard deviation of $\pm$ 5 nsec. Only the timing detectors and the central detector (C + 53 + 33 + 13) have been used as the triggering elements. The overall uncertainty in zenith angle is $\pm 2.0^{\circ}$ and that of the azimuthal angle is $\pm 6.0^{\circ}$.

In determining the above accuracies in shower parameters, various shower features and array properties have been taken into account within the simulation programme. Poissonian fluctuations in the shower particle number at the density measuring detectors and Gaussian fluctuations with standard deviation of $\pm$ 5 nsec. in the arrival times of the shower, the linearity of the electronics and age parameter effects were included. The analysis programme used in the simulation calculations was the same programme as used on the real array data and the same triggering and data selection criteria were applied.

(d) Accuracy of the Determined Muon Momentum

In establishing the muon lateral distribution or muon energy spectrum, not only the shower parameters such as core distance, shower size and arrival directions have to be determined, but also the muons' momenta. The accuracy of the measured momentum is achieved by defining the quantity Δp (Whalley, 1974) such that

$$\Delta p = p \times \sqrt{c^2 + \frac{p^2}{p^2_{m.d.m.}}} \qquad (6.8)$$

where p is the measured muon momentum as determined by the M.A.R.S. analysis programme, c is the scattering correction and $p_{m.d.m.}$ is the maximum detectable momentum (m.d.m) of the spectrograph. Due to the large statistical error on the useful muon data, the scattering correction has not been taken into account, thus equation 6.8 reduces to the following form :-

$$\Delta p = \frac{p^2}{p_{m.d.m.}} \qquad (6.9)$$

Since the value for the m.d.m. of the spectrograph depends on the number of flash tube tray combinations used in determining the momentum of a particular muon, then Δp is a function of the number of flash tube tray combinations. Table 6.5 shows the error in the measured momentum of muons for 1 - 4 tray fits and 1 - 3 tray fits, the m.d.m. being 1572 $\pm$ 60 GeV/c and 520 $\pm$ 50 GeV/c respectively.

6.9 SUMMARY

In this chapter the analysis techniques involved with the muons and air showers have been described. It is seen that for muons detected by the magnetic spectrograph the analysis provides an accurate estimate of the muon's energy.

The powerful package of minimisation subroutines allows the shower analysis programmes to produce an accurate estimation of core location, shower size and arrival direction of shower cores. The errors in core location are quite small such that they do not affect or disturb the shape of the estimated muon lateral distributions. The shower sizes determined by the experiment are underestimated by 10%, and a correction has to be introduced due to this bias, when normalising the muon lateral distribution to ascertain shower size.

	Muon Momentum p GeV/c	Δ p GeV/c	Δ p/p %
4 tray fit (1234)	20	0.25	1.25
	50	1.59	3.2
	100	6.36	6.4
	200	25.45	12.7
	300	57.25	19.1
	500	159.03	31.8
3 tray fit (123)	20	0.77	3.9
	50	4.81	9.6
	100	19.23	19.2
	200	76.92	38.5
	300	173.10	57.7
	500	480.80	96.2

TABLE 6.5 : The calculated error on the measured momenta for 1-4 tray fits and 1-3 tray fits.

CHAPTER 7

THE LATERAL DENSITY DISTRIBUTION OF ULTRA HIGH ENERGY MUONS

7.1 INTRODUCTION

The measurement of the muon lateral distribution at high energies is the most significant result in the present experiment. The measurements have been obtained for near vertical showers having sizes in the range $2 \times 10^5 - 3 \times 10^6$. The experimental data yields not only the shape of the muon lateral distributions,but also the absolute values of the muon measured densities at various muon energies. A determination has been made of the total number of muons traversing the spectrograph above a certain fixed energy and also of the number of showers that are recorded by the array at certain radial distances from the spectrograph. The analysis of experimental results was carried out under the following assumptions :

(1) The spectrograph accepts mainly muons travelling in the near vertical direction.

(2) Muons with energies $\geq$ 50 GeV are almost parallel to the shower core direction.

As a consequence of the two assumptions the experimental results are insensitive to zenith angle and the analysis assumes that all showers arrive from the vertical direction. Further attempts to establish more detailed muon energy spectra have not been made due to the large errors which exist on the determined muon lateral densities.

7.2 BIAS CORRECTION OF EXPERIMENTAL DATA

When deriving the muon densities from the data it is important to

determine some basic parameters concerned with the geometry and design of the spectrograph and the air shower array. The most important factors that are to be taken into account in the case of the spectrograph are the acceptance of the instrument (as a function of momentum), the efficiency of the triggering scintillation detectors and the effect of multiple coulomb scattering in iron. The spectrograph acceptance has been evaluated using a Monte Carlo method following the work of Hawkes (1977) and is explained earlier in section 5.13. The efficiency of the levels 1 and 3 scintillation detectors in the blue-side of the magnet has been found to be 0.92 (Whalley, 1974). Coulomb scattering in the magnet iron has not been considered. Other corrections, possibly necessitated by the flash tubes being inefficient, have been found to have no significant effect on the data, and thus they have not been taken into account. Since the measurements reported here deal with high energy muons ($\geq$50 GeV), effects of the earth's magnetic field and coulomb scattering in the atmosphere have been ignored. In order to obtain the real number of muons observed in the spectrograph, the above biases have to be removed from the observed muon data such that :

$$n_\mu(> E_\mu) = \frac{1}{0.92} \left\{ \frac{\bar{n}_\mu(3)}{\mathrm{Acc}(3)} + \frac{\bar{n}_\mu(4)}{\mathrm{Acc.}(4)} \right\} \qquad (7.1)$$

where $n_\mu(>E_\mu)$ is the real number of muons traversing the spectrograph above a fixed muon energy E_μ(GeV), $\bar{n}_\mu$ is the number of muons observed above that energy and assigned by either a 3-tray or 4-tray fit momenta, Acc is the spectrograph acceptance determined for both tray combination fits and the factor 0.89 represent the value of the three-fold coincidence triggering efficiency of the blue-side of the spectrograph.

The other systematic biases that are concerned with the air shower array are the array detection efficiency

(as a function of shower size and core distance) and the array solid angle of acceptance. The detection efficiency of the array has been obtained following the method of Smith (1977) and is shown in Figure 6.7. The corrected number of showers triggering the array whose cores fell in an annulus of width $R_2 - R_1$, is

$$n_e(N,R_\mu) = \frac{\bar{n}_e(N,R_\mu)}{0.43 \times P(N,R_\mu)} \qquad (7.2)$$

where $\bar{n}_e(N,R_\mu)$ is the observed number of showers of size N falling at a distance R_μ from the spectrograph, $P(N,R_\mu)$ is the detection efficiency of the array triggering elements for showers of size N falling at a distance R_μ from the spectrograph and the factor 0.43 represents the solid angle of the array for showers falling at zenith angles $\leq 30^\circ$.

7.3 THE DISTRIBUTION OF EVENTS WITH RESPECT TO SHOWER SIZE

In order to estimate the densities of muons above a certain energy, it is necessary to obtain the number of showers of a certain size that fell in a certain radial distance range from the spectrograph. Also, it is important to obtain the number of muons observed in the spectrograph that are accompanied by showers and accepted by the muon analysis programmes. Showers were therefore divided into equal logarithmic bins of shower size, the resultant distributions are shown in Figure 7.1 where the number of showers in each logarithmic bin of shower size are plotted for five intervals of core distance from the blue-side of the spectrograph. Within each shower size interval, showers falling inside equal bins of core distance were grouped together, each group being 10 metres wide. In this way the total number of showers is obtained at a certain logarithmic bin of shower size

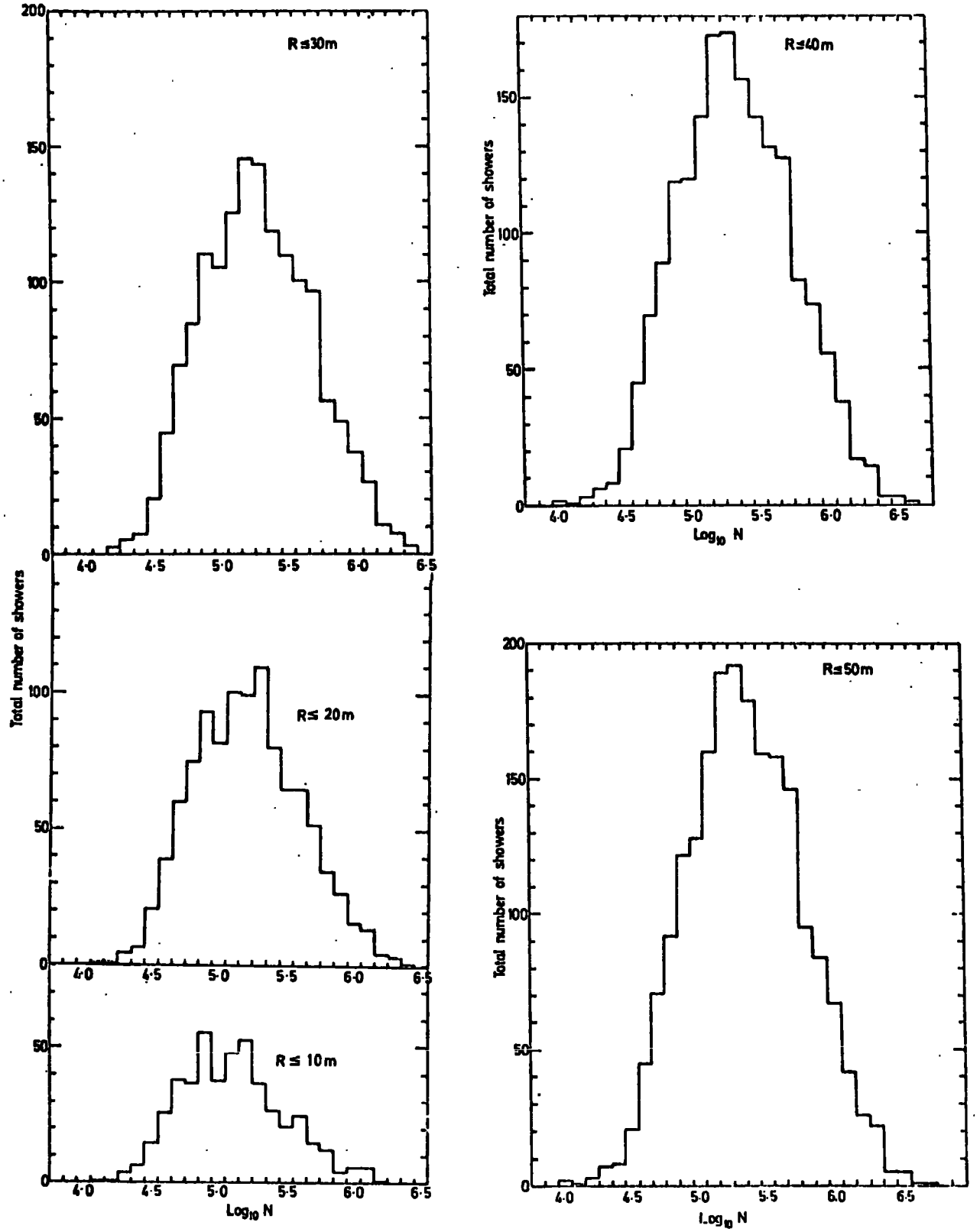

FIGURE 7.1 The shower size distribution of all showers triggered the array whose cores fell at distances ≤R (metre) from the spectrograph.

and radial distance. This is shown in Figure 7.2 (a,b.c,d and e). The mean shower size and mean core distance of each distribution are calculated and the muon densities above a certain muon fixed energy were then calculated as will be explained in section 7.5.

The total number of showers accompanied by muons with energies greater than or equal to 50, 100, 200 and 300 GeV, are plotted in an integral form in Figure 7.3 versus shower size. For each logarithmic bin the number of showers represent the total number of showers falling at distances $\leq$ 50 metres from the shower axis and corrected for the array detection probability. Figure 7.4 shows the distribution of the muons with energies not less than 50 GeV observed in the spectrograph in showers of certain sizes falling at five 10 metre intervals from the spectrograph. The data presented in this figure were used in estimating the muon lateral distributions in this work.

7.4 THE RADIAL DISTRIBUTION OF HIGH ENERGY MUONS

Muon events that are accepted in the present analysis have been grouped into 5 m intervals of core distance from the blue-side of the spectrograph . The resulting distributions for muons in showers whose detection probability is $\geq$ 60% are shown in Figure 7.5. Each distribution is obtained for muons of energies not less than 50, 100, 200 and 300 GeV. It is seen from the figure that there is a general agreement in the shape of the distributions, this agreement is evidence against any possible systematic biases in the analysis of high energy muons that are edited from relatively complicated muon events in which the showers fell almost in the vicinity of the spectrograph. A more general picture of the radial distribution of high energy muons can be obtained by using all muon-accompanied showers such that no cut due to detection probability was imposed on the shower sizes. Figure 7.6 (a,b,c and d) shows a three dimensional plot of

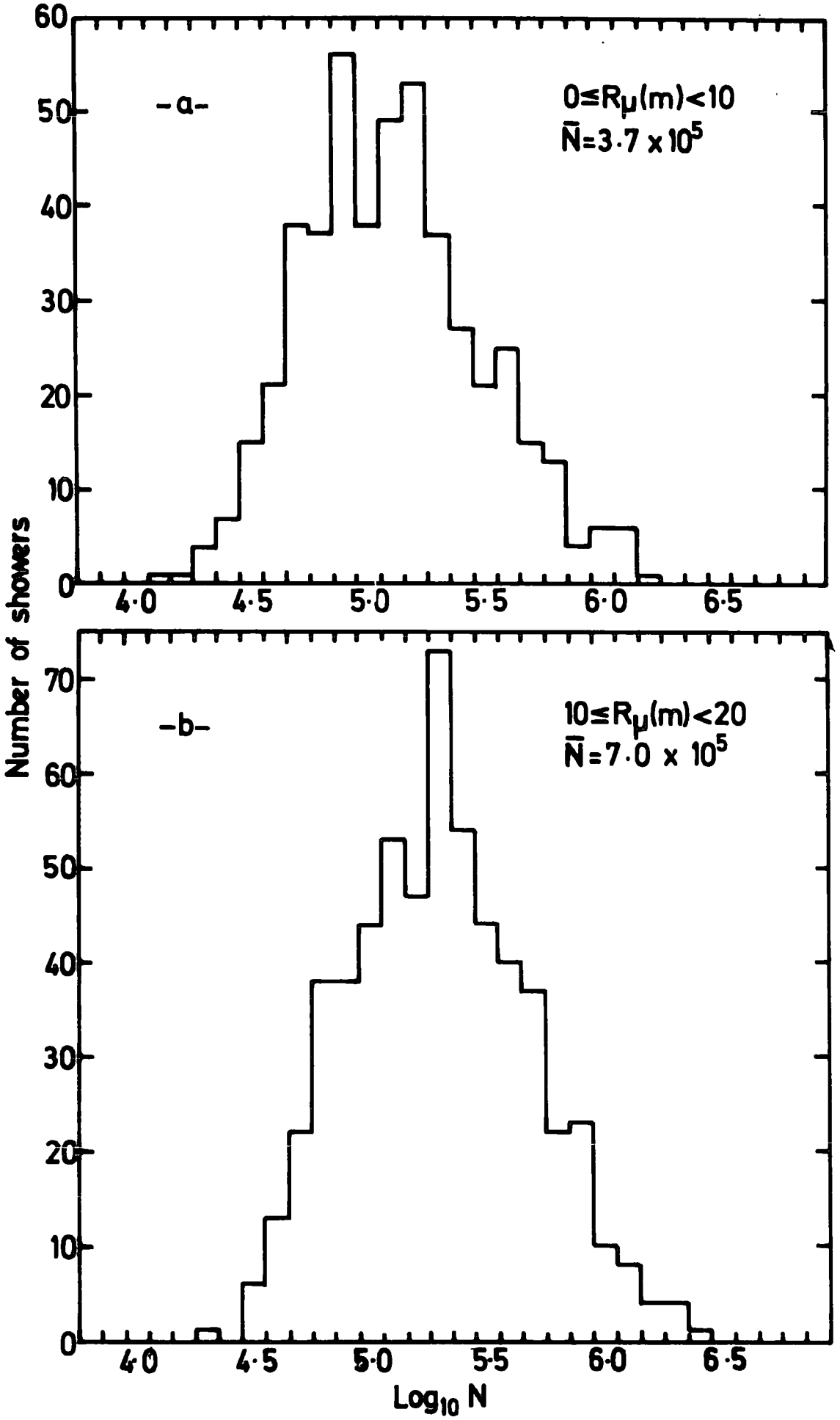

FIGURE 7.2 The distribution of all showers that their cores fell in an annulus $R_{\mu_2} - R_{\mu_1}$

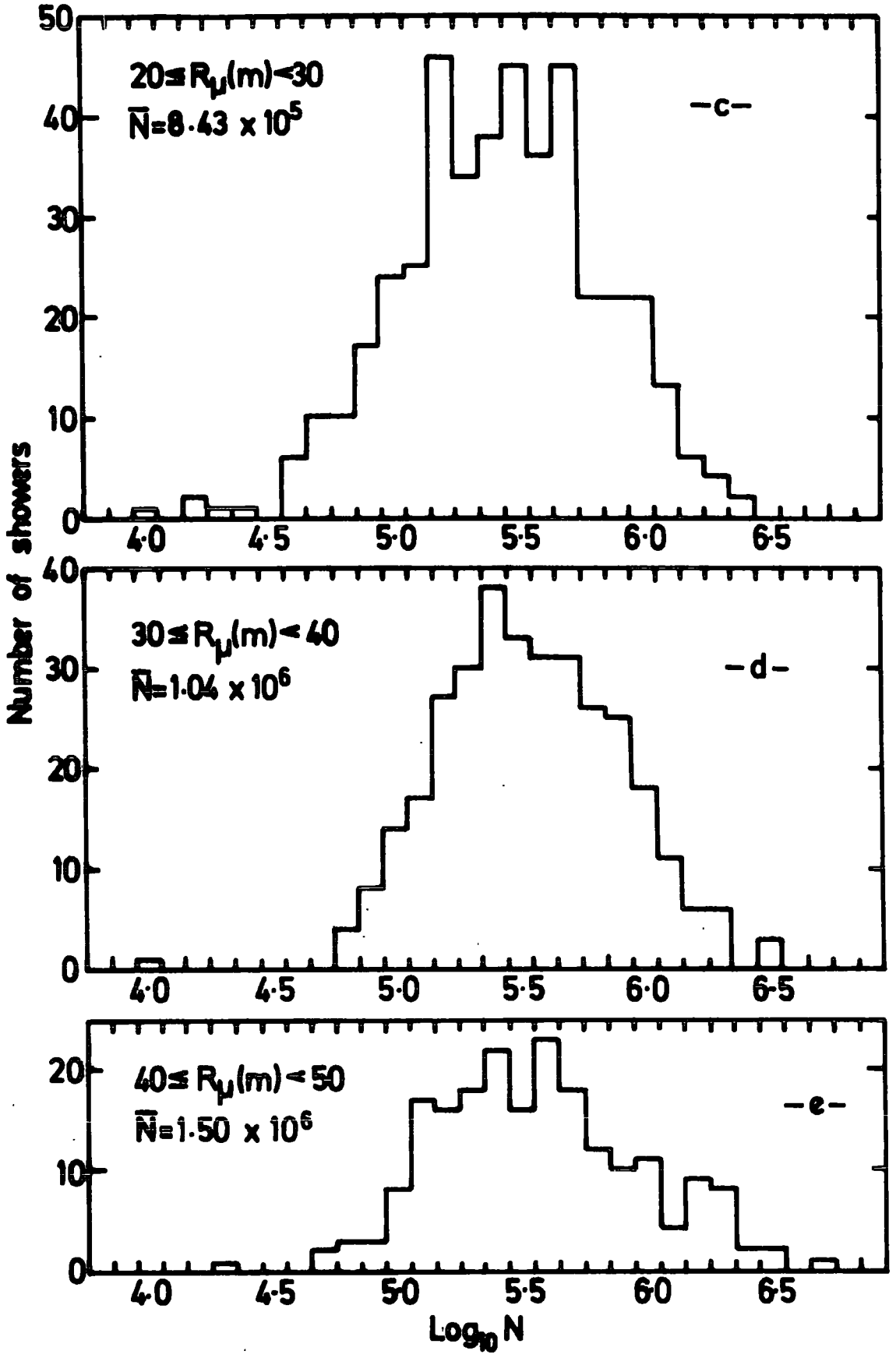

FIGURE 7.2 Continued : The distribution of all showers that their cores fell in an annulus $R_{\mu_2} - R_{\mu_1}$

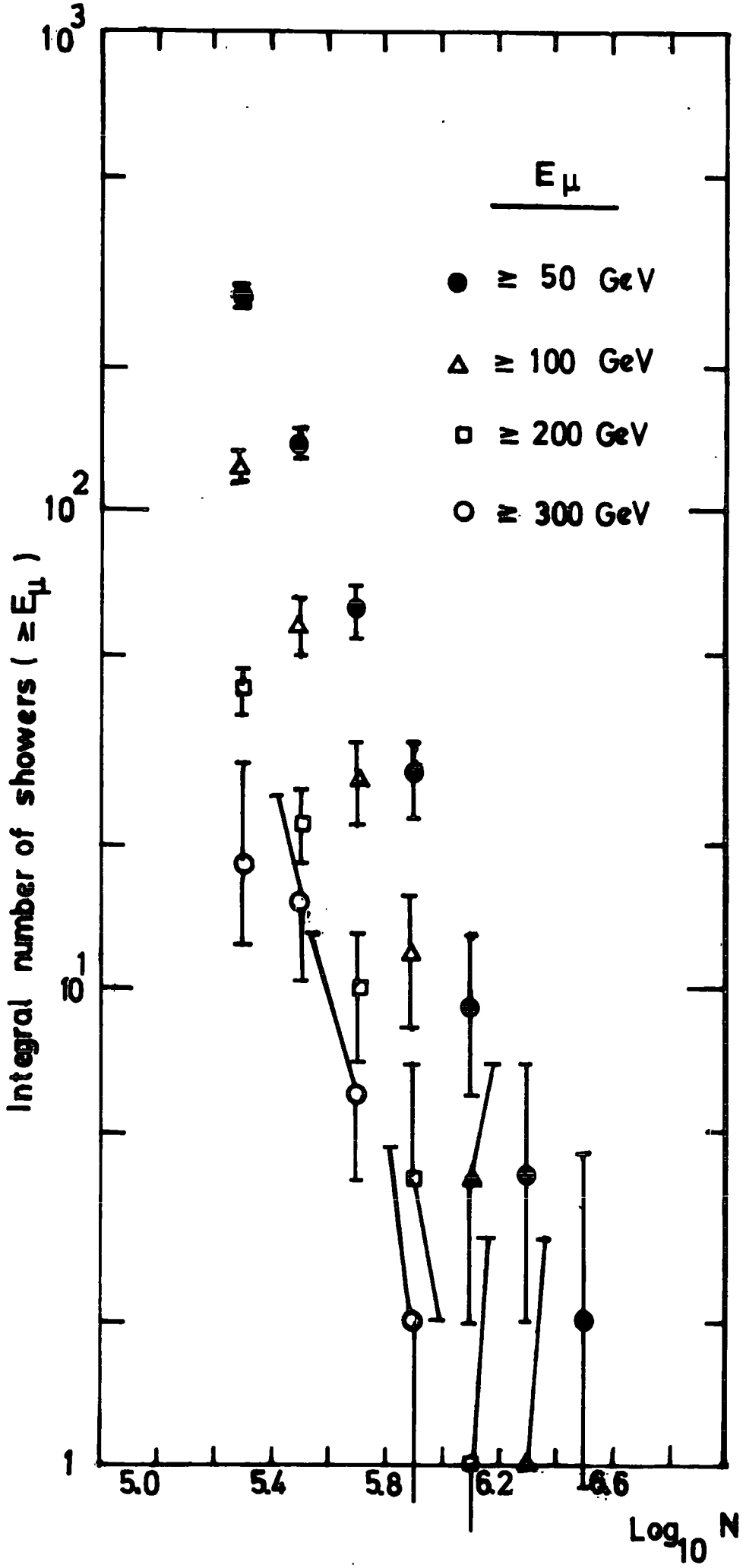

FIGURE 7.3 The shower size distribution for showers accompanied by high energy muons where threshold energies are indicated in the figure.

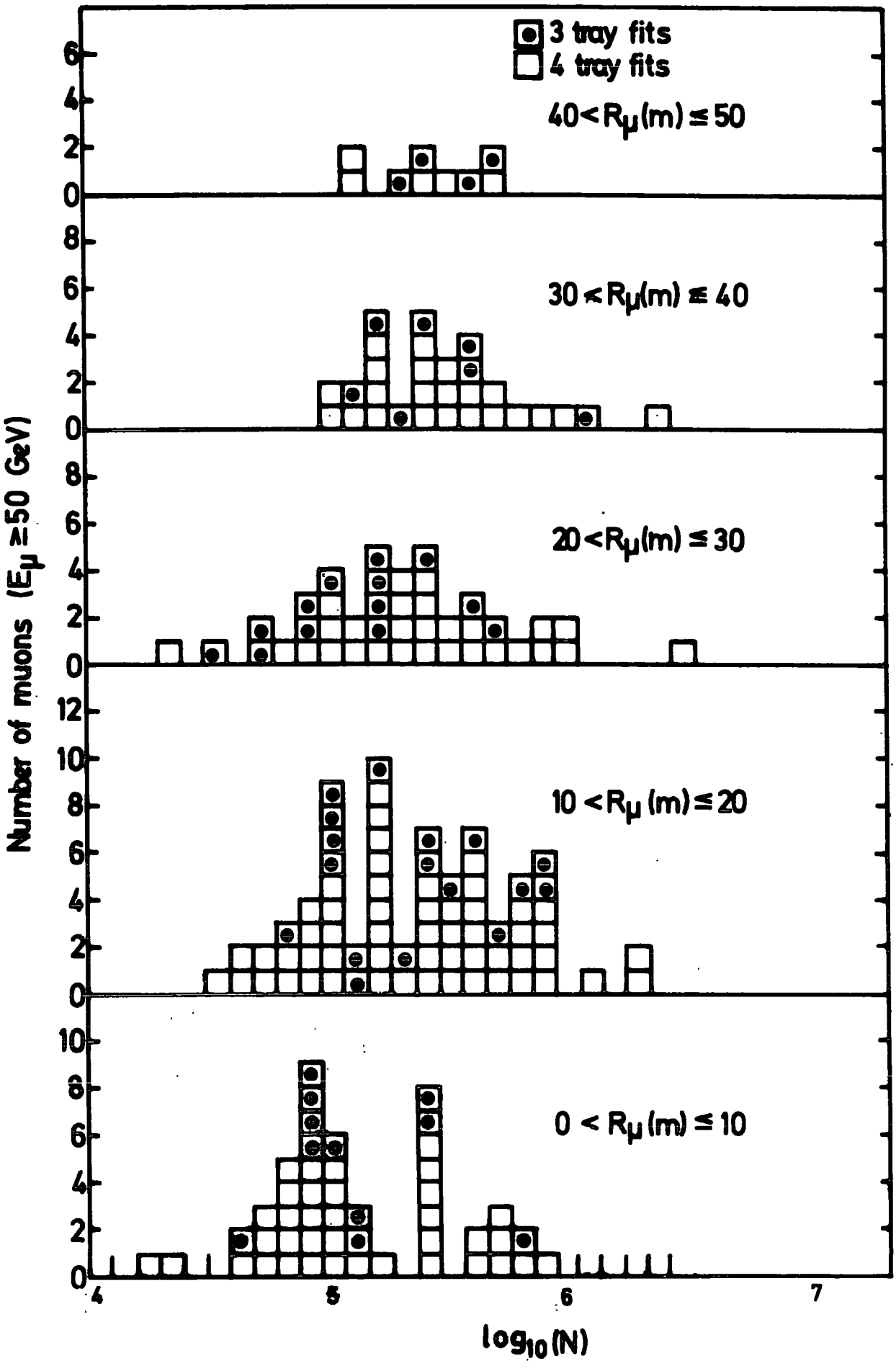

FIGURE 7.4 The observed number of muons per logarithmic bin of shower size for showers whose cores hit in a 10 meter annulus from the spectrograph.

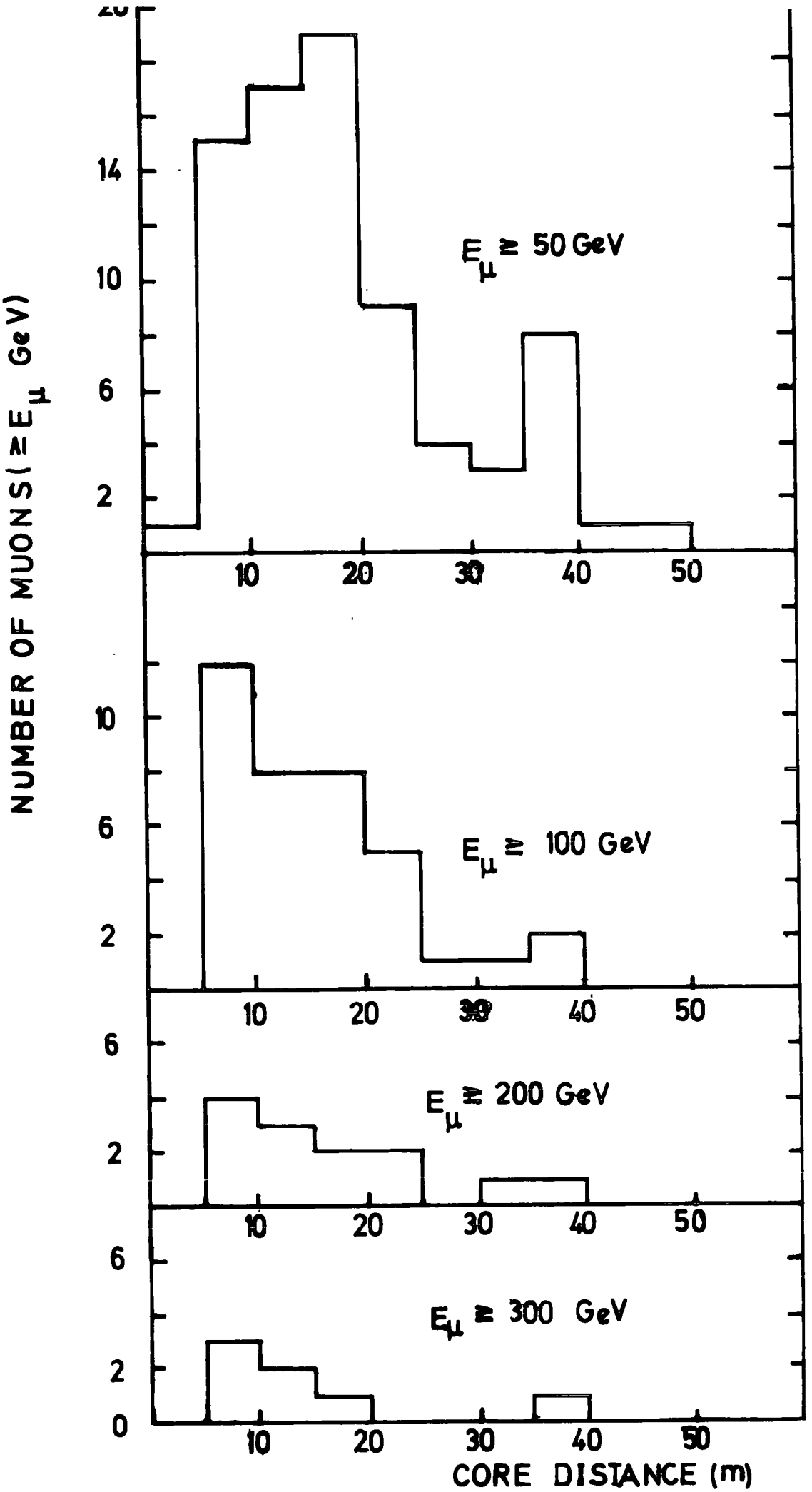

FIGURE 7.5 The radial distance distribution of muons with threshold energies ≥ 50, 100, 200 and 300 GeV associated with showers in the range $2 \times 10^5 - 3 \times 10^6$ particles.

the scatter distribution of the cores of showers that were accompanied by muons having energies above 50,100,200 and 300 GeV. The relative position of the spectrograph and the array triggering detectors are shown in the scatter plot. It is concluded from Figure 7.6 that as the muon energy threshold increases shower cores hit closer to the spectrograph. This fact reflects the overall dependence of the muon energy threshold on the average radial distance, i.e. high energy muons exist closer to the core than those of lower energies.

7.5 ESTIMATION OF MUON DENSITIES

As far as the work reported in this chapter is concerned the main objective is to find as accurately as possible the number of muons traversing the spectrograph above a certain fixed muon energy in a number of showers whose cores have fallen in an annulas R_2-R_1 for a shower size range N_2-N_1. Although the majority of muon trajectories are well defined and determined, the method of estimating muon densities is still subjective to some degree. Many checks were made on the number of observed muons and the number of registered showers, but it was found that there was no significant change in these numbers. The accumulated data of muons have been sub-divided into intervals of size and radial distance as explained in section 7.3. According to the data in Table 7.1, four muon density estimates have been worked out corresponding to four muon energy thresholds (50,100,200 and 300 GeV). Each of the muon densities has been defined as follows :

$$\Delta_\mu (\geq E_\mu) = \frac{n_\mu (\geq E_\mu)/A}{n_e (N, R_\mu)} \qquad (7.3)$$

where Δ_μ is the muon density above a fixed muon energy E_μ(GeV), $n_\mu(\geq E_\mu)$ is

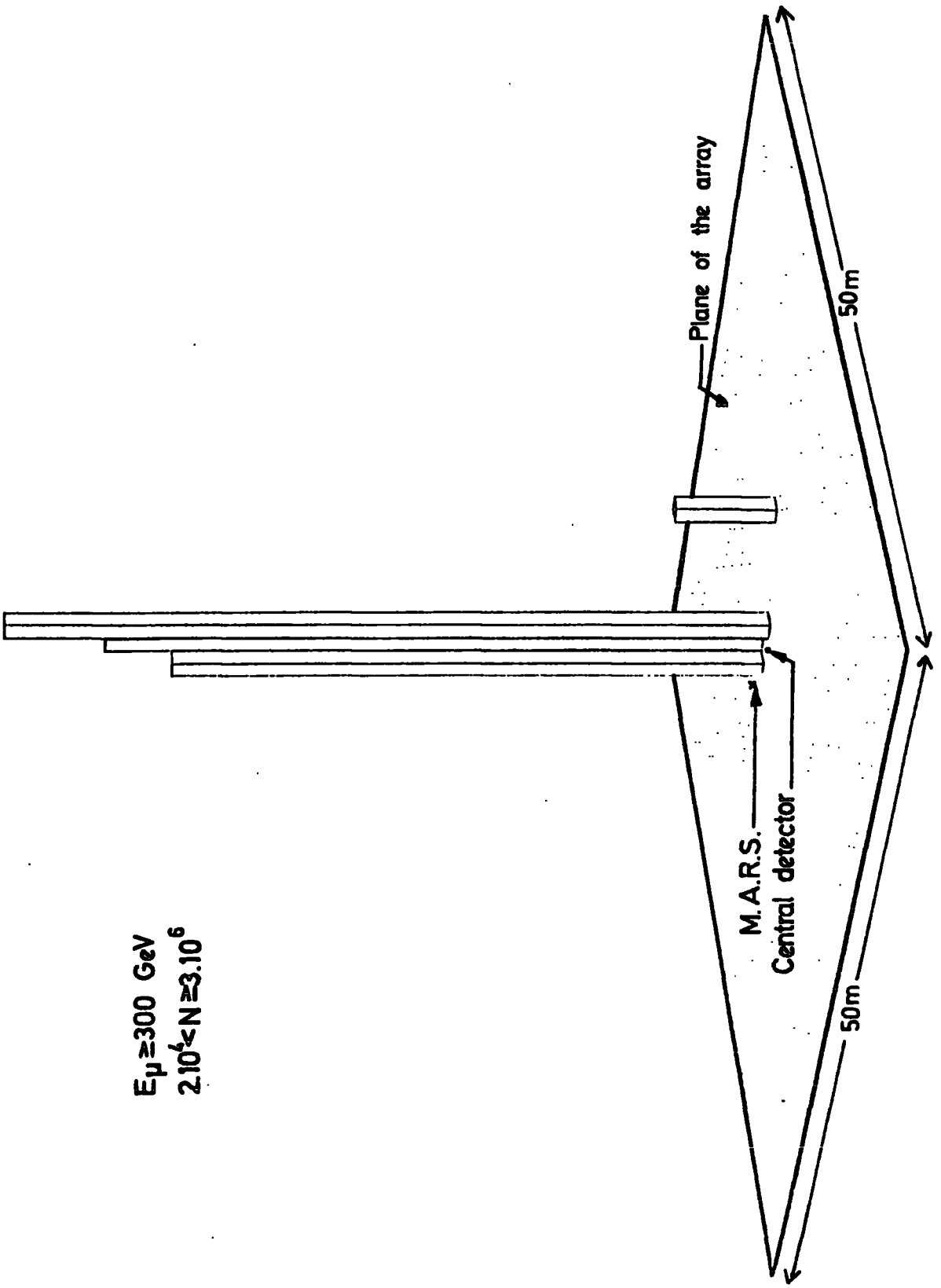

FIGURE 7.6a Three dimensional plot of the core impact distribution of showers associated by muons whose energies are not less than 300 GeV.

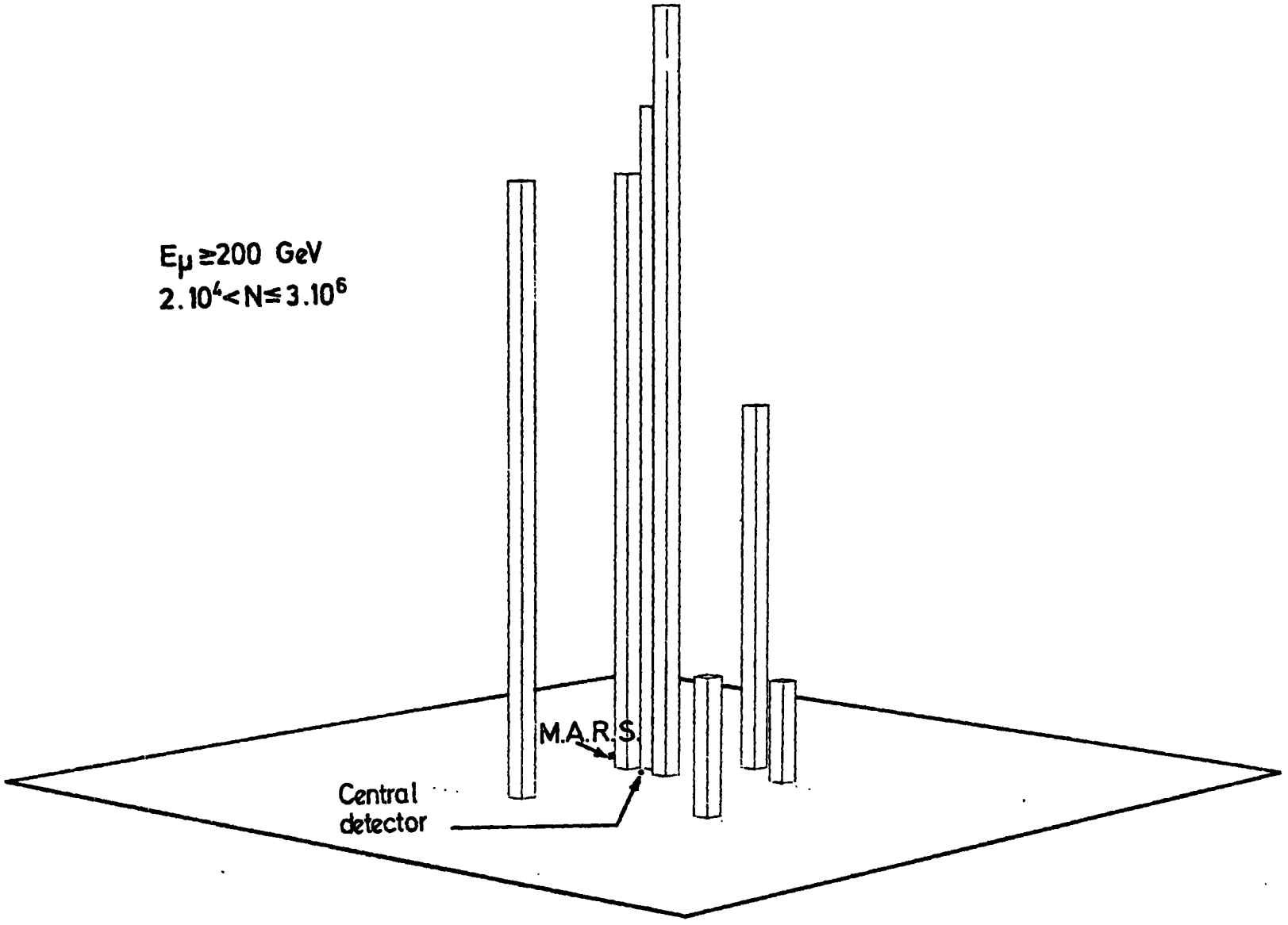

FIGURE 7.6b Three dimensional plot of the core impact distribution of showers associated with muons having energies not less than 200 GeV.

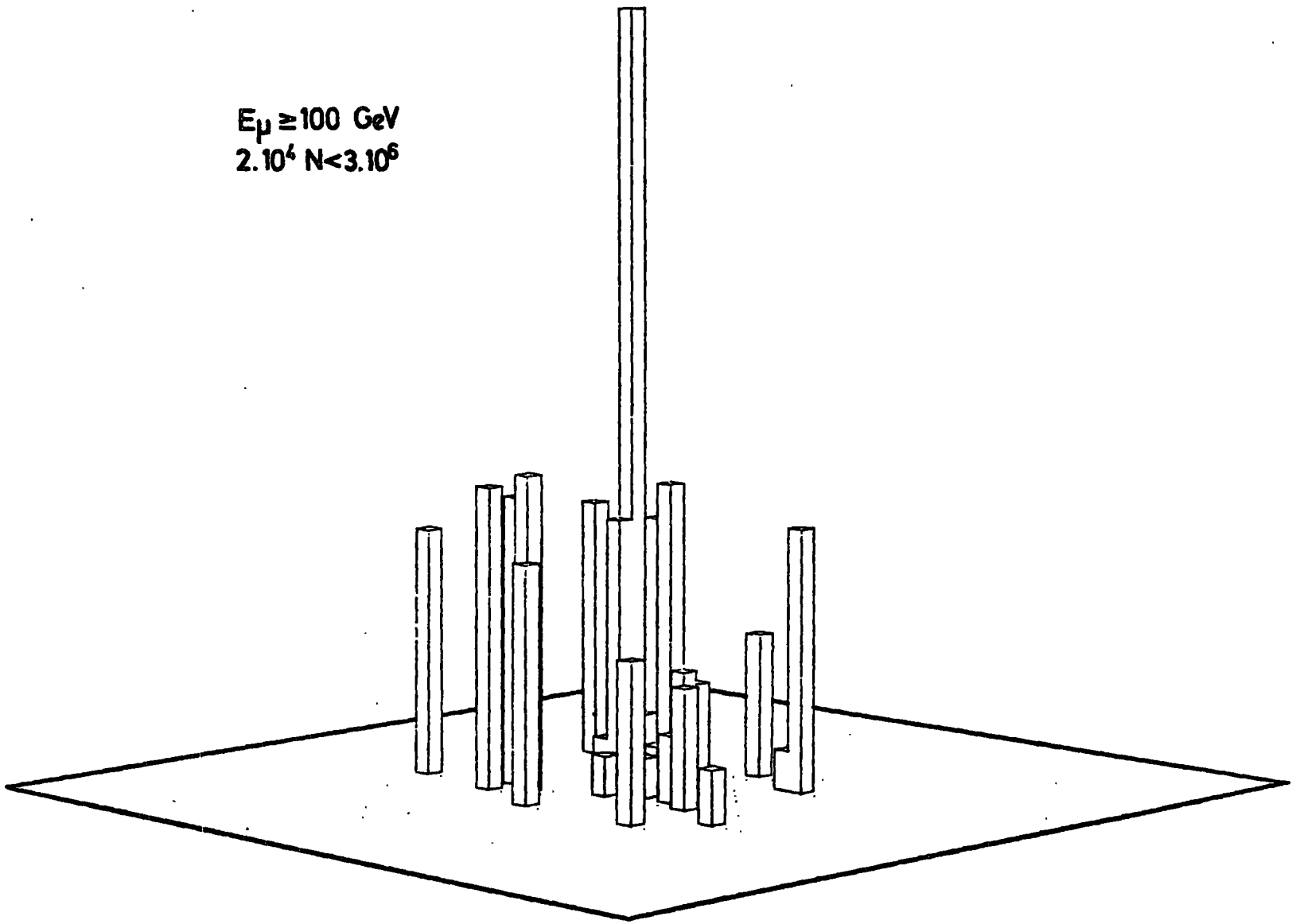

FIGURE 7.6c A three dimensional plot of the core impact distribution of showers associated with muons of energies not less than 100 GeV.

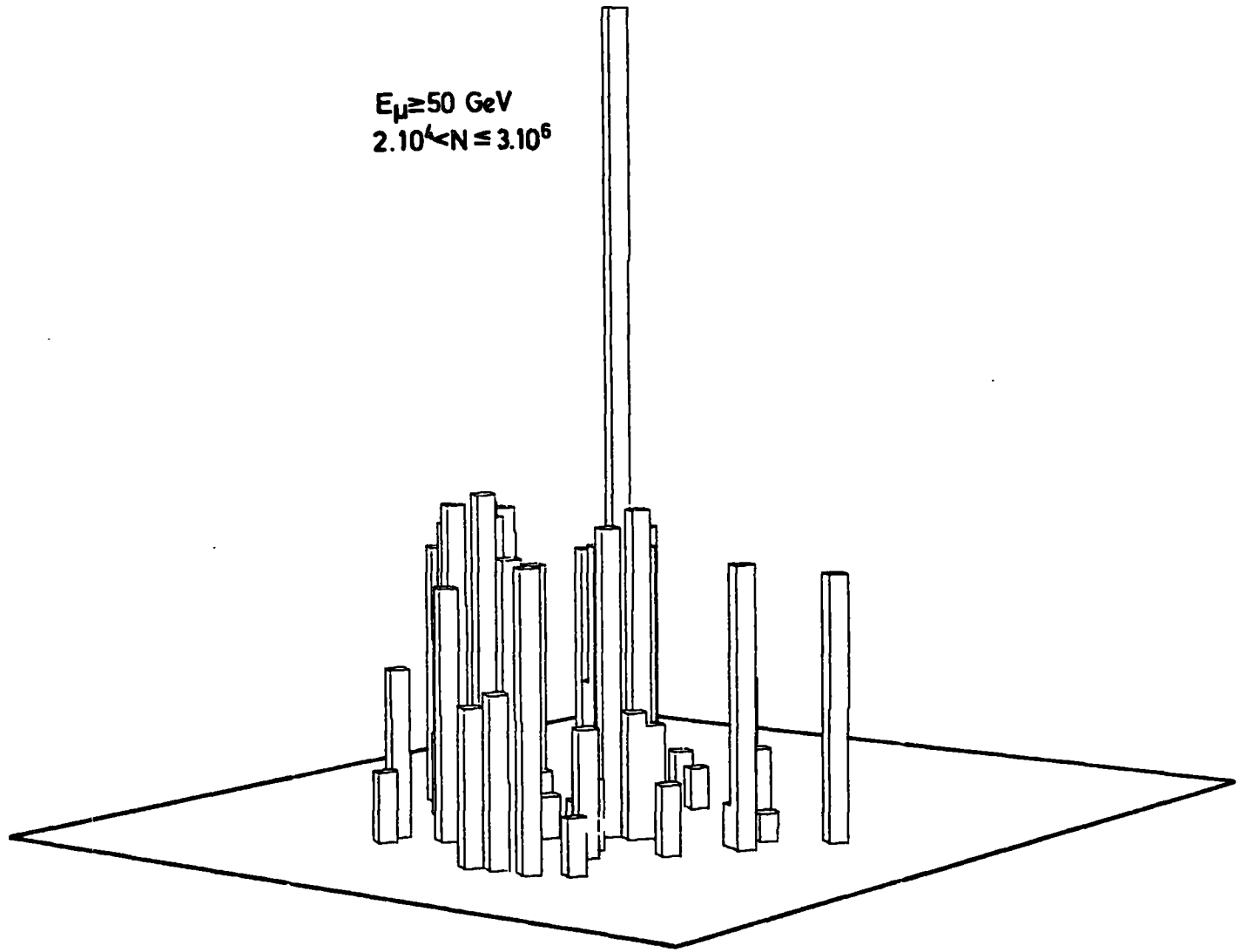

FIGURE 7.6d A three dimensional plot of the core impact distribution of showers associated with muons having energies not less than 50 GeV.

Muon threshold energy (GeV).	Number of muons per radial distance interval				
	0-10	10-20	20-30	30-40	40-50
⩾ 50 GeV	16	36	13	11	2
⩾100 GeV	12	16	6	3	-
⩾200 GeV	5	4	2	2	-
⩾300 GeV	3	3	-	1	-
number of showers per radial distance interval	120	247	217	157	77

TABLE 7.1 : Summary of muons and air showers number data that are selected for estimation of muon densities. (Showers detection probability > 60%).

the corrected number of muons above or equal to an energy E_μ observed in the spectrograph out of a total of n_e showers and A is the geometrical area of the spectrograph obtained considering the acceptance of the spectrograph. A is a function of muon energy (see section 6.10). The errors quoted on the estimated densities in equation 7.3 are the Regener (1951) statistical limits for very small samples. The dependence of muon densities on zenith angle has not been studied since the angular distribution of muons is very narrow and thus the measured muon densities are assumed to be for near vertical showers.

7.6 MEASUREMENTS OF THE LATERAL DENSITY DISTRIBUTION OF ULTRA HIGH ENERGY MUONS

The spectrograph data in association with E.A.S. have enabled the muon densities to be derived above a certain muon threshold energy and at distances $\leqslant$ 50 m from the shower axis to the muon spectrograph. In establishing the muon lateral distribution only showers having a detection efficiency $\geqslant$ 60% have been included. Figure 7.7 shows the lateral density distribution of muons with energies not less than 50 GeV obtained in this experiment for near vertical air showers whose mean sizes are indicated at each point. Each point on the lateral distribution curve represents an average density for a group of showers with similar characteristics and core distances from the muon spectrograph which fell in a certain interval. The abscissa of each point is the mean distance from the shower axis to the spectrograph for that particular group of showers in each radial distance interval. Representing the data in this way enables the measured muon densities to be scaled to a fixed shower size by assuming the shape of the muon lateral density distributions to be independent of shower size. This assumption may be justifiable if, for example, the mass composition of primary cosmic rays does not vary with energy, thus no variation is expected

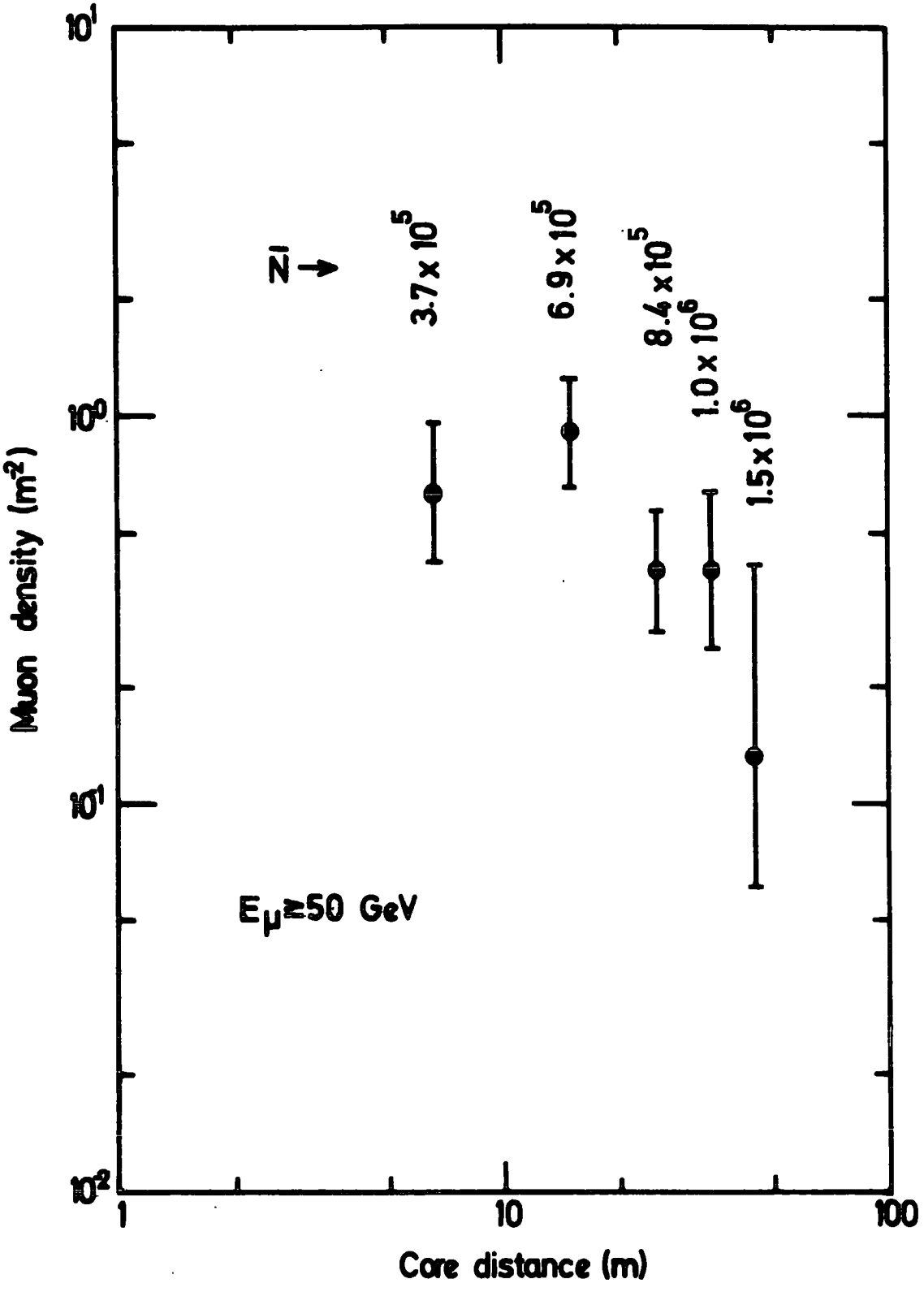

FIGURE 7.7 The measured lateral density distribution of muons having energies ≥ 50 GeV in selected showers (see text).

in the shape and absolute normalization of the muon lateral distributions. In a similar way the lateral density distributions for muons with threshold energies 100, 200 and 300 GeV are established, these distributions are shown in Figures 7.8, 7.9 and 7.10 respectively. All the data presented in the measured muon lateral distributions are eventually scaled to a standard shower size of 10^6 particles by making use of the relation $N_\mu \propto N_e^{0.8}$ and the resultant distributions are presented in the next section. It is found that over the range 0.7 - 0.9 for the exponent of the $N_\mu - N_e$ dependence (see Figure 2.19) the scaled densities do not vary by more than 5%. Thus, variations of the exponent with muon energy and radial core distance may not give significant changes in the shape or absolute normalisation of muon densities. Normalisation of muon densities to a common shower size (10^6 particles) serves two purposes. The first is to correct approximately for any small systematic variation of mean shower size with mean radial distance from the muon spectrograph. The second purpose is to enable the measured lateral distributions to be compared with other experimental and theoretical muon lateral distributions. This will be discussed in the following sections.

7.7 COMPARISON WITH OTHER EXPERIMENTAL RESULTS

In section 2.5 three experiments have been described in which the lateral density of muons have been measured using magnetic deflection technique. Direct comparison of the present results can be made with the results of the Moscow/Lodz collaboration (Rozhdestvensky et al, 1975) for muons of threshold energy $\geq$ 50 GeV covering the same range in radial distance as is used in the present work. The Haverah Park measurements of the lateral density distribution of muons above 50 GeV have been taken from the work of Orford (1968) for a shower of size 2×10^7 particles, zenith angle 22° and distances of 50-500 metres from the shower axis. Muon densities

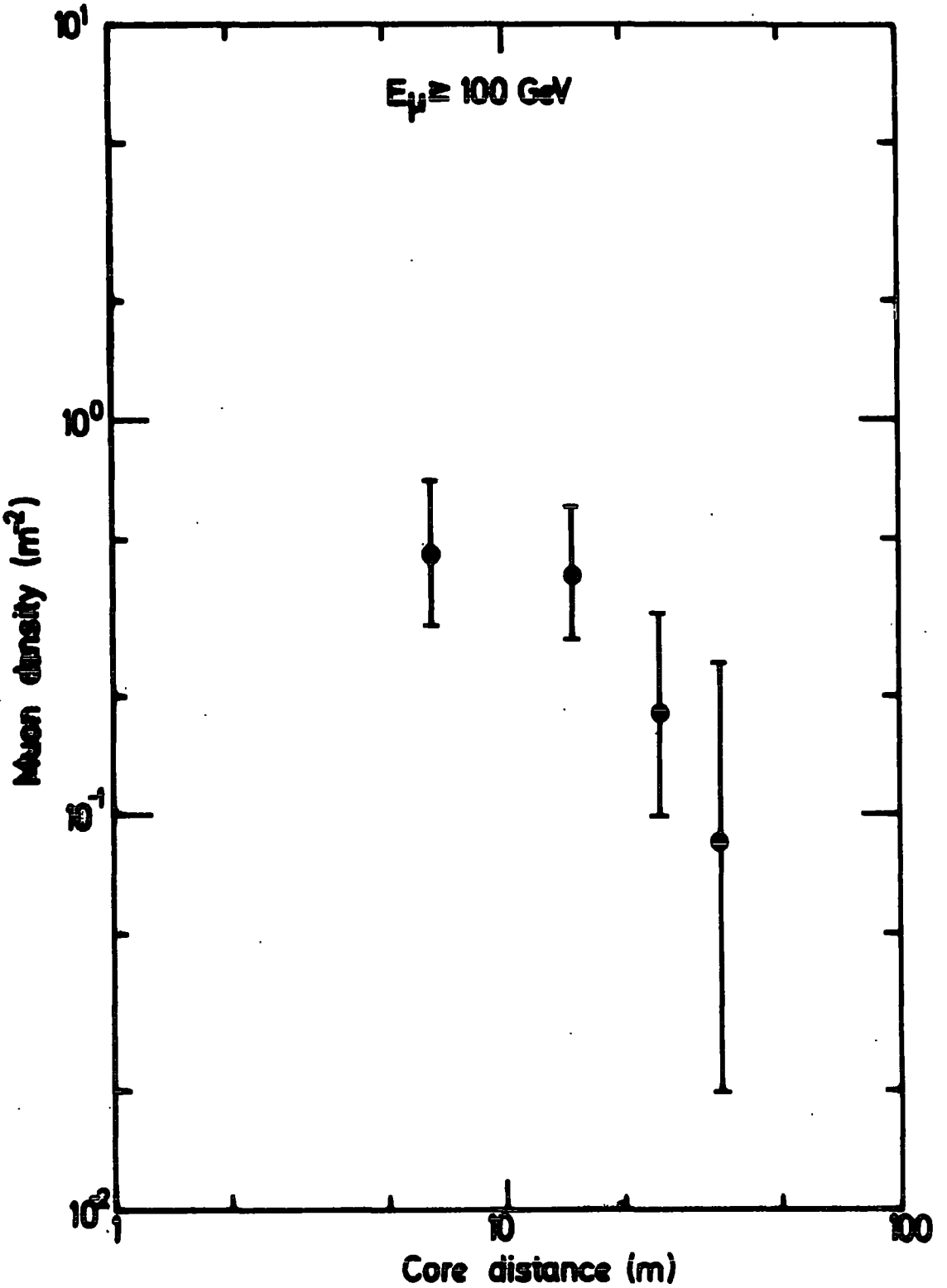

FIGURE 7.8 The measured lateral density distribution of muons of energies ≥ 100 GeV in showers of various mean sizes as indicated in figure 7.7.

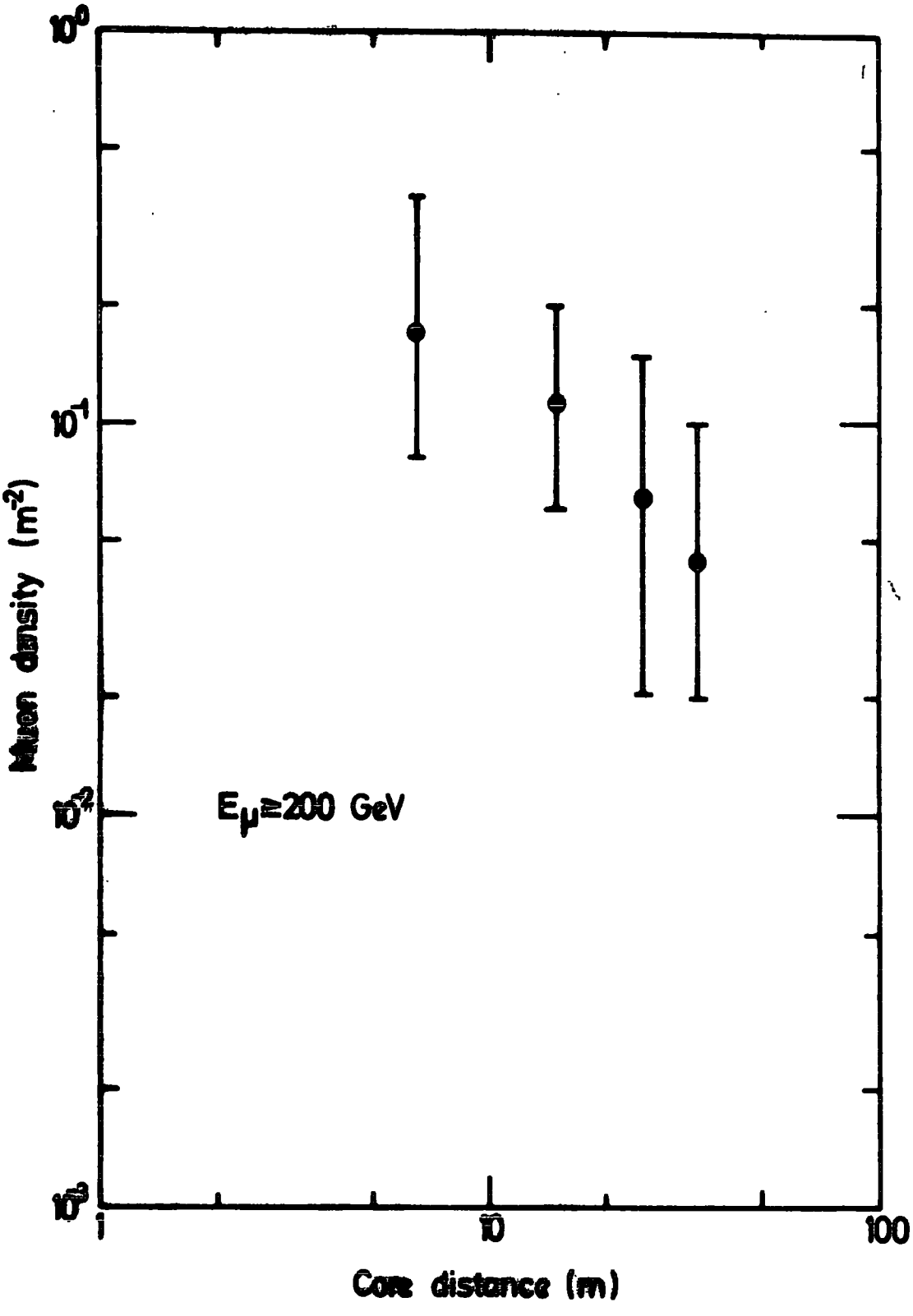

FIGURE 7.9 The measured lateral distribution of muons with energies ≥ 200 GeV in showers of various sizes as indicated in figure 7.2.

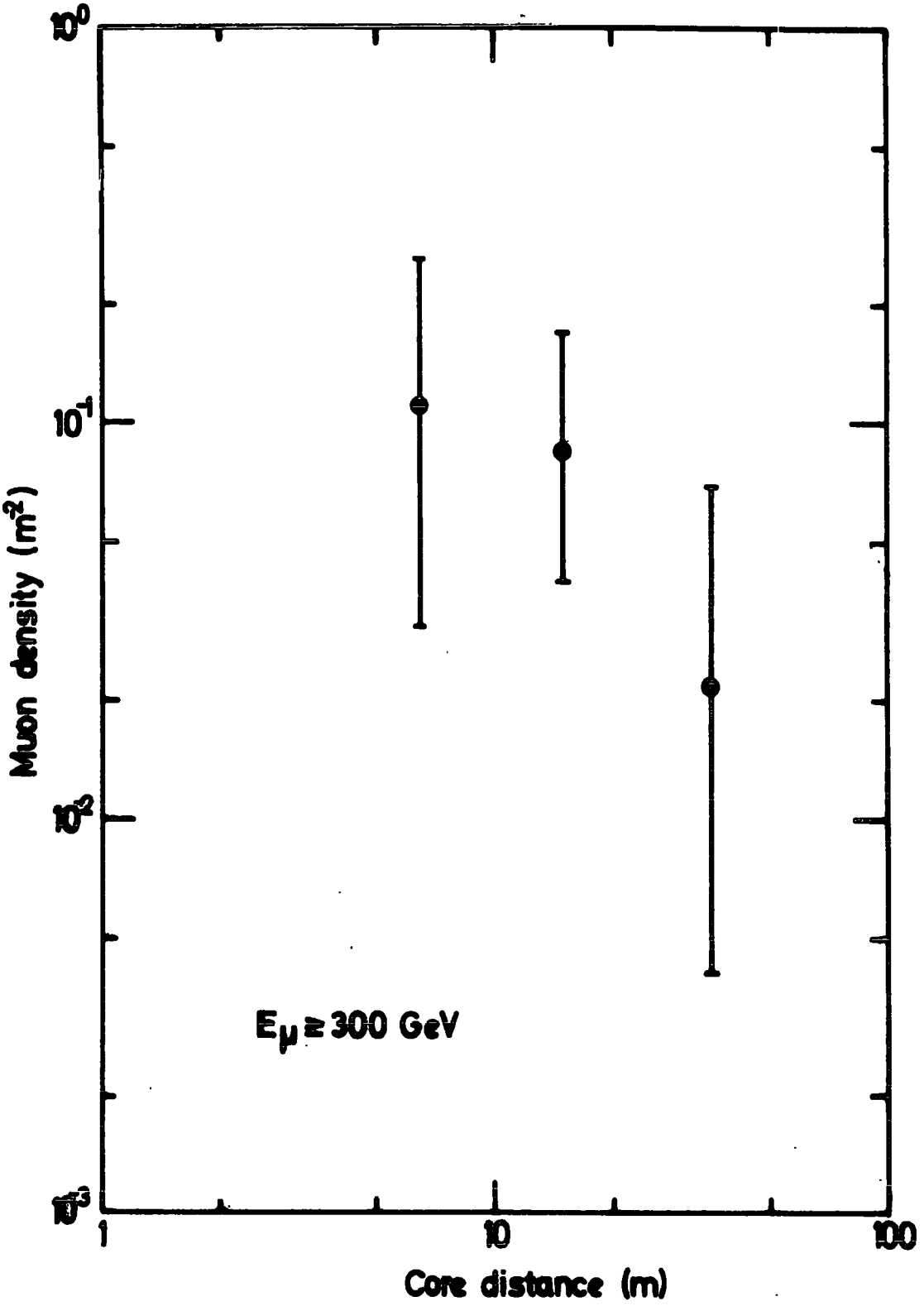

FIGURE 7.10 The measured lateral distribution of muons with energies ≥ 300 GeV in showers of mean sizes indicated in figure 7.7.

at core distances 50, 100 metres were selected and scaled to a common shower size of 10^6 particles using the relation $N_\mu \propto N_e^{0.8}$. A correction was applied to the absolute values of muon densities to convert them from a 22^o zenith angle to those expected for the vertical direction. Figure 7.11 compares the lateral density distribution of muons above 50 GeV as measured by the two groups with the present results. It is clear from the figure that a satisfactory agreement is obtained with the Moscow/Lodz data in both shape and absolute value of the distribution. It is also noticed that the statistical accuracy of the present data is slightly worse than the Moscow/Lodz data, this is attributed to the severe selection criteria imposed on the present data. Figure 7.11 shows that the present experimental data do not contradict the Haverah Park results. An attempt is also made here to compare the present results with the lateral structure function of muons given by Greisen (1960), the density of muons being given by equation 2.10 which is an empirical expression based on the measurements of the muon energy spectrum in the range 1-20 GeV and at core distance 10-500 m from the shower core. Since the Greisen structure function is applicable for muons at threshold energies well below those of the present experiment and in order to allow a comparison to be made with the present results, it is necessary to extrapolate this function to the muon threshold energies used in the present work, this is shown in Figures 7.12, 7.13, 7.14 and 7.15, where the extrapolated lateral structure function is plotted for a shower of size 10^6 particles at various muon threshold energies. Also presented in the same figures are analytical expressions representing the lateral structure of muons fitted by Hawkes (1977) to the data of the Moscow/Lodz collaboration (Rozhdestvensky et al, 1975), this expression has the form

$$\rho_\mu (\geq E_\mu, N, r) = A E_\mu^{B} \; N^{0.8} \; r^{-0.5} \; e^{-C E_\mu^{D}} \times r \qquad (7.4)$$

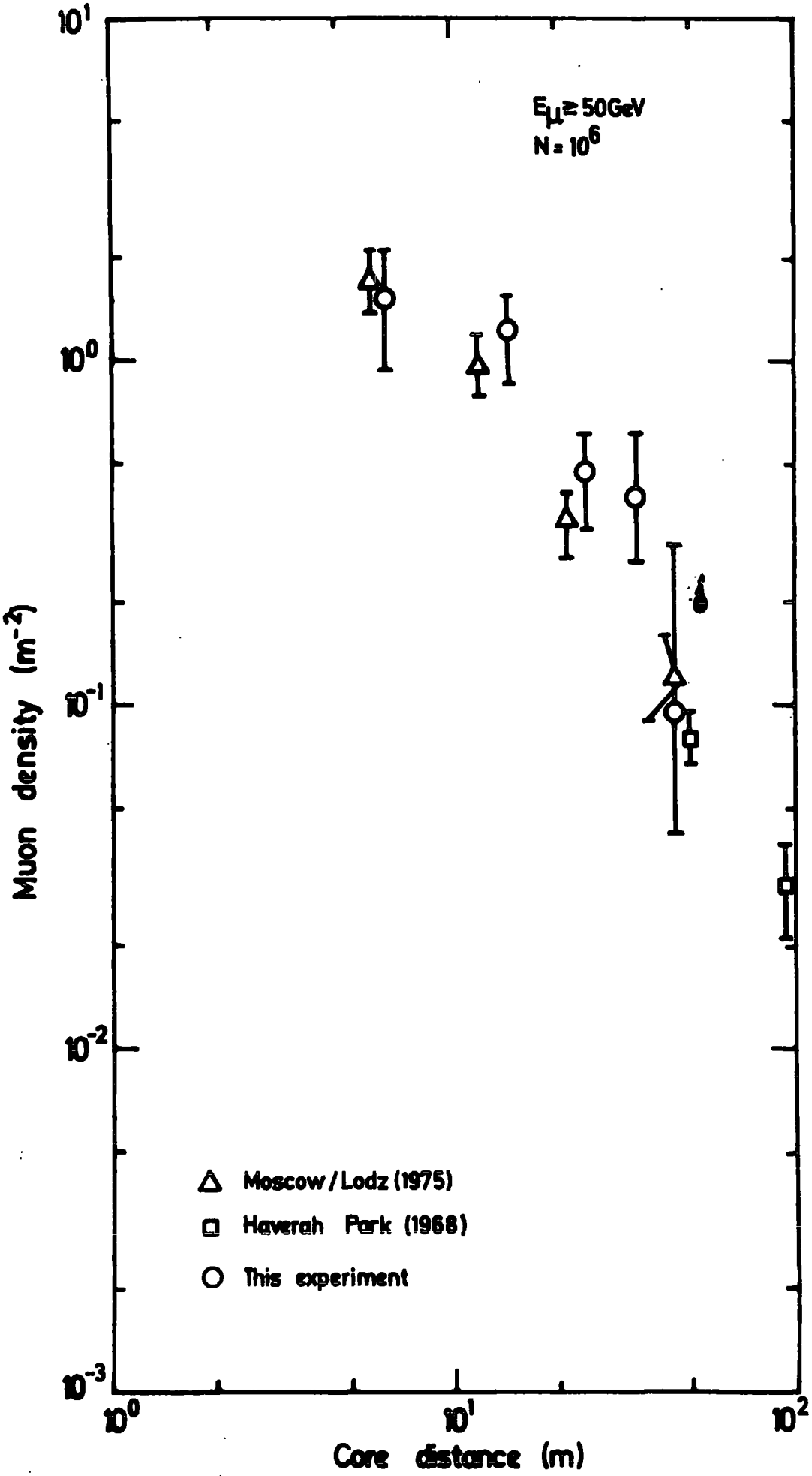

FIGURE 7.11 Comparison of the lateral distribution of muons ($E_\mu \geq 50$ GeV) with the measured distribution of the Moscow/Lodz collaboration (Rozhdestvensky et al, 1975) and the Haverah Park measurement (Orford, 1968). The present data and Haverah Park data are normalised to a shower size of 10^6 particles.

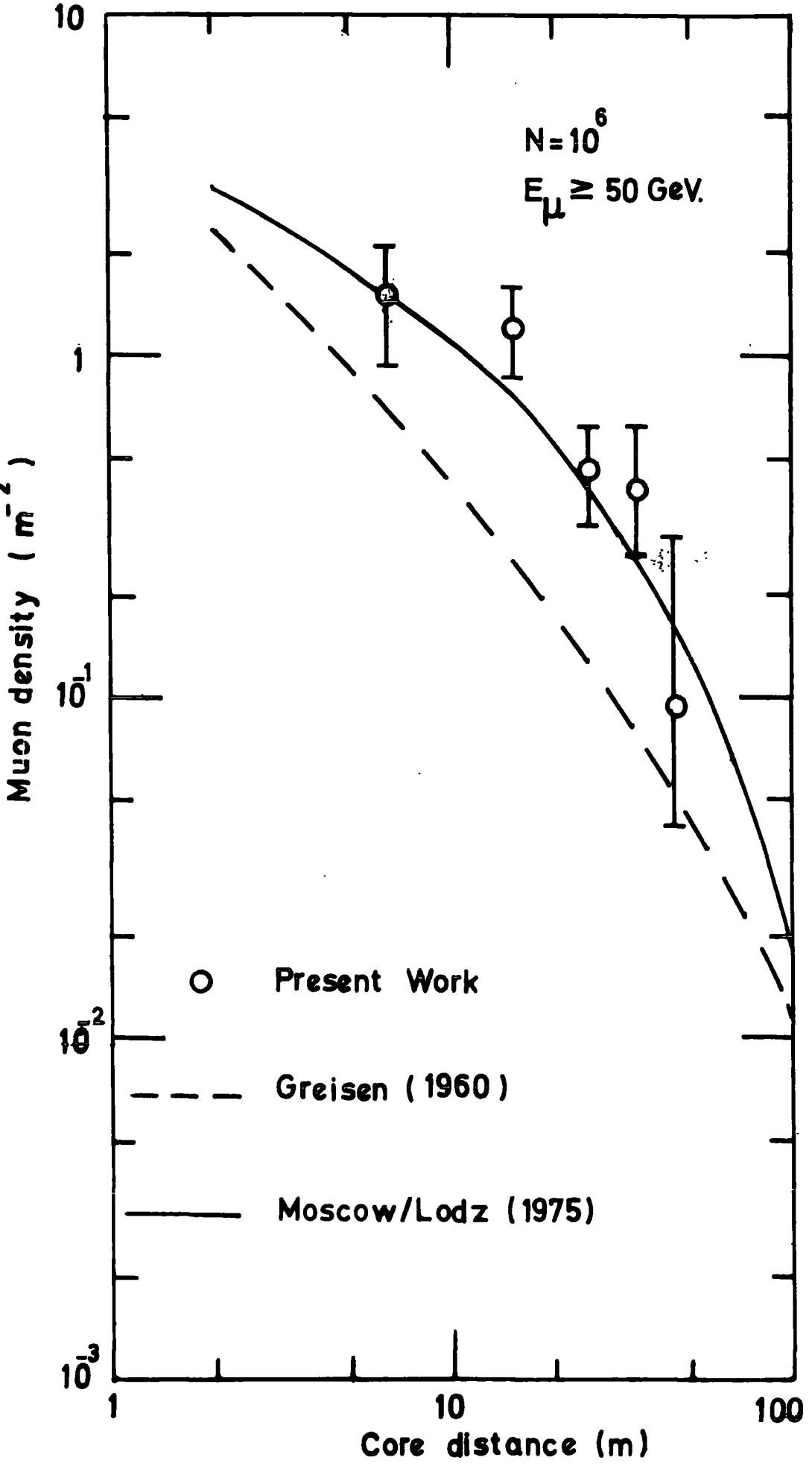

FIGURE 7.12 Comparison of lateral distribution of muons ($E_\mu \geq 50$ GeV) in showers of size 10^6 particles with the predictions of the Greisen's structure function extrapolated to $E_\mu \geq 50$ GeV, and the muon structure function fitted to the Moscow/Lodz data.

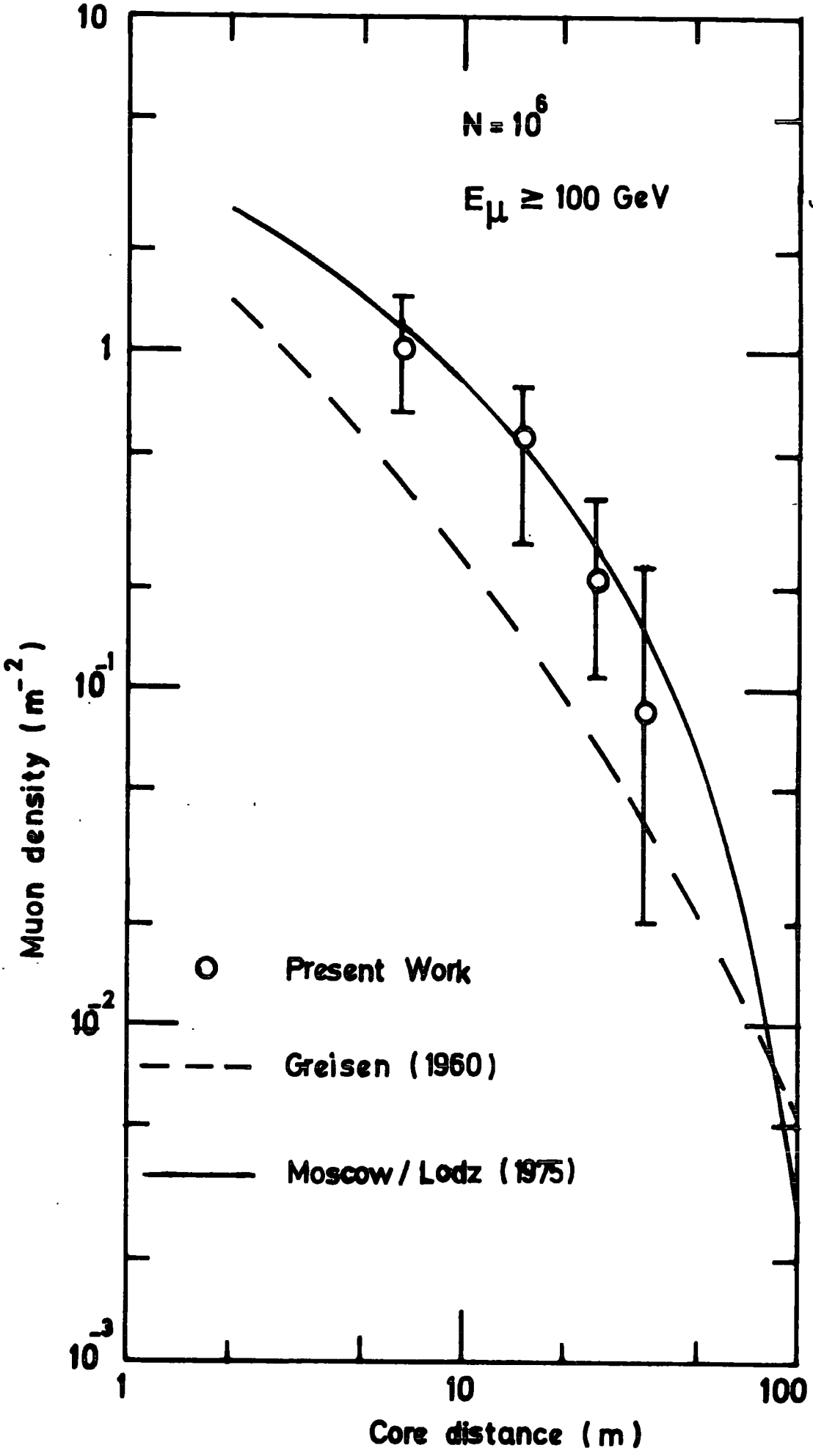

FIGURE 7.13 Comparison of the lateral distribution of muons ($E_\mu \geq 100$ GeV) in showers of size 10^6 particles with the extrapolations of the structure functions of Greisen (1960) and Moscow/Lodz collaboration, (Hawkes, 1977).

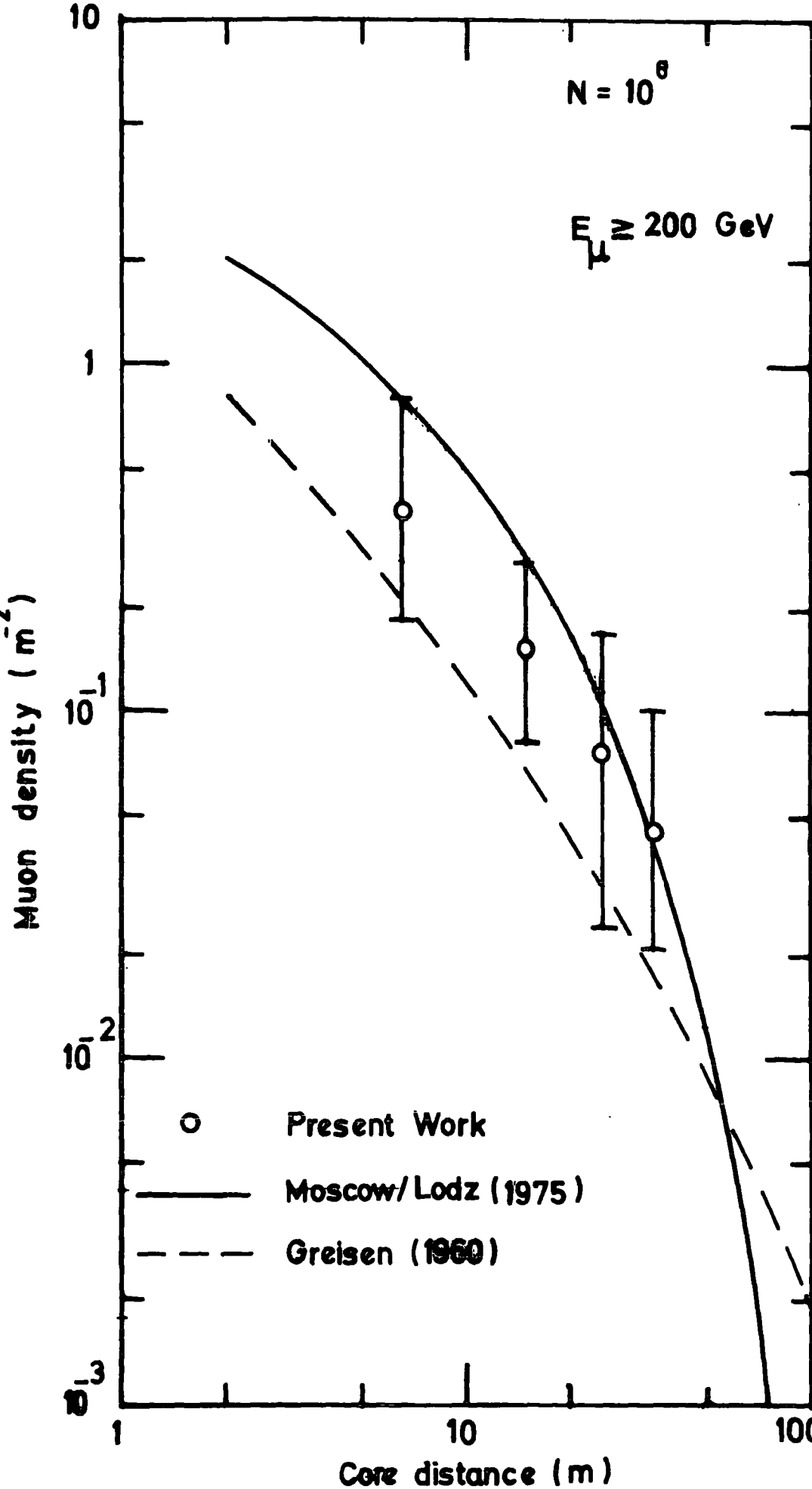

FIGURE 7.14 A comparison of the lateral distribution of muons ($E_\mu \geq 200$ GeV) with the predictions of the muons lateral structure functions of Greisen (1960) [4] and the Moscow/Lodz collaboration (Hawkes, 1977) extrapolated to $E_\mu \geq 200$ GeV.

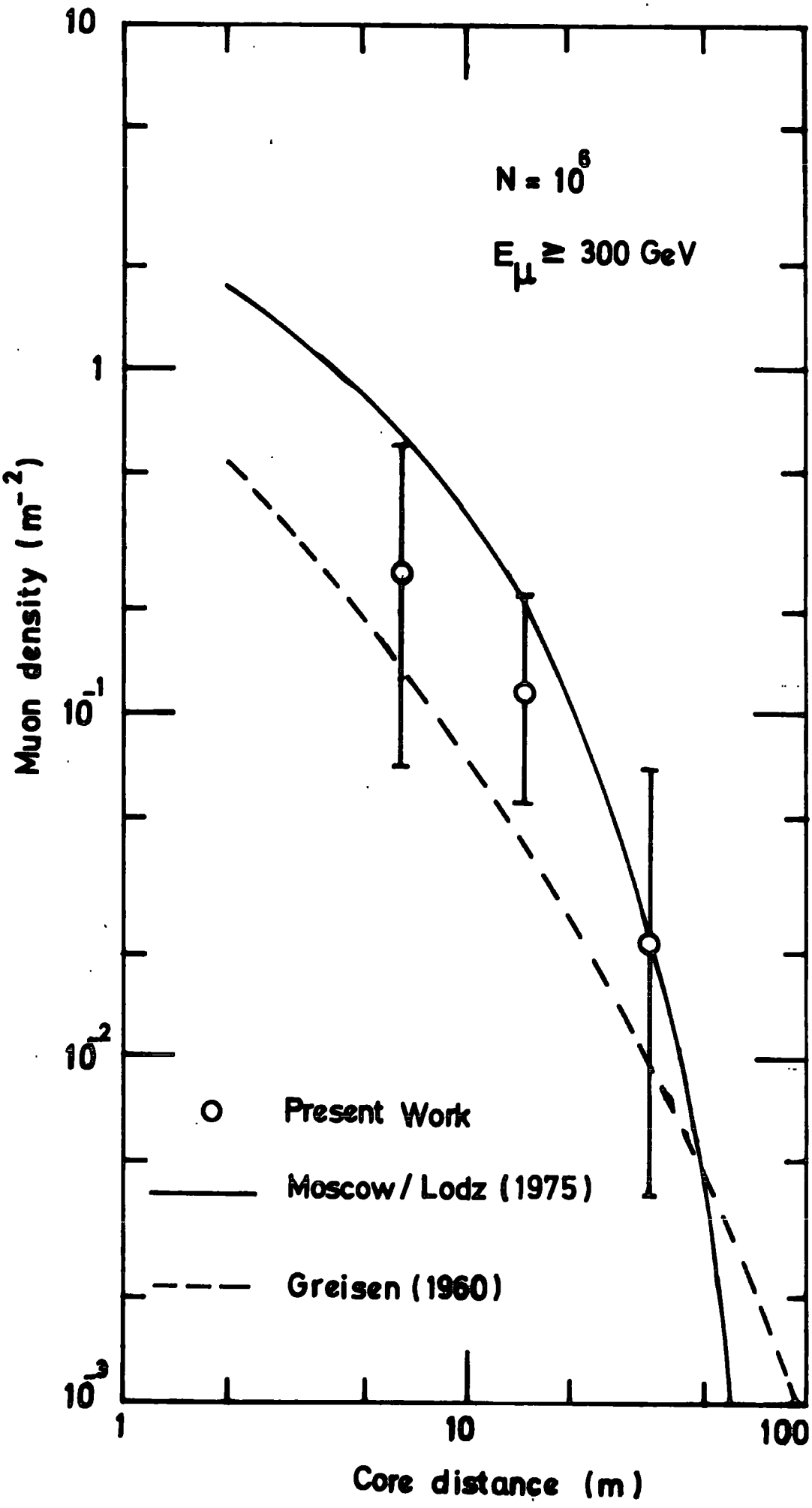

FIGURE 7.15 A comparison of the lateral distribution of muons having energies ≥300 GeV in showers of size 10^6 particles with the predictions of the muon structure function of Greisen (1960) and the Moscow/Lodz collaboration (Hawkes, 1977), both structure functions are extrapolated to $E_\mu \geq 300$ GeV.

where $A = 2.124 \times 10^{4}\ m^{-3/2}$, $B = -0.27$, $C = 3.74 \times 10^{13}\ m^{-2}$ $D = 0.56$, r is the core distance in meter and E_{μ} is the muon threshold energy in GeV. It is immediately clear from the comparison of both structure functions with the experimental results in Figures 7.12 and 7.13 that the Moscow/Lodz lateral structure function at muon threshold energies 50 and 100 GeV is a better fit to the present experimental results than the muon structure function due to Greisen. In order to get agreement between the present results and the muon density of the Greisen structure function the latter must be scaled up by a factor of 3. At higher muon threshold energies (200 and 300 GeV) the accuracy of the experimental data becomes poor such that it is difficult to tell which structure function better fits the data..

7.8 HIGH ENERGY INTERACTION MODELS AND PREDICTIONS OF MUON LATERAL DENSITY DISTRIBUTIONS

7.8.1 Introduction

Elementary particle interactions in E.A.S. are basically nucleon-nucleon and pion-nucleon interactions. Different models have been used to describe these interactions in this section. Three models of high energy nuclear collisions are used to compare the measured muon lateral distributions with model predictions, these models being the C.K.P. model (Cocconi,Koester and Perkins, 1961), the two-component cluster model (Grieder, 1977) and the scaling model (Feynman, 1969). The C.K.P. model predictions of the muon lateral distributions used are due to Olejniczak (1975), those of the two-component cluster model are due to Grieder (1977) while predictions of the muon lateral distributions using the scaling model have been derived by the author following the work of Hawkes (1977).

7.8.2 Similarities between Models

(1) The secondary particles are assumed to be mainly pions, there being on average, equal number of π^{+},π^{-} and π^{o}.

(2) The inelasticity for nucleon-nucleon collisions is 0.5 and assumed to be independent of energy and 1.0 for pion-nucleon collisions.

(3) The interaction mean free paths are taken as 80 gm/cm^2 and 120 gm/cm^2 for nucleon-nucleus and pion-nucleus collisions, respectively.

(4) The distribution of transverse momentum P_t, of the produced pions is given by the following expression suggested by the C.K.P. relation

$$f(P_t) = \frac{P_t}{P_o^2} \exp\left\{ - \frac{P_t}{P_o} \right\} \qquad (7.5)$$

The mean transverse momentum ($2P_o$) is assumed to be independent of energy and equal to 0.4 GeV/C.

The effect of leading particles and the differences between nucleon-nucleon and pion-nucleon interactions such as the productions of anti-nucleons and kaons is taken into account in the two-component cluster model as discussed later in this section.

7.8.3 The C.K.P. Model (Cocconi, Koester and Perkins, 1961)

This model is based on acceleration measurements of proton-light-nucleus interactions in the region of few tens of GeV. With allowance being made for pions in the backward cone, the energy distribution of emitted pions in the laboratory-system is given as follows :

$$S\left[E, E_o\right] = \frac{1}{2} \left\{ \frac{n(E_o)}{T} \exp - \frac{E_R}{T} + \frac{n(E_o)}{G} \exp - \frac{E_\pi}{G} \right\} \qquad (7.6)$$

where $n(E_o)$ is the forward multiplicity of pions produced, E_o being the transferred energy, G is the average energy of pions in the laboratory

system of the backward cone and

$$T = 2 \left\{ E_o - n(E_o) \frac{G}{2} \right\} \left\{ n(E_o) \right\}^{-1} \qquad (7.7)$$

is the average energy of pions emitted in the forward cone.

Pions emitted in the backward cone in the centre of mass system are not taken into account since they have low energies in the laboratory-system. The dependence of multiplicity of pions on primary energy E_p is given by $n_s \alpha E_p^{1/4}$ with E_p in GeV.

Some indications on the validity of this model at air shower energies are given in section 1.4.

The predictions of the lateral muon density distributions based on the C.K.P. model, and used for comparison with the present experimental data, are those due to the calculations of Olejniczak (1975) for proton initiated showers of a fixed size of 10^6 particles. These predictions are shown in Figure 7.16 - 7.19 for a multiplicity dependence of secondaries as $n_s \alpha E_p^{1/4}$ and $n_s \alpha E_p^{1/2}$, respectively, and selected for the four muon energy thresholds ($\geq 50, \geq 100, \geq 200$ and ≥ 300 GeV) that are used in this work.

7.8.4 The Scaling Model (Feynman, 1969)

This model is exhibited by the inclusive proton-proton interactions at the CERN ISR (Intersecting storage rings) energies. The effect of intra-nuclear cascading is not taken into account. The scaling model is characterised by a multiplicity of produced particles which grows logarithmically with energy in hadron-hadron collisions. The model can be described by the differential cross-section in the Lorentz-differential form as follows :

$$E \frac{d^2\sigma}{d(P_t)dP_L} = \frac{d^2\sigma}{d(P_t)dy} = F(X, P_t^2) \qquad (7.8)$$

where X is the Feynman factor which is defined as

$$X = \frac{2 P_L}{S^{\frac{1}{2}}} = \frac{2 m_t \sinh(y)}{S^{\frac{1}{2}}}$$

where P_t and P_L are the centre of mass transverse and longitudinal momenta of the produced particles respectively. The rapidity y is defined as

$$y = \log \left[(E + P_L) \Big/ m_t \right] ,$$

m_t is the transverse mass, $m_t^2 = m_\pi^2 + P_t^2$ and S is the centre of mass energy squared.

This model encounters serious difficulties in connection with air shower simulations, in particular it cannot account for the large number of muons observed in EAS. Also, showers predicted using this model develop late and reach their maxima at an altitude which is too low in comparison with the observations. The main reason for the large discrepancies experienced with calculations using the scaling model lies not only in employing different multiplicity dependence in comparison to other models, but also in the flat rapidity distribution of secondaries emerging from high energy interactions that are exhibited by the scaling model. Several authors (for example (Gaisser and Maurer, 1972) and Fishbane et al 1974) have concluded from such discrepancies that Feynman scaling fails at EAS energies. In order to save the situation, Fishbane et al, (1974) have suggested the following assumptions in conjunction with the scaling hypothesis which can reproduce acceptable air shower particle spectra, These assumptions are:

(1) - Intranuclear cascading

(2) - Rising cross section at very high energies

(3) - Heavy primaries.

Very recently, Olejniczak et al (1977) have examined a variety of cosmic ray data in order to draw some conclusions on the primary spectrum and nature of high energy collisions. They have confirmed that if the primaries are mainly protons then the scaling model, in very high energy collisions, is very unlikely to be valid.

Predictions of the lateral density distributions of muons based on the scaling model have been obtained following the method of Hawkes (1977). In this method the muon lateral distributions have been calculated for primary protons initiated showers as given by Goned (1975). The same method has been used to predict the muon lateral distribution due to iron primaries using the superposition method in which a primary nucleus of a given total energy E and a mass number A can be thought of as A particles of energy E/A whose individual showers are therefore less energetic and develop faster. The predicted muon lateral distributions for protons and iron primaries are shown in Figures 7.16 - 7.19 where they are compared with experimental measurements at various muon energy thresholds.

7.8.5 The Two Component Cluster Model

This model includes two distinct clustering processes being isobar and fireballs (or fragmentation and pionization). The isobar or fragmentation process has a very limited energy dependence and contributes a small number of secondaries that are fast in the centre of mass. The fireballs or pionization region is more energy dependent and responsible for the majority of the particles produced in very high energy collisions. The fraction of the total centre of mass energy given to the fireball component is described by an approximated Gaussian distribution, whose mean value is an energy independent parameter (Grieder, 1977). This fraction of energy is the total energy of one or more fireballs in the centre of mass. Details and kinematical treatment of this model and its modified versions is given by Grieder (1975) and Grieder (1977). In general the gross features of the

model are similar to the C.K.P. formula except that the production of kaons and nucleon-anti-nucleon pairs have been added to a pure pion production and also the effects of leading particles are taken into account. Applications of this model in the work presented in this chapter lies in the predictions of the lateral density distributions of high energy muons. These are shown in Figures 7.16 - 7.19 where the muon lateral distributions as predicted by the so called SMFB model (slow multiple fireball) is compared with experimental results. This model is a modified version of the two component cluster model for protons and iron initiated showers respectively. In such a version the energy is assumed to be shared among two or more fireballs and each share is divided into kinetic and mass portions. The multiplicity is dominated by the fireball component at high energy and was chosen such that

$$n_s \alpha S^{0.4375} \qquad (7.9)$$

where S stands for the centre of mass energy squared.

7.9 COMPARISON WITH THE PREDICTIONS OF HIGH ENERGY INTERACTION MODELS

The importance of high energy nuclear model calculations is to show evidence of the effects of primary mass composition and the nature of high energy collisions on the measured shower parameters. It is always difficult to make statements on the primary mass composition and the nature of high energy interactions because both of them are subject to great uncertainty and several interpretations could be possible from the experimental data by a reasonable adjustment of one of the model variables which can account for any discrepancies between the calculated and observed data. Thus, the present comparison is not expected to give a firm conclusion.

The present experimental results on the lateral density distribution of muons above four threshold energies (50, 100, 200 and 300 GeV) are shown in Figures 7.16, 7.17, 7.18 and 7.19. Muon densities in all the figures have been scaled to a common shower size of 10^6 particles as explained earlier in section 7.6. Also shown in the figures are the theoretical predictions of the high energy interaction models described in section 7.6. Predictions of both scaling and the SMFB models are given for certain fixed primary energies (see Table 7.2), but indirect comparison of the experimental results with these two models only is possible. Converting the primary energies to equivalent shower sizes is somewhat of a problem since the $N_e - E_p$ relationship is uncertain and model dependent. Direct comparison of experimental results with the predictions of the C.K.P. model can be achieved since the calculations of Olejniczak (1975) were performed for a shower of a fixed size of 10^6 particles. Table 7.2 shows the values of shower sizes obtained for the converted primary energies used in both scaling and the SMFB models for protons and iron primary initiated showers. The $N_e - E_p$ relationship used for scaling model is that obtained by Hawkes (1977) as follows

$$N_e = 6.66 \times 10^{-2} \left\{ E_{p,} \right\}^{1.125} \qquad (7.10)$$

E_p being measured in GeV.

This relationship is obtained for proton primaries, constant cross-section and no intranuclear cascading. For iron primaries and the same conditions the $N_e - E_p$ relationship can be derived from equation 7.10 according to the principle of superposition of heavy primaries, and is

$$N_e = 6.66 \times 10^{-2} \times A \times \left\{ E_{p/A} \right\}^{1.125} . \qquad (7.11)$$

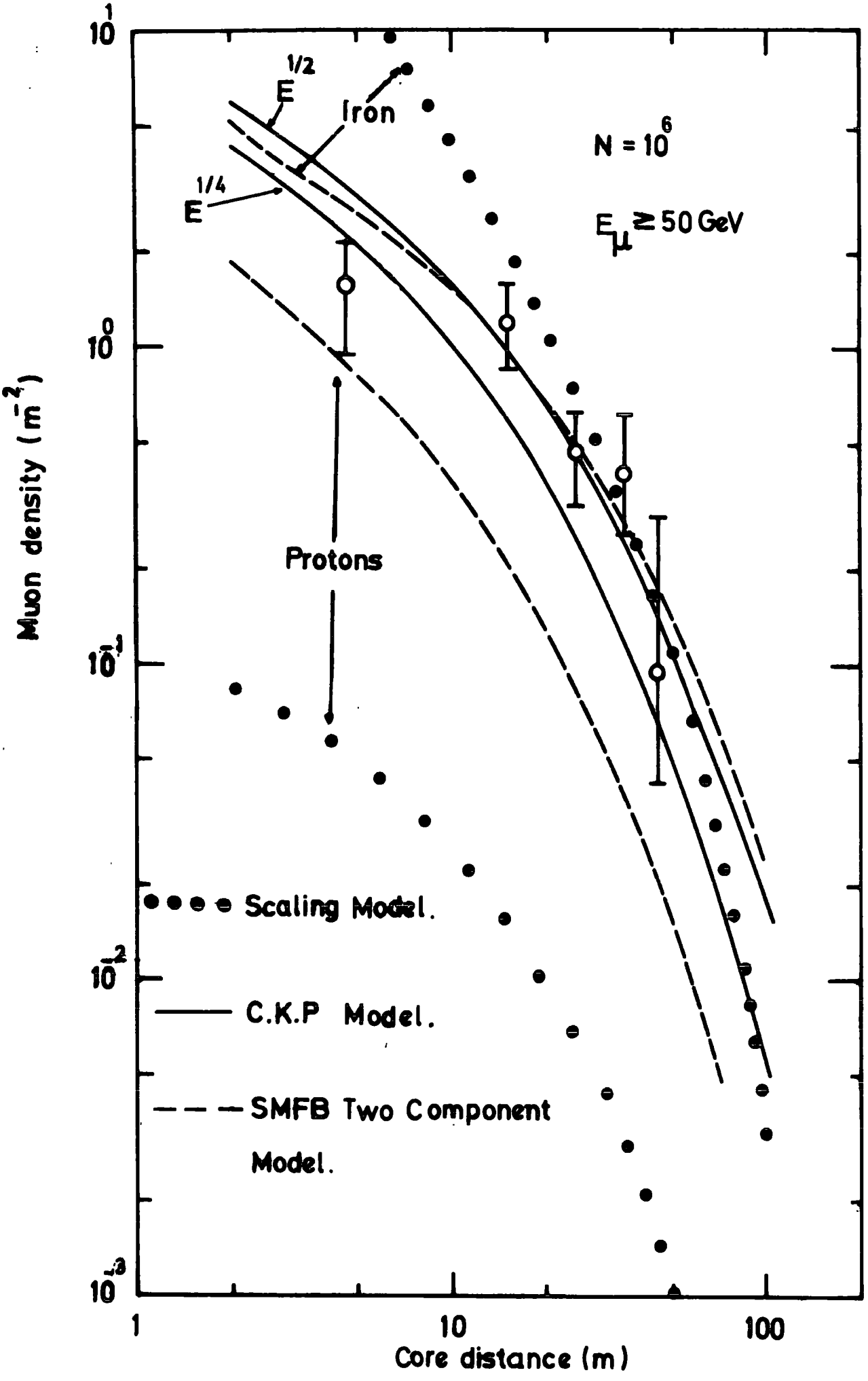

FIGURE 7.16 (See caption overleaf)

FIGURE 7.16 A comparison of lateral distribution of muons ($E_\mu \geq$ 50 GeV) in showers of size 10^6 particles with the predictions of the C.K.P. model (Olejniczak, 1975), the Scaling Model and the SMFB Two Component Model (Grieder, 1977). The former model is for proton primaries and mean multiplicity dependence of $E^{\frac{1}{4}}$ and $E^{\frac{1}{2}}$ while the two latter models are predicted for the case of protons and iron primaries.

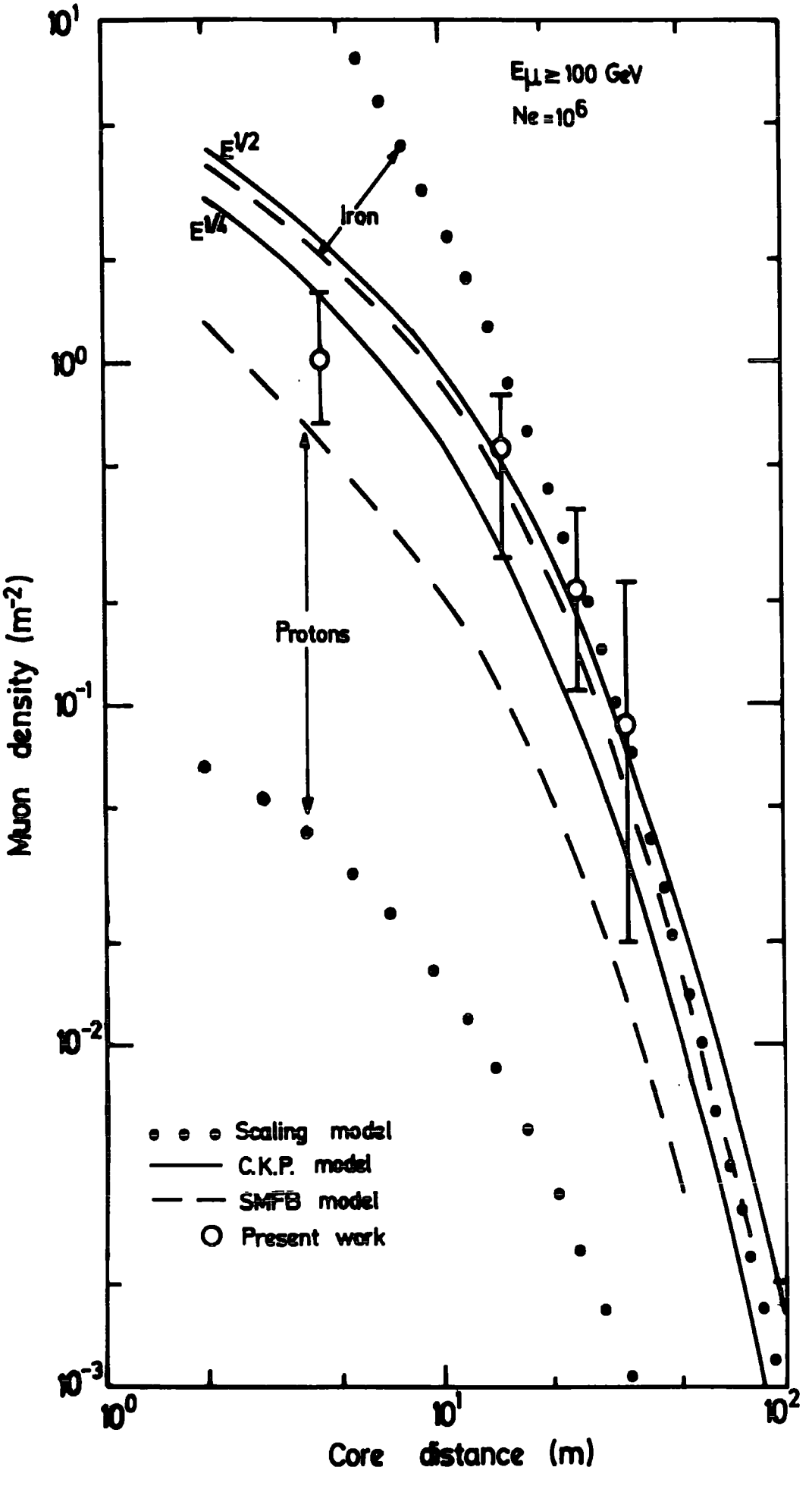

FIGURE 7.17 (See caption overleaf)

FIGURE 7.17 A comparison of lateral distribution of muons ($E_\mu \geq 100$ GeV) in showers of size 10^6 particles with the predictions of the C.K.P. model (Olejniczak, 1975), the Scaling Model and the SMFB Two Component Model (Grieder, 1977). The former model is for proton primaries and mean multiplicity dependence of $E^{\frac{1}{4}}$ and $E^{\frac{1}{2}}$ while the two latter models are predicted for the case of protons and iron primaries.

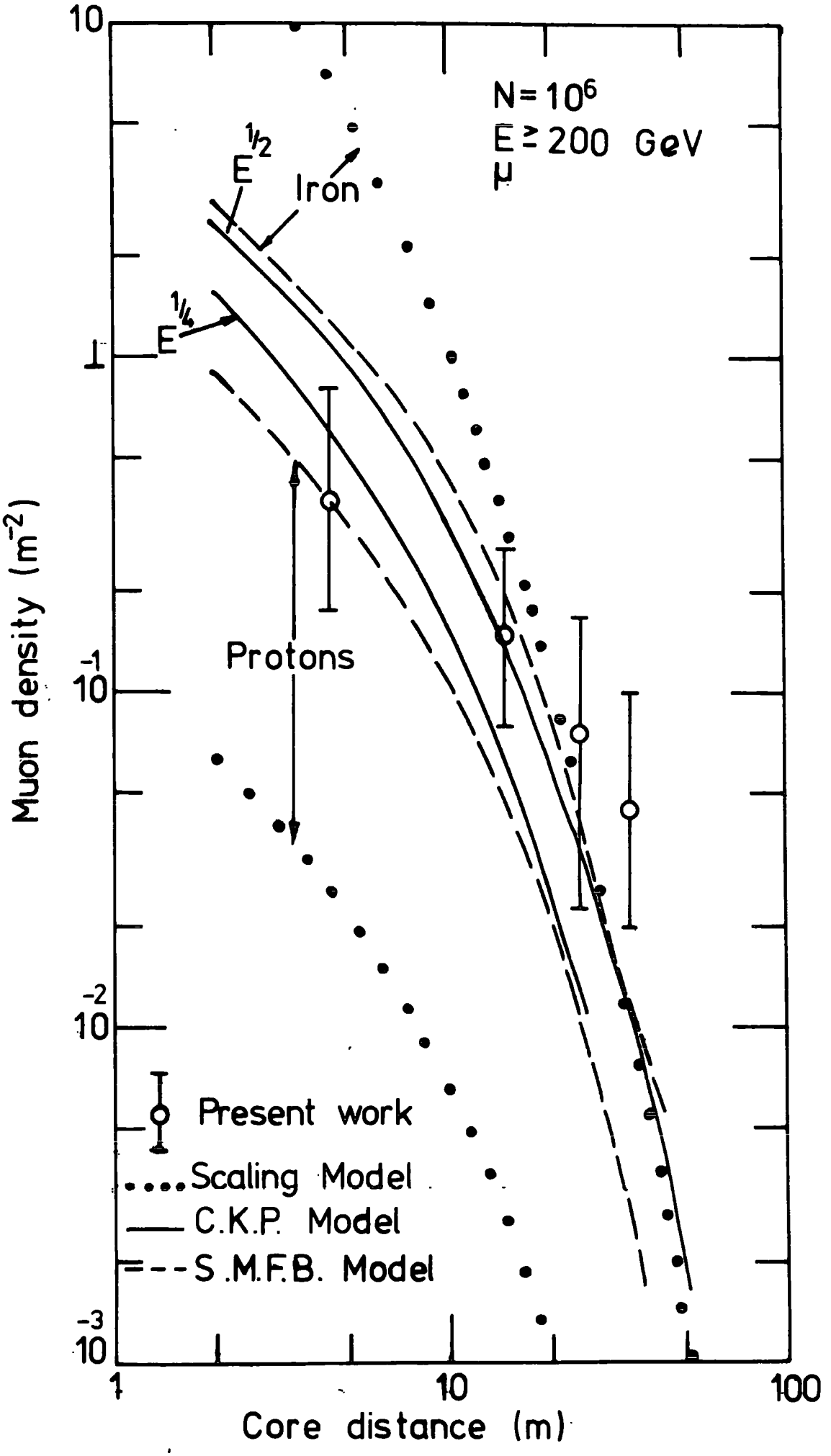

FIGURE 7.18 (See caption overleaf)

FIGURE 7.18 A comparison of lateral distribution of muons ($E_\mu \geq 200$ GeV) in showers of size 10^6 particles with the predictions of the C.K.P. model (Olejniczak, 1975), the Scaling Model and the SMFB Two Component Model (Grieder, 1977). The former model is for proton primaries and mean multiplicity dependence of $E^{\frac{1}{4}}$ and $E^{\frac{1}{2}}$ while the two latter models are predicted for the case of protons and iron primaries.

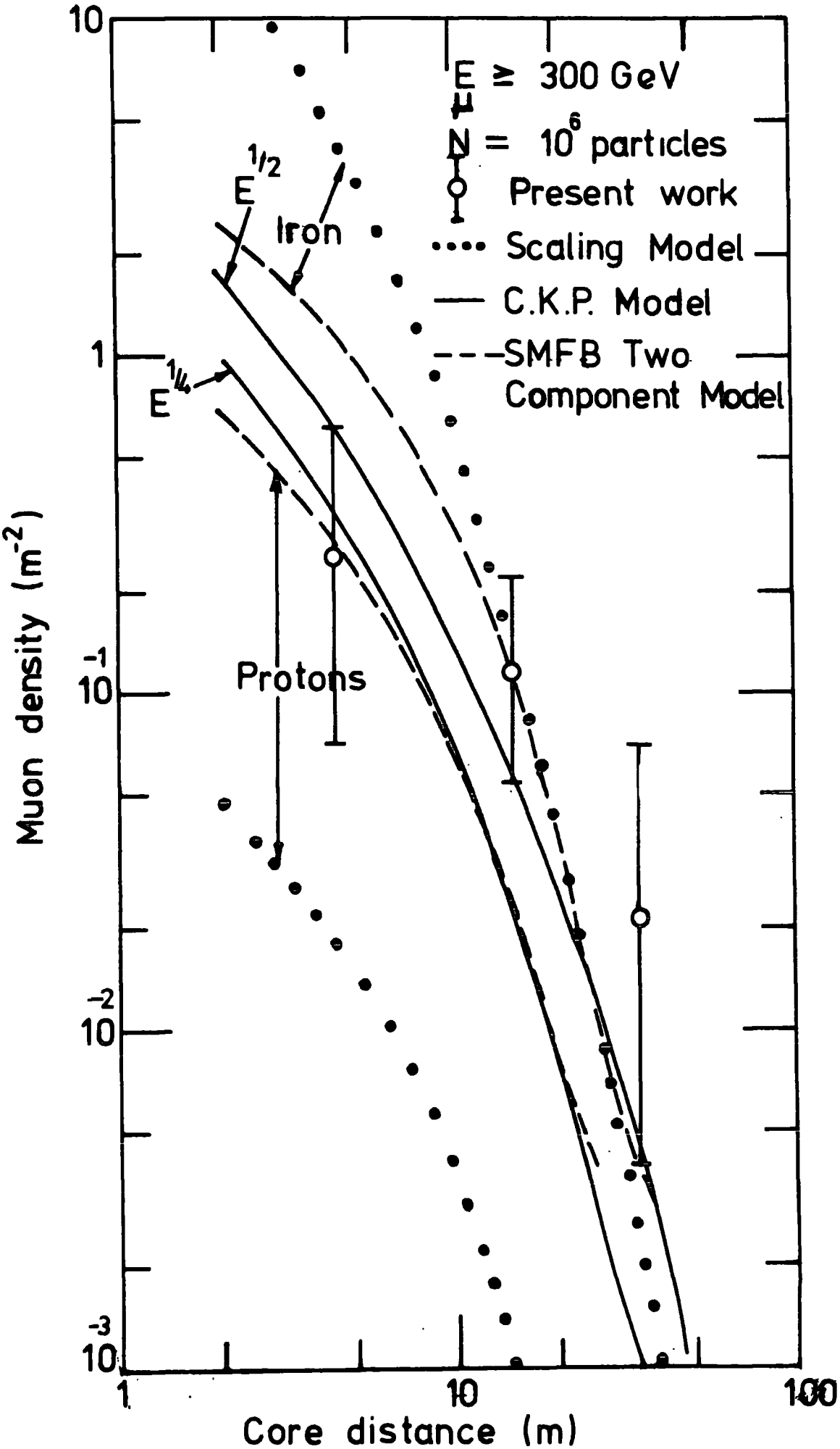

FIGURE 7.19 (See caption overleaf)

FIGURE 7.19 A comparison of lateral distribution of muons ($E_\mu \geq$ 300 GeV) in showers of size 10^6 particles with the predictions of the C.K.P. model (Olejniczak, 1975), the Scaling Model and the SMFB Two Component Model (Grieder, 1977). The former model is for proton primaries and mean multiplicity dependence of $E^{\frac{1}{4}}$ and $E^{\frac{1}{2}}$ while the two latter models are predicted for the case of protons and iron primaries.

	Protons		Iron	
	E_p (GeV)	N_e	E_p (GeV)	N_e
SMFB Model	10^6	1.3×10^5	10^6	4×10^4
Scaling Model	2×10^6	8.17×10^5	5×10^6	1.38×10^6

TABLE 7.2 : The E_p-N_e conversion values for protons and iron initiated showers as given for a fixed primary energy per nucleus in the scaling model and the SMFB Model.

For iron primaries the above equations becomes

$$N_e = 4.03 \times 10^{13} \left(E_p\right)^{1.125}, \qquad (7.12)$$

E_p being measured in GeV in equations 7.12 and 7.13.

For the case of the SMFB model the $N_e - E_p$ conversion was obtained from the survey of figure 2, and the work of Turner (1969).

Before any conclusions are drawn from the present comparison, the accuracy of the experimental data must be taken into consideration. There are two major sources of error which affect the comparison,

(1) large statistical errors on the estimated muon densities.

(2) uncertainty in the location of the shower cores.

The former effect can only change the absolute values of the densities but the latter can effect the shape of the lateral distribution of muons at small distances ($\leq$10 meters from the shower axis). Thus an appropriate correction to the mean radial distance at less than 10 meters from the shower axis has been applied to all the experimental densities. Inspection of Figures 7.16, 7.17, 7.18 and 7.19 show that for most of the muon threshold energies considered the predicted distributions are in a reasonable agreement with the experimental observations. Considering the situation where the C.K.P. model is used, it is clear that within statistical limits good agreement is found between the experimental data and the model predictions for an $E^{\frac{1}{4}}$ multiplicity dependence. However, a better agreement with the $E^{\frac{1}{2}}$ multiplicity can be seen through all the four muon distributions. Thus, the data give a slight suggestion of an increase in multiplicity over that of an $E_p^{\frac{1}{4}}$ law at energies of the order of few x 10^{15} eV. Comparing the experimental results with the predictions of the SMFB two component model, it is clear from Figures 7.16 and 7.17 that the present experimental data, does not support the view that the primaries are protons but rather suggest

a pure iron composition. A similar view point is illustrated when comparing the scaling predictions and iron primaries in which an agreement with the data for all different muon threshold energies is obtained at core distances larger than 15 metres. At distances smaller than 15 m from the shower axis the scaling model predicts higher numbers of muon than experimentally observed. It is clear that the experimental data for the four muon threshold energies are greatly higher than the predictions of the scaling model and primary protons (constant proton-proton cross-section and no intranuclear cascading are assumed). The discrepancy between observed and predicted distributions is a factor of ~ 70 over the whole range of radial distances and various muon threshold energies the experimental data does not support Feynman Scaling and protons at E.A.S. energies.

7.10 CONCLUSIONS

The results presented in this experiment represent only preliminary measurements. As a result of the present work the measurements of the lateral density distribution of muons have been extended to higher muon threshold energies ($\geq$100, $\geq$ 200 and $\geq$300 GeV) than that obtained by the Haverah Park and the Moscow/Lodz experiments and are now known to a limited degree of accuracy.

The measured lateral density distribution of muons with energies not less than 50 GeV has been found to be in good agreement with the measurement of the Moscow/Lodz collaboration in both shape and absolute value of the distribution over the radial distance range 5 - 50 metres from the shower axis. No contradiction has been found when the same measurements are compared with the results of the Haverah Park group at larger radial distance (50 - 100 metres). Furthermore the data at muon energies $\geq$50 and 100 GeV do not confirm the extrapolation of Greisen's

structure function but do agree well with the predictions of the lateral structure expression of muon based on the Moscow/Lodz results when extrapolated to the higher muon threshold energies used in this experiment. The experimental data presented in this experiment has been considered in terms of the predictions of three different models of high energy collisions. A satisfactory agreement with the C.K.P. model is found, but the experimental data are insensitive to either form of multiplicity dependence ($E^{\frac{1}{4}}$, $E^{\frac{1}{2}}$) of secondaries as suggested by the model. The further general alternative conclusion that can be drawn from the data is that agreement is found with the hypothesis of iron primaries together with the prediction of the scaling and the SMFB two-component models. Thus, the results give an evidence for heavy primaries at energies of the order 5×10^{15} eV. It seems clear that the predictions of the scaling model and an assumed primary proton spectra is inconsistent with the observation over the whole radial distances and different muon threshold energies used in this work.

7.11 FUTURE WORK

Because of the non-interacting properties of muons, it is expected that the total number of muons in a shower and the form of the muon lateral distributions and energy spectra will be largely influenced by the parameters that characterize the first interaction. In future experiments linking MARS and the EAS array, the validity of the interpretations of the present experimental results can be established by increasing the number of muon air shower events. In order to carry out crucial and decisive examinations on high energy interaction models and primary mass composition, it is

necessary to obtain measurements of muon spectra and lateral distributions at ultra high energies ; this fact has also been emphasized by many workers (e.g. Grieder, 1977). However, future experiments incorporating MARS and the array may provide many important measurements of the muon component at distances less than 50 m from the shower axis. Measurements such as the charge ratio of E.A.S. muons at high energies, the height of origin of the muons, the dependence of N_μ on N_e, the correlation between the mean radius and threshold energies of muons in individual showers, and the dependence of muon energy spectra and lateral distributions on showers age parameter, can all furnish useful information on the nature of mass composition of the primary cosmic ray spectrum and the kinematic and dynamic features of ultra-high energy interactions. Very recently, eight liquid scintillator detectors have been located in the vicinity of the spectrograph which will increase the accuracy of determination of the shower core as well as extending the shower sizes detected down to a few x 10^4 particles with a reasonable detection efficiency.

APPENDIX 1

CALCULATION OF THE EXPONENT OF THE ANGULAR VARIATION OF COSMIC RAY INTENSITY

The expected exponent m of the zenith angular distribution of all showers recorded at sea level by the apparatus described in Chapter 3 can be obtained from the total observed rate of showers and the knowledge of the intensity of showers incident on this particular experimental set up. By assuming the zenith angle distribution of showers to be of the following form :

$$I(\theta) = I(0) \cos^{m}\theta \quad m^{-2} \sec^{-1} st^{-1} \qquad \text{(A1.1)}$$

where $I(\theta)$ is the intensity of showers incident at an angle θ to the zenith and $I(0)$ is the intensity of showers in the vertical direction. The relationship between $I(\theta)$ and $I(0)$ is shown in figure A1.1 by the spherical co-ordinate system. It follows from the figure that the total number of showers per unit time expected from a small element of solid angle $d\Omega$ (expressed in steradians) is given by $I(\theta)\, d\Omega$. Thus,

$$I_T = \int_{\text{all solid angles}} I(\theta)\, d\Omega \qquad \text{(A1.2)}$$

From figure A1.1, the solid angle ($d\Omega$) subtended by an area dA at O is

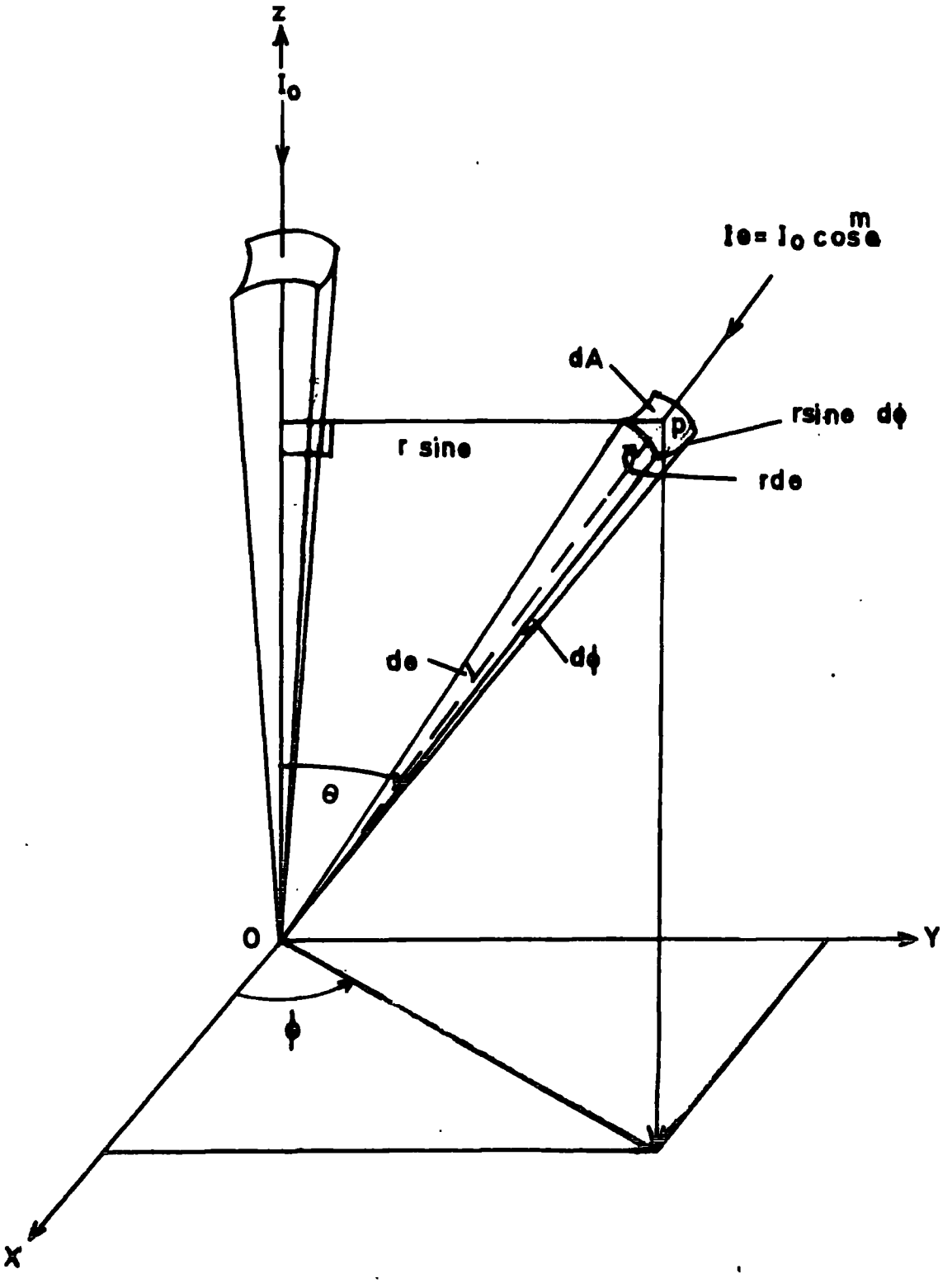

FIGURE A1.1 The spherical co-ordinate system used to represent the angular variation of cosmic ray intensity : θ and ϕ represent the direction of the incident flux in the atmosphere from the origin O and X, Y and Z represent the co-ordinate system axes.

$$d\Omega = \frac{dA}{r^2}$$

$$= \frac{rd\theta r\sin\theta d\phi}{r^2}$$

$$= \sin\theta d\theta d\phi \qquad \text{(A1.3)}$$

Thus

$$I_T = \int_{\phi} d\phi \int_{\theta} I(\theta) \sin\theta d\theta$$

By integrating over all azimuthal and zenith angles the total intensity of air showers can be written as follows :

$$I_T = \int_{o}^{2\pi} d\phi \int_{o}^{\pi/2} I(\theta) \sin\theta d\theta$$

By substituting $I(\theta)$ in equation A1.1, it follows that

$$I_T = 2\pi \int_{o}^{\pi/2} I(O) \cos^{m}\theta \; d(\cos\theta)$$

by solving this integral for the limits of the value of θ, the total cosmic ray intensity becomes

$$I_T = (\sec^{-1}) = \frac{2\pi}{m+1} \; (sr) \times I(O) \; (\sec^{-1} sr^{-1})$$

the term $\frac{2\pi}{m+1}$ is a solid angle term in units of steradians. If I_T

represents the total observed rate of recording air showers per second and I (O) is the calculated vertical intensity of air showers in sec^{-1} st^{-1} (obtained from relation 4.22 after performing the integration over all the sensitive collecting area of the array), then the value of m can be obtained as :

$$m = 2\pi \frac{I(O)}{I_T} - 1. \qquad \text{(A1.4)}$$

This is an indirect estimate of the exponent of the angular variations of air shower particles without the knowledge of the showers incident direction.

REFERENCES

PICCR ≡

PROCEEDINGS OF THE INTERNATIONAL

CONFERENCE ON COSMIC RAYS

ABROSIMOV, A.T., et al, 1974, Izv. Akad. Nauk USSR, Ser.Fiz. Vol., 38, No. 5, 1104.

ADCOCK, C, et al, 1968, J. Phys. A., 1, 82.

ADCOCK, C, et al, 1970, J. Phys. A., 3, 697.

ADCOCK, C, 1971, Ph.D. Thesis, University of Durham.

ADCOCK, C, et al, 1971, J. Phys. A, 4, 276.

ALEXANDER, D, 1968, Ph.D. Thesis, University of Durham.

ASEIKIN, V.S., et al, 1971, PICCR, Hobart, 6, 2152.

ASHTON, F., et al, 1973, PICCR, Denver, 4, 2489.

ASHTON, F,, et al, 1975, PICCR, Munich, 8, 2831.

AUGER, P, et al, 1939, See Wei, J., and Montgomery, G., G., 1949.

AYRE, C.A., and THOMPSON, M.G., 1969, Nucl. Inst. and Meth., 69, 106.

AYRE, C.A., et al, 1969, PICCR, Budapest, 4, 541.

AYRE, C.A., 1971, Ph.D. Thesis, University of Durham.

AYRE, C.A., et al, 1972, Nucl. Inst. and Methods, 102, 29.

BALASUBRAHMANIAN, V.K., and ORMES, J.F., 1973, Nature, 241, 95.

BARNABY, C.F., and BARTON, J.C., 1960, Proc. Phys. Soc., 76, 745.

BELL, C.J., et al., 1974, J. Phys. A., 7, 990.

BELL, M.C., 1974, Ph.D. Thesis, University of Durham.

BENNETT, S., and GREISEN, K., 1961, Phys. Rev., 124, 1982.

BENNETT, S., et al, 1962, J. Phys. Soc. Japan, 17, A3, 196.

BERENZINSKY, V.S., and ZATSEPIN, G.T., 1969, Phys. Let t., 28B, 423.

BERENZINSKY, V.S., and ZATSEPIN, G.T., 1971, Sov. J. Nucl. Phys., 13, 453.

BERGESON, H.E., et al, 1975, Phys. Rev. Lett., 35, 681.

BRADT, H., et al., 1965, PICCR, London, 2, 715.

BROADBENT, D., et al, 1950, Proc. Phys. Soc., A63, 864.

BROWNLEE, R.G., et al., 1970, PICCR, Budapest, 3, 377.

BURGER, J. et al., 1975, PICCR, Munich, 8, 2784.

CANNON, T. M., et al, 1971, J. Phys. A, 4, 266.

CATZ, Ph., et al, 1975, PICCR, Munich, 12, 4329.

CHATTERJEE, B.K., et al, 1968, Canad. J. Phys., 46, S13.

CHATTERJEE, B.K., 1965, PICCR, London, 2, 627.

CLARK, G., et al, 1958, Suppl. Nuovo Cim., 8, 628.

COCCONI, G., KOESTER, L.J., and PERKINS, D.H., 1961, Lawrence Radiation Lab. High Energy Physics Study Seminars, No. 28, 2.

COCCONI, G., Cocconi-Tongiorgi, V., 1949, Phys., Rev., 75, 1058.

COCCONI, G., 1961, Handbuch der Physik, Vol. 46/1., Springer-Verlag, Berlin, 215.

DAKE, S., et al, 1971, PICCR, Hobart, 3, 948.

DE BEER, J.F, et al, 1966, Proc.Phys. Soc., 89, 567.

DE BEER, J.F, et al, 1968, J. Phys. A, 1, 72.

DE BEER, J.F, et al, 1969, J. Phys. A, 2, 354.

DE BEER, J.F, et al, 1962, Phil. Mag., 7, 499.

DIXON, H.E., 1973, Ph.D. Thesis, University of Durham.

DIXON, H.E., and TURVER, K.E., 1974, Proc. Roy.Soc., London, A., 339, 171.

DIXON, H.E.,et al, 1973, PICCR, Denver, 4, 2473.

DZIKOWSKI, T.R., et al, 1975, PICCR, Munich, 8, 2795.

EARNSHAW, J.C., et al, 1973, J. Phys. A., 6, 1244

EARNSHAW, J.C., et al, 1967, Proc. Phys. Soc., 90, 91.

EDGE, D.M, et al, 1973, J. Phys. A., 6, 1612.

FEYNMAN, R.P., 1969, Phys. Rev., Lett., 23, 1415.

FISHBANE, P.M., et al, 1974, Phys. Rev. D.9, 11, 3083.

FOWLER, W.A., 1975, PICCR, Munich, 11, 3550.

GALIBRAITH, W., 1958, Extensive Air Showers, Butterworth Scientific Publications.

GAISSER, T.K., and MAURER, R.H., 1972, Phys. Lett., 42B, 4, 444.

GAISSER, T.K., 1974, Nature, 248, 122.

GEMESY, T., et al, 1964, Nucleonika, 9, 365.

GONED, A., 1975, Il, Nuovo, Cim., 29A, 3, 301.

GREIDER, P.K.F., 1973, PICCR, Denver, 4, 2467.

GREIDER, P.K.F., 1975, PICCR, Munich, 8, 2889.

GREIDER, P.K.F., 1977, Nuovo Cim., 7, Ser.2, No.1, 1

GREIDER, P.K.F., 1970, Acta Phys. Hung., 29, Suppl. 3, 563.

GREIDER, P.K.F., 1971, PICCR, Hobart, 3, 976.

GREISEN, K., 1956, Progress in Cosmic Ray Physics, III, 1

GREISEN, K., 1966, Phys. Rev., Lett., 16, 748.

GREISEN, K., 1960, Annual Review of Nuclear Science, 10, 63.

GRIGOROV, N.L., et al, 1971, PICCR, Hobart, 3, 970.

GUSEVA, U.V., et al, 1962, PICCR, Koyoto, 3, 375.

HALZEN, F., and GAISSER, T.K., 1975, PICCR, Munich, 7, 2216.

HANSEN, S., 1975, Ph.D. Thesis, University of Durham.

HASEGAWA, H., et al, 1966, Piccr, London, 2, 642.

HASEGAWA, H., et al, 1962, J. Phys. Soc. Japan, 17, Suppl. A3, 86.

HAWKES, R.C., 1977, Ph. D. Thesis, University of Durham.

HAWKES, R.C., et al, to appear in PICCR,Plovdiv.

HAYAKAWA, S., 1969, Cosmic Ray Physics, (Wiley-Interscience), 299.

HAZEN, W.E., et al, 1973, PICCR, Denver, 3, 2087.

HILLAS, A.M., 1966, PICCR, London, 2, 758.

HILLAS, A.M., 1970, PICCR, Budapest, 3, 355.

HUME, C.,1975, Ph.D. Thesis, University of Durham.

JACOB, M., 1973, See Wdowczyk, J., and Wolfendale, A.W., 1973.

JAMES, F., and ROOSE, M., 1971, C.E.R.N. Computer 7600 Programme Library, D505, D605.

JULLIUSON, E., 1974, Ap. J., 191, 331.

KALMYKOV., N.N., and KHRISTIANSEN, G.B., 1975, PICCR, Munich, 8, 2861.

KAMATA, K., and NISHIMURA, J., 1958, Prog. Theor. Phys., Suppl. 6, 93.

KARAKULA, S., 1968, See Wdowczyk, J., 1973.

KARAKULA, S., et al, 1974, J. Phys. A., 7, 437.

KEMPA, J., et al, 1974, J. Phys. A., 7, 1213.

KHRISTIANSEN, G.B., 1975, PICCR, London, 2, 774.

KULIKOV., G.V., et al, 1960, PICCR, Moscow, 2, 85.

LA-POINTE, M., et al, 1968, Can. J. Phys., 46, S68.

LINSLEY, J., 1963, PICCR, Jaipur, 4, 77.

MACHIN, A.C., et al, 1969, PICCR, Budapest, 3, 579.

MACLEOD, G.R., 1956, Nuovo Cim, III, 118.

MASON, G.W., et al, 1975, PICCR., Munich, 8, 2943.

McCAUGHAN, J.B., et al, 1965, Nuovo Cim., 38, 693.

MIYAKE, S., et al., 1970, PICCR., Budapest, 3, 463.

MIYAKE, S., 1973, PICCR, Denver, 5, 3220.

MURAKI, Y., 1975, PICCR, 7, 2209.

MURDOCH, H.S., 1958, Nucl. Phys., 8, 157.

NORMAN, R.J., 1956, Proc. Phys., Soc., A69, 804.

NISHIMURA, J., and KAMATA, K., 1952, Prog. Theor.Phys., 1, 185.

NISHIMURA, J. and KAMATA, K., 1958, (See Kamata, K, and Nishimura J., (1958)).

OLEJNICZAK, J., et al., 1977, J. Phys., G., 3, 847.

OLEJNICZAK, J., 1975, Ph.D. Thesis, University of Lodz, Poland.

ORFORD, K. J., 1968, Ph.D. Thesis, University of Durham.

ORFORD, K.J., and TURVER, K.E., 1969, PICCR, Budapest, 3, 585.

PENZIAS, A.A., and WILSON, R.W., 1965, Ap. J., 142, 419.

PIGGOTT, J.L., 1975, Ph.D. Thesis, University of Durham.

PRESCOTT, J.R., 1956, Proc. Phys. Soc., A69, 870.

PICKERSGILL, D.R., 1973, Ph.D. Thesis, University of Durham

REGENER, V.H., 1951, Phys. Rev., 81, 161.

REID, R. J., et al, 1961, Proc. Phys. Soc., 78, 103.

ROLL, P.G., and WILKINSON, D.T., 1966, Phys. Rev. Lett., 16, 405.

ROZHDESTVENSKY, S.M., et al., 1975, PICCR, Munich, 8, 2790.

RYAN, M.J., et al., 1972, Phys. Rev. Lett., 28, 985.

SCHMIDT, W.K.H., et al, 1975, Astron. and Astrophys. 46, 49.

SHAPIRO, M., et al, 1971, PICCR, Hobart, 1, 221.

SHIBATA, S., et al, 1965, PICCR, London, 2, 672.

SMITH, A.C., 1976, Ph.D. Thesis, University of Durham.

SMITH, A.C., and THOMPSON, M.G., 1977, Nucl. Inst. and Methods, 145, 289.

SMITH, A.C., 1977, Nucl. Inst. and Methods (accepted for publication).

STAUBURT, R., et al, 1970, PICCR, Budapest, 3, 661.

THOMPSON, M.G., 1973, Cosmic Rays at Ground Level, (Ed.Wolfendale,A.W, The Institute of Physics, London).

THOMPSON, M.G., and WELLS, S., 1972, Nucl. Inst. and Methods, 102, 102, 35.

TURNER, M.J.L., 1969, Ph.D. Thesis, University of Durham.

TURVER, K.E., 1973, Cosmic Rays at Ground Level, (Ed.Wolfendale, A.W, The Institute of Physics, London).

TURVER, K.E., 1974, Survey of Computer Simulations of Air Showers, Internal Report, University of Durham.

VERNOV, S.N., et al, 1970, Acta. Phys., Hung, 3, 429.

VERNOV, S.N., et al, 1968, Canad. J. Phys., S46, 197.

WDOWCZYK, J., and WOLFENDALE, A.W., 1972, Nature, 236, 29.

WDOWCZYK, J., and WOLFENDALE, A.W., 1973, J.Phys. A, 6, 1594.

WDOWCZYK, J., 1975, PICCR, Munich, 11, 4002.

WDOWCZYK, J., 1976, Reprint, University of Durham.

WDOWCZYK, J., 1973, Cosmic Rays at Ground Level (Ed. Wolfendale,A.W, The Institute of Physics, London).

WEI, J., and MONTGOMERY, G.G., 1949, Phys.Rev., 76, 1488.

WHALLEY, M.R., 1974, Ph.D. Thesis, University of Durham.

WOLFENDALE, A.W., 1973, Cosmic Rays at Ground Level, (Ed.Wolfendale,A.W, (Ed.Wolfendale, A.W., The Institute of Physics, London).

WOLFENDALE, A.W., 1972, See Wdowczyk, J. and Wolfendale, A.W., 1972.

ZATSEPIN, G.T., and Kuzmin, V.A., 1966, Sov. Phys. J.E.T.P, Lett., 4, 78.